Radicals in Organometallic Coordination Complexes

Inaugural Dissertation

Towards the Academic Degree

Doctor Rerum Naturalium (Dr. rer. nat.)

Submitted to the

Department of Biology and Chemistry

of the University of Bremen

by

Dirk Schlüter

from Bremen

July 2023

This work was carried out under the supervision of Prof. Dr. Jens Beckmann from November 2014 to July 2023 at the Institute of Inorganic Chemistry and Crystallography, Department of Biology and Chemistry of the University of Bremen.

REVIEWERS

1. Prof. Dr. Jens Beckmann (University of Bremen)
2. Prof. Dr. Anne Staubitz (University of Bremen)

Date of Disputation: 26.09.2023

Diese Dissertation wurde in Absprache mit der Prüfungskommission überarbeitet. Es wurden keine wesentlichen inhaltlichen Änderungen vorgenommen.

Eidesstattliche Erklärung

Ich, Dirk Schlüter

versichere an Eides statt durch meine Unterschrift, dass ich die vorliegende Arbeit selbstständig und ohne fremde Hilfe angefertigt und alle Stellen, die ich wörtlich dem Sinne nach aus Veröffentlichungen entnommen habe, als solche kenntlich gemacht und mich auch keiner anderen als der angegebenen Literatur oder sonstiger Hilfsmittel bedient habe. Die aus fremden Quellen direkt oder indirekt übernommenen Formulierungen und Gedanken – einschließlich Abbildungen, Tabellen etc. – sind als solche kenntlich gemacht. Diese schriftliche Arbeit wurde bisher weder ganz noch in Teilen als Prüfungsleistung vorgelegt.

Ich versichere eidesstattlich, dass ich die vorgenannten Angaben nach bestem Wissen und Gewissen gemacht und dass die Angaben der Wahrheit entsprechen und ich nichts verschwiegen habe.

Die Strafbarkeit einer falschen eidesstattlichen Versicherung ist mir bekannt, namentlich die Strafandrohung gemäß § 156 StGB bis zu drei Jahren Freiheitsstrafe oder Geldstrafe bei vorsätzlicher Begehung der Tat bzw. Gemäß § 161 Abs. 1 StGB bis zu einem Jahr Freiheitsstrafe oder Geldstrafe bei fahrlässiger Begehung.

_____ _____

Ort, Datum Dirk Schlüter

Im Gedenken an Christoph Nickel

Danksagung

Ein großer Dank gilt Dr. Matthias Vogt für das Bereitstellen des interessanten Themas meiner Doktorarbeit sowie seiner Hilfe beim Erstellen der veröffentlichten Manuskripte; zudem danke ich ihm für den wissenschaftlichen Diskurs.

Ferner möchte ich mich bei meinem Doktorvater Prof. Dr. Jens Beckmann für die Möglichkeit, die Promotionsarbeit in seinen Laboren durchführen zu können, danken. Ebenso gilt mein Dank seinen Ideen und Anregungen, mit denen er mich auf meinem Weg begleitet hat.

Frau Prof. Dr. Anne Staubitz danke ich für die Anfertigung des Zweitgutachtens. Ferner gilt mein Dank Herrn Prof. Dr. Peter Spiteller für die Übernahme des Vorsitzes des Prüfungsausschusses sowie den übrigen Mitgliedern desselben, Herrn Dr. Emanuel Hupf, Marvin Janßen und Frau Leonie Knecht.

Des Weiteren danke ich allen Mitarbeitern der verschiedenen Analytikmethoden: Dr. Enno Lork, Dr. Marian Olaru, Daniel Duvinage und Sarah Matz danke ich für die Aufnahme und Strukturverfeinerung der Röntgenstrukturanalysen; Herrn Johannes Stelten danke ich für seine große Hilfsbereitschaft bei der Durchführung komplexerer NMR-Messungen sowie seine Zeit, die er für die Wartung der NMR-Geräte aufbrachte, um einen reibungslosen Einsatz derselben zu ermöglichen; Dr. Thomas Dülcks und Dorit Kemken danke ich für die Messungen zahlreicher Massespektren und insbesondere ihre Zeit und Geduld, die hierbei bei mancher Verbindung vonnöten war. Ein besonderer Dank geht zudem an Jeffrey R. Harmer von der Universität Queensland für die Erstellung und Auswertung komplexer Elektronenspinresonanzspektren der Vanadium-Verbindungen.

Ich möchte mich zudem bei allen Mitgliedern der AG Beckmann für die große Hilsbereitschaft, Diskussionsfreude und die wunderbare Arbeitsatmosphäre bedanken. Ein großer Dank gilt nochmals gesondert Dr. Marian Olaru für die regen Diskussionen und das Korrekturlesen meiner Arbeit.

Ebenso richte ich einen großen Dank an meine Familie und Freunde, insbesondere Zork d. Z. und Dr. Rimbedim, die immer an mich geglaubt und meinen Weg mit großem Beistand begleitet haben. Ganz besonders danke ich zudem meiner Lebensgefährtin, Dr. Nalin Sinas Furan für das Korrekturlesen dieser Arbeit, ihre aufmunternden Worte, ihre Geduld und Liebe, die mir viel Kraft gegeben haben.

List of Publications

Published Articles

- Dirk Schlüter, Florian Kleemiss, Malte Fugel, Enno Lork, Kunihisa Sugimoto, Simon Grabowsky, Jeffrey R. Harmer, Matthias Vogt*, "Non-Oxido-Vanadium(IV) Metalloradical Complexes with Bidentate 1,2-Dithienylethene Ligands: Observation of Reversible Cyclization of the Ligand Scaffold in Solution", *Chemistry – A European Journal,* **2020**, *26*, 1335 – 1343.
  DOI: 10.1002/chem.201904103

- Dirk Schlüter, Daniel Duvinage, Robert Langer, Matthias Vogt*, "Hexacoordinated M^{IV} (M = Ti, Zr, Hf) Tetrachlorido Complexes with Chelating Dithienylethane Based 1,2 Diketone Ligand – π-Conjugation as Decisive Factor for Axial Chirality Mode", *European Journal of Inorganic Chemistry*, **2023**, e202300276.
  DOI: 10.1002/ejic.202300276

Poster at Conferences

- Dirk Schlüter, Matthias Vogt*, "Photo-Switchable Electromeric Complexes Bearing Dithienylethene Ligand Motifs – Controllable Redox Non-Innocence Induced by External Stimuli", *18th Norddeutsches Doktorandenkolloquium* **2015**, Goslar, Germany.

- Dirk Schlüter, Enno Lork, Matthias Vogt*, "Photo-Switchable Electromeric Complexes Bearing Dithienylethene Ligand Motifs – Controllable Redox Non-Innocence Induced by External Stimuli", *19th Norddeutsches Doktorandenkolloquium* **2016**, Hamburg, Germany.

List of Abbreviations, Acronyms and Symbols

°C	degree Celsius
Å	Ångström
Ar	aryl
Bu	butyl
BPY	2,2´-bipyridine
Cat	catecholate
cf.	*confer* (compare)
CV	cyclic voltammogram
δ	chemical shift
DCM	dichloromethane
DTE	dithienylethene
E_A	activation energy
EPR	electron paramagnetic resonance
eq	equivalent
et al.	*et alii* (and others)
FLP	frustrated Lewis pair
h	hour
h	Planck constant
HOMO	highest occupied molecular orbital
HR-MS	high resolution mass spectrometry
i	iso
LUMO	lowest unoccupied molecular orbital
m	meta
M	metal
Me	methyl
MeCN	acetonitrile
Mes	mesityl
mol	mole
MS	mass spectrometry

NIL	non-innocent ligand
NMR	nuclear magnetic resonance
MO	molecular orbital
n	normal
nm	nanometer
o	ortho
p	para
PCET	proton-coupled electron transfer
Ph	phenyl
ppm	parts per million
Pr	propyl
Q	quinone
SI	supporting information
SQ	semiquinonate
t	tertiary
THF	tetrahydrofuran
UV/Vis	ultraviolet/visible
v	temporal frequency

Table of Contents

List of Figures

Figures assigned with a literature reference in the description are reproductions of the corresponding authors

List of Tables

In den Wissenschaften ist viel Gewisses, sobald man sich von den Ausnahmen nicht irremachen läßt und die Probleme zu ehren weiß.

- Johann Wolfgang von Goethe

1 Introduction

Over the last eight decades, technological progress has rapidly increased: the first modern computer was built, TVs conquered the living room of every household, the mobile phone was invented and became 'smart', nowadays comprising of computing power beyond the imagination of early modern computer's creators; the internet was born, entwining people all over the world, making it possible to access any information within a few seconds, just to name a few achievements. However, the cost of this progress combined with Earth's growing population is a rising demand for energy and resources, causing global warming and destruction of the environment. Over the past few years, green technologies, such as solar and wind energy, therefore have come to the fore as a substitute for fossil fuels; a development that is additionally fueled by the most recent geopolitical tensions. Many companies are trying to reduce their carbon footprint, e.g. by use of recyclable plastic or no plastic at all in their packaging or by lowering their need for energy with modern production technology; people overall pay more attention to sustainability.

Chemistry is no exempt to this development, as 'green chemistry', which can be described as "to design chemicals, chemical processes and commercial products in a way that, at the very least, avoids the creation of toxics and waste",[1] shows. Nonetheless, one of the important fields of chemistry, catalysis, still mainly relies on noble metals although unearthing of those as well as their application modification pose a hazard to the environment. Yet there is hope that with help of so called 'non-innocent' ligands base metals could provide for a valid substitution.

While not part of this work, but as a desired application in the future and to pay tribute to the importance catalysis plays in chemistry, a brief historical background of it is given in the next chapter, before the concept of non-innocent ligands and its application in catalysis will be explained. Thereafter molecular switches, especially dithienylethene, the ligand of choice for this work, its advantages as well as the overall motivation for this work will be discussed.

Although only a small step in the desired direction, this work may inspire ongoing research in the field of dithienylethene as a non-innocent ligand and provide useful information for compositions and design of such. A marathon yet to absolve, but it is always the first step to get it started.

1.1 Catalysis

The term 'catalysis', derived from Greek word '*κατάλυσις*' for 'annulation', 'untie'[2] was coined by Swedish chemist J. J. Berzelius in 1835 as he tried to describe results of his studies and to refer to a phenomenon known since the antique: that even the addition of smallest amounts of a material could greatly effect the composition of others; an action, which was attributed to the 'philosopher's stone' during the Middle Ages.[3] Berzelius wrote: "In order to avail myself of a derivation well-known in chemistry I will call both the catalytic force of matter and the decomposition by this matter, catalysis, just like we understand with the word analysis the separation of the constituents."[3, 4]

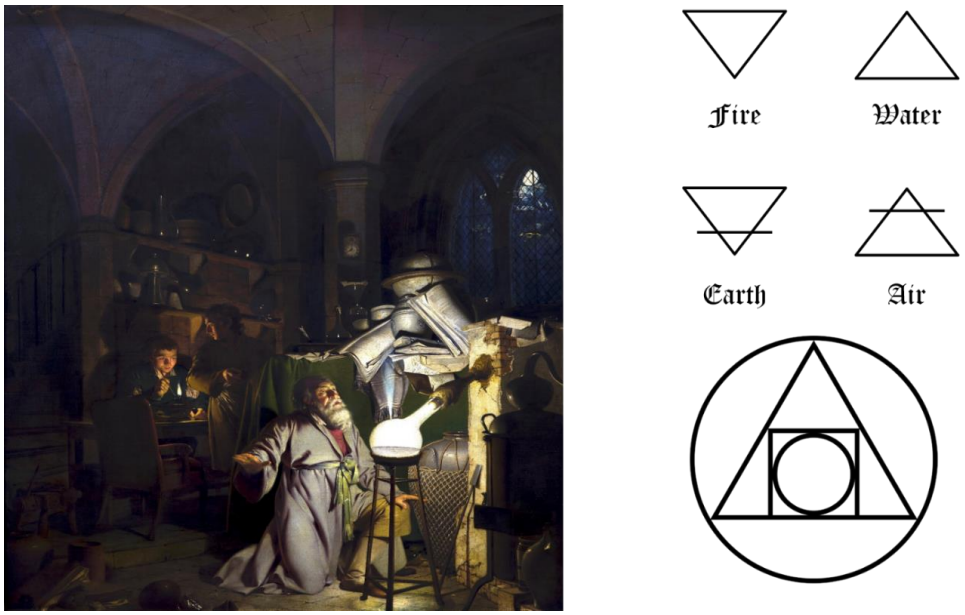

Figure 1: *Left: Alchemist searching for the philosopher's stone (by Joseph Wright of Derby, 1771);[5] upper right: alchemical symbols for the four elements; lower right: 17th century alchemical symbol for the philosopher's stone, illustrated as the interplay of the four elements of matter (fire, water, earth, air).*

The first modern definition of catalysis was given by W. Ostwald in 1894 when he stated that "catalysis is the acceleration of a slow chemical process by the presence of a foreign material",[3, 6] which he changed to his final definition in 1901 at the meeting of the Gesellschaft Deutscher Naturforscher und Ärzte: "A calatyst is a material that changes the rate of a chemical reaction without appearing in the final product."[3, 7]

Nowadays a catalyst would be described as a material that accelerates a chemical reaction. Since it is not being consumed in the process and therefore able to undergo multiple catalytic cycles, no stoichiometric amounts of the catalyst are needed. Catalysts have *no effect* on the thermodynamic equilibrium, however they provide for a *faster* adjustment of it. The reason for the acceleration is a thermodynamically more beneficial transition state that can be formed by substrate and catalyst,

leading to a lower activation energy needed compared to when the reaction is without a catalyst (*Figure 2*).[8]

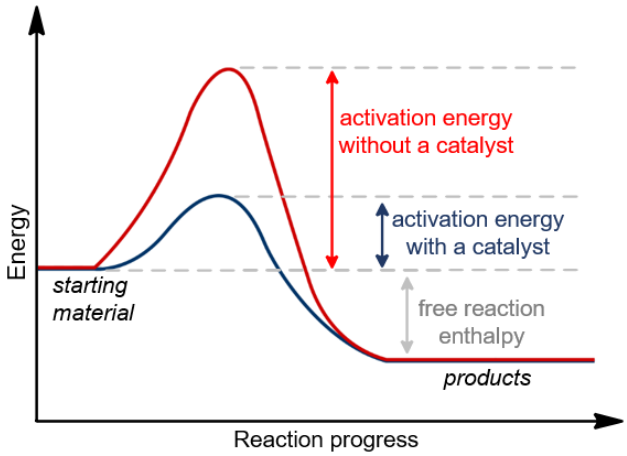

Figure 2: *Simple energy profile of a reaction with and without a catalyst.*

The first technical processes based on catalysis (without knowledge of the enzymatic reaction taking place) were used by advanced civilizations like the Sumerians as long ago as 6000 B.C. who produced beer through fermentation of cereals. Egyptians have used yeast for baking their bread; consumption and therefore the knowledge of fermentation of wine has been known since Bible's first book Genesis.[9] Nonetheless, it was not until the end of 18th and early beginnings of the 19th centuries when a whole series of new catalytic reactions were discovered, e.g. the decomposition of alcohol to ethylene and water upon contact with heated aluminum oxide by J. Priestley in 1793, the decomposition of ammonia upon contact with heated metals in 1813 by L. J. Thénard, the cleavage of hydrogen cyanide when in contact with iron in 1817 by H. Davy, or the ignition of hydrogen at room temperature in the presence of a platinum sponge in 1823 by J. W. Döbereiner, which led to the development of one of the first modern lighters: the 'Döbereiner's lamp'.[10]

Figure 3: *Left: Cylinder seal showing the consumption of (most likely) beer (ca. 1800 B.C.) © Staatliche Museen zu Berlin-Vorderasiatisches Museum, photo: Olaf M. Teßmer; right: Döbereiner's lamp (created around 1825 – 1850).*[11]

However, catalysis' most shining hours took place in 20th century when processes have been developed that can be accounted as some of the most important in chemical industry. One of them is the Haber-Bosch process, named after German chemists F. Haber and C. Bosch, which made it possible to produce ammonia through hydrogen and *atmospheric* nitrogen. This is achieved through high pressure (> 100 bar), high temperatures (ca. 400 - 500 °C; originally up to 600 °C) and the help of an iron-based catalyst.[10, 12, 13] Ammonia is a key chemical in the production of fertilizers as a source for nitrogen. At beginning of the 20th century approximately 200.000 tons of nitrogen in form of Chile saltpeter could be used as fertilizer for agriculture.[14] Nowadays ammonia gets produced in a scale of 150.000.000 tons / year (2019),[15] making it the second largest synthetic chemical product with ca. 80% of it being used for production of fertilizers. The share of ammonia produced by Haber-Bosch process exceeds 90%, thus making it by far the most important for production of this chemical.[13] The Haber-Bosch process therefore has played / plays a significant role in nutrition of world's population.[13, 14]

Another outstanding process based on catalysis is the Ziegler-Natta polymerization for production of polyolefins. Before its use polyethylene could only be produced *via* radicalic polymerization, taking place at elevated temperatures (200 °C) and under high pressure (1.000 – 2.000 bar).[12] The result of this procedure is a polyethylene of low density due to its heavily branched structure and the contained amorphous parts.[12, 16] With help of the Ziegler catalyst, polyethylene can be obtained at room temperature and under atmospheric pressure. Produced this way it is far less branched, leading to a higher crystallinity and density.[12, 17] The Ziegler Catalyst is made of a combination of titanium-(IV)tetrachloride and triethylaluminium and is named after German chemist Karl Ziegler. The second eponym behind the Ziegler-Natta polymerization is Italian scientist Giulio Natta who studied the impact of the Ziegler catalyst on the polymerization of propene shortly after its invention (1953). With it he was not only able to produce polymers with completely new properties; he also discovered that polymerization using a Ziegler catalyst is stereoregular, meaning that polymers produced this way contain a certain tacticity. Both, the invention of the metalorganic mixed catalyst and the proof of the stereoselective polymerization it offers marked the beginning of modern plastics production.[12]

Ostwald (1909), Haber (1918), Ziegler and Natta (1963) all received the honor of the Nobel Prize. Overall achievements related to chemical and enzymatic catalysis have been recognized by the Nobel Foundation at least 16 times, accounting for about 14 % of the awarded prizes and 18 % of the prize winners in chemistry. Numbers, that underline the importance of catalysis for chemistry - and the world.[18, 19]

1.2 Non-innocent Ligands (NILs)

The term *'innocent'* and therefore the implied term of *'non-innocent'* with reference to ligands was first used and invented by Danish chemist C. K. Jørgensen in 1966.[20, 21] It became popular and widely accepted within the community since the 90's when interest in complexes bearing NILs greatly increased.[22] Ever since, the concept of NILs is under running investigation in research topics like optical materials, catalysis, energy storage and conversion, data storage, group-transfer chemistry and many more.[23-28]

Why is that? What opportunities do NILs offer and what exactly makes a ligand 'non-innocent'?

1.2.1 A Brief Historical Background

In 1962 Schrauzer and Mayweg reported on an 'unusual' nickel complex with the formula $NiS_4C_4Ph_4$.[29, 30] Only a few weeks later Gray and co-workers independently described metal complexes of the form $[MS_4C_4(CN)_4]^{2-}$ with M = Ni, Pd, Pt amongst others.[31]

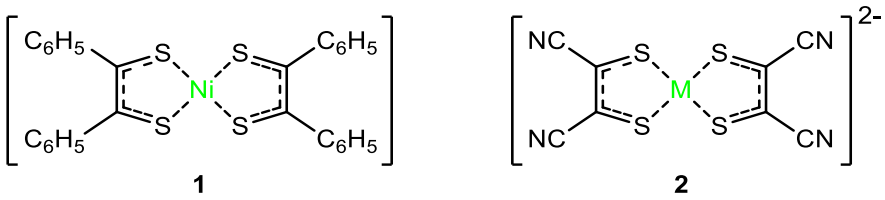

Figure 4: *Left: Schrauzer and Mayweg's nickel dithiolene complex (**1**);[30] right: Gray and co-worker's metal dithiolene complexes (**2**) with M = Ni, Pd, Pt.[31]*

The peculiarity about these complexes was how to distribute the electrons among the central metal atom and the dithiolene ligands, namely what exact oxidation state the metal atom is in. *Figure 5* shows some possible resonance descriptions for **1**.

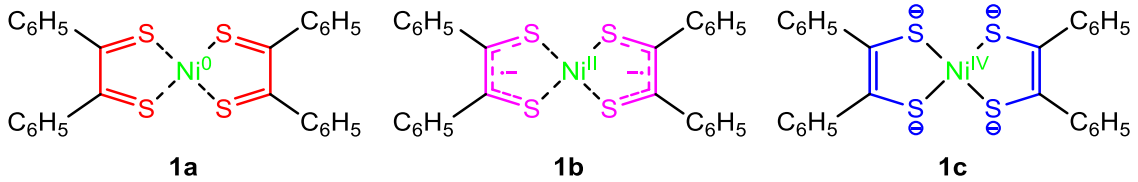

Figure 5: *Three possible resonance descriptions for **1**.[32]*

1a depicts nickel in a zerovalent state with the dithioketones remaining in their neutral structure. **1c** depicts the other extreme, where both ligands have been reduced to the dianionic species, leaving nickel in the oxidation state of +4. Case **1b** shows an intermediate situation between **1a** and **1c** with two radical monoanions and nickel in the oxidation state of +2.[23, 32]

The ambiguity in assignment of the metal's - and therefore the ligand's - oxidation state and the subsequent difficulties in interpretation of the electrochemical and electric spectroscopic properties led to a discussion about their true nature for many years.[23] Particularly worth mentioning in this controversy besides the groups of Schrauzer[30, 32-38] and Gray[31, 39-42] are R. H. Holm and co-workers.[43-45] They indicated that the complexes of Schrauzer and Gray, in terms of valence electrons, differed only by two electrons and that it should be possible to reduce the neutral species to the dianionic species and the other way around.[43] They proofed this assumption to be correct and generated the monoanion and dianion for **1** as well as the monoanion and the neutral complex for **2** along with other group 10 complexes.[44]

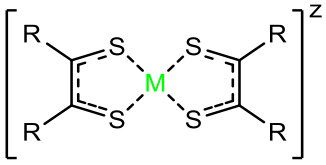

3

Figure 6: *Holm and co-worker's chemically and electrochemically obtained dithiolene complexes with R = C_6H_5, CN, CF_3; M = Ni, Pd, Pt; z = 0, 1-, 2-.*[44]

However their postulation about nickel being in the oxidation state +3 having an electron configuration of d^7 for complex **3** with R = CN, z = 1-, 2-[45] was proven wrong since their calculation was based solely on pure 3d-functions.[42]

In the end, intensive studies of the mentioned complexes and their derivatives (e.g. $Ni(S_2C_2H_2)_2$ (**4**) with z = 0, 1-, 2-) in terms of their X-ray powder diffraction patterns, UV- and IR spectra, magnetic- and electrochemical spectroscopic properties as well as charge density and molecular orbitals (MOs) calculations consolidated the fact that these complexes are square planar d^8 metal complexes with both ligands as radical monoanions and the metal center in the spectroscopically determined oxidation state of +2.[30-45] Furthermore Schrauzer and co-workers concluded that reducing the neutral complex to the mono- or dianion does *not* change the oxidation state of the metal which remains at +2.[35]

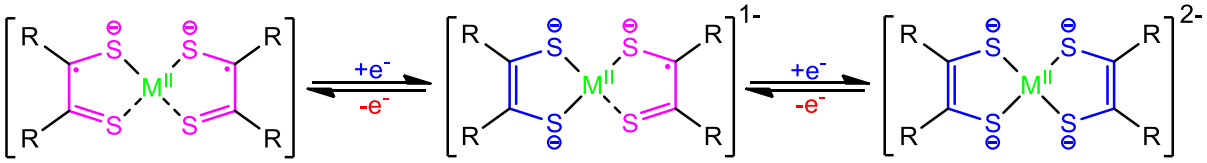

4a **4b** **4c**

Figure 7: *Reduction/oxidation of complexes **4** occurs on the ligand, the central metal atom remains in its bivalent state. M = Ni, Pd, Pt; R = H, C_6H_5, CN, CF_3.*[35]

Due to cases like these, as mentioned in the beginning, Jørgensen coined the term 'innocent' for ligands: "Ligands are innocent when they allow oxidation states of the central atoms to be defined."[20]

1.2.2 *Formal* Oxidation State VS *Spectroscopic* Oxidation State

Besides the term 'innocent' for ligands, Jørgensen also proposed the term of a *spectroscopic* oxidation state.[46] The term 'oxidation state' was invented by German chemist F. Wöhler and, as the word implies, was originally defined as the number of oxygen equivalents an element can bind to.[47] A modern definition of the oxidation state by L. S. Hegedus describes it as "the charge left on the metal atom after all ligands have been removed in their normal, closed-shell configuration – that is with their electron pairs".[48] As Hegedus points out, the oxidation state is a pure formalism and *not* a physical property of the atom thus it cannot be measured.[48] In contrast, the spectroscopic oxidation state *is* a measurable physical property and can be determined by various spectroscopic methods, e.g. resonance Raman or Mössbauer spectroscopy.[46, 49] Often, formal and spectroscopic oxidation state are uniform.[22, 49] This accounts for complexes with unequivocally charge defined ligands such as H_2O or NH_3.[50, 51] One example is the low-spin cobalt d^6 complex $[Co(NH_3)_6]Cl_3$ in which both, formal and spectroscopic oxidation state, are identical (+3).[22, 49] *Figure 8* depicts the framework of an O-coordinated phenolato- and the corresponding phenoxyl radical Fe(III)-complex K. Wieghardt and co-workers studied for a prolonged time.[52-55]

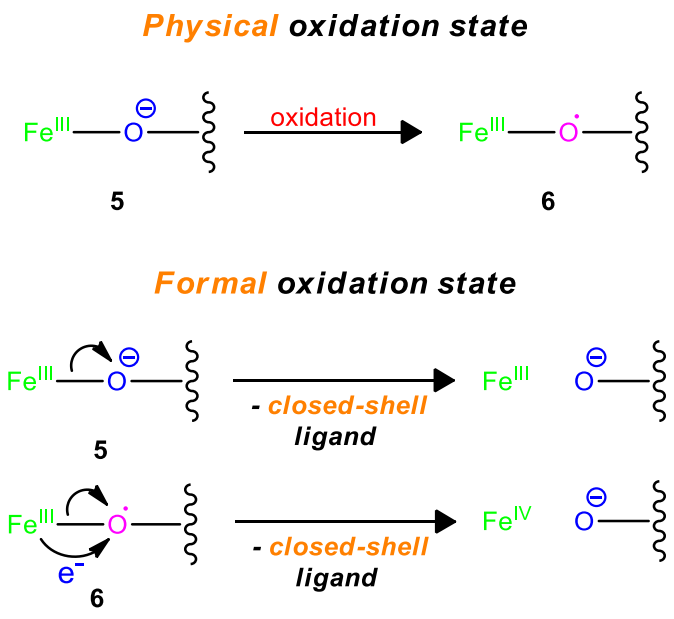

Figure 8: *Framework of a phenolato- (**5**) and the corresponding phenoxyl radical iron complex **6**.*[53]

Photoionization or electrochemical oxidation converts **5** into **6**. *Via* Mössbauer-, resonance Raman spectroscopy and X-ray diffraction crystallography Wieghardt and co-workers proved that the oxidation takes place on the ligand rather than iron; the latter therefore retains its d^5 configuration, leading to a *spectroscopic* oxidation state of +3 for both, the phenolato- (**5**) and the oxidized phenoxyl radical complex **6**.[52-55] On the other hand the *formal* oxidation state changes from +3 for **5** to +4 for **6**

(*Figure 8*, bottom). Discrepancies therefore arise for transition metal complexes with organic radical open-shell ligands since the ligand formally gets removed with a closed-shell for the formal oxidation state.[49] On that account when referring to an 'oxidation state' of a metal center in a complex with NILs it is important to distinguish between *formal* and *spectroscopic* oxidation state. It is also noteworthy that while a priori the *physical* oxidation state in such a complex might be difficult to predict, it is by no means ambiguous at a given time since it is a measurable physical property.[26]

1.2.3 MO Interactions Between Metal and NIL

In complexes with NILs, redox reactions can take place on the ligand rather than the metal and it is difficult to assign actual oxidation states a priori. Why is that?

The answer can be found in the energy differences between the highest occupied molecular orbital (HOMO) and the lowest unoccupied molecular orbital (LUMO) of such complexes. Since a detailed description of MO interactions is far too complex and would lead beyond the scope of this work, the following approximation will be used: electron transfer mainly contains involvement of the HOMO or LUMO frontier orbitals. In the process of an oxidation, an electron is removed from the HOMO while in the process of a reduction an electron is added to the LUMO. HOMO and LUMO are therefore referred to as redox orbitals. As mentioned before this is a vast approximation since electron transfers affect more than one MO and can effectively re-determine all energy levels in the frontier orbital system.[56-58]

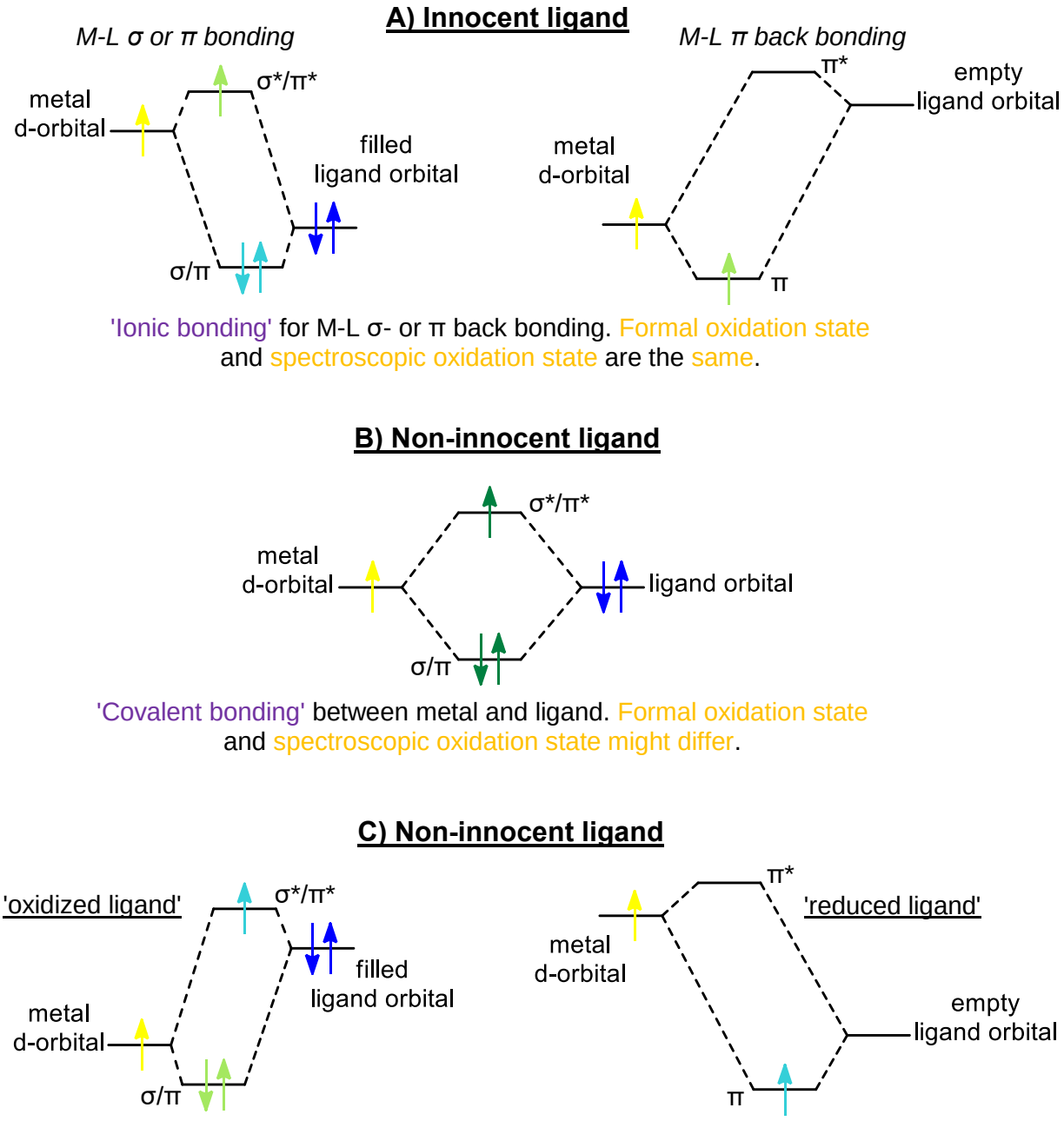

Figure 9: *Simplified orbital schemes for possible bondings between metal and ligand. Metal's electrons are illustrated in yellow, ligand's electrons in blue. The color for electrons in the MOs depends on the mixing of metal's and ligand's atom orbitals.*[59]

In 'classic' coordination complexes the filled σ-donor type ligand orbitals are significantly lower in energy than the metal's d-orbitals, which are slightly lower in energy than the σ*/π*-orbitals. Unpaired electrons are therefore usually located at the metal and radical reactions also typically occur there.[59] The σ/π MOs contain a strong ligand character (*Figure 9, **A** left*). Since numerous ligands, e. g. olefins, CO, NO possess relatively low-lying empty π*-orbitals, M-L-π-backbonding is possible. The suitable metal d-orbitals are substantially lower in energy than the empty π*-ligand orbitals thus the

corresponding MOs contain a strong metal character (*Figure 9, **A** right*).[59, 60] Electrons for the π-back bonding therefore can be described as 'metal electrons', in the σ/π MOs as 'ligand electrons'. In this case both, formal oxidation state and physical oxidation state are the same. The ligand acts innocently.[59]

In a complex with NILs, the relative metal's and ligand's orbital energies might be inversed. In that case the filled σ-donor type ligand orbitals are higher in energy than the d-orbitals of the metal. This effectively leads to a reduction of the latter and an oxidation of the ligand also meaning that unpaired spin-density now is located on the ligand rather than the metal (*Figure 9, **C** left*). This redox non-innocent behavior might also apply when empty π-acceptor ligand orbitals are lower in energy than the metal's d-orbitals, leading effectively to a reduction of the ligand and an oxidation of the metal (*Figure 9, **C** right*). In this case, again, is the unpaired electron located on the ligand. Formal oxidation state and spectroscopic oxidation state are different since in the first case the actual filling of the metal d-orbitals is higher while in the second case lower than predicted by the formal oxidation state.[59]

While ***A*** and ***C*** describe the metal-ligand bonding as ionic, ***B*** depicts a situation with covalent bonds. Due to strong mixing of energetically close orbitals of metal and ligand, spin density is located on either the first or the last and possibly switches in-between. Formal oxidation state and physical oxidation state might be different, depending on where the spin density is actually located.[59]

1.2.4 Valence Tautomers

Open-shell complexes can be categorized in one of three ways as shown in *Figure 10*: as a metal centered radical (left), a ligand centered radical (right) or as an intermediate of both (middle).[59]

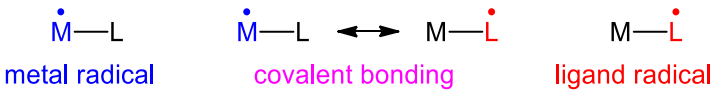

***Figure 10:** Possible electronic configurations for an open-shell complex.[59]*

This intermediate state with covalent bonds between metal and non-innocent ligand can be further specified 1) as a resonance stabilized species with a single minimum due to delocalized valences or 2) as an equilibrium of two species, so called 'redox' or 'valence tautomers', each with its own minimum (see *Figure 11*).[51, 61, 62]

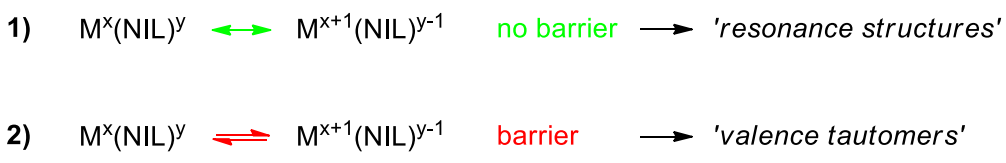

***Figure 11**: Difference between resonance structures and valence tautomers.*[51]

The first valence tautomers of a redox isomeric cobalt quinone complex have been reported in 1980 by Pierpont and Buchanan.[63-65] *Figure 12* shows the structure **(A)** and the electronic configuration of the cobalt atom of the two species **(B)**.[28, 66]

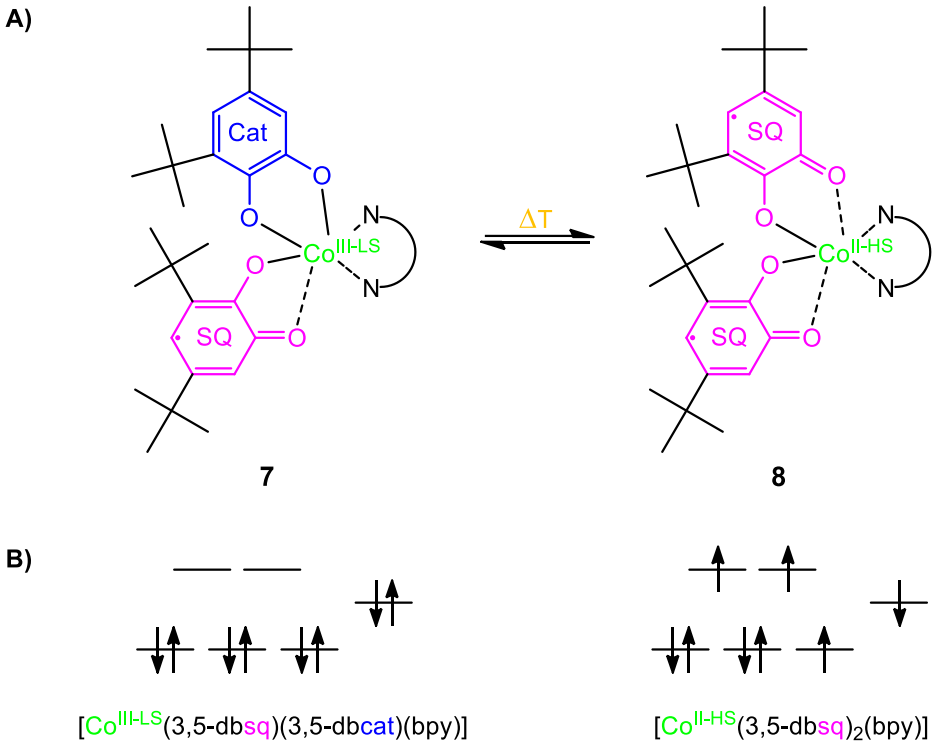

***Figure 12**: **A)** Equilibrium between $[Co^{III-LS}(3,5\text{-dbsq})(3,5\text{-dbcat})(bpy)]$ **7** and $[Co^{II-HS}(3,5\text{-dbsq})_2(bpy)]$ **8** in solution. LS = low spin; 3,5-dbsq = 3,5-di-tert-butyl-1,2-semiquinonate; 3,5-dbcat = 3,5-di-tert-butyl-1,2-catecholate; bpy = 2,2'-bypriridine; HS = high spin **B)** Electronic configuration of Co.*[28, 66]

Lower temperatures shift the equilibrium towards the low-spin complex $[Co^{III-LS}(3,5\text{-dbsq})(3,5\text{ dbcat})(bpy)]$ (**7**) with one ligand in the form of a semiquinonate, the other in the form of the corresponding catecholate. Higher temperatures lead to a shift of the equilibrium towards high-spin complex $[Co^{II-HS}(3,5\text{-dbsq})_2(bpy)]$ (**8**), which effectively forms due to an oxidation of the catecholate to the semiquinonate and a reduction of Co^{III} to Co^{II} (see *Figure 12* for abbreviations).[63-65] Both valence tautomers show distinct differences in their structure and charge distribution; therefore they possess varying optical and magnetic properties, which can be obtained *via* external stimuli due to reversible switching. Valence tautomers like these are highly interesting for applications as molecular switches, sensors and as molecule-based magnets and optical and/or magnetic data storage media.[66-72]

1.2.5 Redox Active Ligands and NILs

The non-innocent ligands of complexes **1**–**8** all exhibit redox active behavior, as *Figure 13* shows exemplary for dioxolene 3,5-cyclohexadiene-1,2-dione from complex **7** and **8**.[73]

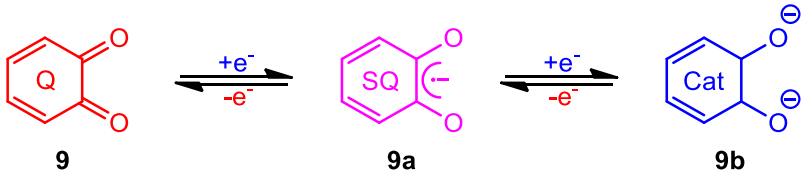

Figure 13: *Redox series of dioxolene 3,5-Cyclohexadiene-1,2-dione. Q = quinone; SQ = semiquinonate; Cat = catecholate.*[73]

Quinone **9** can be reduced in two one electron steps: first to its radical anionic form, the semiquinonate **9a**, then to dianionic catecholate **9b**. These steps are reversible as the catecholate can be oxidized back to the prior mentioned forms.[73] The same applies for 1,2-dithiolligands (cf. *Figure 5*) since they can exist in the neutral dithiol-, the radical anionic dithiolate- and the corresponding dithiolato form.[23, 74] Nonetheless, this does not mean that every redox active ligand is automatically a non-innocent ligand. *Figure 14* depicts the redox series for another redox active ligand, 2,2'-bipyridine (**10**).

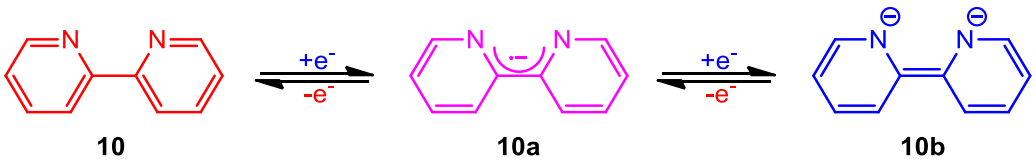

Figure 14: *Redox series of 2,2'-bipyridine.*[75]

As can be seen, **10** also exists in the neutral, the radical anionic and the dianionic form.[75] *Figure 15* shows two complexes, both containing 2,2'-bipyridine as ligands: $[Ru(bpy)_3]^{2+}$ and $[Cr(bpy)_3]^{3+}$.

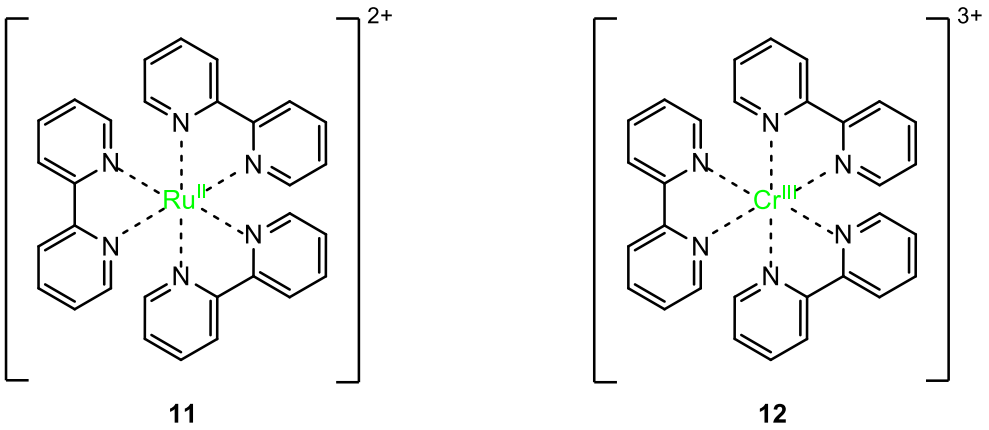

Figure 15: *Structure of $[Ru(bpy)_3]^{2+}$ (**11**)*[76] *and $[Cr(bpy)_3^{2+}$ (**12**)*[77].

Electrochemical investigations of **11** show that at +1.26 V an oxidation takes place on the metal and starting at -1.35 V three reduction steps for the ligand can be observed. Since HOMO (strong influence

of metal d(π) orbitals) and LUMO (strong influence of ligand π* orbitals) differ substantially in energy, these redox processes can unambiguously be described as metal- or ligand centred.[22, 23, 76]

Compound **12** also displays a couple of one electron reduction steps.[78] However, while the first reduction can clearly be assigned as metal centred ($[Cr^{III}(bpy)_3]^{3+} \rightarrow [Cr^{II}(bpy)_3]^{2+}$), the following reduction leads, presumably *via* transfer of two electrons into the π* orbitals of the ligand, to a species that can be described as $[Cr^{III}(bpy)(bpy^{\cdot-})_2]^{+}$ (or possibly $[Cr^{II}(bpy)_2(bpy^{\cdot-})]^{+}$). Successive reduction steps also result in 'delocalized behavior'.[22, 23, 77, 79, 80] Although both complexes **11** and **12** contain the same redox active ligand, 2,2'-bipyridine, one can see why the term 'non-innocent' is more applicable for complex **12**, in which, due to the energetically great similarity of the metal's and ligand's redox orbitals, strong mixing among them can be observed. Non-innocent behavior therefore is, as implied by Jørgensen's definition, not a function of the ligand alone, but of the entire complex.[20, 22, 23]

1.2.6 NILs in Catalysis

In the past, even though acknowledged as crucial for the catalytic system as a whole and therefore subject of tuning for reactivity and selectivity, ligands in inorganic chemistry have just been spectators in the actual catalytic process. They were well defined closed-shell molecules, e. g. triphenylphospines or ammonia, unable to be part of redox reactions due to the large amount of energy needed to oxidize or reduce them. Catalytic complexes with non-innocent ligands go a different way as they try to use a synergetic interplay between metal and ligand.[25, 27, 81, 82]

Up to now numerous chemicals are industrially prepared *via* catalysts (approximately 80% of all chemical and pharmaceutical products),[83] relying on precious metals like rhodium, palladium, platinum or iridium.[25, 81, 84] Their advantage lies in the ability of reacting in well-defined two-electron redox reactions, while base metals often favor one-electron redox changes, leading to a possible lack of controlling reactivity, dysfunction or even decomposition of the catalyst.[25, 27, 81] However, noble metals are expensive, become more and more scarce and tend to generate toxic waste.[25, 81, 85] Base metals like copper or iron on the other hand are abundant (iron is the second most metal and the fourth most common element of Earth's crust)[60, 86], cheap and much more environmentally benign.[81, 85] But how to compensate for the limiting deficits?

One answer lies in the above mentioned synergetic interplay between metal and ligand. Nature, as a true pioneer of non-innocent redox active ligands, is utilizing this fortune of possibilities for a long time already in its catalytic systems, the enzymes.[26] One example for a metalloprotein complex with a non-innocent ligand is galactose oxidase (GO). This fungal enzyme catalyzes the aerobic oxidation of

D-galactose (R-CH_2-OH) into D-galactohexodialdose (R-CHO) and hydrogen peroxide. The catalytic mechanism, which proceeds *via* a radical-type reaction, has been studied in detail by several working groups (*Figure 16*).[27, 87-91]

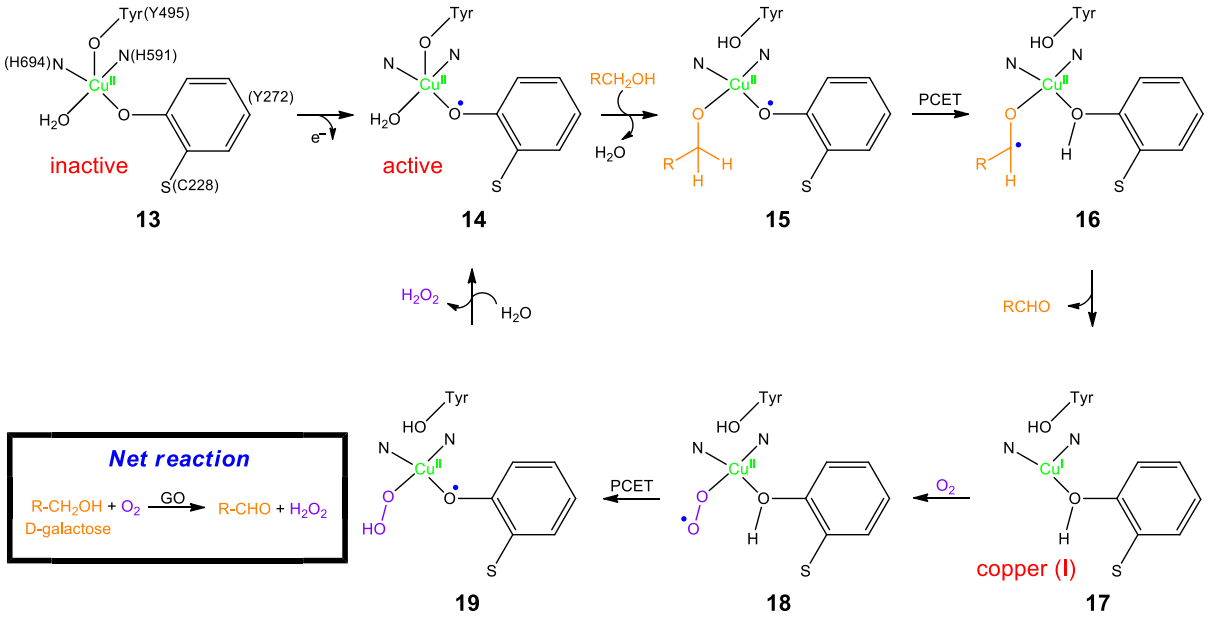

Figure 16: *Catalytic mechanism of galactose oxidase. Amino acid residues are not shown for overview purposes. GO = galactose oxidase; PCET = proton-coupled electron transfer.*[27]

Galactose oxidase consists of a copper(II) center surrounded by H_2O, two histidine and two tyrosine moieties. Oxidation of Tyr(Y272) leads to the active form of the complex with a phenoxyl radical (**14**). After binding of D-galactose to the copper center through elimination of Tyr(Y495), an intramolecular proton-coupled electron transfer (PCET) takes place (**15** → **16**), followed by a reductive elimination step, in which the oxidation state of copper changes from Cu(II) to Cu(I) (**16** → **17**). Addition of molecular oxygen brings the copper back to an oxidation state of +2 (**17** → **18**). Again an intramolecular proton-coupled electron transfer takes place, regenerating the oxygen-centered radical of Tyr(Y272) (**18** → **19**). Release of hydrogen peroxide upon addition of water and forming back the bond to Tyr(495) closes the catalytic cycle (**19** → **14**). As net reaction the alcohol group of D-galactose became oxidized to the corresponding carbonyl group *via* oxygen. Obviously in this catalytic process the redox-active ligand plays a major part and is an active participant: while the substrate's binding takes place first at the copper(II)-center, bringing it close to the active site of the ligand, it is between the substrate and the non-innocent ligand where the bond-breaking process effectively takes place.[27]

Inspired by this, Wieghardt and Chaudhuri developed a Cu(II)-thiophenol catalyst (**20**) which is, like galacose oxidase, able to convert primary alcohols *via* oxygen into the corresponding aldehyds and hydrogen peroxide. The catalyst is furthermore capable, unlike galactose oxidase, of forming diols out of secondary alcohols, leading to a new C-C-bond formation.[27, 92]

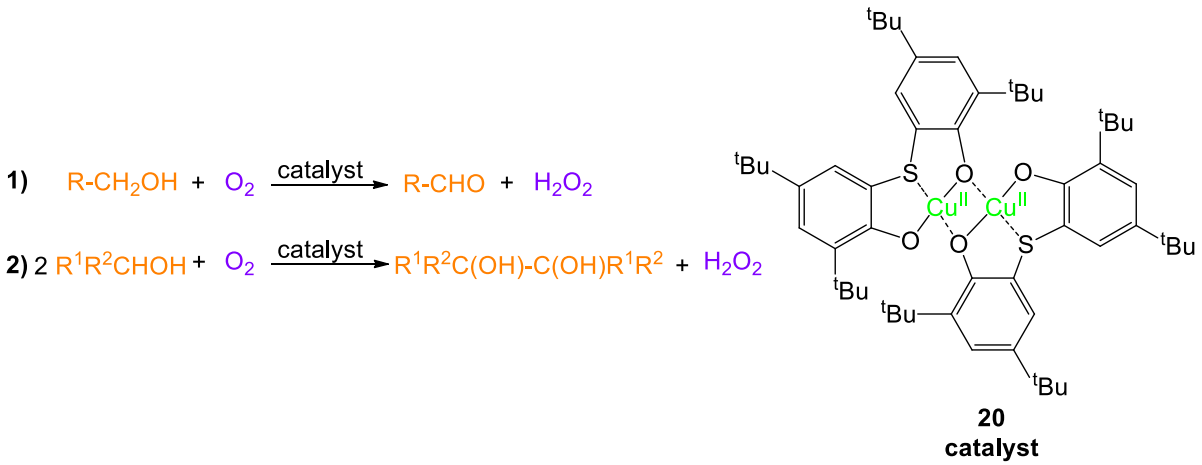

Figure 17: *Structure of Wieghardt's and Chaudhuri's Cu(II)-catalyst. 1) Oxidation of a primary alcohol; 2) Oxidation of a secondary alcohol.*[27]

Not inspired by nature, but the observations of Schrauzer et al. and Wing et al. that nickeldithiolenes react with norbonadienes and 2,3-dimethyl-1,3-dibutadiene to form the corresponding [1+1] adducts,[35, 93, 94] Stiefel and Wang found a way to improve purification of olefins *via* a catalytic process (*Figure 18*).[95]

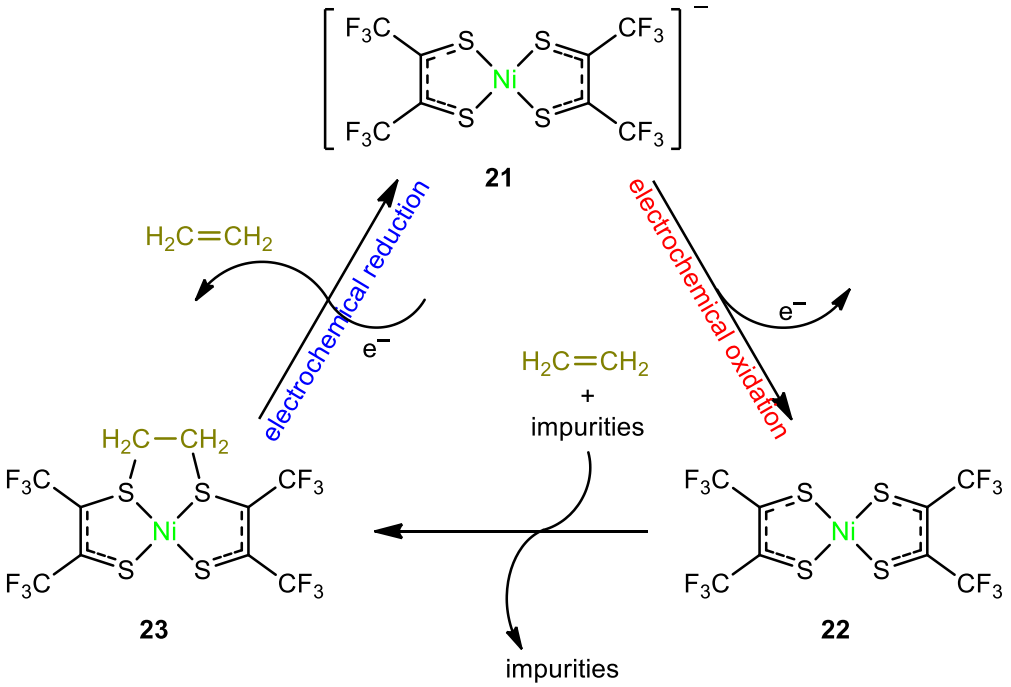

Figure 18*: Electrochemical purification of ethene via a nickel-dithiolene complex (**21**).*[27]

Anionic complex **21** can electrochemically be oxidized to neutral compound **22.** Unlike **21**, **22** possesses a great affinity to olefins, especially ethene, and forms with it adduct complex **23**. Other impure gaseous components like CO, C_2H_2, alkanes, do not interact with complex **22** and can therefore be

removed. Upon electrochemical reduction of adduct complex **23** the ethene, now purified, can be released and the cycle is closed.[27, 95]

Another interesting example of a catalyst where the non-innocent ligand plays an active part is complex **24**, reported by Chirik and co-workers (*Figure 19*).[96]

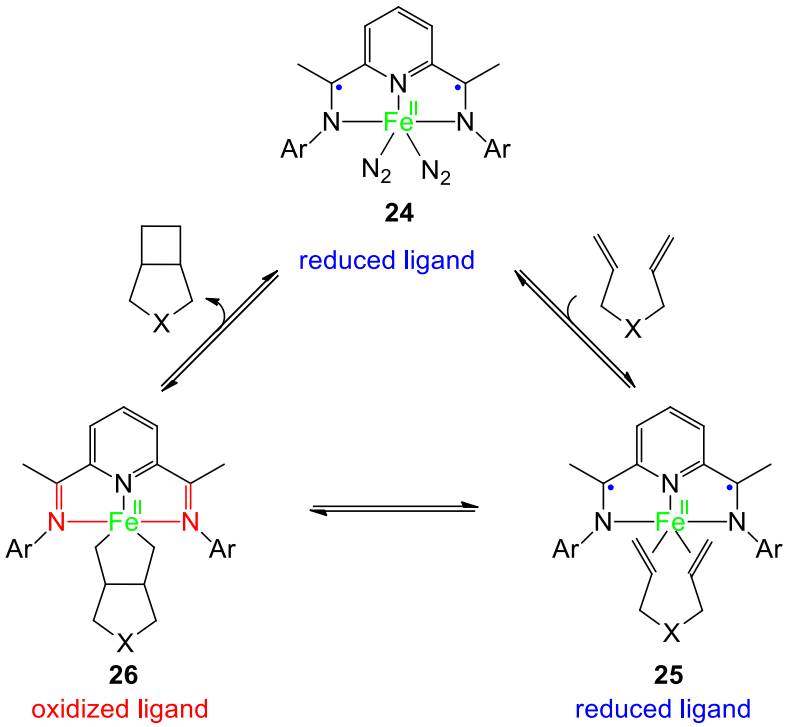

***Figure 19**: Intramolecular [2π + 2π] cycloaddition of two terminal olefins promoted by a Fe(II)-complex (**24**). X = CH_2, $C(CO_2Et)_2$, N-alkyl.*[27]

Iron complex **24**, containing a dianionic tridentate N_3-ligand which is derived from the redox-active ligand 2,6-diiminepyridine,[97, 98] reacts with a terminal diene upon release of the N_2-ligands to π-complex **25**. This π-complex can react in a formally two-electron oxidative addition step to compound **26**; however, the electrons necessary for this transition do not originate from iron, but from the dianionic 2,6-diiminepyridine. This leads to an oxidation of the ligand, while iron remains in bivalent state. In the following reductive elimination step, upon release of the cyclized product, iron again can maintain its oxidation state of +2, while the ligand becomes reduced back to its original state. Hence, in the whole catalytic cycle the ligand's ability to store and release electron density allows iron to avoid high-energy and therefore unstable oxidation states (like Fe^0 upon release of the substrate *via* reductive elimination). This way, due to the help of the non-innocent ligand, iron can mimic a noble metal and is able to react in well-defined two-electron redox reactions.[25, 27] Other related Fe(II)-complexes feature e.g. the intermolecular [2π + 2π] cycloaddition of ethylene and butadiene,[99] the polymerization of ethylene[100] or the intramolecular cyclization of enzynes and diynes.[101]

1.3 Molecular Switches

In electrical engineering a 'switch' is defined as a device in an electrical circuit that is able to open or close the conducting path, thus intercepting or redirecting the electric current.[102] *Figure 20* depicts a simplistic scheme of a switch that can be toggled between the states 'off' (open conducting path) and 'on' (closed conducting path).

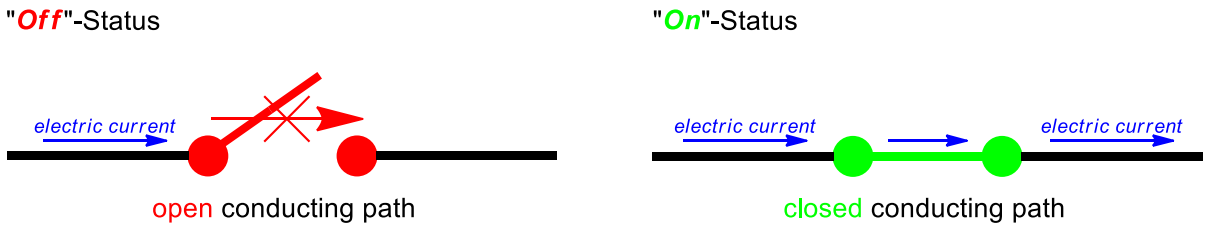

Figure 20: *Simplistic scheme of a switch.*

The term 'switch' also has found its way into the field of chemistry: molecular-level systems that can undergo reversible interconversion between two (or more) stable states *via* an external stimulus are referred to as 'molecular switches'.[103-107] Unlike in electrical engineering this term is used quite liberally by chemists as in a molecule there are numerous features that could be interconverted like structural-, magnetic-, electronical-, optical or luminescence properties. There also exists a vast selection of external stimuli to achieve the switching, e.g. changes in the electrochemical potential, pH, temperature, the presence (or absence) of other chemicals or absorption of light.[103, 108-111] Therefore a wide range of molecules can be accounted as 'molecular switches' in some way.[108] However, these can be classified as *thermodynamically* or *kinetically* controlled.[103, 105, 106, 108] In the first case the molecule is in a thermodynamic equilibrium with its environment as long as it is receiving the stimulus. Upon removal of the stimulus, the molecule will revert into its original state. An example for this kind of behavior are pH indicators. They undergo a distinct color change due to their altered optical absorption spectrum when they become protonated or deprotonated.[108] *Figure 21* shows the pH indicator phenolphthalein, which is colorless in aqueous ethanol at a pH range of 0 – 8.2. At a pH above 8.2, due to deprotonation and opening of the lactone ring, the molecule switches into a wide conjugated π-system, leading to a purple colored solution.[112-114]

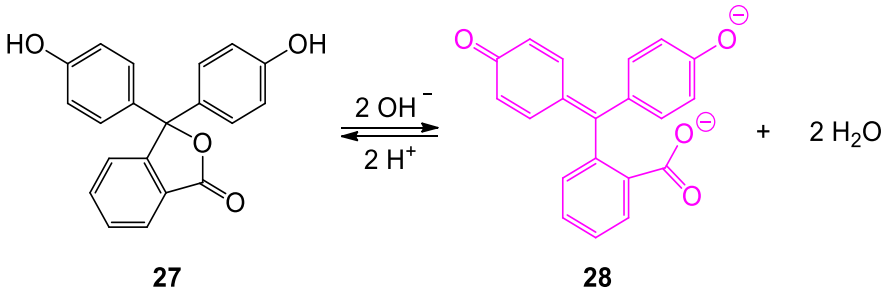

27 **28**

Figure 21: *pH indicator phenolphtalein undergoes structural changes depending on the pH of the solution. The conjugated π-system of* ***28*** *leads to a purple color.*[112]

Nonetheless, this transformation is not permanent. As soon as the pH shifts back below 8.2 **28** will return to its former form **27**. Preservation of **28** therefore is not possible when the pH change is reversed.[108]

This aspect is different in case of a kinetically controlled molecular switch. Here the stimulus does lead to a kinetically stable new state which will *not* return to its prior form even upon removal of the original stimulus due to a kinetic barrier. To bring it back to the original state, a second stimulus is needed.[103, 105, 106, 108] This type of switch is intuitively easier to understand as it can be compared on a macroscopic scale with an ordinary light switch: once the switch was pushed to turn on the light, the light would stay on indefinitely without need of the switch permanently being pressed.[108] A switch of this kind can normally be found in systems prone to photonic stimulation.[105] An example for this sort of switch is 11-*cis*-retinal (**29**), which plays a crucial part in the visual process of mammals (*Figure 22*).[8]

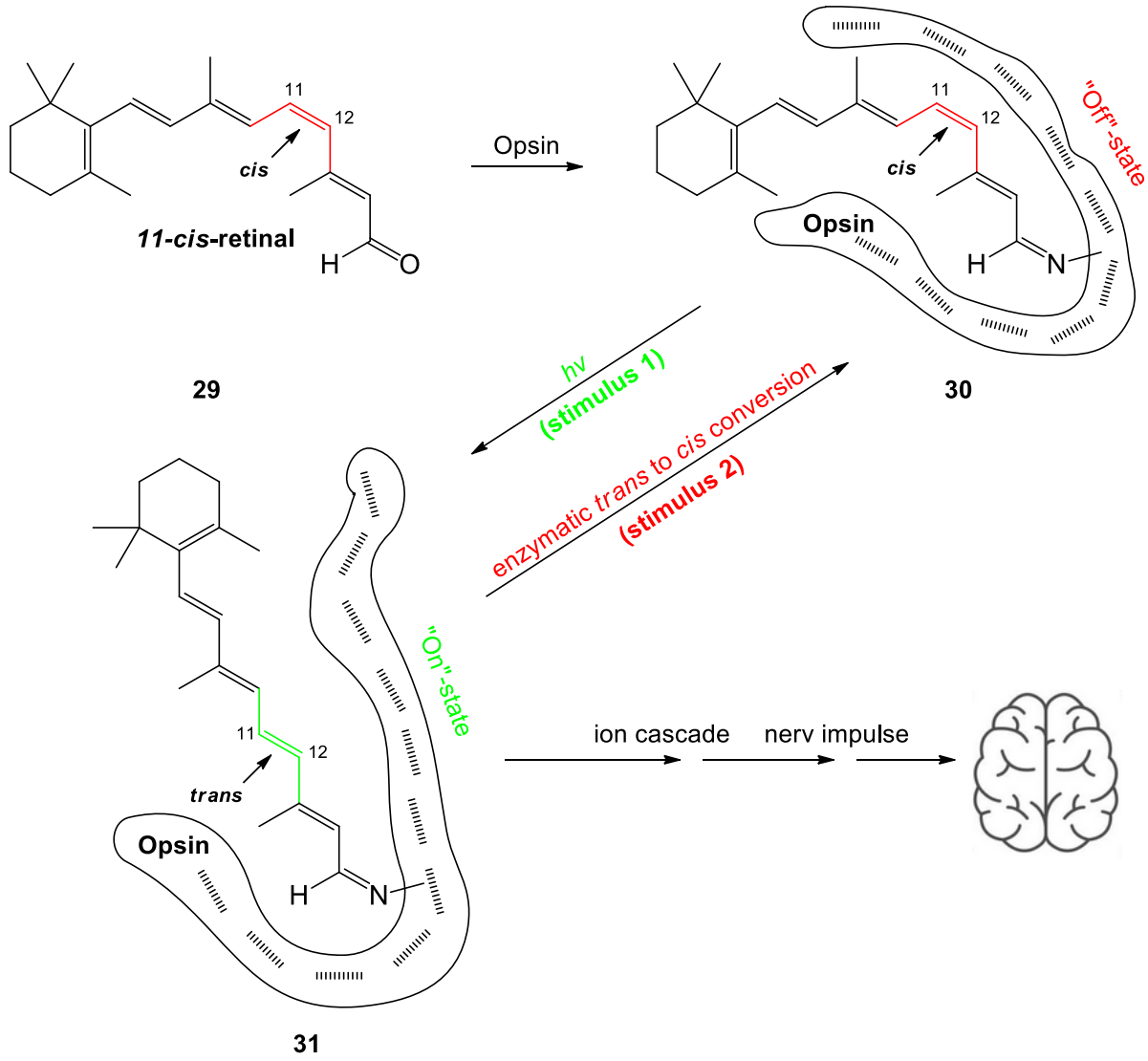

Figure 22: *Activation and regeneration of cis-rhodopsin (**30**) via two different stimuli.*[8]

11-*cis*-retinal **29**, or its Schiff base **30** when bound to the protein opsin, contains a prolonged conjugated π-system with all double bonds between carbon atoms in *trans*-conformation – except for the one between C11 and C12. Upon absorption of visible light the 11-*cis*-isomer undergoes a photoisomerization into the all-*trans*-isomer and stays in this state since a large enough kinetic barrier hampers the conversion back to the *cis*-isomer. This state can be described as the 'on'-state of the molecular switch. The all-*trans*-isomer **31** is more stretched than the 'buckled' *cis*-isomer **30** and the opsin therefore undergoes a conformational change which leads to an ion cascade. The resulting nerve impulse gets transmitted to the brain and becomes processed. The 'off'-state of the molecular switch rhodopsin (**30**) is achieved *via* a slow acting *trans*- to *cis*-isomerization enzyme.[8, 106, 115, 116]

1.4 Photochromism

'*Photochromism*' is defined as a reversible interconversion between two forms of a chemical species induced by light excitation in at least one direction with both forms having different absorption spectra (besides other physical properties).[106, 117] Since the occurring photoreaction only leads to changes in the electronic structure of the molecule or its arrangement of atoms in space (with or without reversible bond breaking) the transforming species are isomers.[106] Excitation with light converts the stable isomer **A** into the higher-energy isomer **B** (*Figure 23*).[106, 117] This conversion can take place on a timescale as small as several femtoseconds.[118-121] Photoreactions are therefore kinetically controlled. Upon overcoming a certain energy barrier, Isomer **B** can convert back to isomer **A**. Depending on the system this reconversion can occur fast, slow or not at all (within a reasonable timescale) without a second stimulus.[106]

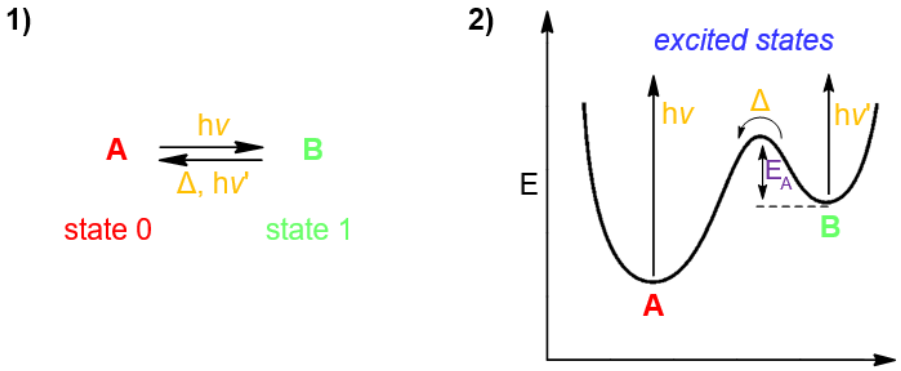

Figure 23: *1) Scheme of a simple photochromic reaction; 2) corresponding simplified energy profile.*[106]

If isomer **B** is thermally stable and no back reaction takes place even when the photogenerated isomer is exposed to higher temperatures for a prolonged time, this system can be classified as a P-Type (photochemically reversible type). If isomer **B** is not thermally stable and converts back to isomer **A**, the system can be described as the T-type (thermally reversible type).[106, 117]

1.5 Molecular Switches based on Photochromism

1.5.1 Spiropyrans

Although observation of photochromism was already reported by Fritzsche as early as in 1867,[122] it was not before the 1950's when major interest settled in due to the discovery and exploitation of photochromism in spiropyrans,[106, 123-126] indicating technical applications e.g. as photochemical erasable memory.[106, 127] Spiropyrans, as the name indicates, are 2H-pyran derivatives where a second ring system (normally heterocyclic) is connected to position two of the pyran, making this atom a spiro atom.

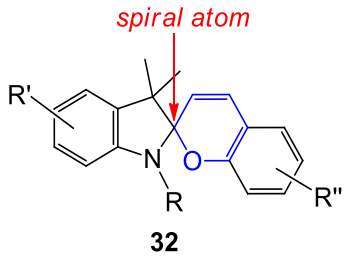

Figure 24: *Typical structure of a spiropyran.*[106]

When irradiated with UV light the usually colorless spiropyrans (and their analogues) undergo a ring opening reaction, leading to the corresponding colored merocyanine. The intensive color of the latter is caused by the extended conjugated π-system.[106, 128]

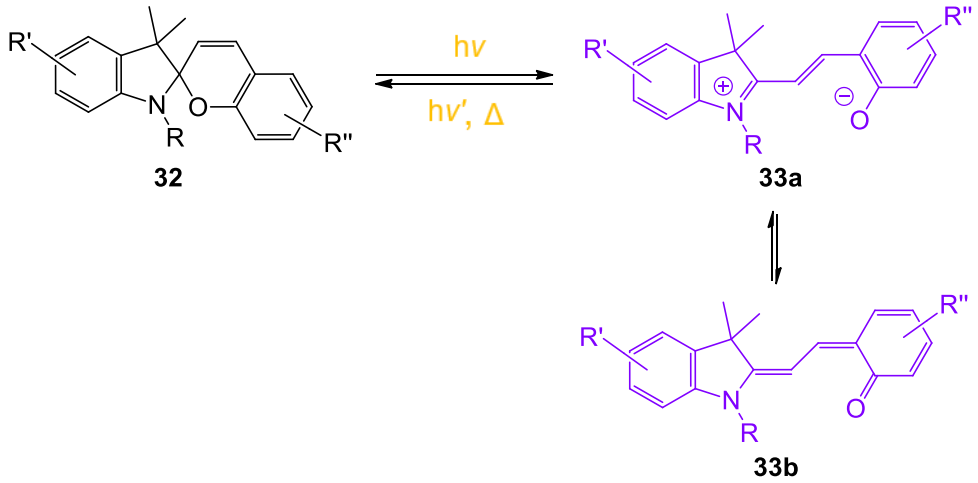

Figure 25: *Scheme of a spiropyran and its corresponding merocyanine form.*[106, 128]

Upon exposure to visible light or even when stored in darkness, the merocyanine will convert back to the original spiropyran. Hence the merocyanine form is not thermally stable and spiropyrans can be accounted as T-type photochromic systems.[106]

In comparison with other photochromic systems, spiropyrans have several advantages: they are synthetically easy to obtain and modify, they display great quantum efficiencies, their isomers possess significant different properties and their reversible isomerization can be triggered by a wide range of stimuli, e.g. irradiation, solvent, temperature, redox potential, pH, mechanical force and metal ions.[106, 126, 128-132] *Figure 26* shows an interesting example of a spiropyran that responds reversibly and selectively to zinc ions.[131, 132]

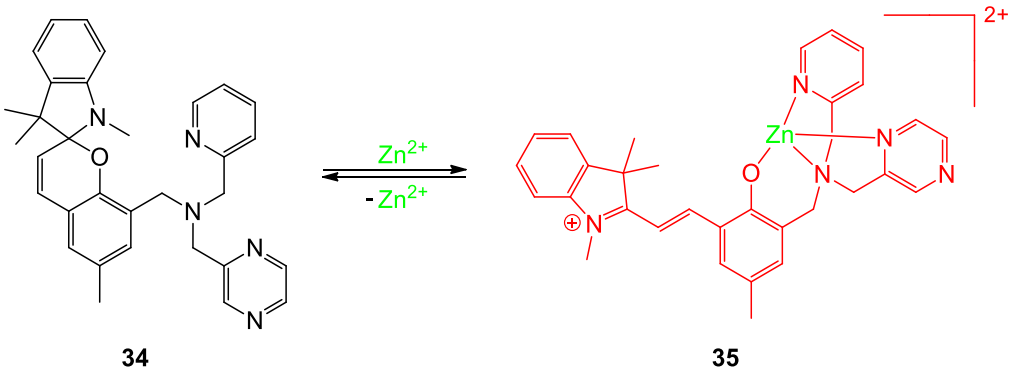

Figure 26: *Addition of zinc ions leads to conversion of* ***34*** *to the merocyanine* ***35****. This is accompanied by a color change of the solution from pale yellow to deep red.*[131, 132]

However, one of the biggest disadvantages of spiropyrans is their lack of thermal stability against the back reaction when the initial stimulus is no longer provided and therefore their limited potential in applications where a prolonged stability of both isomers is needed.[106]

1.5.2 Azobenzenes

Another well studied and widely used photochromic compound is azobenzene.[106] Although synthesized already in 1834 by E. Mitscherlich,[133, 134] it took more than three decades before F. A. Kekulé postulated its correct structure: two phenyl rings that are connected to one another by a N=N double bond.[135] After another 71 years, in 1937, G. S. Hartley accidently discovered that upon irradiation azobenzene enters a second modification which can reversibly convert back to the starting compound.[136] Shortly after, both forms, different in chromatographic behavior, color, solubility, melting point etc.,[137] were measured *via* X-ray crystallography and identified as *trans*- and *cis*-azobenzene.[138]

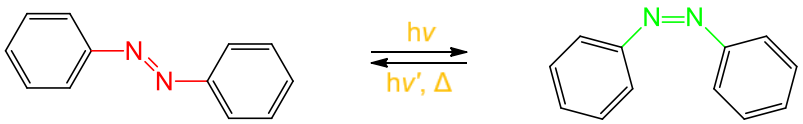

36 *trans*-azobenzene **37** *cis*-azobenzene

Figure 27: *Interconversion of trans- and cis-azobenzene.*[106]

It is this ability to switch between the two geometrical isomers and the accompanying large amplitude change in size that makes azobenzenes so popular amongst photosensitive compounds.[106] *Figure 28* shows an example of an azobenzene working as a 'phototweezer' in solvent extraction and ion-transport systems, as *trans*-diazobenzene **39** exhibits a much greater binding affinity for larger alkali metals due to formation of intramolecular sandwich type complexation. [139-141]

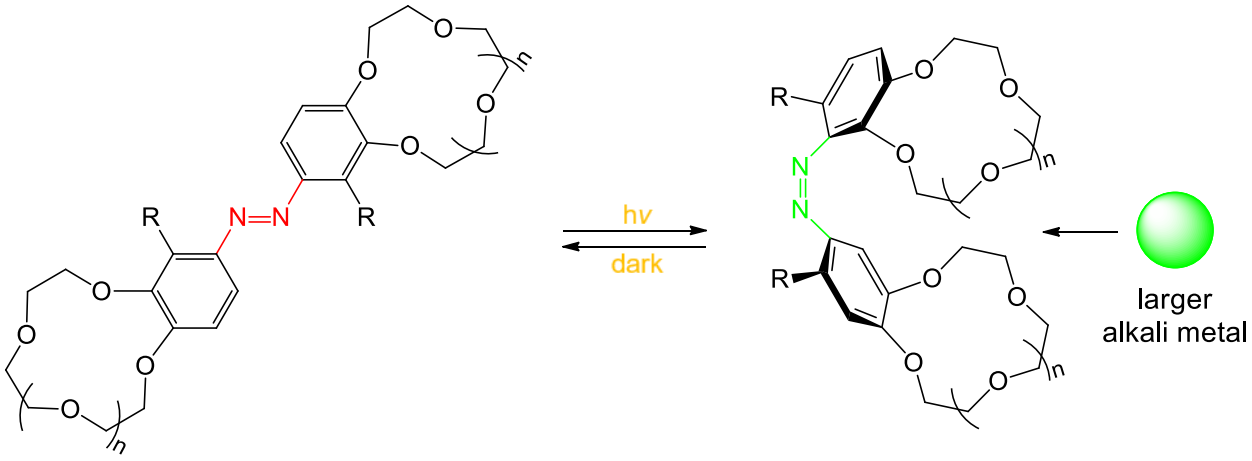

38 **39**

Figure 28: *Azobenzene as a 'phototweezer'.*[140]

Other advantages of azobenzenes, besides the large amplitude change in size, are their easy accessibility and tunability. However, like spiropyrans, azobenzenes are T-type photochromic systems and the *cis*-isomer usually is not thermally stable, meaning a re-isomerization will take place in the absence of light. Another demerit is the lacking efficiency of the photoinduced reconversion *cis*- to *trans*, which usually lies below 80%, thus a fast and *complete* switching between the two states is not possible.[106]

1.5.3 Stilbene and Stilbene-derived Diarylethenes

Another very well studied family of photochromic compounds are diarylethenes with stilbene as its simplest representative.[106]

Stilbene, discovered in 1843 by Auguste Laurent and named by him after the greek word '*στίλβω*' (*stilbo* = 'I shine') due to its lustrous appearance[142, 143] is a 1,2-diphenylated ethene which, like azobenzene, consists of the two stereoisomers *trans*- and *cis*-stilbene (*Figure 29*).[144, 145]

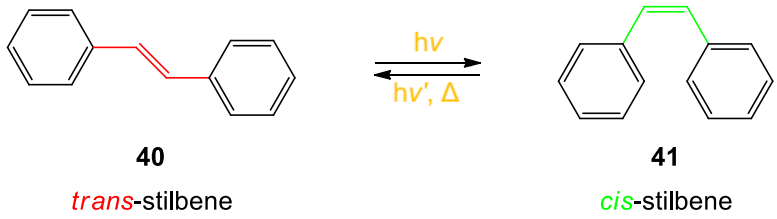

Figure 29: *Interconversion of trans- and cis-stilbene.*[145, 146]

The *cis*-isomer **41** can furthermore undergo a photocyclization reaction leading to dihydro-phenantrene (**42**).[117, 147, 148] The latter reverts, when stored under oxygen-free conditions in darkness, back to *cis*-stilbene. However, under oxygenic conditions dihydrophenantrene **42** reacts *via* hydrogen-elimination irreversibly to phenantrene **43** (*Figure 30*).[149]

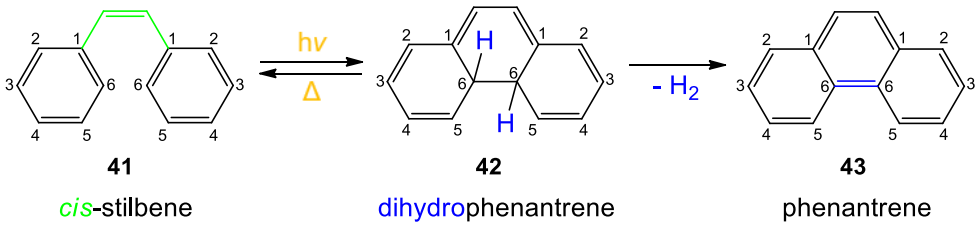

Figure 30: *Photocyclization of cis-stilbene and following irreversible dehydration.*[149] *It applies: 2 and 6, 3 and 5 are chemically equivalent.*

In order to suppress the unwanted hydrogen-elimination in positions 2 and 6, Irie and Mohri exchanged the phenyl rings with mesitylene. Their 2,3-dimesityl-2-butene **44** proofed to be reversibly interconvertible between the ring-open and ring-closed isomer even when exposed to air (*Figure 31*).[150]

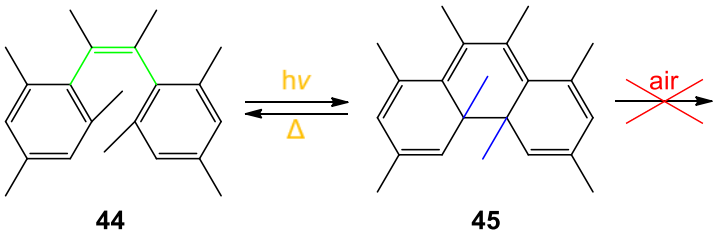

Figure 31: *Ring-open and ring-closed form of 2,3-dimesityl-2-butene.* ***45*** *does not react with oxygen.*[150]

Though this was a big step towards a photochromic system suitable as optical molecular switch or memory device, one problem remained: the lifetime of the ring-closed isomer (**45**) was way too short for the desired applications ($t_{1/2}$ = 1.5 min at 20 °C).[150] Inspired by the findings of Kellogg and co-workers[151] two decades earlier that substitution of the phenyl rings with heterocyclic ring systems leads to prolonged lifetimes of the ring-closed isomers and their own observations, Irie and Mohri prepared two new diarylethenes, shown in *Figure 32*.[149, 150]

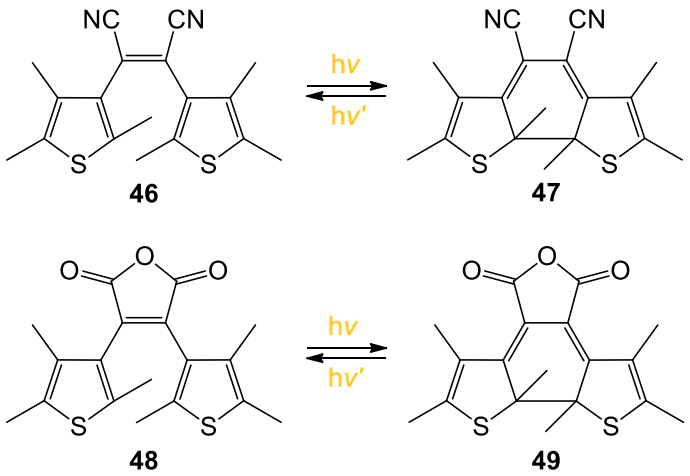

Figure 32: *First P-type dithienylethenes synthesized by Irie and Mohri.*[149, 150]

The designed molecules **46** and **48** both were a great success as their closed forms **47** and **49** showed thermal stability when stored at 80 °C for several month or even when heated up to 300 °C. Only when irradiated with visible light they readily returned to the corresponding open-ring isomer.[149, 150] Shortly after Irie and co-workers showed that dithienylethenes are fatigue-resistant photochromic systems (photocyclization / back reaction can be repeated more than 10^4 times)[152, 153] and furthermore that conversion from the ring-open to the ring-closed isomer can be as high as > 99 %.[153, 154] Ever since dithienylethenes have gained massive attention as key elements in chemical systems and molecular devices.[106] As this work is also based on dithienylethene ligands, a more detailed view on this chemical species regarding its properties and opportunities for applications is given in the following chapter.

1.5.4 Dithienylethenes

Dithienylethenes (DTE) are stilbene-derived P-type photochromic systems with excellent yields in terms of conversion between the ring-open and ring-closed isomer while being fatigue resistant (in case there are no hydrogen atoms in position 2 on the thienyl-rings) on this reaction, which in addition occurs extremely fast.[106, 149, 150, 152, 154-158] DTEs are also responsive in the solid state.[159-163]

1.5.4.1 Electronic Communication of Substituents on the DTE Scaffold

Figure 33 shows the backbone of DTEs, the properties of the ring-open and ring-closed isomers and the communication of the substituents among each other on both isomers.[106]

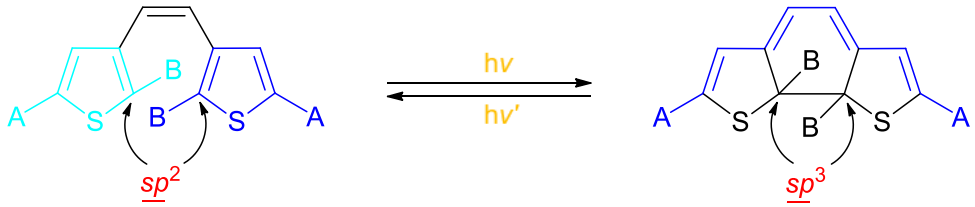

50

ring-open
colourless
cross-conjugated
flexible

groups A and B are affected by each other
groups A are not affected by each other
groups B are not affected by each other

51

ring-closed
coloured
linearly conjugated
rigid

groups A and B are not affected by each other
groups A are affected by each other
groups B are not affected by each other

Figure 33: *Properties and group interaction among each other on the ring-open and ring-closed isomer.*[106]

In the ring-open isomer (**50**) groups A are not affected by one another on behalf of their electron-accepting or electron-donating character and act independently. On the contrary groups A are affected by one another on the ring-closed isomer (**51**) *via* the π-conjugated backbone. The opposite is true for communication between groups A and B: on the ring-open isomer (**50**) they can communicate directly with each other while this communication breaks off on the ring-closed isomer (**51**) due to the change in hybridization from sp^2 to sp^3 of the carbon-atoms groups B are connected to.[106] These interactions are well demonstrated with two examples in *Figure 34*.

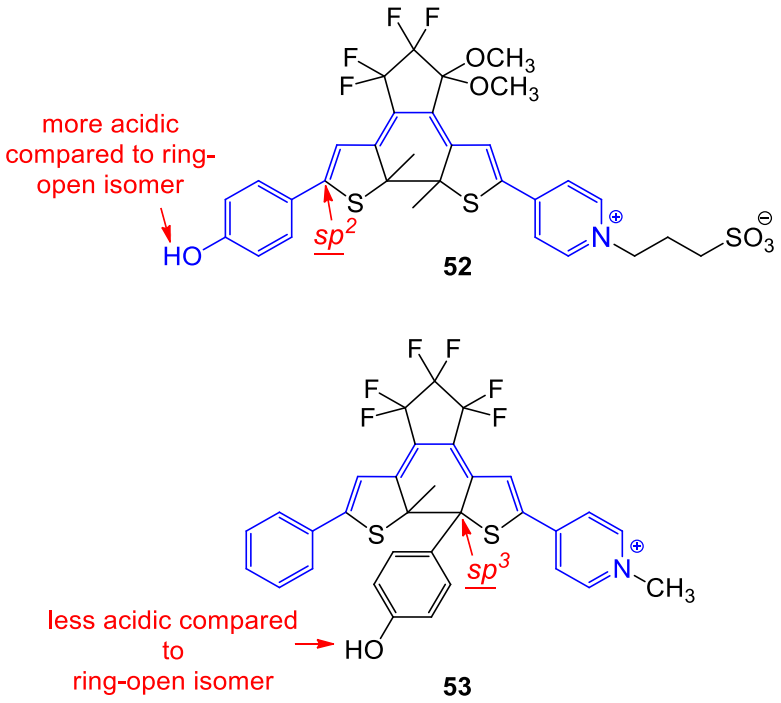

Figure 34: *Group affection on two different DTE derivatives (ring-open forms are not shown).*[106, 164, 165]

In both DTEs (**52** and **53**) the acidity of the –OH group is dependent on whether the respective phenol unit is connected with the pyridinium group or not. The pyridinium group, as an electron-withdrawing group, is able to stabilize the conjugated base of the phenol when both groups can communicate electronically. For DTE **52** this is the case in the ring-closed form, as the phenol- and pyridinium group are conjugated *via* π-backbone. As a result, the pK_a is lower (9.3) for the ring-closed isomer compared to the ring-open isomer (10.5) due to break of conjugation between the phenol- and pyridinium group when the ring is opened.[106, 164] For DTE **53** it is the other way around: on the ring-closed isomer there is no communication between the phenol- and the pyridinium group, which is achieved upon ring-opening. The pK_a therefore is lower for the ring-open isomer.[106, 165]

Figure 35 shows the ring-open DTE **54** with a crown ether unit effectively binding Ca^{2+}-cations. Upon ring-closure (**55**) the electron withdrawing aldehyde group becomes electronically connected to the crown ether *via* π-backbone. As a result the nucleophilicity and therefore the binding affinity towards Ca^{2+}-ions becomes reduced by four order of magnitude.[106, 166]

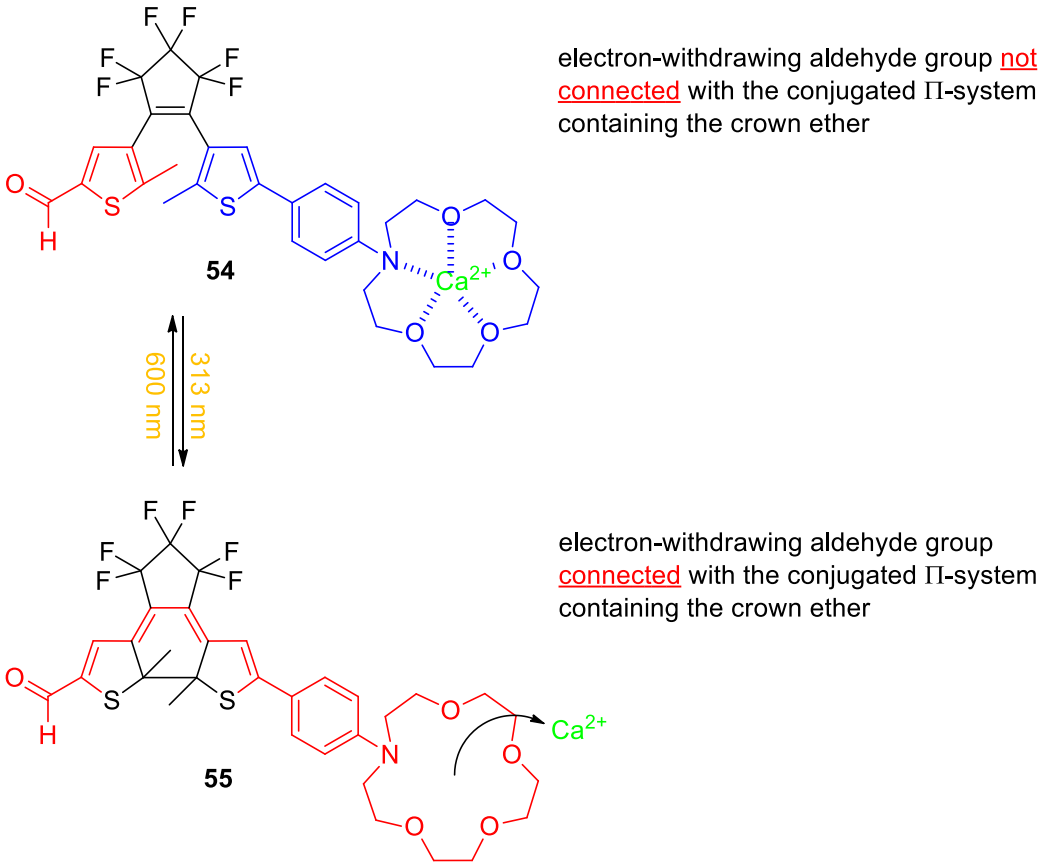

Figure 35: *DTE that can bind and release Ca^{2+}-cations.*[166]

1.5.4.2 Concurring Side Reaction to Photocyclization

DTEs are (almost always) designed with a ring system bridging the central alkene bond. This is in order to avoid unwanted photoreactions concurring with the photocyclization, namely the *cis-trans* isomerization (*Figure 36*).[106, 149]

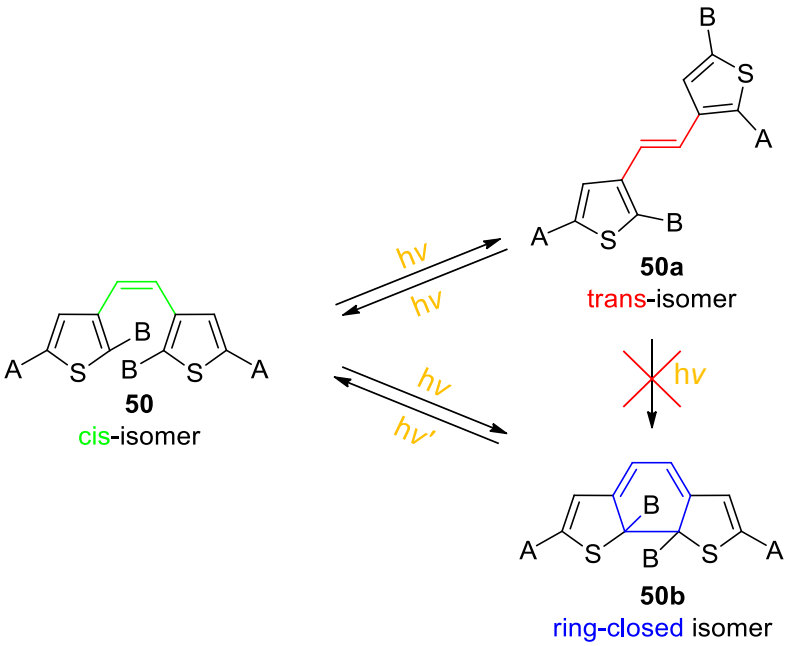

Figure 36: *Concurring photoreaction: cis-trans isomerization.*

trans-isomers of DTEs (**50a**) are unable to undergo a photocyclization reaction due to positioning of the thiophene rings.

1.5.4.3 Conformers

While the electronic communication within the DTE scaffold plays an important role, so do steric effects. As already raised in *Figure 33*, the scaffold of the ring-open isomer is flexible meaning that the thienyl units can rotate freely around the C-C σ-bonds. This leads to rapid conversion between two conformers, one with both thienyl rings in parallel and one with both rings in antiparallel alignment (*Figure 37*).[106, 155] Note: helicity will be addressed in the following chapter.

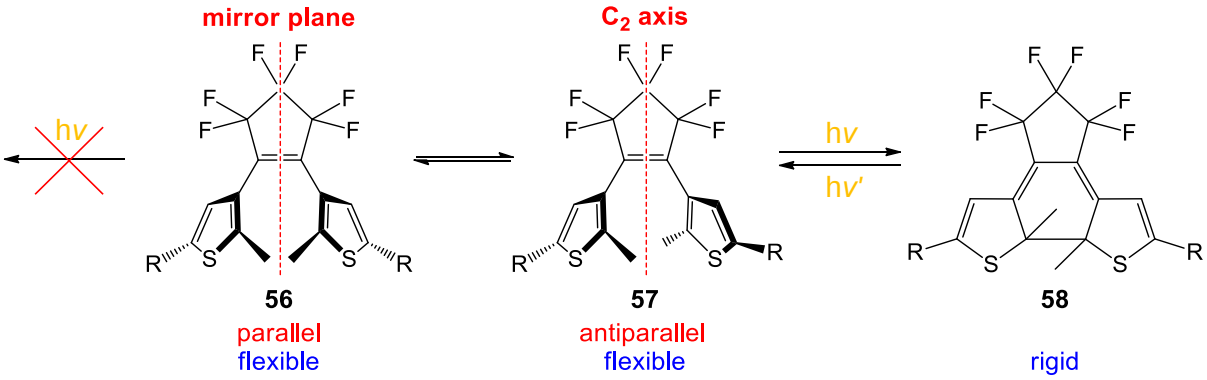

Figure 37: *Conformers of DTE.[106] Only DTE **57** with both rings in antiparallel alignment is able to undergo photocyclization.[106, 155]*

It is important to point out that only DTEs with antiparallel alignment of the thienyl rings are able to undergo the conrotatory 6π-electron photochemical electrocyclization.[106, 155] Upon ring-closure the former flexible DTE backbone becomes rigid and groups located on the 'outer' ring positions are forced to diverge from each other. An example that illustrates the use of this feature of DTEs is shown in *Figure 38*.[167]

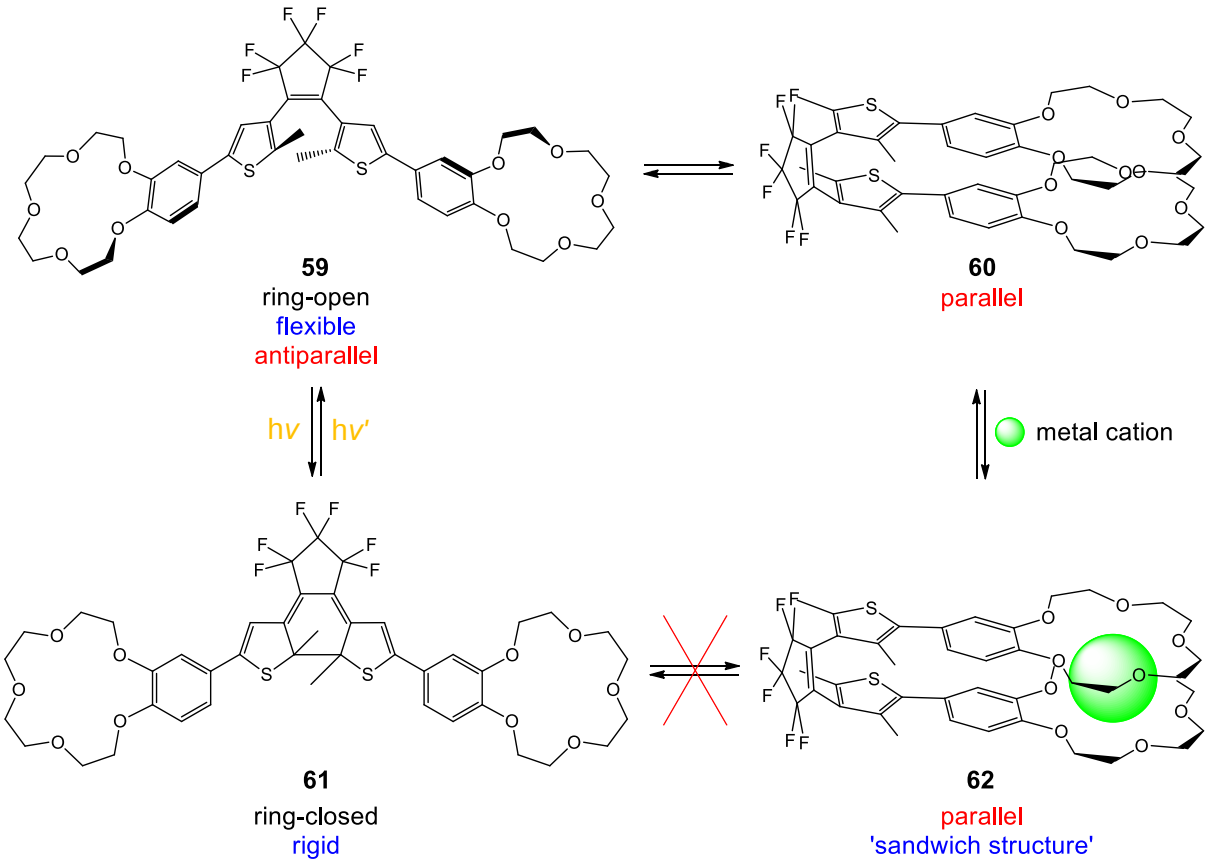

Figure 38: *Enhanced performance in binding large metal cations of DTE **59** compared to DTE **61** due to flexible thienyl units.*[167]

The ring-open isomer **59** with antiparallel thienyl rings is in equilibrium with its parallel form **60**. In the latter, both crown ether units are stacked above each other. This makes a synergetic effect between both units possible, resulting in an enhanced binding of larger metal cations e.g. rubidium or cesium ions (**62**). The ring-closed isomer **61** lacks this possibility and both crown ether units act independently as ionophores. Capability of binding large cations is therefore significantly decreased for **61**.[106, 167]

1.5.4.4 Helicity on DTE Scaffolds

Due to free rotation of the thienyl rings about the C-C σ-bonds, two conformers are present for the ring-open isomer, one with parallel and one with antiparallel alignment. Furthermore, the antiparallel form itself exists of two rapidly interconverting helical species.[106] Helicity, derived from greek word '*ἕλιξ*' for 'helix', meaning 'twisted' or 'spiral',[2] describes a special case of axial chirality. Like 'normal' enantiomers are molecules with helicity present in two forms behaving like image and mirror image towards each other, yet without the need of a chiral center.[168] *Figure 39* illustrates this aspect with an example on a macroscopic scale.

Figure 39: *Snail shell with P-helicity (left) and M-helicity (right) (beginning from the center).*

The spiral on the left snail shell runs clockwise, while the spiral of the right runs anti-clockwise. One cannot be brought in superposition with the other. The same holds true on a microscopic scale: a given molecule containing a helix (a fragment looking like a spiral staircase) can, according to the Cahn-Ingold-Prelog system, be assigned with 'plus-helicity' (*P*-helicity = spiral running clockwise down) or 'minus-helicity' (*M*-helicity = spiral running counterclockwise down), depending on the running direction of that helix (from up to down).[168, 169]

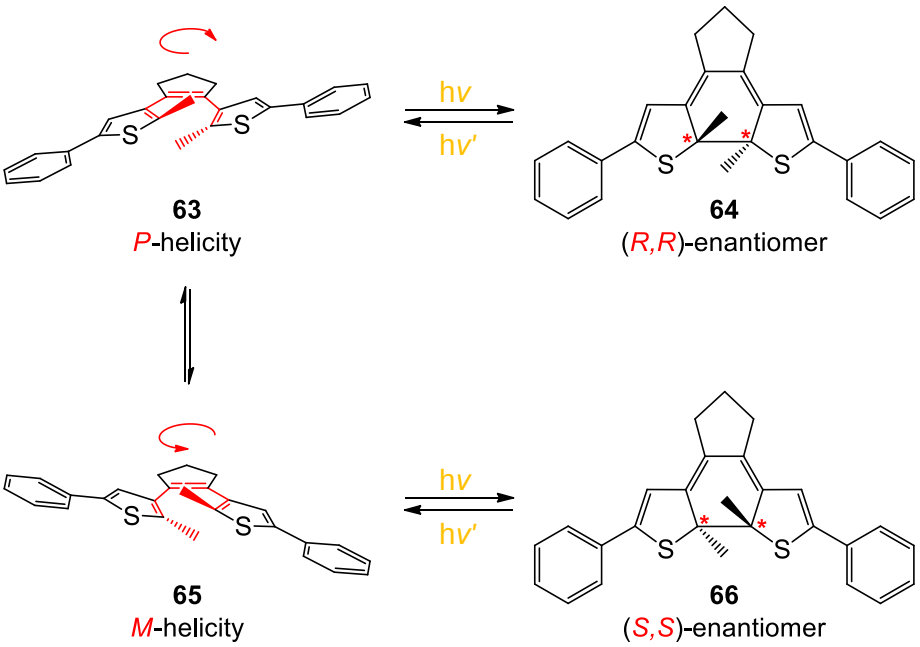

Figure 40: *Helicity on DTE scaffolds and the resulting enantiomers upon photocyclization.*[106]

Figure 40 shows both forms of the ring-open isomer with antiparallel alignment.[106] As can be seen, irradiation of **63** and **65** with UV-light leads to the formation of two new stereocenters and a racemate of the ring-closed isomers ((*R,R*) and (*S,S*)).[106, 170] **63** converts to the (*R,R*)-enantiomer **64**, **65** to (*S,S*)-enantiomer **66**. Hence DTEs contain stereospecific information in their ring-open (helicity) as well as in their closed-ring form (chiral centers) and are therefore interesting building blocks for chiral ligand systems.[106, 170-172] Several working groups also have shown that it is possible to obtain in great excess or even selectively only one of the ring-closed isomers by altering the chemical environment or irradiation conditions.[170, 173-175]

1.5.4.5 Atropisomerism

Atropisomers, named after the greek word 'άτροπος', 'atropos', meaning 'not turning', are stereoisomers (rotamers), which occur due to a restricted rotation about a single bond leading to effectively 'locked up' configurations of a 'plus' or 'minus' isomer. Those can often be visualized as containing helicity.[176] To distinguish atropisomers from rotamers, Oki defined them to be fully resolvable at ambient temperature for ≥ 1000 seconds which corresponds to a barrier of interconversion of >23.3 kcal mol^{-1}.[177] Atropisomers have been described for the first time in 1922 by Christie and Kenner in case of 6,6'-dinitro-2,2'-diphenic acid (*Figure 41*).[178]

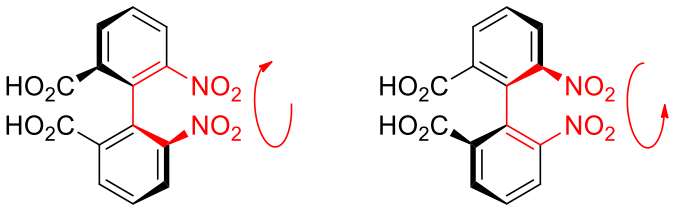

67 *P*-helicity **68** *M*-helicity

Figure 41: *Atropisomers of 6,6'-dinitro-2,2'-diphenic acid.*[178]

Referring to DTE in *Figure 40* this means that if the interconversion of isomers **63** and **65** would be hampered by a large enough barrier, they could be assigned as atropisomers, if not and a rapid equilibrium exists, as conformers.

Atropisomerism becomes exploited in designs of chiral ligand systems with applications e.g. in asymmetric catalysis,[179-183] medicinal chemistry[184] or as an alternative source for production of chiral drugs[185]. It becomes also applied in the design of molecular machines, where a conformational change about a single bond is crucial.[186] Atropisomerism, as mentioned, is a possible feature of DTEs.[187]

1.5.4.6 Gated Photochromism

Until now, examples have been shown where photochemistry dictates how a molecule reacts. However, it is also possible to design molecules in a way so that *their reactivity* dictates their photochemistry.[106] This is called 'gated photochromism' and can be described as a type of photochromism "where the photochromic process is controlled by passing through a gate, the opening and closing of which is governed by a non-photochemical process, which can be chemical or by physical means."[188] Among the most popular photo-switches, gated photochromism has been most successfully exploited in DTEs.[188] *Figure 42* shows an example of such.[189]

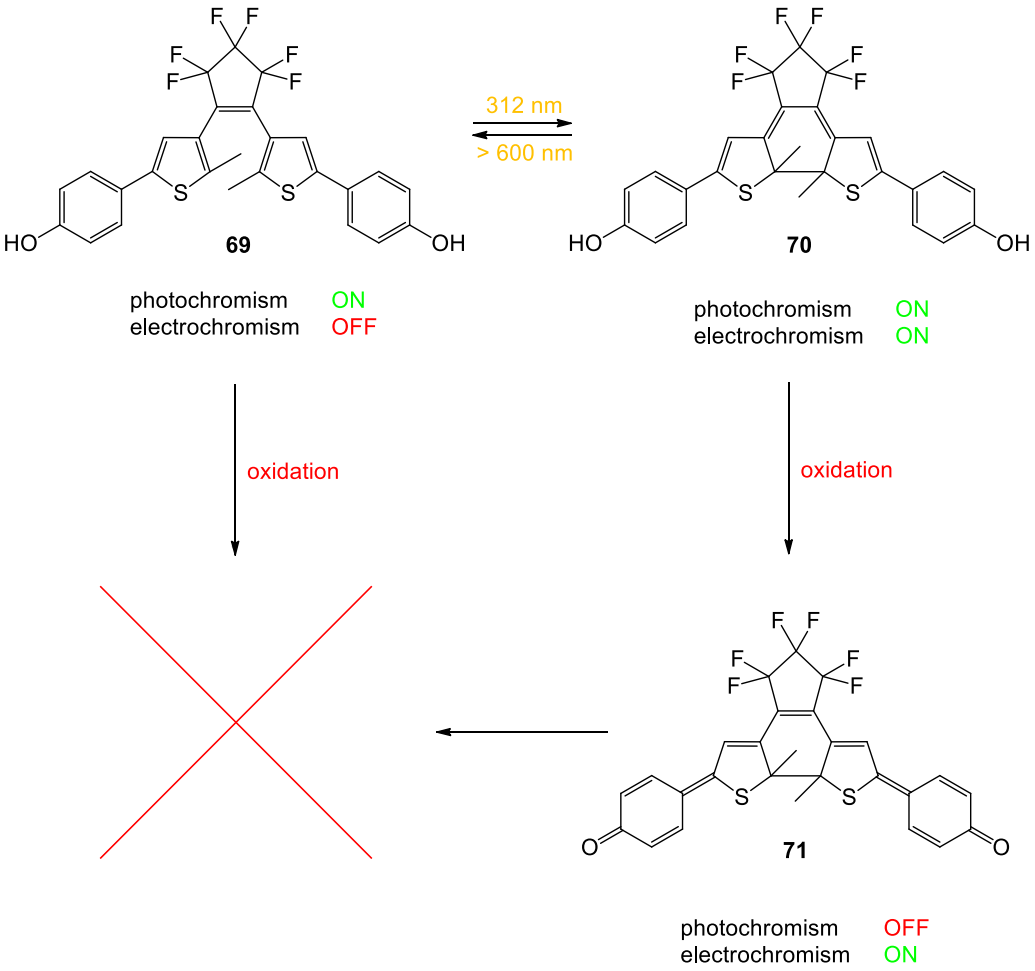

Figure 42: *Gated photochromism via electrochemistry.*[189, 190]

Ring-open isomer **69** does not undergo an oxidation at 735 mV while ring-closed **70**, due to its conjugated π-backbone connecting both phenol groups, does. Since quinone **71** does not possess the cyclohexadiene unit necessary for the ring-opening, no photochemical reaction can occur. Only when reduced back to diphenol **70** a ring-opening to restore **69** is possible again. The photochemical response can therefore be controlled in this case by oxidation/reduction; electrochemistry is 'gating' the photochemistry.[106, 189, 190]

1.5.4.7 DTE Scaffolds Containing (Transition) Metals

The previous chapters showed several examples how properties of DTEs can be altered and controlled by introducing different organic functional groups on the thienyl units. However, there are also plenty of possibilities to modify properties of DTEs *via* e.g. complexation with metals or transition metals. Likewise interesting is the influence of DTEs towards the metal's properties due to electronical changes upon ring closure/opening. The following examples illustrate some of these interactions.

1.5.4.7.1 Influence of Metal Center on DTE

Figure 43 shows the ring-open and ring-closed forms of Yam and co-workers' DTE **72** as free ligand and in a complex with a rhenium species (**74**).[191]

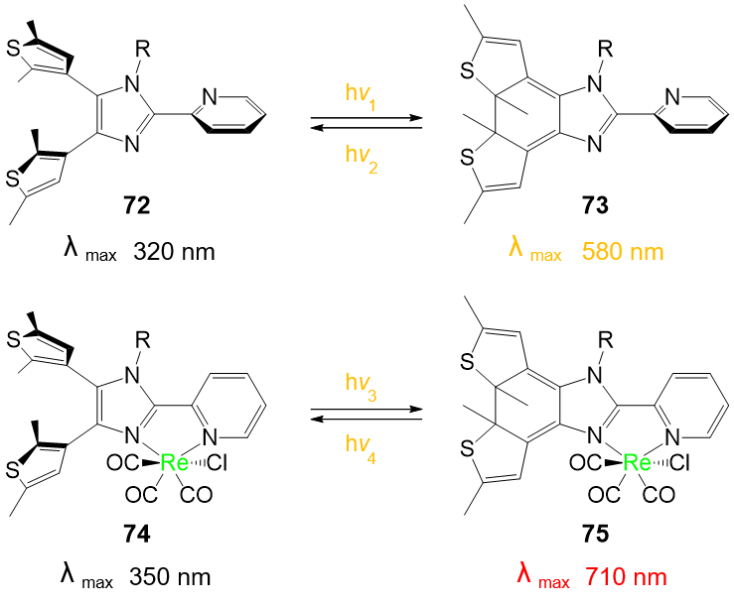

Figure 43: *Observed bathochromic shift of a DTE containing rhenium in its vicinity.*[191]

As can be seen, both, the ring-open and ring-closed form containing the rhenium moiety (**74** and **75**) receive a significant bathochromic shift when compared to free ligand **72** and **73** (open: 320 nm → 350 nm; closed: 580 nm → 710 nm). This is likely due to the fact that the imidazoyl and pyridyl rings are twisted with respect to each other and are not in coplanar arrangement in the free ligand whereas the rhenium moiety forces them into coplanarity, thus leading to a prolonged conjugated π-system.[191] Photochromic compounds showing absorption and reactivity in the near-infrared region are of high interest for applications in optical memory storage devices.[117, 191, 192]

Complexation with a metal containing moiety not only may cause shifts of the absorption maxima – it often causes (major) changes for all spectroscopic properties of the DTE e.g. overall state of energy, fluorescence, phosphorescence or lifetime and 'quality' of excitation states *via* metal to ligand charge transfer effects.[191-195] Depending on the metal and how metal and photochromic moiety are connected (geometry, length, electronic conditions), weakly or strongly interacting systems can be designed to amplify the desired property. However, too strong an electronic coupling may even cause loss of the ability for photocyclization (*Figure 44*).[195]

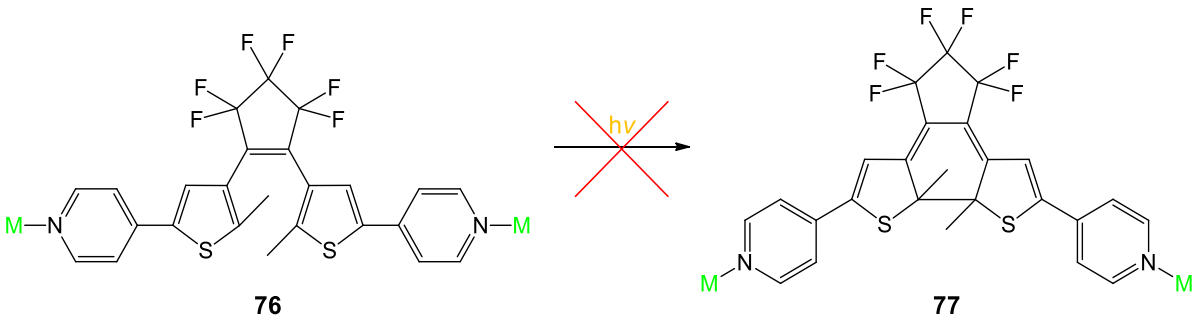

Figure 44: *DTE not able to undergo photocyclization due to strong electronic coupling with a metal moiety. M = [Ru(NH₃)₅](PF₆)₂.* [194]

1.5.4.7.2 Influence of DTEs on Metal Center

Another interesting field of research on DTEs is the impact the ring-closing/ring-opening induces on moieties that are electronically connected with the photochromic unit. *Figure 45* depicts a DTE incorporated in a *N*-heterocyclic carbene (NHC) backbone with a metal moiety attached to it.[196]

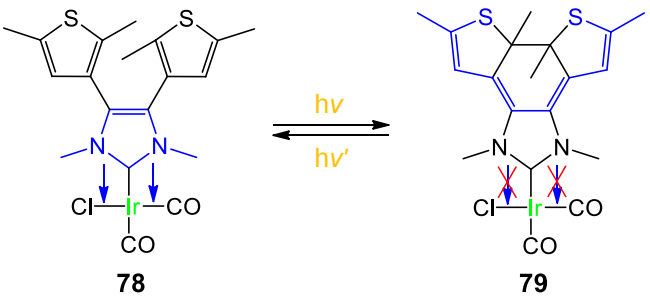

Figure 45: *Relocation of electron density upon ring-opening/ring-closure.*[196]

While in **78** the NHC is able to donate electron density to the metal center, this is no longer possible after photocyclization (**79**). Upon ring-closure the central ring's electrons, namely those of the bridging ethene unit, become delocalized on the DTE scaffold and are therefore no longer part of the original key component providing electron density to the metal center. Switching between the ring-open and ring-closed isomer therefore leads to control over the electron density at the metal center – a feature with possible applications for photomodulation of catalytic activities.[196]

Based on the same principle is DTE **80** (*Figure 46*). Here the bridging ethene unit is part of the DTE backbone as well as of the heterocyclic containing boron.[197] It is worth mentioning that the boron atom in this example is directly connected to the DTE scaffold without a spacer.

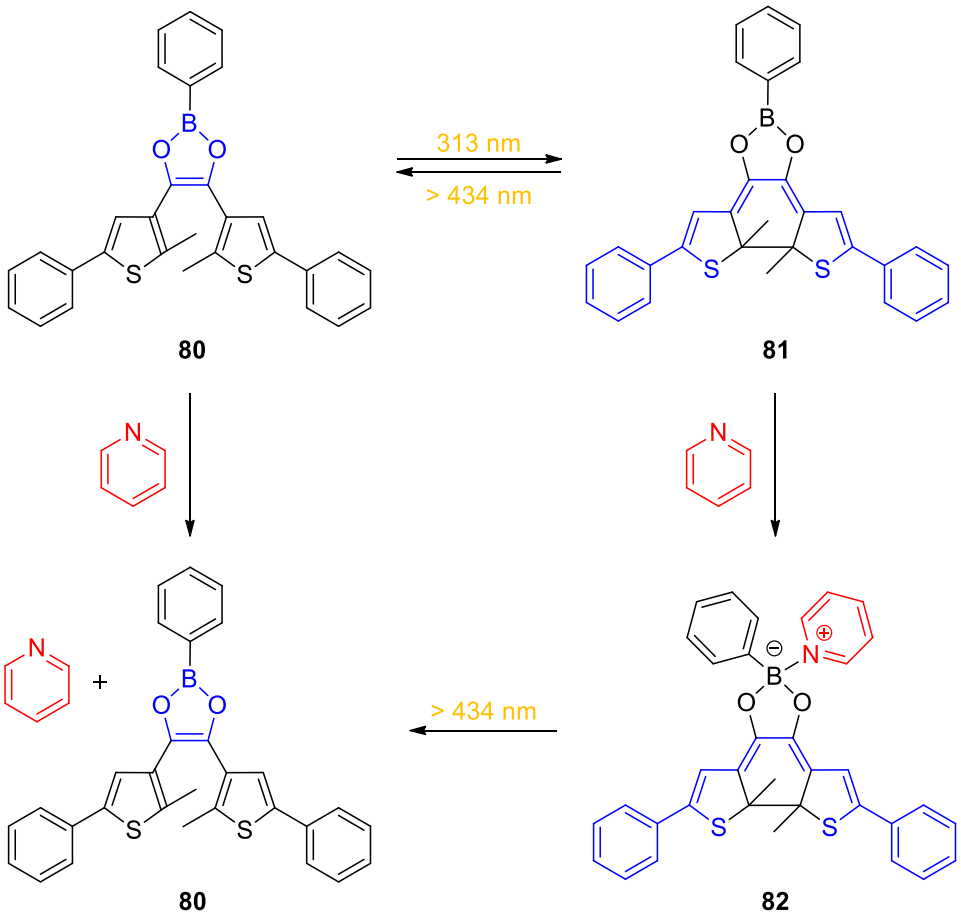

Figure 46: *Change of boron's acidity due to relocation of electron density upon ring-opening/ring-closure.*[106, 197]

In ring-open form **80** the five-membered heterocyclic boron ring contains six delocalized π-electrons, leading to a substantial aromatic character for that moiety. When exposed to pyridine no reaction therefore takes place since the boron atom's p-orbital is already occupied and not able to interact with a Lewis base. Upon photocyclization and formation of the typically DTE ring-closed π-backbone (**81**), the dioxaborole ring loses its aromatic character thus leading to boron now acting as Lewis acid able to bind the pyridine (**81** → **82**). Irradiation with suitable wavelength leads to ring-open isomer **80** and release of the pyridine.[106, 197] This example also shows the possibility to control whether electron density on a certain moiety is increased or decreased *via* reversible photocyclization of the DTE.

1.6 Motivation

As illustrated in the previous chapters, DTEs are interesting building blocks as molecular switches, offering various opportunities to tune their photochromic and the associated electronic properties by altering their framework and/or by interaction with metalloids/metals. However, while there have been numerous reports about DTEs with a metal incorporated in a moiety connected to the DTE *via* spacer (cf. *Chapter 1.5.4.7* for examples), no reports have been found in the beginning of this project about DTEs with a metal incorporated in the ring containing the DTE's ethene bridge so that a *direct* communication between both, metal and DTE-backbone, exists (*Figure 47* bottom).

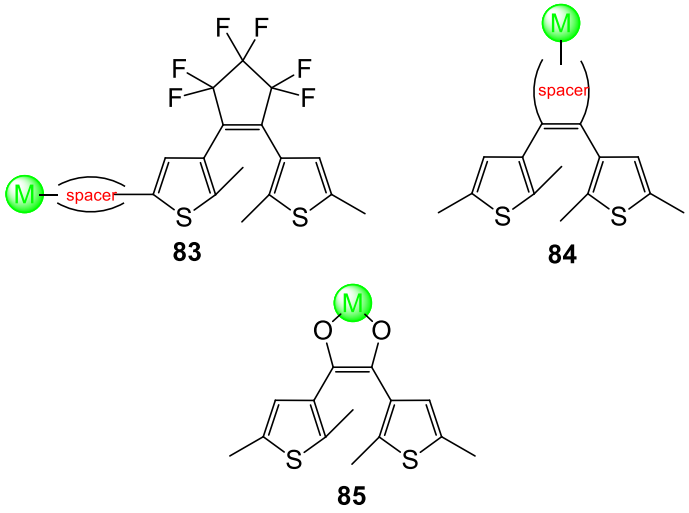

Figure 47: *Examples of DTEs connected to a metal via spacer (top) and DTE with a metal directly incorporated in the ring containing the ethene bridge (bottom).*

This project therefore started with the idea to synthesize complexes containing a DTE ligand directly coordinated to a metal center and to study their properties in regard of stereochemistry, a possible photocyclization and furthermore if the DTE ligand could be capable of showing non-innocent behavior (*Figure 48*).

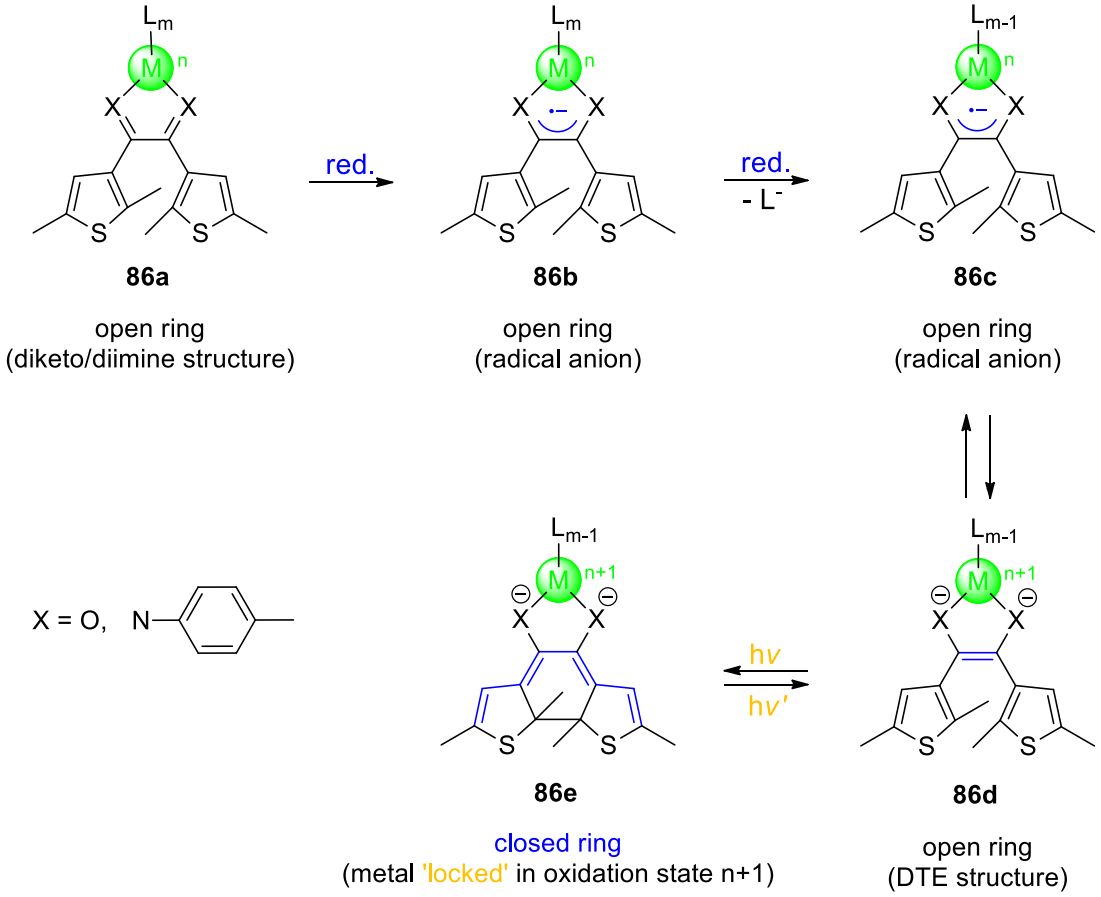

Figure 48: *Possible non-innocent behavior of DTE.*

As shown, reduction of **86a** leads to formation of radical anion **86b**. A second reduction could take place on the metal, which remains in its oxidation state *n* upon elimination of a ligand (likely a halogenide). Complex **86c** and **86d** might coexist in an equilibrium with **86d** containing the hexatriene motif necessary for a photocyclization. When exposed to suitable wavelength, **86d** might undergo a ring-closure reaction, leading to complex **86e** in which the oxidation state of the metal is 'locked' in as long as the ring remains closed. This would serve as an example of a DTE acting as a non-innocent photoswitch allowing to toggle between two oxidation states of the metal center it is bound to.

2 Results and Discussion

2.1 Non-Oxido-Vanadium(IV) Metalloradical Complexes with Bidentate 1,2-Dithienylethene Ligands: Observation of Reversible Cyclization of the Ligand Scaffold in Solution

In this work I carried out the synthesis of all compounds and most of its characterization. I wrote large parts of the result and discussion chapter as well as the experimental section. Dr. Matthias Vogt was the principal investigator and designed the concept of the project. He also wrote the manuscript with other contributors, mainly Jeffrey R. Harmer. Single crystal X-ray diffraction measurements and structure refinements have been carried out by Dr. Enno Lork, Dr. Florian Kleemiss, Dr. Malte Fugel and Prof. Dr. Kunihisa Sugimoto.

Percentage of my contribution of the total workload: experimental concept and design: ca. 80 %, experimental work and acquisition of experimental data: 80 %, data analysis and interpretation: 70 %, preparation of Figures and Tables: ca. 80 %, drafting of the manuscript: ca. 70 %.

The article was published in the journal “Chemistry – A European Journal“ in 2020 as an open access article:

Dirk Schlüter, Florian Kleemiss, Malte Fugel, Enno Lork, Kunihisa Sugimoto, Simon Grabowsky, Jeffrey R. Harmer, Matthias Vogt*, *Chem. Eur. J.* **2020**, *26*, 1335 – 1343.

DOI: 10.1002/chem.201904103

The Supporting Information includes charts of all X-ray crystallographic data and structure refinement and is available free of charge on the journal’s website:

https://chemistry-europe.onlinelibrary.wiley.com/doi/full/10.1002/chem.201904103

ChemPubSoc Europe
DOI: 10.1002/chem.201904103
CHEMISTRY A European Journal Full Paper

Coordination Chemistry

Non-Oxido-Vanadium(IV) Metalloradical Complexes with Bidentate 1,2-Dithienylethene Ligands: Observation of Reversible Cyclization of the Ligand Scaffold in Solution

Dirk Schlüter,[a] Florian Kleemiss,[a, e] Malte Fugel,[a] Enno Lork,[a] Kunihisa Sugimoto,[b, d] Simon Grabowsky,[a, e] Jeffrey R. Harmer,[c] and Matthias Vogt*[a]

Abstract: Derivatives of 1,2-dithienylethene (DTE) have superb photochromic properties due to an efficient reversible photocyclization reaction of their hexatriene structure and, thus, have application potential in materials for optoelectronics and (multi-responsive) molecular switches. Transition-metal complexes bearing switchable DTE motifs commonly incorporate their coordination site rather distant from the hexatriene system. In this work the redox active ligand 1,2-bis(2,5-dimethylthiophen-3-yl)ethane-1,2-dione is described, which reacts with $[V(TMEDA)_2Cl_2]$ to give a rare non-oxido vanadium(IV) species **3(*M,M/P,P*)**. This blue complex has two bidentate en-diolato ligands which chelate the V^{IV} center and give rise to two five-membered metallacycles with the adjacent hexatriene DTE backbone bearing axial chirality. Upon irradiation with UVA light or prolonged heating in solution, the blue compound **3(*M,M/P,P*)** converts into the purple atropisomer **4(*para,M/para,P*)**. Both complexes were isolated and structurally characterized by single-crystal X-ray diffraction analysis (using lab source and synchrotron radiation). The antiparallel configuration (*M* or *P* helicity) present in both **3(*M,M/P,P*)** and **4(*para,M/para,P*)** is a prerequisite for (reversible) 6π cyclization reactions. A CW EPR spectroscopic study reveals the metalloradical character for **3(*M,M/P,P*)** and **4(*para,M/para,P*)** and indicates dynamic reversible cyclization of the DTE backbone in complex **3(*M,M/P,P*)** at ambient temperature in solution.

Introduction

Oxido-vanadium compounds, mostly in the oxidation state +V and +VI, are intensively studied for applications in a diverse range of areas. For instance, vanadate and vanadyl derivatives possess significant importance as biologically active species,[1,2] have been shown to possess insulin-mimetic properties[3–6] and are important catalytic species in various oxidation reactions.[7–9] In contrast, non-oxido vanadium(IV) compounds are less frequently reported in the literature. Sproules, Wieghardt and co-workers described V^{IV} complexes with non-innocent ligand-sets.[10] A prominent compound is amavadin, which is a naturally occurring example of a non-oxido V^{IV} coordination complex,[11] which was initially isolated from the toadstool *Amanita muscaria*.[12] Vanadocene dichloride and derivatives thereof have been investigated with respect to their antitumor activity.[13] Vanadium coordination compounds show a broad range of potential applications in medicinal chemistry including the treatment of endemic tropical and various heart muscle diseases. A concise overview was recently given by Rehder.[9]

Herein, we characterize a class of non-oxido vanadium(IV) complexes bearing two chelating en-diolato ligands with a 1,2 dithienylethene (DTE) motif as backbone, Scheme 1 **F**, **G**. DTE motifs have received considerable attention due to their superior photochromic properties, that is, DTEs undergo reversible photocyclization reactions with an associated characteristic color change. They have a significant application potential as a new photoswitchable material for optoelectronics and (multiresponsive) molecular switches. The photochromic properties of DTEs are characterized, for instance, by a high fatigue resistance, high quantum yields, the robust thermal stability of

[a] D. Schlüter, F. Kleemiss, Dr. M. Fugel, Dr. E. Lork, PD Dr. S. Grabowsky, Dr. M. Vogt
Institut für Anorganische Chemie und Kristallographie
Universität Bremen, Leobener Str. 3 and 7, 28359 Bremen (Germany)
E-mail: mavogt@uni-bremen.de
[b] Prof. Dr. K. Sugimoto
SPring-8/JASRI, 1-1-1 Kouto, Sayo-cho, Sayo-gun, Hyogo 679-5198 (Japan)
[c] Prof. Dr. J. R. Harmer
Center of Advanced Imaging (CAI), University of Queensland
St. Lucia, QL (Australia)
[d] Prof. Dr. K. Sugimoto
Institute for Integrated Cell-Material Sciences (iCeMS), Kyoto University
Yoshida-Ushinomiya-cho, Sakyo-ku, Kyoto 606-8501 (Japan)
[e] F. Kleemiss, PD Dr. S. Grabowsky
Current address:Abteilung für Chemie und Biochemie
Universität Bern, Freiestrasse 3, 3012 Bern (Switzerland)
Supporting information and the ORCID identification number(s) for the author(s) of this article can be found under: https://doi.org/10.1002/chem.201904103.

© 2019 The Authors. Published by Wiley-VCH Verlag GmbH & Co. KGaA. This is an open access article under the terms of Creative Commons Attribution NonCommercial License, which permits use, distribution and reproduction in any medium, provided the original work is properly cited and is not used for commercial purposes.

ChemPubSoc Europe

CHEMISTRY A European Journal Full Paper

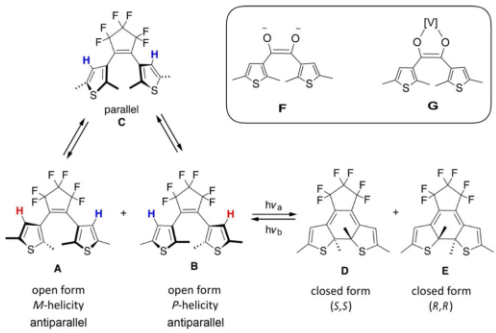

Scheme 1. Atropisomers and photocyclization of 1,2-bis(2,5-dimethyl-3-thienyl)perfluorocyclopentane.

all isomers, and a rapid response to the external stimulus. They are also responsive in the solid state.[14–17] DTEs have been discussed as functional key components in a range of applications including conductive polymers,[18] multiresponsive molecular switches,[19] optical memory devices,[20] photoresponsive building blocks that can regulate supramolecular architectures,[21,22] a selective fluorescent probe for the detection of metal ions,[23] and photoresponsive self-assemblies at liquid–solid interfaces.[24] DTE derivatives that show turn-on mode fluorescence are promising candidates for applications in super-resolution fluorescence microscopy[24] and all-optical transistors.[26] A current active field of research addresses the control of motion in covalently bonded molecular systems, which is closely associated with the design of "molecular machines". In this aspect, the control of conformational change is crucial. For instance, an established approach is the control of conformational change about a single bond triggered by an external stimulus.[27] Against this background, DTEs are reported to possess axial chirality resulting in the formation of atropisomers. Atropisomers (from Greek *atropos* = not turning) are stereoisomers (rotamers) occurring due to a hindered rotation about a single bond. Their rotational interconversion is hampered by a large-enough barrier to allow the individual "minus" (*M* or R_a) and "plus" (*P* or S_a) atropisomers to be "locked" (see Scheme 1 **A**, **B**,).[28] Oki defines atropisomers and distinguishes them from rotamers on the basis that they are fully resolvable at ambient temperature, corresponding to a barrier of interconversion of $>23.3\ kcal\,mol^{-1}$.[29] Atropisomerism, especially in biaryl derivatives bearing a chiral axis between two aromatic moieties, has been intensively exploited for the design of chiral ligand systems that find numerous applications in the field of asymmetric catalysis.[30–35] Atropisomeric chirality, not only restricted to biarylic systems, is important in medicinal chemistry,[36] has pharmaceutical implications as an alternative source for the production of chiral drugs,[37] and can be found in a variety of natural products.[28,38]

1,2-Bis(2,5-dimethyl-3-thienyl)perfluorocyclopentane, a typical example for a photochromic DTE-based derivative with axial chirality, is shown in Scheme 1 **A**–**E**.[15,16] The compound forms the open-ring isomer with parallel aligned thienyl groups (**C**) and the respective enantiomeric antiparallel forms with *M* (**A**) and *P* helicity (**B**).[21,39] The photoinduced cyclization reaction can only occur from the antiparallel conformers **A** and **B** and gives rise to the closed enantiomeric forms **D** and **E** with (*S*,*S*) and (*R*,*R*) configurations,[21] respectively, based on the asymmetric carbon atoms in 2-position of the thiophene units (see Scheme 1).[39] It must be noted that the parallel atropisomer cannot directly undergo photochemical cyclization,[40] and its coexistence with the antiparallel isomers lowers the efficiency of the switching process. Consequently, effort has been spent to increase the relative amount of the antiparallel atropisomers **A** and **B**.[41]

With this background, we now report on the DTE-based bidentate ligand (**F**) equipped with an en-diolato motif. Chelation of a vanadium(IV) metal center gives rise to the formation of a five-membered metallacycle (**G**). These non-oxido vanadium(IV) atropisomeric complexes with metalloradical character were then isolated and structurally characterized by single crystal X-ray (lab source and synchrotron radiation) diffraction analysis, UV/Vis, and EPR spectroscopy.

Results and Discussion

1,2-Bis(2,5-dimethylthiophen-3-yl)ethane-1,2-dione (**1**) reacts with an equimolar amount of vanadium(II)bis-*N*,*N*,*N*′,*N*′-tetramethylethylenediamine-dichloride ($[V(TMEDA)_2Cl_2]$, **2**) to give the vanadium(IV) enantiomeric species $[V(DTE_{(apM)})_2TMEDA]$ **3(*M*,*M*)** and $[V(DTE_{(apP)})_2TMEDA]$ **3(*P*,*P*)** (Scheme 2). It must be noted that the conversion of **1** to the en-diolato ligand is a two-electron reduction. Therefore half of the vanadium must lead to a side product, presumably a "VCl_4" chlorido species, which was not further investigated. The racemic mixture **3(*M*,*M*/*P*,*P*)** was isolated as a deep blue micro-crystalline solid in 43% yield with respect to starting material **2**. In 1998, Rehder and co-workers gave structural precedence to a non-oxido bisenolato complex of vanadium(IV). Specifically, the redox reaction of compound **2** and benzil was reported to give the corresponding bis benzoin vanadium(IV) complex $[V(Ph(O)C{=}C(O)Ph)_2(TMEDA)]$.[42] We applied a similar synthesis strategy; the V^{II} compound **2** serves as both metal precursor complex and reducing agent for the redox-active ligand precursor **1**. Therefore, the 1,2 diketone motif in **1** is reduced to an enediolate, which is stabilized upon coordination to a vanadium(IV) center to form the non-oxido en-diolato complex **3(*M*,*M*/*P*,*P*)**. Thus, a hexatrien motif is formed which is a prerequisite for a (reversible) 6π peri-cyclic reaction. Consistently, the cyclic voltammogram of **1** in THF reveals a quasi-reversible redox-wave at a half potential of $E^1_{1/2} = -1.93$ V with respect to the ferrocene/ferrocenium (Fc/Fc^+) redox couple. However, although the voltammogram suggests a reversible process for the first redox step, the second redox process is observed at very low potential ($E^2_{red} = -2.80$ V and $E^2_{ox} = -2.63$ V) and is not fully reversible (see Figure 1).

To the best of our knowledge, no five-membered metallacycle with a dithienylethene (DTE) backbone has been reported to date. The compounds entail two axially chiral en-diolato li-

 © 2019 The Authors. Published by Wiley-VCH Verlag GmbH & Co. KGaA, Weinheim

ChemPubSoc Europe

CHEMISTRY A European Journal Full Paper

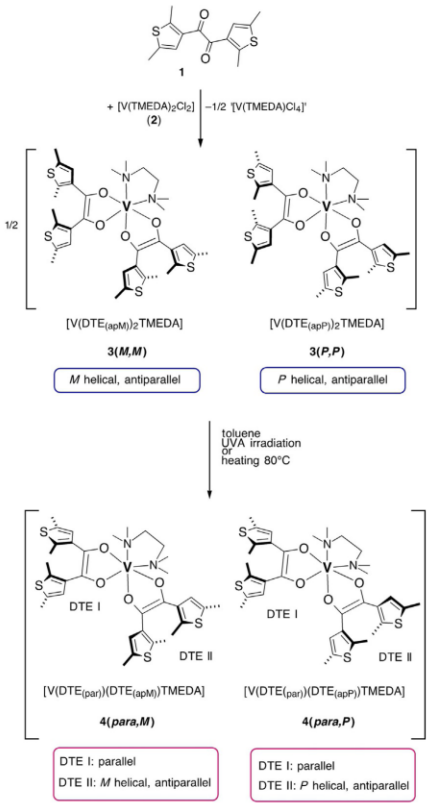

Scheme 2. Synthesis of the racemic vanadium(IV) compounds **3(*M,M/P,P*)** and **4(*para,M/para,P*)**.

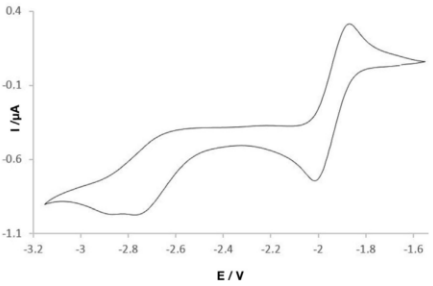

Figure 1. Cyclic voltammogram of **1** (3.9 mM) at 298 K, in 0.1 M $[TBA]PF_6$ in THF, scan rate 100 mV s^{-1}, referenced to Fc/Fc^+. Quasi-reversible redox wave at half potential $E^1_{1/2} = -1.93$ V; $E^2_{ox} = -2.60$ V, $E^2_{red} = -2.80$ V.

gands with both DTE ligands in each enantiomer exhibiting antiparallel configurations with *M,M* helicity **3(*M,M*)** and *P,P* helicity **3(*P,P*)**. Upon irradiation of crystalline **3(*M,M/P,P*)** dissolved in toluene with UVA light ($\lambda_{max} = 370$ nm) or prolonged heating of a toluene solution at 80 °C, the racemate **3(*M,M/P,P*)** is converted to the closely related $[V(DTE_{(par)})(DTE_{(apM)})TMEDA]$ **4(*para,M*)** and $[V(DTE_{(par)})(DTE_{(apP)})TMEDA]$ **4(*para,P*)**. Each of the formed enantiomers exhibits one DTE ligand in an open parallel arrangement and one DTE ligand in an antiparallel arrangement with the respective *M*-helical **4(*para,M*)** or *P*-helical **4(*para,P*)** configuration. The isomerization reaction is not reversible and is characterized by a significant color change from deep blue to purple (images are shown in Figure 3). The reaction can be followed in situ in consecutively recorded UV/Vis absorption spectra of crystalline **3(*M,M/P,P*)** in toluene under concomitant irradiation with UVA light as shown in Figure 2.

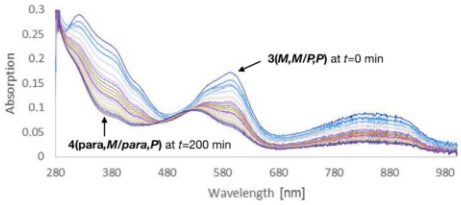

Figure 2. Stacked UV/Vis spectra of complex **3(M,M/P,P)** (0.1 mM single crystals dissolved in toluene) under irradiation of UVA light $\lambda_{max} = 370$ nm for $t = 0$–200 min (10 min interval) results in the formation of **4(*para*,M/*para*,P)**.

The characteristic shoulder at 593 nm associated with **3(*M,M/P,P*)** starts to decrease upon irradiation, as well as a decrease in intensity for the strong absorption band at 836 nm and for the signal in the range of 315–430 nm can be observed. After 200 min, the racemic mixture **4(*para,M*)/4(*para*,*P*)** is formed as the major component. In this regard, it is worth noting that photochromic DTE motifs in switchable transition-metal complexes commonly feature the coordination site rather remotely located from the DTE moiety.[43] For instance, Wing-Wah Yam,[44] Bielawski[45,46] and co-workers reported the incorporation of the photochromic DTE motif in the backbone of an N-heterocyclic carbene. The coordination of such a NHC ligand to Rh^I was reported by Bielawski and co-workers to possess switchable catalytic properties in alkene and alkyne hydroborations, which are triggered by the photoinduced reversible cyclization of the DTE motif.[47] Recently, the same group described a photoswitchable olefin metathesis catalyst using a similar NHC ligand.[48] Photochromic and luminescence switching properties of a Re^I triscarbonyl complex with dithienylphenanthroline were published by Wing-Wah Yam, Phillips and coworkers.[49,50] However, non-switching coordination complexes with DTE entities were reported for which no cyclization reaction was observed.[51]

Single-crystal X-ray diffraction analysis

The racemic mixture of compound **3(*M,M/P,P*)** crystallizes in the monoclinic centrosymmetric space group $P2_1/n$. Therefore, both enantiomers are present in equal amount in the unit cell, that is, the two DTE ligands in each enantiomer are either in

 © 2019 The Authors. Published by Wiley-VCH Verlag GmbH & Co. KGaA, Weinheim

ChemPubSoc Europe

CHEMISTRY A European Journal Full Paper

an antiparallel *M*-helical **3(*M,M*)** or antiparallel *P*-helical **3(*P,P*)** arrangement with respect to the assignment of the highest priority to the methyl groups. Single crystals suitable for X-ray diffraction analysis were obtained by slow diffusion of *n*-pentane into a THF solution of **3(*M,M/P,P*)**. The determined molecular structure is shown for complex **3(*M,M*)** in Figure 3, top left. The structure reveals the vanadium metal center in an octahedral coordination sphere, which consists of four oxygen donors associated with two bidentate DTE en-diolato ligands and the two nitrogen donors of the TMEDA ligand. The en-diolate motif is characterized by short C=C double bonds (C7–C8 = 1.369(7) Å and C21–C22 = 1.365(7) Å) and O–C single bonds (O1–C7 = 1.330(5) Å; O2–C8 = 1.345(5) Å and O3–C21 = 1.344(5) Å; O4–C22 = 1.349(6) Å) suggesting two dianionic en-diolato ligand motifs coordinated to a formal vanadium(IV) center. Most significantly, due to a restricted rotation about the C–C bond connecting the thiophene units and the ethylene backbone, both DTE ligands in complex **3(*M,M/P,P*)** bear axial chirality and the enantiomeric complexes are atropisomers. Multiple attempts to grow single crystals of **4(*para,M/para,P*)** suitable for an X-ray diffraction study proved to be difficult due to the extraordinarily small size of the crystals obtained. This prompted us to undertake an X-ray diffraction study by using a synchrotron radiation source (beamline BL02B1 at SPring-8, Japan). A representative molecular structure is shown in Figure 3 top, right [**4(*para,M*)**]. The racemic mixture **4(*para,M/para,P*)** crystallizes in the monoclinic centrosymmetric space group $P2_1/c$ with both enantiomers present in the unit cell. The molecular structures of **4(*para,M/para,P*)** exhibit similar interatomic distances around the vanadium center and in the en-diolato backbone with respect to **3(*M,M/P,P*)** [C=C double bond (C7–C8 = 1.366(7) Å and C21–C22 = 1.368(7) Å) and O–C single bonds (O1–C7 = 1.349(6) Å; O2–C8 = 1.339(6) Å and O3–C21 = 1.345(6) Å; O4–C22 = 1.351(5) Å)]. However, the structure unambiguously indicates a change to the parallel configuration in only one of the DTE ligands due to a rotation about the C–C bond connecting the thiophene rings and en-diolato backbone. The other DTE unit retains its corresponding antiparallel *M* or *P* helicity to give the enantiomers **4(*para,M*)** and **4(*para,P*)**, respectively. An overlay plot of the blue compound **3(*M,M*)** and purple compound **4(*para,M*)** is shown in Figure 3, bottom. The crystallographic investigation of single crystals of **3(*M,M/P,P*)** and **4(*para,M/para,P*)** allows for the unambiguous structural characterization of the four atropisomers.

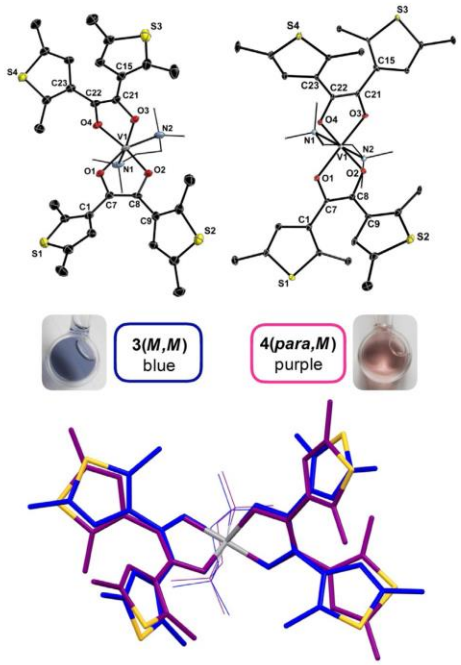

Figure 3. Top: Mercury plot of exemplary complex **3(*M,M*)** (left) and **4(*para,M*)** (right) at 50% ellipsoid probability. Bottom: Wireframe structural overlap of **3(*M,M*)** (blue) and **4(*para,M*)** (purple). Hydrogen atoms are omitted for clarity. Selected bond lengths [Å]: **3(*M,M*)**: C1–C7 = 1.473(6), C7–C8 = 1.369(7), C8–C9 = 1.467(6), O1–C7 = 1.330(5), O2–C8 = 1.345(5), C15–C21 = 1.481(7), C21–C22 = 1.365(7), C22–C23 = 1.473(7), O3–C21 = 1.344(5), O4–C22 = 1.349(6), V–N1 = 2.238(5), V1–N2 = 2.200(5). **4(*para,M*)**: C1–C7 = 1.475(7), C7–C8 = 1.366(7), C8–C9 = 1.471(7), O1–C7 = 1.349(6), O2–C8 = 1.339(6), C15–C21 = 1.476(7), C21–C22 = 1.368(7), C22–C23 = 1.472(6), O3–C21 = 1.345(6), O4–C22 = 1.351(5), V–N1 = 2.195(5), V–N2 = 2.215(5).

EPR spectroscopic study

With the aim of gaining insight into the solution structure, the blue **3(*M,M/P,P*)** and purple **4(*para,M/para,P*)** compounds were investigated by dissolving crystalline samples in THF. We cannot exclude isomerization upon dissolution, however, both solutions exhibit the characteristic blue and purple color, respectively. Both samples give similar but distinctly different EPR spectra as shown in Figure 4, which indicates the existence of two (or more) atropisomers. All experimental EPR spectra indicate metal-centered radicals, that is, V^{IV} metalloradicals. The purple solution spectrum at both room temperature and in frozen-solution is accurately simulated with a single EPR component denoted **4**. These data were modelled with an electron Zeeman (principal g values g_1, g_2, g_3) and a ^{51}V hyperfine (A_1, A_2, A_3) interaction with the isotropic values g_{iso} and A_{iso} used for the room temperature spectrum being the average of the three principal values of the corresponding interaction, for example, $g_{iso} = (g_1 + g_2 + g_3)/3$ and $A_{iso} = (A_1 + A_2 + A_3)/3$.

The blue solution was more complicated. Accurately simulating its isotropic room temperature spectrum requires a two component EPR model comprising of the same component **4** as observed in the purple solution and a new EPR component denoted **3** which again was modelled by an isotropic g value and isotropic vanadium hyperfine coupling (Table 1). In the room temperature spectrum, the two resolved EPR components have the relative weighting $0.54 \times \mathbf{3}^{RT} + 0.46 \times \mathbf{4}$. However, in frozen solution there are at least three EPR components resolved as can be deduced by examination of the high-field feature in the CW EPR spectrum that arises from the largest

 © 2019 The Authors. Published by Wiley-VCH Verlag GmbH & Co. KGaA, Weinheim

ChemPubSoc Europe

CHEMISTRY A European Journal Full Paper

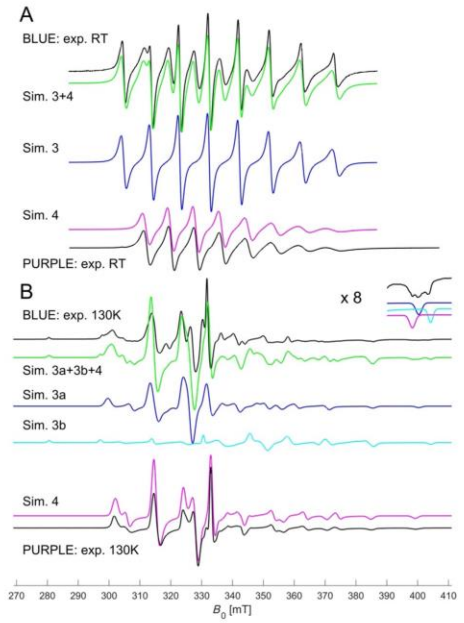

Figure 4. X-band (9.3810 GHz) CW EPR spectra measured at room temperature (A) and at 130 K (B) for the blue and purple solutions in THF. Simulated EPR model components and the sum are shown next to each experimental spectrum.

principal value of the ^{51}V hyperfine interaction, see the blowup of the region around 400 mT in Figure 4B. The appearance of three resolved features indicates the presence of three resolved EPR components. The observation of only two components at room temperature in the blue solution may be because of the presence of several species that interconvert rapidly in solution at room temperature to give an average spectrum **3**^{RT}, whereas in frozen-solution the individual components of this average are observed. In the simulation of the frozen-solution data, these components are denoted **3a** and **3b**. It must be noted that EPR component **4** does not appear to be involved in any room temperature averaging process as it is present in both the room temperature and frozen-solution data. A reasonable model for the blue spectrum was obtained with a simulation employing three EPR components (**3ab**, **4**) with approximately equal relative weights. Spin Hamiltonian parameters for all EPR model components are listed in Table 1. It must be noted that the largest hyperfine value of **3a** and **3b** is accurately determined but the other *g* and *A* values are estimates because they are difficult to determine given the complexity of the spectrum particularly in terms of EPR component number. For example, component **3b** accurately accounts for the largest ^{51}V hyperfine coupling observed in the experiment with its spectrum ranging from 280 to 403 mT, a range quite distinct from **3a** and **4**.

Table 1. EPR parameters for the blue and purple samples derived from experimental and DFT data. Simulation of the CW EPR spectra provide for each component the principal *g* values, ^{51}V hyperfine couplings (MHz), linewidth (MHz), and for room temperature data, the rotational correlation time τ_R (ns). For the DFT geometry optimized structures EPR parameters are computed (*g* values and ^{51}V hyperfine couplings) and compared to the experimental parameters.

EPR parameters		Principal values	Isotropic
"Purple" component			
Model **4**	*g*	1.9114, 1.9694, 1.9886	1.9564
	^{51}V[a]	−371, −268, −69	−236
	LW	58, 42, 23	
	τ_R	0.14	
4^{DFT}***(para,M/para,P)***	*g*	1.9276, 1.9682, 1.9757	1.9571
	^{51}V	−365, −226, −81	−224
"Blue" component			
Model **3**^{RT} (RT)	*g*	NA	1.9735
	^{51}V[a]	NA	−271.8
	LW	NA	–
	τ_R	NA	0.44
Model **3a** (130 K)	*g*	1.910, ≈1.97, ≈1.98	ND
	^{51}V[a]	−385, ≈−260, ≈−70	ND
	LW	57, 42, 30	ND
Model **3b** (130 K)	*g*	≈1.92, ≈1.94, 1.970[b]	ND
	^{51}V[a]	≈−260, ≈−250, −475	ND
	LW	57, 42, 30	ND
DFT optimized structures			
3^{DFT}***(M,M/P,P)***	*g*	1.9276, 1.9670, 1.9730	1.9560
	^{51}V	−363, −232, −92	−167
5^{DFT}***(M,closed-S,S)***	*g*	1.9083, 1.9377, 1.9752[c]	1.9404
	^{51}V	−131, −306, −413	−283
6^{DFT}***(closed-S,S,closed-S,S)***	*g*	1.9160, 1.9357, 1.9640[c]	1.9385
	^{51}V	−308, −223, −498	−343
7^{DFT}***(M,P)***	*g*	1.9345, 1.9530, 1.9629	1.9501
	^{51}V	−390, −198, −270	−286
8^{DFT}***(para,para)***	*g*	1.9284, 1.9674, 1.9749	1.9570
	^{51}V	−365, −224, −85	−225
9^{DFT}***(closed-R,R,closed-S,S)***	*g*	1.9149, 1.9328, 2.0386	1.9621
	^{51}V	−156, −323, −435	−305
10^{DFT}***(P,closed-S,S)***	*g*	1.8989, 1.9400, 1.9887	1.9425
	^{51}V	−109, −306, −431	−282

[a] CW EPR only determines the absolute values of the hyperfine coupling; the sign was set according to the DFT data. [b] Principal *g* values and ^{51}V hyperfine coupling not collinear, the hyperfine interaction in the *g*-matrix frame is given as $A = R^*A_{diagonal}{}^*R^T$, in which R = [0.5121611 0.0082016 −0.8588503; −0.0021891 0.9999636 0.0082437; 0.8588866 −0.0023421 0.5121604]. [c] Principal *g* values and ^{51}V hyperfine coupling not collinear. NA = not available; ND = not defined.

To help assign the EPR components **3a**, **b** and **4** to a chemical structure, various models were tested. For each structural model, density functional theory (DFT) was used to obtain a geometry optimized structure which was subsequently used to compute EPR parameters for comparison to the experimental data as shown in Table 1. The optimized geometries are listed in the Supporting Information. The DFT computed EPR parameters for the structure of the model **4(*para,M/para,P*)** fit the EPR parameters from the purple solution very accurately (Table 1) and, thus, allow EPR component **4** to be assigned to atropisomer **4(*para,M/para,P*)** with metalloradical character in solution. However, assignment of the EPR components **3a** and

 © 2019 The Authors. Published by Wiley-VCH Verlag GmbH & Co. KGaA, Weinheim

ChemPubSoc Europe

CHEMISTRY A European Journal Full Paper

3b from the blue solution on the basis of the EPR parameters (*g* values and ^{51}V hyperfine couplings) was not as definitive as for **4**. Seven structural models were investigated: The model for compound **3(*M,M/P,P*)** and the (partially) closed compounds **5^{DFT}(*M,closed-S,S*)**, **6^{DFT}(*closed-S,S,closed-S,S*)** **9^{DFT}(*closed-R,R,closed-S,S*)**, and **10^{DFT}(*P,closed-S,S*)**, in which the DTE moiety underwent a pericyclic ring closure. Model **7^{DFT}(*M,P*)** has two DTE ligands with *M* and *P* helicity, respectively. Structural model **8^{DFT}(*para,para*)** carries both DTE ligands in a parallel alignment. Component **3b** exhibits a large and well determined ^{51}V principal hyperfine coupling value of $A_3(^{51}V) = -475$ MHz, which is best matched by the group of (partially) closed compounds **5^{DFT}(*M,closed-S,S*)**, **6^{DFT}(*closed-S,S,closed-S,S*)**, **9^{DFT}(*closed-R,R,closed-S,S*)**, and **10^{DFT}(*P,closed-S,S*)** with $A_3^{DFT}(^{51}V)$ ranging from −413 to −498 MHz. The other models all have significantly lower largest $A^{DFT}(^{51}V)$ values in the 300 MHz range. On this basis, EPR component **3b** is tentatively assigned to a compound class bearing cyclized DTE ligands. Component **3a** has $A_3(^{51}V) = -385$ MHz and given the limited experimental accuracy of the other *A* and g principal values, the signal could arise from a compound with both DTE in their non-cyclized form such as in **3^{DFT}(*M,M/P,P*)**, **7^{DFT}(*M,P*)** or **8^{DFT}(*para,para*)** (see Scheme 3). These three DFT models all have similar *A* and *g* values. Given the complexity of the experimental spectrum, we cannot rule out either that a combination of EPR components with slightly different EPR parameters are required to accurately explain the **3b** CW EPR signals.

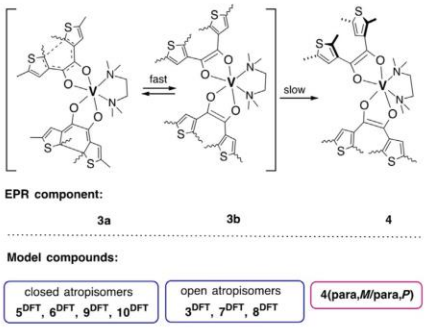

Scheme 3. Dynamic interconversion of EPR components **3ab** and **4** in solution and assignment of DFT models.

Conclusion

The redox-active ligand 1,2-bis(2,5-dimethylthiophen-3-yl)-ethane-1,2-dione (**1**) reacts with $[V(TMEDA)_2Cl_2]$ (**2**) in a disproportionation reaction to give rare non-oxido vanadium(IV) species encompassing two bis-enolato ligands with 1,2-dithienylethene (DTE) backbone. A blue crystalline product was isolated from the reaction mixture. Upon irradiation with a UVA-light source or heating of a toluene solution, a color change occurs from blue to purple and a purple crystalline material was obtained from the solution. Our single-crystal XRD analysis of both isolated compounds reveals the structure of the racemic complex **3(*M,M/P,P*)** (blue) and **4(*para,M/para,P*)** (purple). The antiparallel configuration of the thiophene rings of the DTE ligands in both complexes display axial chirality corresponding to *M* or *P* helicity. A parallel configuration is observed in complex **4(*para,M/para,P*)**.

The vanadium(IV) center is chelated through the en-diolate of each DTE ligand giving rise to five-membered metallacycles with a hexatriene motif formed in the DTE scaffold. The antiparallel alignment present in both **3(*M,M/P,P*)** and **4(*para,M/para,P*)** is a prerequisite for potential (reversible) 6π cyclization reactions (Scheme 1) and thus for the development of for example, photoswitchable metalloradicals.

With the aim of characterizing the solution structures, X-band CW EPR spectra were recorded of solutions of crystalline samples of **3(*M,M/P,P*)** and **4(*para,M/para,P*)** dissolved in THF at room temperature and in frozen solution. All obtained EPR spectra indicate vanadium-centered radicals. The purple solution spectrum of **4(*para,M/para,P*)** at both room temperature and in frozen-solution contained a single EPR-active component **4**, which is assigned to **4(*para,M/para,P*)**. The X-band EPR solution spectrum of the blue **3(*M,M/P,P*)** indicates a complex dynamic behavior; two EPR components are resolved at room temperature comprising of **4** and another denoted **3^{RT}**. We assume that **3^{RT}** is an average spectrum of rapidly interconverting species as there are three (or more) components in the frozen-solution spectrum (including **4**). The frozen-solution spectrum was modelled by **4** and components **3a** and **3b**. Although **3b** may be described as a complex with one or two cyclized DTE units represented by model compounds **5^{DFT}**, **6^{DFT}**, **9^{DFT}**, or **10^{DFT}**, component **3a** is best described as a complex involving only open DTE units represented here by model compounds **3^{DFT}**, **7^{DFT}**, or **8^{DFT}** or a combination thereof (see Scheme 3). Component **4** does not appear to be involved in dynamic averaging processes as **4** is definitively detected at room temperature as well as in frozen solution. Compound **4** thus appears to be the thermodynamically stable atropisomer because it forms slowly from **3(*M,M/P,P*)** solutions. The formation of the blue component **3** is kinetically controlled in the course of the synthesis of **3(*M,M/P,P*)** starting from ligand precursor **1** and complex **2**.

In conclusion, switchable transition-metal complexes bearing photochromic DTE motifs commonly have the coordination site rather distant from the DTE backbone and its hexatriene system. Here, we report the bidentate en-diolato ligand **F**, which directly chelates V^{IV} centers giving rise to five-membered metallacycles with adjacent DTE hexatriene backbone. Although we do not observe well-defined photochemically triggered cyclization, we found evidence for dynamic reversible cyclization reactions starting from **3(*M,M/P,P*)** at ambient temperature in solution.

 © 2019 The Authors. Published by Wiley-VCH Verlag GmbH & Co. KGaA, Weinheim

ChemPubSoc Europe

CHEMISTRY A European Journal Full Paper

Experimental Section

Crystallographic data

Experimental details for single crystal X-ray diffraction analysis of complexes 3(*M,M/P,P*) and 4(para,*M*/para,*P*): Diffraction experiments were performed on a Bruker D8 Venture in-house diffractometer using $Mo_{K\alpha}$ radiation and at the beamline BL02B1 of SPring-8 in Hyogo, Japan, using a wavelength of 0.3567 Å. The collection of the dataset of compound **4(*para,M/para,P*)** was done under exclusion of light and oxygen by using argon atmosphere while preparing crystals. Further details are shown in Table 2 and in the crystallographic information files (CIFs) deposited with the Cambridge Structural Database. CCDC 1946375 and 1946376 contain the supplementary crystallographic data for this paper. These data are provided free of charge by The Cambridge Crystallographic Data Centre.

Table 2. Details on the measurements and refinements of compound **3(*M,M/P,P*)** and **4(*para*,M/*para*,P)**.

Structure	**3(*M,M*)/(*P,P*)**	**4(*para,M*)/(*para,P*)**
Sum formula	$C_{34}H_{44}N_2O_4S_4V$	$C_{34}H_{44}N_2O_4S_4V$
Mol. mass (g mol^{-1})	723.89	723.89
Space group	$P2_1/n$	$P2_1/c$
a [Å]	10.4187(5)	28.109(6)
b [Å]	25.2837(11)	8.9569(18)
c [Å]	13.8148(7)	14.529(3)
β [°]	108.345(2)	94.47(3)
V [Å^3]	3454.2(3)	3646.8(13)
Z	4	4
F_{000}	1524	1524
Radiation	Mo-K_α (0.71073 Å)	Synchr. (0.3567 Å)
T [K]	100(1)	20(1)
Crystal color	blue	purple
Diffractometer	Bruker D8 Venture	SPring-8 Rigaku CCD
Max. resolution [Å]	0.82	0.75
R_{int}	0.089	0.173
hkl (−min = max)	12/30/16	37/11/19
# of reflns	35517	63595
# of indep. reflns	6455	9032
R	0.064	0.089
wR(F^2)	0.131	0.188
GoF	1.14	1.11
Residual [e Å^{-3}]	0.60/−0.38	1.14/−0.73
Obsv. criteria	$F^2 > 2\sigma(F^2)$	$F^2 > 2\sigma(F^2)$
CCDC entry[a]	1946375	1946376

[a] See also the Experimental Section.

Method and materials

If not mentioned otherwise, all reactions were carried out in a heavy-walled Schlenk tube with a wide bore Teflon screw stopcock under an atmosphere of dry argon. Solvents and chemicals were used without further purification.

UV/Vis spectroscopy: Experiments were carried out at 298 K on a Varian Cary 50 UV/Vis spectrophotometer. Cuvettes: 10 mm, synthetic quartz (QS) with Teflon cap. Probes were prepared under an inert atmosphere of argon.

Cyclic voltammetry: Experiments were carried out at 298 K with a Metrohm potentiostat running the NOVA 2.1 software package using a RHD Instruments electrochemical cell TSC 1600 closed. Solvent: THF; Electrolyte: [TBA]PF6; Electrodes: Pt working electrode, Ag/AgCl pseudo reference electrode, Pt counter electrode.

Continuous-wave (CW) electron paramagnetic resonance: X-band (9.3810 GHz) CW EPR measurements were carried out on a Bruker ElexSys E540 spectrometer equipped with a Bruker super-high-Q cavity and a Eurotherm LN_2 cooling system. Room temperature measurements were made under non-saturating conditions using a microwave power of 20 mW with a modulation frequency of 100 KHz and a modulation amplitude of 0.1 mT. Measurement in frozen solution used a microwave power of 5.0 mW (non-saturating) with a modulation frequency of 100 KHz and modulation amplitude of 0.3 mT. The spectrometer field was calibrated with 2,2-diphenyl-1-picrylhydrazyl (DPPH: $g = 2.0036$). Simulations used the XSophe[52] and Easyspin[53] software.

Density functional theory: Calculations to compute EPR parameters were performed using ORCA 3.0.3.[54,55] Geometry optimization was performed using the UKS B3LYP functional, a T2V basis set and a frozen core for all electrons, and a COSMO model for THF. The g-, hyperfine and nuclear quadrupole tensors were calculated using a spin-unrestricted Kohn–Sham self-consistent field calculation method with a ZORA scalar relativistic Hamiltonian and the B3LYP functional, using the Def2QZVPP basis set for V and the def2TZVPP basis set for all other nuclei,[56] and tighter convergence constraints. The spin-orbit coupling was calculated using the SOMF(1X) option in ORCA.

Synthetic protocols

$[V_2(\mu\text{-}Cl)_3(THF)_6]_2[Zn_2Cl_6]$: the compound was prepared following a slightly modified literature procedure:[57] 1) **$VCl_3(THF)_3$**: VCl_3 (0.50 g, 3.18 mmol, 1.00 equiv) was suspended in THF (40 mL) and stirred for 48 h at 75 °C. The formed light purple solution was subsequently filtered and the solvent removed under reduced pressure. Yield: 1.18 g (3.15 mmol, 99%). 2) **$VCl_3(THF)_3$** (1.00 g, 2.68 mmol, 1.00 equiv), dissolved in THF (50 mL), was treated with zinc powder (0.44 g, 6.69 mmol, 2.50 equiv) and stirred for 48 h at room temperature. After removal of the solvent under reduced pressure, the green product was dissolved in DCM, filtered, dried and washed with small portions of *n*-pentane. Yield: 0.87 g (0.54 mmol, 80%).

$VCl_2(TMEDA)_2$: the compound was prepared following a modified literature procedure:[58] $[V_2(\mu\text{-}Cl)_3(THF)_6]_2[Zn_2Cl_6]$ (0.70 g, 0.43 mmol, 1.00 equiv) was suspended in THF (30 mL), treated with *N,N,N′,N′*-tetramethylethylenediamine (2.3 mL, 15.07 mmol, 35.00 equiv), stirred at 75 °C for 6 h and then at room temperature for 16 h. After partial removal of the solvent under reduced pressure, blue crystals separated from the red solution upon standing overnight in a cryostat at 5 °C. The supernatant was decanted and the product washed with small portions of cold THF. Yield: 0.53 g (1.51 mmol, 87%).

1,2-Bis(2,5-dimethylthiophen-3-yl)ethane-1,2-dione (**DTE**, **1**): the compound was prepared following a modified literature procedure:[59] In a three neck flask, $AlCl_3$ (9.39 g, 70.42 mmol, 1.00 equiv) was suspended in DCM (40 mL), cooled to −15 °C and treated with pyridine (2.8 mL, $\rho = 0.978$ g cm^{-3}, 35.21 mmol, 0.50 equiv) and 2,5-dimethylthiophene (8.0 mL, $\rho = 0.985$ g cm^{-3}, 70.42 mmol, 1.00 equiv), each dissolved in DCM (40 mL). Over a time period of 40 minutes, oxalyl chloride (3.6 mL, $\rho = 1.48$ g cm^{-3}, 42.25 mmol, 0.60 equiv), dissolved in CH_2Cl_2 (40 mL), was added to the red solution. After stirring for 40 min at −5 °C and 1 h at 5–10 °C, the mixture was poured onto ice. The organic layer was separated and the aqueous layer extracted with chloroform. The combined organic phases were then washed with water, sodium carbonate solution and saturated NaCl solution subsequently. Filtering through hot

 © 2019 The Authors. Published by Wiley-VCH Verlag GmbH & Co. KGaA, Weinheim

ChemPubSoc Europe

CHEMISTRY A European Journal Full Paper

cotton and removal of the solvent under reduced pressure was followed by flash chromatography (cyclohexane/ethylacetate, 100:3) of the viscous oil and led to pure orange-brown product. Yield: 4.12 g (14.80 mmol, 42%), $R_f = 0.38$.

[V(DTE$_{(apM)}$)$_2$TMEDA]/ [V(DTE$_{(apP)}$)$_2$TMEDA] (3(*M,M/P,P*)): Compound **1** (0.20 g, 0.71 mmol, 1.00 equiv) was added to a suspension of [VCl_2(TMEDA)$_2$] (0.25 g, 0.71 mmol, 1.00 equiv) in THF (15 mL). The resulting dark-blue solution was stirred at 75 °C for 24 h. After filtration and partial removal of the solvent under reduced pressure, *n*-pentane was allowed to diffuse into the saturated solution for seven days, allowing for the crystallization of product **3**. The supernatant was decanted and the product was washed with small portions of *n*-pentane and subsequently dried in a stream of argon. Yield: 0.22 g (0.30 mmol, 43%).

[V(DTE$_{(par)}$)(DTE$_{(apM)}$)TMEDA]/[V(DTE$_{(par)}$)(DTE$_{(apP)}$)TMEDA] [4(*para,M/para,P*)]: *Photochemical isomerization*: In a typical experiment, a 20 mL fused-quartz Schlenk tube with Teflon valve was charged with a toluene solution of compound **3(*M,M/P,P*)** (0.01–0.02 mM). The sample was irradiated with UVA light (λ_{max} = 370 nm), performed in a custom-built photoreactor with two 11 W UVA lamps (Philips UV-A PL-S 11 W/10/2P, 28 mm diameter, 236 mm total length) equipped with a cooling ventilator. Distance to probe: 10 cm. The reaction is characterized by a color change from deep blue to purple. The solvent was removed under reduced pressure after 4–6 h reaction time. The product was isolated as purple powder in quantitative yield. Crystals suitable for single-crystal X-ray diffraction analysis by using synchrotron radiation at the BL02B1 beamline at SPring-8 in Hyogo, Japan, were obtained from a saturated solution of **4(*para,M/para,P*)** in toluene upon standing for several days. *Thermal isomerization:* A toluene solution of **3(*M,M/P,P*)** (0.1–0.2 mM) was transferred in a Schlenk tube with a wide bore Teflon screw stopcock and heated to 80 °C for 12 h. The reaction is characterized by a color change from deep blue to purple. The supernatant was removed in vacuo leaving compound **4(*para,M/para,P*)** as a purple solid.

Acknowledgements

This work was funded by the central research and development fund of the University of Bremen. M.V. thanks the Fonds der Chemischen Industrie for generous financial support. J.R.H. thanks the Australian Research Council (ARC) FT120100421 for financial support. Synchrotron measurements were made possible through funding of S.G. within the Emmy Noether Scheme of the DFG (Deutsche Forschungsgemeinschaft), project GR 4451/1-1, and were supported by SPring-8 within proposal no. 2017A1233.

Conflict of interest

The authors declare no conflict of interest.

Keywords: axial chirality · cooperative effects · dithienylethene · EPR spectroscopy · ligand design · reversible ligand cyclization · vanadium

[1] D. C. Crans, J. J. Smee, E. Gaidamauskas, L. Yang, *Chem. Rev.* **2004**, *104*, 849–902.
[2] J. Costa Pessoa, E. Garribba, M. F. A. Santos, T. Santos-Silva, *Coord. Chem. Rev.* **2015**, *301–302*, 49–86.
[3] K. H. Thompson, J. H. McNeill, C. Orvig, *Chem. Rev.* **1999**, *99*, 2561–2572.
[4] K. H. Thompson, J. Lichter, C. LeBel, M. C. Scaife, J. H. McNeill, C. Orvig, *J. Inorg. Biochem.* **2009**, *103*, 554–558.
[5] Y. Wei, C. Zhang, P. Zhao, X. Yang, K. Wang, *J. Inorg. Biochem.* **2011**, *105*, 1081–1085.
[6] D. Sanna, G. Micera, E. Garribba, *Inorg. Chem.* **2013**, *52*, 11975–11985.
[7] M. Sutradhar, L. M. D. R. S. Martins, M. F. C. Guedes da Silva, A. J. L. Pombeiro, *Coord. Chem. Rev.* **2015**, *301–302*, 200–239.
[8] E. Amadio, R. Di Lorenzo, C. Zonta, G. Licini, *Coord. Chem. Rev.* **2015**, *301–302*, 147–162.
[9] D. Rehder, *Dalton Trans.* **2013**, *42*, 11749–11761.
[10] a) G. H. Spikes, S. Sproules, E. Bill, T. Weyhermüller, K. Wieghardt, *Inorg. Chem.* **2008**, *47*, 10935–10944; b) S. Sproules, T. Weyhermüller, S. DeBeer, K. Wieghardt, *Inorg. Chem.* **2010**, *49*, 5241–5261.
[11] R. E. Berry, E. M. Armstrong, R. L. Beddoes, D. Collison, S. N. Ertok, M. Helliwell, C. D. Garner, *Angew. Chem. Int. Ed.* **1999**, *38*, 795–797; *Angew. Chem.* **1999**, *111*, 871–873.
[12] E. Bayer, H. Kneifel, *Z. Naturforschung Sect. B* **1972**, *27*, 207.
[13] D. Sanna, V. Ugone, G. Micera, T. Pivetta, E. Valletta, E. Garribba, *Inorg. Chem.* **2015**, *54*, 8237–8250.
[14] M. Irie, T. Fukaminato, K. Matsuda, S. Kobatake, *Chem. Rev.* **2014**, *114*, 12174–12277.
[15] M. Irie, *Proc. Jpn. Acad. Ser. B* **2010**, *86*, 472–483.
[16] M. Irie, *Photochem. Photobiol. Sci.* **2010**, *9*, 1535–1542.
[17] C. Yun, J. You, J. Kim, J. Huh, E. Kim, *J. Photochem. Photobiol. C* **2009**, *10*, 111–129.
[18] C. P. Harvey, J. D. Tovar, *Polym. Chem.* **2011**, *2*, 2699–2706.
[19] S.-Z. Pu, Q. Sun, C.-B. Fan, R.-J. Wang, G. Liu, *J. Mater. Chem. C* **2016**, *4*, 3075–3093.
[20] M. Irie, *Chem. Rev.* **2000**, *100*, 1685–1716.
[21] T. Hirose, K. Matsuda, *Org. Biomol. Chem.* **2013**, *11*, 873–880.
[22] C. Xiao, W.-Y. Zhao, D.-Y. Zhou, Y. Huang, Y. Tao, W.-H. Wu, C. Yang, *Chin. Chem. Lett.* **2015**, *26*, 817–824.
[23] S. Cui, G. Liu, S. Pu, B. Chen, *Dyes Pigm.* **2013**, *99*, 950–956.
[24] D. Frath, S. Yokoyama, T. Hirose, K. Matsuda, *J. Photochem. Photobiol. C* **2018**, *34*, 29–40.
[25] Y. Takagi, M. Morimoto, R. Kashihara, S. Fujinami, S. Ito, H. Miyasaka, M. Irie, *Tetrahedron* **2017**, *73*, 4918–4924.
[26] C. Li, H. Yan, L.-X. Zhao, G.-F. Zhang, Z. Hu, Z.-L. Huang, M.-Q. Zhu, *Nat. Commun.* **2014**, *5*, 5709.
[27] S. Erbas-Cakmak, D. A. Leigh, C. T. McTernan, A. L. Nussbaumer, *Chem. Rev.* **2015**, *115*, 10081–10206.
[28] J. E. Smyth, N. M. Butler, P. A. Keller, *Nat. Prod. Rep.* **2015**, *32*, 1562–1583.
[29] M. Öki in *Topics in Stereochemistry, Vol. 14* (Eds.: N. L. Allinger, E. L. Eliel, S. H. Wilen), Wiley, New York, **1983**, pp. 1–81.
[30] K. Mikami, M. Yamanaka, *Chem. Rev.* **2003**, *103*, 3369–3400.
[31] L. Pu, *Chem. Rev.* **1998**, *98*, 2405–2494.
[32] F. Leroux, *ChemBioChem* **2004**, *5*, 644–649.
[33] R. Noyori, *Angew. Chem. Int. Ed.* **2002**, *41*, 2008–2022; *Angew. Chem.* **2002**, *114*, 2108–2123.
[34] A. Miyashita, A. Yasuda, H. Takaya, K. Toriumi, T. Ito, T. Souchi, R. Noyori, *J. Am. Chem. Soc.* **1980**, *102*, 7932–7934.
[35] E. Kumarasamy, R. Raghunathan, M. P. Sibi, J. Sivaguru, *Chem. Rev.* **2015**, *115*, 11239–11300.
[36] P. W. Glunz, *Bioorg. Med. Chem. Lett.* **2018**, *28*, 53–60.
[37] J. Clayden, W. J. Moran, P. J. Edwards, S. R. LaPlante, *Angew. Chem. Int. Ed.* **2009**, *48*, 6398–6401; *Angew. Chem.* **2009**, *121*, 6516–6520.
[38] A. Zask, J. Murphy, G. A. Ellestad, *Chirality* **2013**, *25*, 265–274.
[39] M. Fukagawa, I. Kawamura, T. Ubukata, Y. Yokoyama, *Chem. Eur. J.* **2013**, *19*, 9434–9437.
[40] H. Tian, S. Yang, *Chem. Soc. Rev.* **2004**, *33*, 85–97.
[41] M. Walko, Ben L. Feringa, *Chem. Commun.* **2007**, 1745–1747.
[42] M. Farahbakhsh, H. Schmidt, D. Rehder, *Chem. Commun.* **1998**, 2009–2010.
[43] C.-C. Ko, V. W.-W. Yam, *Acc. Chem. Res.* **2018**, *51*, 149–159.
[44] V. W.-W. Yam, J. K.-W. Lee, C.-C. Ko, N. Zhu, *J. Am. Chem. Soc.* **2009**, *131*, 912–913.
[45] B. M. Neilson, V. M. Lynch, C. W. Bielawski, *Angew. Chem. Int. Ed.* **2011**, *50*, 10322–10326; *Angew. Chem.* **2011**, *123*, 10506–10510.

 © 2019 The Authors. Published by Wiley-VCH Verlag GmbH & Co. KGaA, Weinheim

ChemPubSoc Europe

CHEMISTRY A European Journal Full Paper

[46] B. M. Neilson, C. W. Bielawski, *J. Am. Chem. Soc.* **2012**, *134*, 12693 – 12699.
[47] B. M. Neilson, C. W. Bielawski, *Organometallics* **2013**, *32*, 3121 – 3128.
[48] A. J. Teator, H. Shao, G. Lu, P. Liu, C. W. Bielawski, *Organometallics* **2017**, *36*, 490 – 497.
[49] C.-C. Ko, W. M. Kwok, V. W.-W. Yam, D. L. Phillips, *Chem. Eur. J.* **2006**, *12*, 5840 – 5848.
[50] V. W. W. Yam, C.-C. Ko, N. Zhu, *J. Am. Chem. Soc.* **2004**, *126*, 12734 – 12735.
[51] A. Presa, L. Barrios, J. Cirera, L. Korrodi-Gregorio, R. Perez-Tomas, S. J. Teat, P. Gamez, *Inorg. Chem.* **2016**, *55*, 5356 – 5364.
[52] G. R. Hanson, K. E. Gates, C. J. Noble, M. Griffin, A. Mitchell, S. Benson, *J. Inorg. Biochem.* **2004**, *98*, 903 – 916.
[53] S. Stoll, A. Schweiger, *J. Magn. Reson.* **2006**, *178*, 42 – 55.
[54] F. Neese, *WIREs Comput. Mol. Sci.* **2012**, *2*, 73 – 78.
[55] a) A. Schäfer, H. Horn, R. Ahlrichs, *J. Chem. Phys.* **1992**, *97*, 2571 – 2577; b) F. Weigend, R. Ahlrichs, *Phys. Chem. Chem. Phys.* **2005**, *7*, 3297 – 3305.
[56] a) D. A. Pantazis, X.-Y. Chen, C. R. Landis, F. Neese, *J. Chem. Theory Comput.* **2008**, *4*, 908 – 919; b) D. A. Pantazis, F. Neese, *J. Chem. Theory Comput.* **2009**, *5*, 2229 – 2238; c) D. A. Pantazis, F. Neese, *J. Chem. Theory Comput.* **2011**, *7*, 677 – 684; d) D. A. Pantazis, F. Neese, *Theor. Chem. Acc.* **2012**, *131*, 1292.
[57] R. J. Bouma, J. H. Teuben, W. R. Beukema, R. L. Bansemer, J. C. Huffman, K. G. Caulton, *Inorg. Chem.* **1984**, *23*, 2715 – 2718.
[58] J. J. H. Edema, W. Stauthamer, F. Van Bolhuis, S. Gambarotta, W. J. J. Smeets, A. L. Spek, *Inorg. Chem.* **1990**, *29*, 1302 – 1306.
[59] L. I. Belen'kii, V. Z. Shirinyan, G. P. Gromova, A. V. Kolotaev, Y. A. Strelenko, S. N. Tandura, A. N. Shumskii, M. M. Krayushkin, *Chem. Heterocycl. Compd.* **2003**, *39*, 1570 – 1579.

Manuscript received: September 6, 2019
Accepted manuscript online: November 13, 2019
Version of record online: January 21, 2020

 © 2019 The Authors. Published by Wiley-VCH Verlag GmbH & Co. KGaA, Weinheim

2.2 Investigation of M(IV) (M = Ti, Zr, Hf, Sn) Tetrachlorido Complexes based on α-Diketone **90** and α-Diimine **91**

As reported in *Chapter 2.1*, the initial approach to a metal complex bearing the 1,2-endiolato DTE motif entailed a reaction, in which α-diketone **90** was reduced by a V(II) precursor and concomitantly furnished the corresponding V(IV) complexes. Since this reaction is very specific and an intrinsic yield limitation of 50% cannot be overcome, it was reached out to find a more universal approach for the synthesis of DTE-metallacycles: that is to induce a pre-coordination of the DTEthane-precursor to a suitable metal center, followed by a two-electron reduction to give rise to the (potentially) photoswitchable hexatriene motif.

Inspired by Clark's report on the reduction of (α-diimino)$TiCl_4$ complex **87** to complex **88** or **89** with a double bond being formed between the carbon atoms of the former imine groups,[198] it was decided to convert α-diketone **90** at hand to α-diimine **91** and form with it the corresponding $TiCl_4$ complex **92**. Reduction of **92** could lead to the desired DTE-backbone necessary for photocyclization (*Figure 49*).

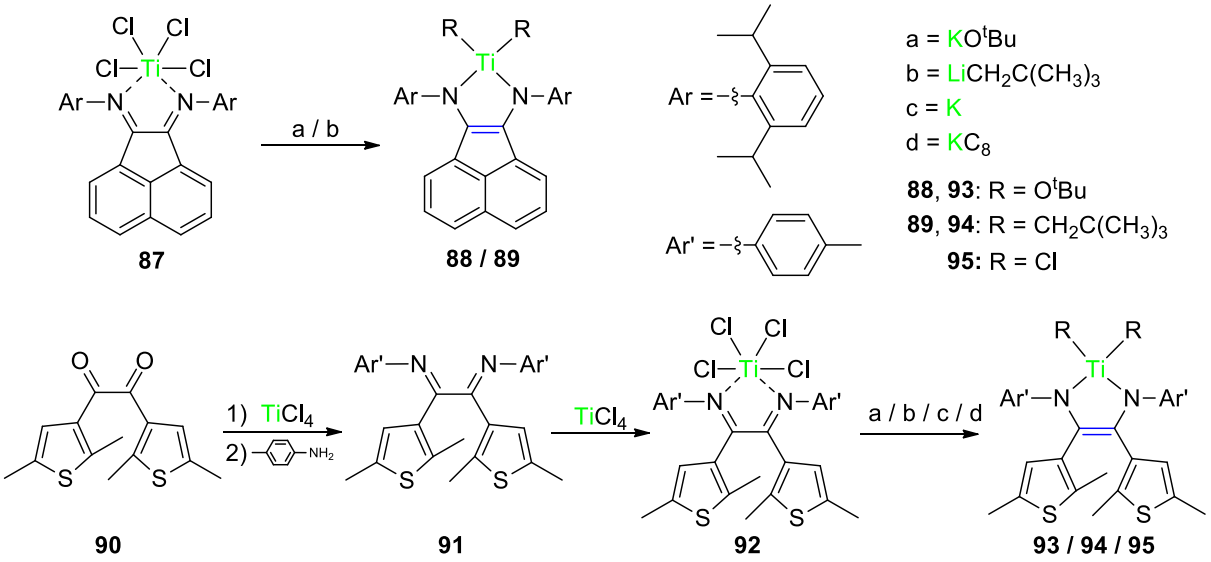

Figure 49: *Reported reduction of (α-diimino)$TiCl_4$ complex **87**[198] (upper part); synthesis of **91** via a modified synthetic route for similar transformations reported by Ragogna and Price[199] and intended reduction of **92** to complex **93**, **94** or **95** (lower part).*

Several attempts for a condensation reaction commonly used for conversion of ketones/α-diketones to the corresponding imines/diimines[8, 168, 200] have failed, which probably is owed to the high stability of **90**'s keto groups as a result of the prolonged π-conjugation. However, α-diimine **91** could finally be obtained *via* a slightly modified synthetic route reported by Ragogna and Price[199] by the use of $TiCl_4$ as an activation reagent for the desired condensation reaction: after formation of a complex of **90** with $TiCl_4$ in DCM, *p*-toluidine was added, the reaction mixture stirred for 24 h and then quenched with water. Filtering and workup of the crude product led to **91** in a yield of 65%. *p*-Toluidine was used as

reagent due to its nucleophilic character and the fact that no sterically obstructive groups are present at positions 2' and 6'. Complex **92** could then be obtained in quantitative yield by addition of **91** to a solution of $TiCl_4$ in DCM.

Unfortunately reduction of **92**, although CV experiments looked promising (cf. *Chapter 2.2.1.5*) with KO^tBu or neopentyllithium in toluene led to complex mixtures and it was neither possible to isolate the desired products **93** or **94** nor obtain proof for their presence. The use of stronger reducing agents like potassium or KC_8 to form complex **95** led to similar results.

In order to investigate if 1) the higher and easier to polarize group four metals zirconium and hafnium and/or 2) the corresponding complexes bearing *α*-diketone **90** as ligand could serve as suitable compounds for a reduction, those complexes were synthesized/tried to be synthesized as well; unfortunately results in regard of a well-defined reduction were the same as for **92**. *Figure 50* shows all obtained complexes in the course of addition of *α*-diketone **90** or *α*-diimine **91** to the corresponding MCl_4 precursor (M = Ti, Zr, Hf, Sn) and an overall view of the synthetic pathways. $SnCl_4$ was used in addition to gain access to another NMR active nucleus.

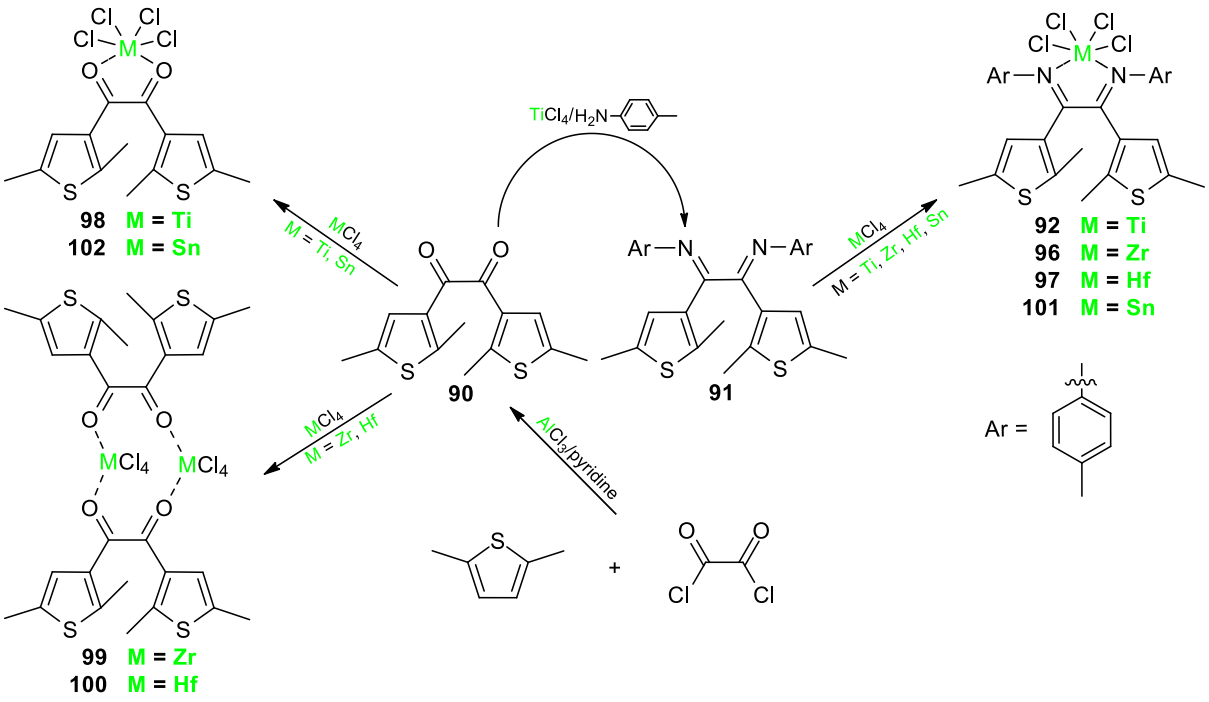

Figure 50: *Complete overview of the synthetic pathways for α-diketone **90**, α-diimine **91** and corresponding complexes **92**, **96** - **102** formed with metal precursors MCl_4 (M = Ti, Zr, Hf, Sn).*

As can be seen, reaction of *α*-diketone **90** with $ZrCl_4$ and $HfCl_4$ unexpectedly gave rise to formation of a 10-membered metallacycle with two MCl_4 fragments being bridged by two {μ^2,η^1,η^1-*O*,*O'*-DTEthane} ligands. This finding, overall description of complexes **98** - **100** and detailed investigations in regard of their stereochemistry is described in *Chapter 2.3*.

In case of *α*-diimine **91** no formation of [2+2] complexes could be observed, a result likely caused by the presence of the sterically demanding phenyl rings. Another effect of those bulky substituents of *α*-diimine **91** results in a limited ability for the thienyl rings to rotate along the C-C-σ-bonds C1-C7 and C8-C9, thus leading to two chiral axes and the presence of atropisomers. *Figure 51* shows the crystal structures of complex **92** in parallel alignment (upper part) and zirconium complex **96** in antiparallel alignment with *P*- and *M*-helicity, respectively (middle and lower part).

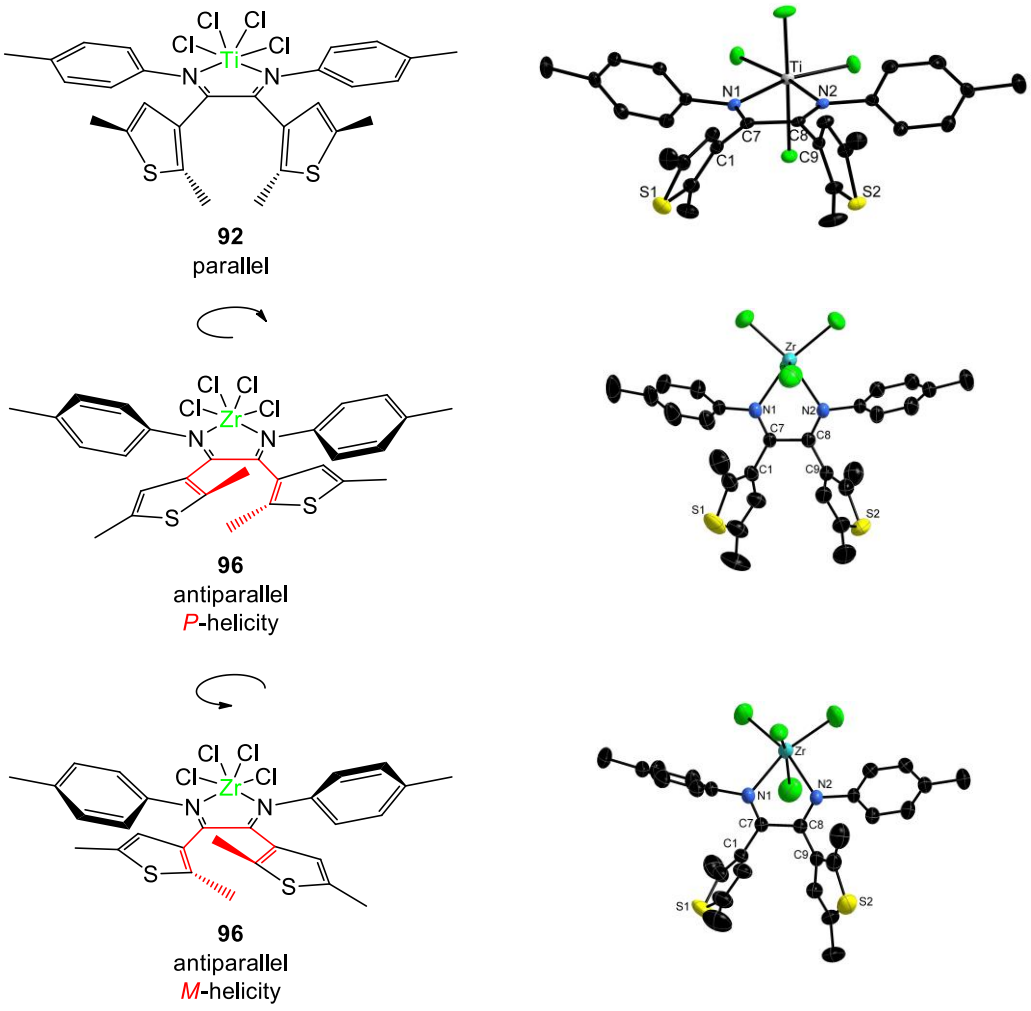

Figure 51: *Parallel atropisomer of **92** (top) and antiparallel atropisomers of **96** with P-helicity (middle) and M-helicity (bottom). Complexes' ligand structures on the left side being shown after slight rotation of the thienyl rings for better visualization of their stereochemistry.*

It was found that both, the pair of helical atropisomers and the non-helical atropisomer are equally present in solution, as the NMR spectra for complexes **92, 96, 97** and **101** display two sets of signals in a ratio of 1:1. (Note that both helical atropisomers, like enantiomers, have identical NMR spectra.)

In order to exclude the possibility that the two sets of signals were caused by the presence of an unsymmetrical molecule rather than atropisomers, it was decided to synthesize $SnCl_4$ complexes **101** and **102** (*Figure 50*). As expected, complex **101**, like **92, 96** and **97**, displays two similar sets of signals

in the ^{1}H and ^{13}C, as well as two signals in the ^{119}Sn NMR spectra, supporting the stated assumption. Reaction of *α*-diketone **90** with $SnCl_4$ led, as anticipated due to tin's small atom radius, to [1+1] product **102** with only one signal present in the ^{119}Sn NMR spectrum.

In a further experiment a solution of **101** in d_6-benzene was heated up (stepwise to 70 °C) to see if interconversion between the distinct atropisomers could be observed; however monitoring of the ^{119}Sn NMR signals showed no significant changes upon heating, implying that a much higher temperature would be of need for an interconversion (NMR spectra can be found in *Chapter 2.2.1.2* and in SI).

In the following *α*-diimine **91** as well as the obtained complexes **92**, **96**, **97** and **101** are described in more detail.

2.2.1 Characterization of *α*-Diimine **91** and Complexes **92**, **96, 97**, **101**

2.2.1.1 Solubility of *α*-Diimine **91** and Complexes **92**, **96**, **97**, **101**

α-Diimine **91** is, like *α*-diketone **90** readily soluble in most organic solvents, such as THF, MeCN, chloroform, DCM, and toluene and also slightly soluble in unpolar solvents, such as *n*-hexane, which proofs useful in removing remaining ligand after the reaction. Complexes formed with *α*-diimine **91** (**92, 96, 97** and **101**) remain soluble in the above stated solvents except *n*-hexane and are – in contrast to complexes formed with *α*-diketone **90** (**98** – **100**, **102**), where facile dissociation in coordinating solvents like MeCN or THF was observed – stable in solution.

2.2.1.2 NMR Investigations of α-Diimine **91** and Complexes **92**, **96, 97**, **101**

While [1+1] complexes formed with α-diketone **90** show only slight deviation when compared to free ligand α-diketone **90** (cf. *Chapter 2.3*), complexes formed with α-diimine (**92, 96**, **97**, **101**) exhibit drastic change in the NMR spectra in comparison to free ligand α-diimine **91**, that is, besides overall large chemical shifts, the presence of two sets of signals. This can be seen best in the ^{13}C NMR spectrum of **101** in CD_2Cl_2, where all signals, except for the phenyl ring's methyl group, can be seen without overlaps. When measured in d_6-benzene, **101** also exhibits each methyl group's signals individually in the ^{1}H NMR spectrum (*Figure 52*).

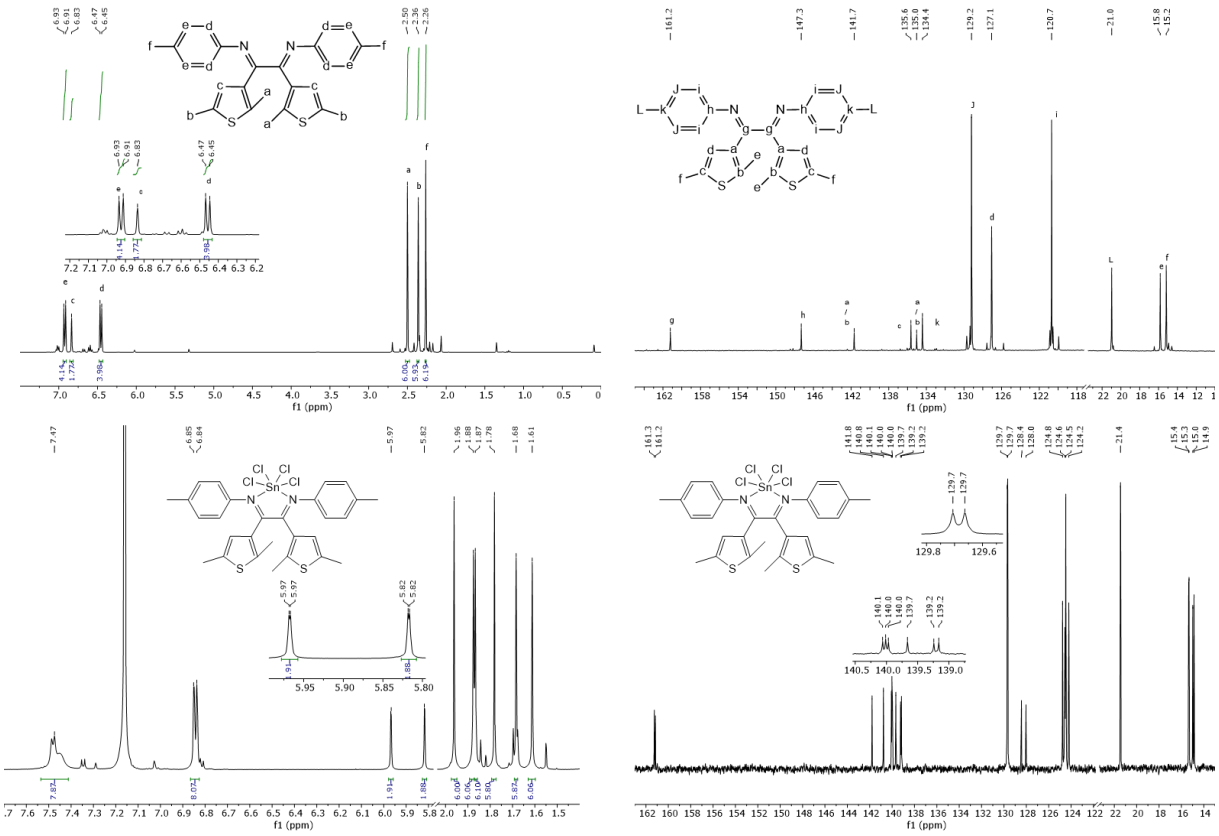

Figure 52: *^{1}H (360 MHz, CD_2Cl_2) and $^{13}C\{^{1}H\}$ (90 MHz, CD_2Cl_2) NMR spectra of α-diimine **91** (top); ^{1}H (600 MHz, C_6D_6) and $^{13}C\{^{1}H\}$ (150 MHz, CD_2Cl_2) NMR spectra of complex **101** (bottom).*

The ^{119}Sn NMR spectrum of **101** (*Figure 53*) consists of two signals and supports the thesis of presence of two compounds: that is the pair of helical atropisomers (*M*- or *P*-helicity due to antiparallel alignment of the thineyl rings) and the atropisomer without helicity (parallel alignment of the thienyl rings).

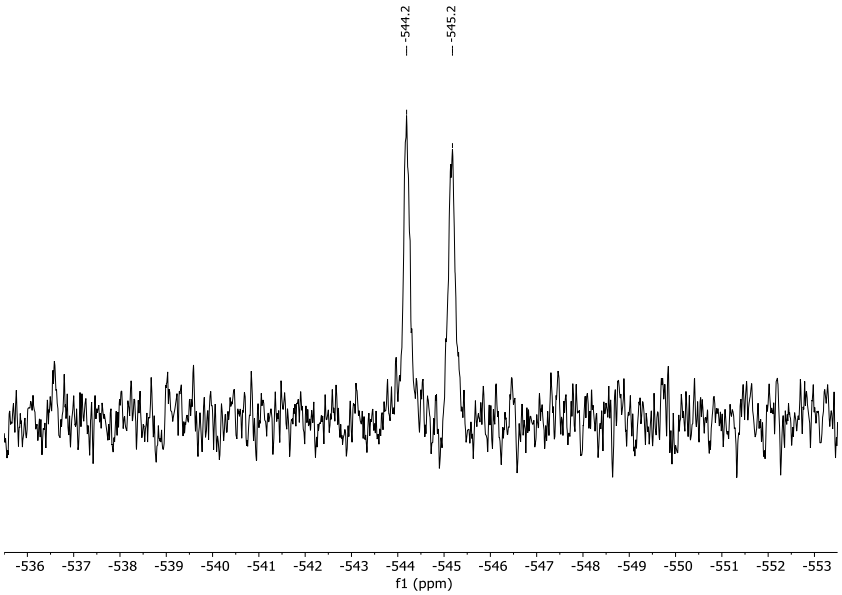

Figure 53: *^{119}Sn (220 MHz, C_6D_6) NMR spectrum of complex **101**.*

To investigate an influence of the temperature in regard of a possible interconversion of the atropisomers, **101** in d_6-benzene was heated up to 70°C (*Figure 54*).

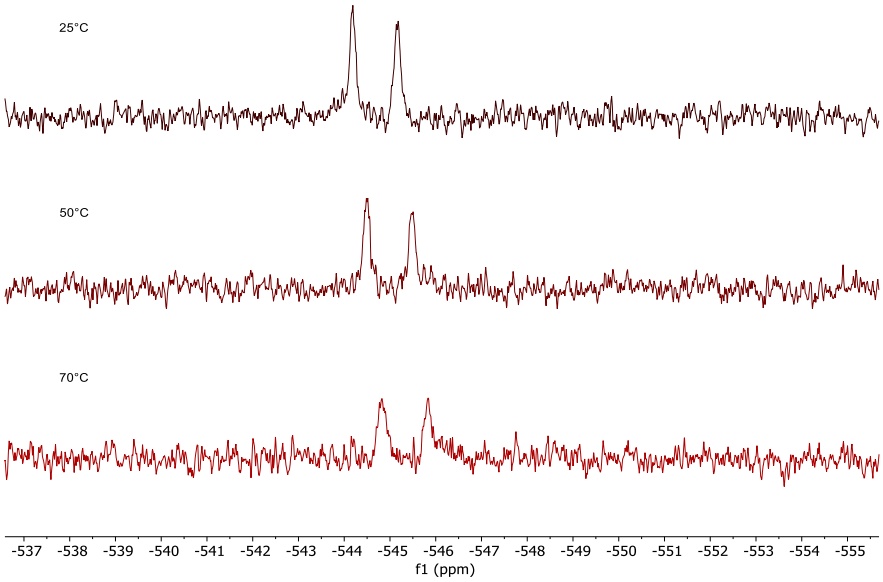

Figure 54: *^{119}Sn (220 MHz, C_6D_6) NMR spectra of **101** at different temperatures.*

However, distance between the signals in the ^{119}Sn NMR spectrum did not remarkably change and it is likely that a much higher temperature is needed to reach a state of rapid interconversion.

2.2.1.3 X-ray Crystal Structures of α-Diimine **91** and Complexes **92**, **96**, **97**

Figure 55 depicts the received crystal structures of α-diimine **91** and corresponding complexes **92**, **96** and **97**.

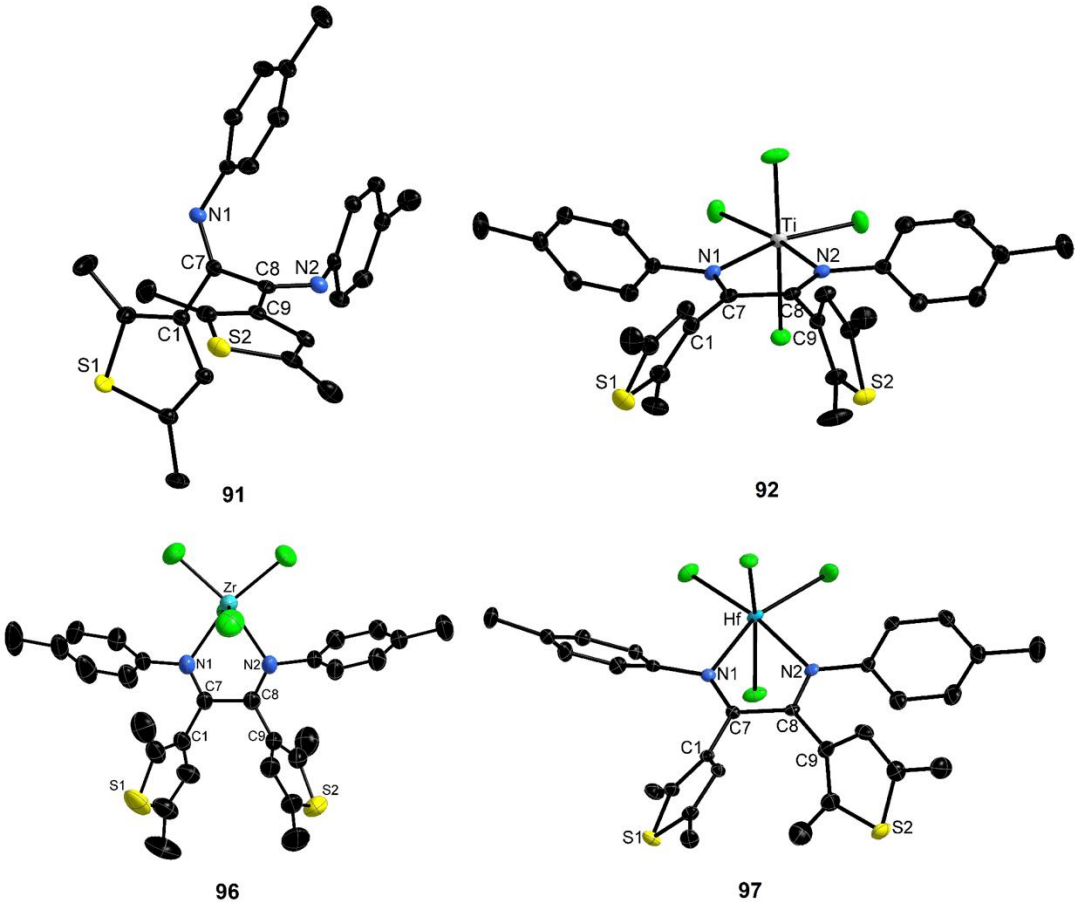

Figure 55: *X-ray crystal structures of α-diimine **91** and complexes **92**, **96**, **97** at 50% ellipsoid probability. Hydrogen atoms are omitted for clarity.*

α-Diimine **91** crystalizes in the triclinic space group P-1 in an asymmetrical unit cell containing two structures, which mainly show differences for the torsion angles of N1-C7-C8-N2 and C1-C7-C8-C9. Bond lengths display only narrow differences. In order to create as much space as possible between the bulky toluene and thiophene rings, bonds C7-N1 and C8-N2 as well as C1-C7 and C8-C9 are tilted against each other along the C7-C8 axis, leading to torsion angles of 77.2(3)° (2nd structure: 68.5(3)°) for N1-C7-C8-N2 and 74.2(2)° (2nd structure: 68.7(2)°) for C1-C7-C8-C9. Upon formation of a complex with MCl_4 (M = Ti, Zr, Hf) these angles become as low as 2.0(6)° in **97** for N1-C7-C8-N2 and 0.6(2)° in **92** for C1-C7-C8-C9 (*Table 1* and *Table 2*).

Table 1: *Selected bond lengths for α-diimine **91** and corresponding complexes **92, 96, 97** in Å.*

	91	**91** 2nd	**92** (M = Ti)	**96** (M = Zr)	**97** (M = Hf)
C1-C7	1.475(2)	1.478(2)	1.479(2)	1.476(5)	1.476(6)
C7-C8	1.519(2)	1.519(2)	1.499(2)	1.503(5)	1.501(6)
C8-C9	1.479(2)	1.479(2)	1.482(2)	1.470(5)	1.482(6)
C7-N1	1.284(2)	1.284(2)	1.287(2)	1.284(4)	1.294(6)
C8-N2	1.276(2)	1.278(2)	1.283(2)	1.283(4)	1.298(6)
N1-M1	-	-	2.225(2)	2.358(3)	2.331(4)
N2-M1	-	-	2.213(2)	2.349(3)	2.338(4)

Table 2: *Selected torsion angles for α-diimine **91** and corresponding complexes **92, 96, 97** in °.*

	Torsion Angle (N1-C7-C8-N2)	**Torsion Angle (C1-C7-C8-C9)**
91	77.2(3)	74.2(2)
91 (2nd)	68.5(3)	68.7(2)
92 (M = Ti)	2.7(2)	0.6(2)
96 (M = Zr)	3.6(5)	2.0(5)
97 (M = Hf)	2.0(6)	1.6(6)

Complexes **92**, **96** and **97** crystalize in the monoclinic space group $P2_1/n$ and form a 6-coordinated distorted octahedral structure around the metal center. In order to reduce steric strains, the toluene and thiophene ring of each side as well as the thiophene rings in regard to each other stand in staggered formation. Crystal structures of **92** and **97** were received with thienyl rings in parallel alignment, the unit cell of **96** contained both helical structures in a 1:1 ratio with thienyl rings in an antiparallel alignment (*Figure 55* shows **96** with *P*-helicity). While several crystals have been measured, only the prior described configuration for each complex was received, indicating this form to be favoured in the crystallization progress. However, NMR spectra clearly point towards the presence of all atropisomers in solution for those complexes. The largest distance between nitrogens and metal center can be observed for **96** (N1-M1: 2.358(3) Å; N2-M1: 2.349(3) Å; M = Zr), the shortest for **92** (N1-M1: 2.225(2) Å; N2-M1: 2.213(2) Å; M = Ti).

Unfortunately it was not possible to obtain crystals of **101** large enough for measurements, even though several methods and various combinations of solvents have been tried out.

2.2.1.4 UV/Vis Spectra of α-Diimine **91** and Complexes **92**, **96**, **97**, **101**

UV/Vis spectra of α-diimine complexes **96, 97**, **101** in DCM show a broad absorption from 300 nm to 500 nm, with a maximum around 415 nm. In contrast to those **92** exhibits an absorption maximum at 300 nm and a steadily decreasing absorption from 300 nm to 750 nm (*Figure 56*).

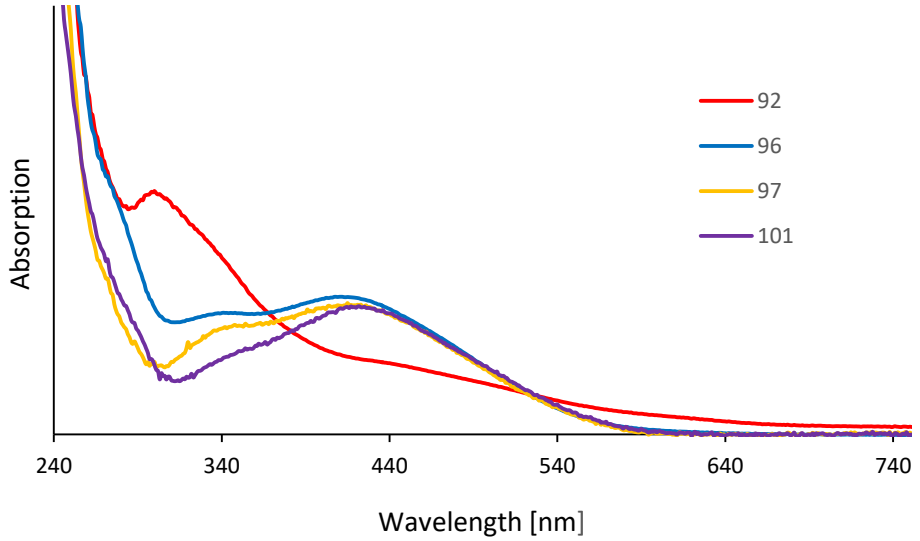

Figure 56: *UV/Vis spectra of **92**, **96**, **97** and **101** in DCM. Note: solutions differ in concentration; spectra of **96**, **97** and **101** were calibrated at 415 nm for better comparability.*

Despite that difference all α-diimine complexes share an orange color when dissolved in DCM. Complexes formed with α-diketone **90** in DCM are deep red in color. α-Diimine **91** exhibits no absorption beyond 430 nm and appears, like α-diketone **90**, yellow in solution (*Figure 57*, cf. SI).

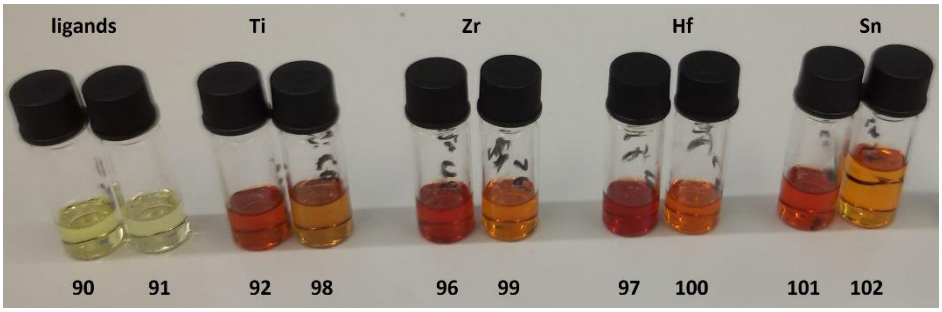

Figure 57: *Solutions of α-diketone **90**, α-diimine **91** and complexes **92**, **96** – **102** in DCM.*

2.2.1.5 Cyclic Voltammograms of α-Diketone **90**, α-Diimine **91** and Complexes **92** and **98**

Cyclic voltammetry measurements were carried out to gain information of the electrochemical redox behavior of α-diketone **90**, α-diimine **91** and their corresponding formed complexes with $TiCl_4$ **92** and **98**. The experiments were carried out in a closed cell (Pt working electrode) under an inert atmosphere of argon with DCM and acetonitrile as solvents and $[TBA]PF_6$ as electrolyte. *Table 3* displays the obtained voltammetric data.

Table 3: *Voltammetric data for α-diketone **90**, α-diimine **91** and complexes **92** and **98**.*

	E^c_p (V)	E^a_p (V)	$E_{1/2}^{red}$ (V)
α-diketone **90** (DCM)	E^c_{p1} =-2.17	E^a_{p1} = -2.08	$E_{1/2}^{red}$ = -2.13
α-diketone **90** (MeCN)	E^c_{p1} =-2.04	E^a_{p1} = -1.83	$E_{1/2}^{red1}$ = -1.94
	E^c_{p2} = -3.00	E^a_{p2} = -2.82	$E_{1/2}^{red2}$ = -2.91
(α-diketone)$TiCl_4$ **98** (DCM)	E^c_{p1} = -0.43	E^a_{p1} = -1,43	
	E^c_{p2} = -1.16	E^a_{p2} = -1,90	
	E^c_{p1} = -1.62	E^a_{p1} = -2.16	
	E^c_{p2} = -2.06		
α-diimine **91** (MeCN)	E^c_{p1} = -2.01	E^a_{p1} = - 2.33	
	E^c_{p2} = -2.66		
(α-diimine)$TiCl_4$ **92** (MeCN)	E^c_{p1} = -0.58	E^a_{p1} = -0.37 / -0.48	$E_{1/2}^{red}$ = -0.50
	E^c_{p2} = -0.92	E^a_{p2} = -0.75	
	E^c_{p3} = -1.16	E^c_{p3} = -1.02	

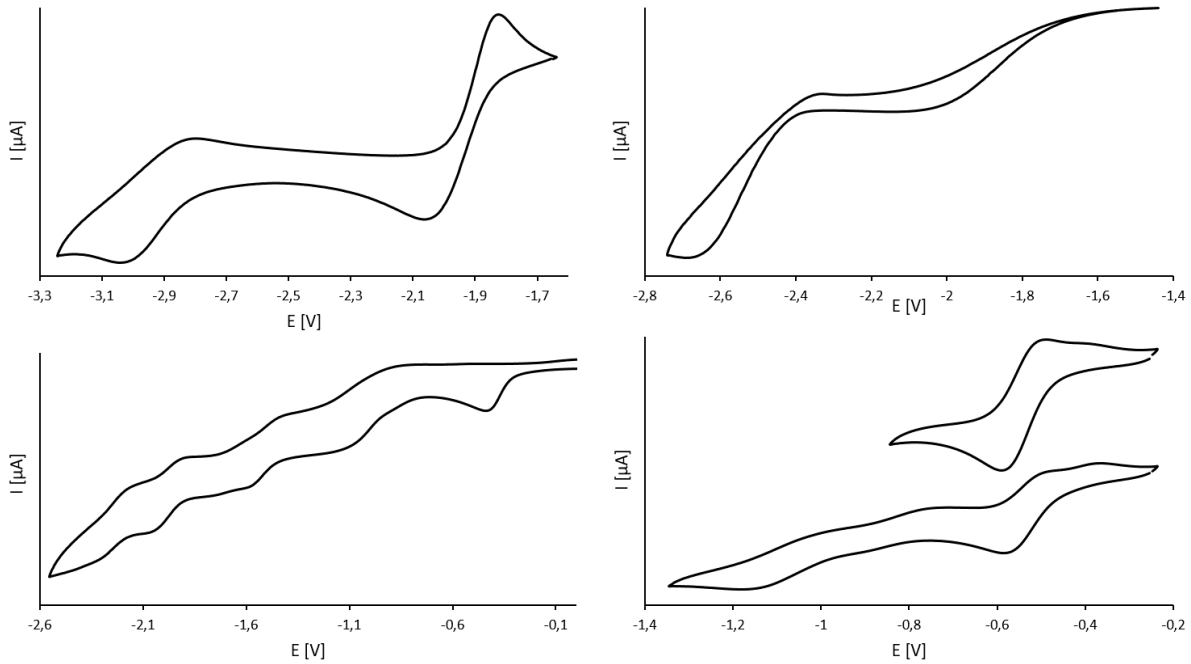

Figure 58: *Cyclic voltammograms of α-diketone **90** (top left), α-diimine **91** (top right), **92** (bottom right) and **98** (bottom left) at 298 K in 0.1 M [TBA]PF_6 in DCM (**98**) and MeCN (**90 – 92**), scan rate 200 mV/s, referenced to Fc/Fc^+.*

CVs of *α*-diketone **90** show a quasireversible redox wave at half potential $E^1_{1/2}$ = -1.94 V and $E^2_{1/2}$ = -2.91 V when measured in acetonitrile and a quasireversible redox wave at half potential $E^1_{1/2}$ = -2.13 V when measured in DCM (*Figure 58*, *Table 3*). The second half potential lies below the possible range for an anodic measurement in DCM and was taken to allow for a comparison with complex **98**, which is not stable in acetonitrile. The CV of **98** looks undefined as several overlapping oxidation- and reduction peak potentials in the area of -0.7 V to -2.2 V can be observed. At -0.42 V an irreversible reduction (E^c_{p1}) occurs, giving rise to the assumption that the following reduction/oxidation processes could be based on the species formed in the first electrochemical irreversible reduction step. However, an electrochemically irreversible mechanism does not automatically exclude a chemically reversible one.

For the CVs of *α*-diimine **91** and complex **92** it is the other way around: since a plain conformation of the nitrogens and C7 and C8 is preferred for the radical anion due to possible electron delocalization, larger structural and geometrical changes occur during reduction of **91** (bonds C7-N1 and C8-N2 are tilted away from each other along C7-C8 in free *α*-diimine **91**, *Figure 59*), leading to a significantly slowed heterogeneous electron transfer rate and therefore an electrochemical irreversible behavior. This ‘rearrangement’ process is not needed for complex **92** and its CV looks defined, although several redox processes are overlapping in the area of -0.7 V to -1.2 V. It furthermore exhibits a quasireversible redox wave at half potential $E^1_{1/2}$ = -0.50 V with two anodic peak potentials (-0.37 V/-0.48 V) overlapping, which likely is caused by the different atropisomers.

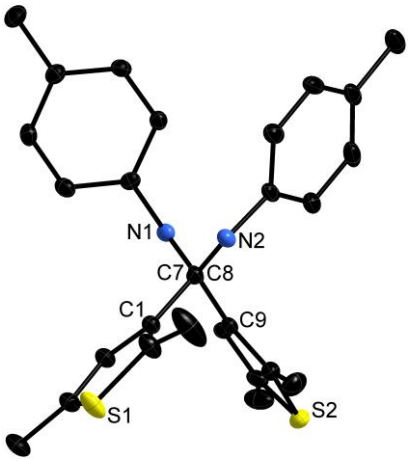

Figure 59: *X-ray crystal structure of α-diimine **91** with view on C7-C8 axis at 50% ellipsoid probability. Hydrogen atoms are omitted for clarity.*

The obtained CVs clearly show that both ligands, *α*-diketone **90** and *α*-diimine **91**, become much more prone for a reduction after formation of the corresponding $TiCl_4$ complexes, as intended. While the CV for **98** points towards electrochemically irreversible behavior upon reduction, the CV of **92** shows no obvious signs of such.

2.2.2 Conclusion and Outlook

As intended, it was possible to synthesize various complexes bearing a DTEthane motif; furthermore could precursor *α*-diimine ligand **91** be prepared. However, reduction of the obtained complexes to achieve the desired DTE structures necessary for photocyclization turned out unsuccessful. Nontheless were interesting findings in regard of those complexes' stereochemistry made, which are described for (*α*-diketone)MCl_4 complexes (M = Ti, Zr, Hf) in *Chapter 2.3* and will soon be described in more detail for the (*α*-diimine)MCl_4 complexes (M = Ti, Zr, Hf, Sn) (manuscript in progress).

2.3 Hexacoordinated M(IV) (M = Ti, Zr, Hf) Tetrachlorido Complexes with Chelating Dithienylethane based 1,2 Diketone Ligand – π-Conjugation as Decisive Factor for Axial Chirality Mode

In this work I carried out the synthesis and characterization of all compounds. I wrote large parts of the result and discussion chapter as well as the experimental section. Dr. Matthias Vogt was the principal investigator and designed the concept of the project. He also wrote the manuscript with other contributors, mainly Robert Langer. Single crystal X-ray diffraction measurements and structure refinements have been carried out by Daniel Duvinage.

Percentage of my contribution of the total workload: experimental concept and design: ca. 80 %, experimental work and acquisition of experimental data: 80 %, data analysis and interpretation: 70 %, preparation of Figures and Tables: ca. 70 %, drafting of the manuscript: ca. 80 %.

The article was published in the journal “European Journal of Inorganic Chemistry“ in 2023 as an open access article:

Dirk Schlüter, Daniel Duvinage, Robert Langer, Matthias Vogt*, *Eur. J. Inorg. Chem.* **2023**, *e202300276*.

DOI: 10.1002/ejic.202300276

The Supporting Information includes charts of all recorded NMR and CV spectra as well as all X-ray crystallographic data and structure refinement and is available free of charge on the journal’s website:

https://chemistry-europe.onlinelibrary.wiley.com/doi/full/10.1002/ejic.202300276

Check for updates

EurJIC
European Journal of Inorganic Chemistry

Research Article
doi.org/10.1002/ejic.202300276

Chemistry Europe
European Chemical Societies Publishing

www.eurjic.org

Hexacoordinated M^{IV} (M=Ti, Zr, Hf) Tetrachlorido Complexes with Chelating Dithienylethane Based 1,2 Diketone Ligand – π-Conjugation as Decisive Factor for Axial Chirality Mode

Dirk Schlüter,[a] Daniel Duvinage,[a] Robert Langer,[b] and Matthias Vogt*[a, b]

1,2-bis(2,5-dimethylthiophen-3-yl)ethane-1,2-dione (**1**, *DTEthane*) reacts with MCl_4 metal precursors of group four (M=Ti, Zr, Hf) via coordination of the carbonyl groups. The molecular structure of complex **2–4** were determined in scXRD studies in the solid state and characterized by means of multi-nuclear and multi-dimensional NMR spectroscopy in solution. While the resulting titanium complex [$TiCl_4$(*DTEthane*)] **2** shows a monomeric structure, where **1** binds in a bidentate fashion, complexes with a Zr (**3**) and Hf (**4**) center have dimeric scaffolds in which the ligands adopt a bridging mode. Quantum chemical calculations using density functional theory (G16, B97D3/def2-TZVP) were used to evaluate the general trend of dimer formation (Ti < Zr < Hf). The molecular structures derived from both scXRD and the DFT optimized structures reveal the carbonyl groups in conjugation with the adjacent thiophene substituent. As a result, they are coplanar and rotation about the two C–C axes (C1–C7; C8–C9) is restricted allowing for only one chiral axis along C7–C8. This gains special importance with respect to previously described complexes carrying the closely related 1,2-endiolato ligand (1,2-bis(2,5-dimethylthiophen-3-yl)ethene-1,2-diolate), in which no coplanarity of the thiophene rings to their neighboring metallacycle was observed allowing for two chiral axes. Noteworthy, further DFT calculations addressing the pathway of racemization found transition states, which are characterized by contrary rotations of both thiophene rings and a loss of conjugation rather than a direct rotation around the axis C7–C8.

Introduction

Ever since their first synthesis by Irie and Mohri in the late 1980s, dithienylethenes (DTE) have gained significant attention as photochemically reversible photochromic compounds.[1] Bearing a hexatriene-motif, they are able to undergo a light-induced switching between the ring-open and the ring-closed isomer (Scheme 1 **A**), which often is accompanied by a significant color change. They can therefore be considered to feature an 'on'- and 'off'-state (ring-closed *vs.* ring open-isomer) in analogy to '0' and '1' of the binary system.[2,3] Due to their excellent photochromic properties[1] they are often regarded to hold potential for applications, such as high density optical memory devices,[1,4] logic gates,[5,6] multi responsive molecular switches,[3,7,8] photochromic conducting polymers,[9] selective fluorescent probes for detection of metal ions,[10] photo-responsive self-assemblies at liquid/solid interfaces,[11] photo-responsive building blocks being able to regulate supramolecular architectures,[12,13] photochromic molecular capsules,[14] light-driven actuators,[15,16] and photo-modulating catalysis.[17]

The typical alkene motif, as part of a (metalla) cyclic system[18–20] with the two thiophene groups in mutual *cis*-arrangement, gives rise to two C–C rotational axes and therefore different rotameric configurations can occur. The rotamers can be described according to the alignment of the thiophenes and the observed helicity: That is, two helical structures with antiparallel alignment of the thiophene units in M- and P-helicity, respectively, can arise, as well as a conformer in parallel alignment (see Scheme 1, **A**).[21] As a result, photoirradiation of the helical isomers (P and M) can lead to the ring closed structures encompassing two stereogenic centers with (*R*,*R*) and (*S*,*S*) configuration, respectively. These stereogenic centers are located at the carbon atoms involved in the formation of the new C–C bond.[21,22] Note that only the antiparallel conformers can react via photocyclization.

A particular case of axial chirality with respect to the above mentioned rotamers occurs when they are fully resolvable at ambient temperature meaning that the individual rotamers are 'locked' due to a sufficiently high barrier of interconversion caused by the (sterically) hindered rotation about the two C–C rotational axes.[23] Then, by definition of Ôki,[24] those rotamers

[a] *D. Schlüter, D. Duvinage, Dr. M. Vogt*
Institut für Anorganische Chemie und Kristallographie
Universität Bremen, 28359 Bremen (Germany)
[b] *Prof. Dr. R. Langer, Dr. M. Vogt*
Martin-Luther-Universität Halle Wittenberg
Naturwissenschaftliche Fakultät II
Institut für Chemie – Anorganische Chemie;
Kurt-Mothes-Str. 2, 06120 Halle (Saale) (Germany)
E-mail: matthias.vogt@chemie.uni-halle.de
www.chemie.uni-halle.de

Supporting information for this article is available on the WWW under https://doi.org/10.1002/ejic.202300276

© 2023 The Authors. European Journal of Inorganic Chemistry published by Wiley-VCH GmbH. This is an open access article under the terms of the Creative Commons Attribution Non-Commercial NoDerivs License, which permits use and distribution in any medium, provided the original work is properly cited, the use is non-commercial and no modifications or adaptations are made.

© 2023 The Authors. European Journal of Inorganic Chemistry published by Wiley-VCH GmbH

EurJIC
European Journal of Inorganic Chemistry

Research Article
doi.org/10.1002/ejic.202300276

Chemistry Europe
European Chemical Societies Publishing

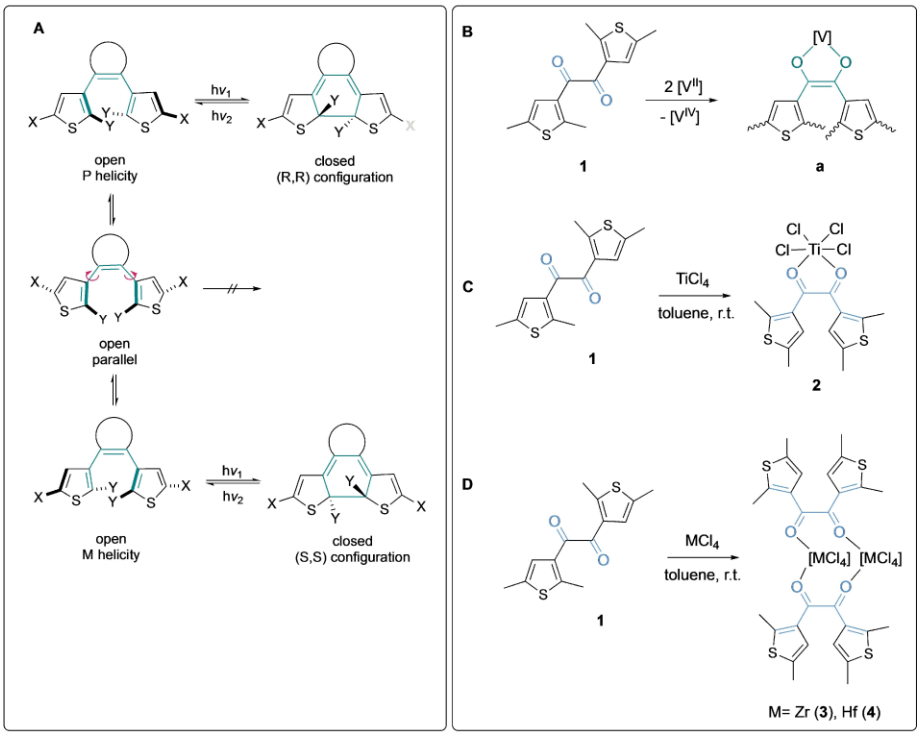

Scheme 1. A Generalization of the rotameric structures in dithienylethene photochromic switches (DTE); B *in-situ* reduction of 1,2-diketone (1) by V(II) to form a $[VO_2C_2]$ en-diolato metallacycle;[18] C and D Synthesis of complex **2**–**4.**

can be referred to as atropisomers. Atropisomerism, derived from Greek *'atropos'* = not turning, describes the hampered interconversion of rotamers about single bonds[23] and was first observed and studied in biaryl derivatives.[25] Atropisomerism finds application in design of chiral ligand systems, being applied in e.g. asymmetric catalysis,[26–30] medicinal chemistry[31] or as an alternative source for the production of chiral drugs.[32] It can also play an important role in modulation of molecular machines, where conformational change about a single bond is crucial.[33] Atropisomerism is a possible feature of DTEs.[22,34]

We have recently reported on the novel DTE-based complexes encompassing a five-membered metallacycle including an chelating en-diolato motif, which coordinates a vanadium(IV) metal center in direct proximity of the hexa-trien system (Scheme 1, **B**). The obtained compounds showed interesting interconversion of distinct atropisomers upon irradiation with UV light and evidence was observed for dynamic reversible C–C bond formation within the ligand backbone, indicating a fast cyclization/ring-opening in solution.[18] The synthesis involved the *in-situ* reduction of the pre-ligand 1,2-bis(2,5-dimethylthiophen-3-yl)ethane-1,2-dione (**1**, *DTEthane*) to the corresponding en-diolato motif (1,2-bis(2,5-dimethylthiophen-3-yl)ethene-1,2-diolate) by an excess of the V(II) precursor. Against this background, we now report on the direct complexation of **1** to MCl_4 metal precursors of the titanium triad (M=Ti, Zr, Hf) as schown in Scheme 1 **C** and **D**..

Results and Discussion

A solution of **1** in toluene reacts instantaneously with the respective MCl_4 (M=Ti, Zr, Hf) precursors to furnish dark red to black precipitates, which could be recrystallized from DCM/*n*-hexane. The obtained crystals were also suitable for single crystal X-ray diffraction (scXRD) analysis, which gave rise to the molecular structures of complex [Ti(κ^2-*O,O*-DTEthane)Cl_4] (**2**), [Zr(μ^2,η^1,η^1-*O,O'*-DTEthane)$Cl_4]_2$ (**3**), and [Hf(μ^2,η^1,η^1-*O,O'*-DTEthane)$Cl_4]_2$ (**4**). Selected interatomic distances for **1**-**4** are summarized in Table 1. As the Ti(IV) metal precursor is fully oxidized an *in-situ* reduction of **1** as previously observed for V(II) precursors,[18] is precluded and **1** gives rise to a chelating 1,2-diketone ligand (k^2-*O,O*-DTEthane, **1**). This is reflected in the obtained structure of **2** by a rather typically C=O interatomic distance of 1.247(2) Å and 1.251(2) Å, respectively only margin-

© 2023 The Authors. European Journal of Inorganic Chemistry published by Wiley-VCH GmbH

10990682c, 0, Downloaded from https://chemistry-europe.onlinelibrary.wiley.com/doi/10.1002/ejic.202300276 by Cochrane Germany, Wiley Online Library on [17/06/2023]. See the Terms and Conditions (https://onlinelibrary.wiley.com/terms-and-conditions) on Wiley Online Library for rules of use; OA articles are governed by the applicable Creative Commons License

EurJIC
European Journal of Inorganic Chemistry

Research Article
doi.org/10.1002/ejic.202300276

Chemistry Europe
European Chemical Societies Publishing

19990682c, 0, Downloaded from https://chemistry-europe.onlinelibrary.wiley.com/doi/10.1002/ejic.202300276 by Cochrane Germany, Wiley Online Library on [17/06/2023]. See the Terms and Conditions (https://onlinelibrary.wiley.com/terms-and-conditions) on Wiley Online Library for rules of use; OA articles are governed by the applicable Creative Commons License

Table 1. Selected bond lengths for diketone ligand **1** and complexes **2**–**4** in Å.

	1[i]	**2** (M=Ti)	**3** (M=Zr)	**4** (M=Hf)
C1–C7	1.467(2)	1.432(2)	1.414(4)	1.418(3)
C7–C8	1.540(2)	1.541(3)	1.527(4)	1.531(3)
C8–C9	1.467(2)	1.425(2)	1.428(4)	1.420(3)
C7–O1	1.224(2)	1.247(2)	1.245(4)	1.253(3)
C8–O2	1.224(2)	1.251(2)	1.244(4)	1.252(3)
O1–M1	–	2.137(1)	2.179(2)	2.171(2)
O2–M1	–	2.112(2)	2.192(2)	2.158(2)

[i]P. Pakulski, D. Pinkowicz.[35]

ally elongated with respect to the free ligand (1.224(2) Å in **1**)[35] and a C7–C8 interatomic distance of 1.541(3) Å, which is in good agreement for a typical C–C single bond. The coordinated carbonyl groups exhibit a O–C–C–O torsion angle of 19.2°. The Ti center resides in an octahedral coordination sphere built by four chlorido ligands and the chelating k^2-*O,O*-DTEthane ligand.

The thiophene rings in the coordinated ligand **1** reside in mutual *syn* alignment with respect to the C–H moiety and remain only slightly shifted from coplanarity with respect to the adjacent carbonyl group (torsion angles in **2**: O2–C8–C9–C10 = 17.9°; O1–C7–C1–C2 = 26.6°). This remarkable structural feature may imply that the π-conjugation in ligand **1** is effective and gives rise to coplanarity (which can be also observed in the structure of the free ligand)[35] resulting in one possible chiral axis along the C7–C8 bond (Figure 1, Scheme 2 **F**, **G**). Consequently, two enantiomers (*R* and *S*) exist for complex **2** (Scheme 2 **G**). In fact, compound **2** crystallizes as racemic mixture in the monoclinic space group $P2_1/n$ with a full molecule in the asymmetric unit.

In sharp contrast, the previously reported related en-diolato complexes[18] (Scheme 1, **a**) show strictly planar –V-(–O–C=C–O–) metallacycles with very small –O–C=C–O– torsions around 0.4°–4.5° and short C=C bonds with thiophene rings strongly deviating from coplanarity with respect to the metallacycle suggesting the presence of two possible C–C chiral axes along the 3-position of the thiophene rings and the endiolato backbone (Scheme 2, **E**). Similar structural features for five-membered metal chelated rings are reported by Sheng-Hua Liu, Zhong-Ning Chen and co-workers for related dithienyldithiolene chelated species **b**[19] and by Wolf and co-workers for copper complexes with DTE ligands carrying an 1,2-bisphosphane motif **c**.[20]

Complex **3** and **4** crystallize in the triclinic space group P-1 with half of the molecule in the asymmetric unit. In contrast to **2**, the molecular structures obtained for complexes **3** and **4**, formed between **1** and $ZrCl_4$ or $HfCl_4$, respectively, are dimeric: Two MCl_4 metal fragments are bridged by two {μ^2,η^1,η^1-*O,O′*-DTEthane} ligands furnishing a 10-membered metallacycle $(MO_2C_2)_2$. This structural composition may be preferred due to the larger ionic radii of the heavier congeners zirconium and hafnium (see also analysis based on DFT calculations below). The two DTEthane ligands bind with their respective μ^2,η^1,η^1-*O,O′* donors each metal center in mutual *cis*-position. Both diketone ligands in **3** and **4**, respectively, show O1–C7–C8–O2 torsions of almost 90° with the thiophene rings located almost orthogonal to each other and with inter plane angles (calculated as average planes through the five-membered thiophene rings) of 86° (**3**) and 84° (**4**), respectively. Similar to complex **2**, the molecular structures of **3** and **4** suggest that π-conjugation in ligand **1** results in coplanarity of the thiophene rings and the adjacent carbonyl group giving rise to only one possible chiral axis (C7–C8) as rotation about the C8–C9 and C1–C7 bonds may be hampered (Scheme 2, **F**). The two centrosymmetric molecular scXRD structures of **3** and **4** exhibit their two respective DTEthane ligands in *R* and *S* configuration and can therefore be identified as achiral *meso* isomers.

The ^{1}H NMR chemical shifts of complex **2** remained similar with respect to free ligand **1** except for the methyl group adjacent to the 2-position of the thiophene ring (see SI, CH_3 group label a), which displays a more significant shift from 2.70 ppm to 2.96 ppm upon coordination of **1** to the titanium

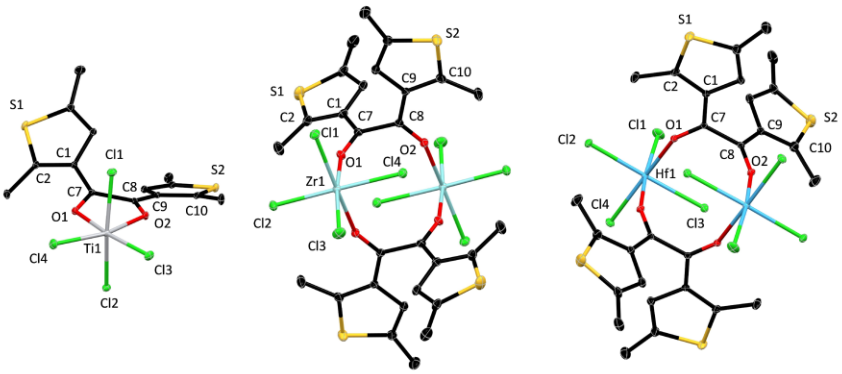

Figure 1. Mercury plots of the molecular structures of complex **2**–**4** derived from scXRD analysis. Thermal ellipsoids drawn at 30% probability. H-Atoms omitted for clarity.

© 2023 The Authors. European Journal of Inorganic Chemistry published by Wiley-VCH GmbH

EurJIC
European Journal of Inorganic Chemistry

Research Article
doi.org/10.1002/ejic.202300276

Chemistry Europe
European Chemical Societies Publishing

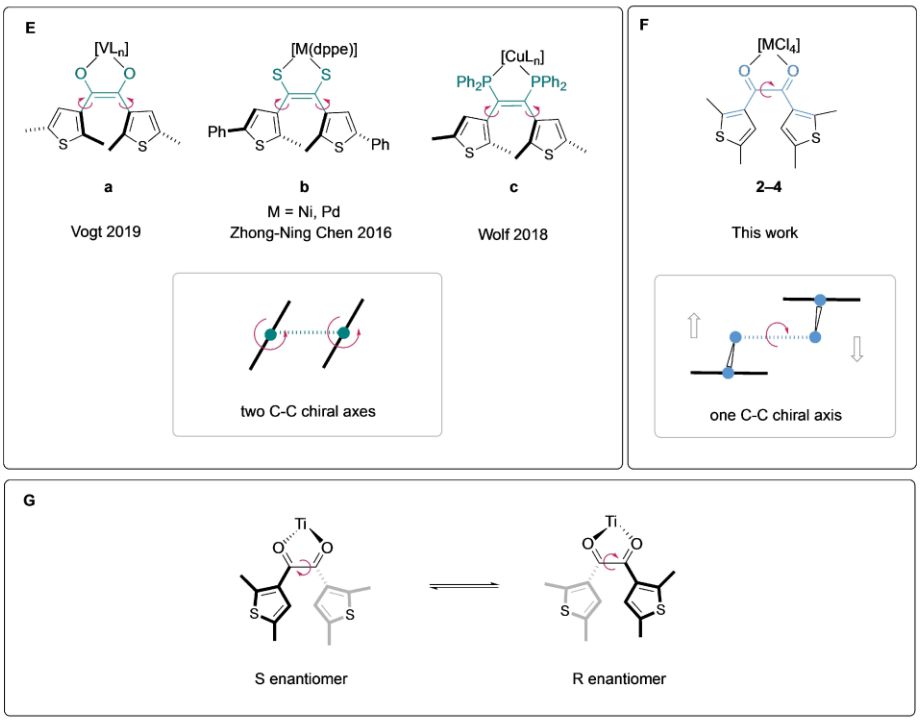

Scheme 2. Axial chirality features in complex **2**–**4** (F,G) and the previously reported examples **a**–**c** (E).

center. The resonances in the $^{13}C\{^1H\}$-NMR spectrum are marginally shifted with exception of the signals associated with the carbonyl-group (coordination shift of almost 3.2 ppm upfield), the quaternary C nucleus in 2-position of the thiophene ring (shift of 18.0 ppm downfield, see SI label b) and the C-atom of the methyl group adjacent to the 2-position of the thiophene ring, showing a shift from 16.1 ppm to 18.8 ppm upon coordination to the $TiCl_4$-fragment. Overall the $^{13}C\{^1H\}$-NMR chemical shifts suggest the conservation of the 1,2-ketone structural motif in **2**.

Complexes **3** and **4** are poorly soluble in dcm-d_2 and show rapid decomposition in coordinating solvents such as thf or acetonitrile. The ^1H NMR spectra of complex **3** and **4** are similar to **2**. However significant broadening is observed, which points toward solution dynamic processes. The $^{13}C\{^1H\}$ NMR spectra are substantially different: We observe seven resonances for **2** (half set) indicating a central molecular plane of symmetry.

In contrast, $^{13}C\{^1H\}$-NMR spectra of **3** and **4** reveal 28 resonances indicating significantly reduced symmetry with respect to **2**. Such an observation might be caused by partial dissociation[36] or a non-centrosymmetric arrangement of the diketone ligand in solution.

DFT Calculations

Quantum chemical investigations based on density functional theory (DFT) were performed on B97D3[38]/def2-TZVP[37,39] level of theory to gain further insights on the relative stability of monomers and dimers as well as the potential racemization pathways within this series. In line with the experimental findings we found that the monomeric complex **2** is 2.8 kcal·mol^{-1} more stable in Gibbs energy than the corresponding dimer, whereas for zirconium (**3**, ΔG =-3.9 kcal·mol^{-1}) and hafnium (**4**, ΔG =-5.9 kcal·mol^{-1}) the dimer was calculated to be more stable in solution (Table 2). A closer look at the optimized geometries of **2**–**4** reveal that each carbonyl group remains conjugated to the attached thiophene substituent and therewith in the same plane with respect to the substituent. This holds true for the monomeric, as well as the dimeric species. For the monomeric species the increased distance of the ligating atoms from titanium to hafnium results in an increased twist angle ($\angle_{OCCO}$ 26.0°… 36.4°), which in case of zirconium and hafnium leads to an increased stability of the dimer ($\angle_{OCCO}$ 98.8°/98.0°).

With view on the monomeric species we investigated the pathway of isomerization for the group four metals and found

© 2023 The Authors. European Journal of Inorganic Chemistry published by Wiley-VCH GmbH

10990682c, 0, Downloaded from https://chemistry-europe.onlinelibrary.wiley.com/doi/10.1002/ejic.202300276 by Cochrane Germany, Wiley Online Library on [17/06/2023]. See the Terms and Conditions (https://onlinelibrary.wiley.com/terms-and-conditions) on Wiley Online Library for rules of use; OA articles are governed by the applicable Creative Commons License

EurJIC
European Journal of Inorganic Chemistry

Research Article
doi.org/10.1002/ejic.202300276

Chemistry Europe
European Chemical Societies Publishing

19990682c, 0, Downloaded from https://chemistry-europe.onlinelibrary.wiley.com/doi/10.1002/ejic.202300276 by Cochrane Germany, Wiley Online Library on [17/06/2023]. See the Terms and Conditions (https://onlinelibrary.wiley.com/terms-and-conditions) on Wiley Online Library for rules of use; OA articles are governed by the applicable Creative Commons License

Table 2. Relative Gibbs energies based on DFT calculation (G16, B97D3/def2-TZVP).

metal	ΔG(dimer – 2·monomers)* kcal·mol^{-1}	ΔG_{rel}(R-isomer)/kcal·mol^{-1}	ΔG_{rel}(TS)/kcal·mol^{-1}	ΔG_{rel}(S-isomer)/kcal·mol^{-1}
Ti	+2.8	0	+13.1	+0.9
Zr	−3.9	0	+12.3	-0.8
Hf	−5.9	0	+12.2	+0.7

*SMD solvation model for CH_2Cl_2 was used.

that the difference in Gibbs energy between the *S*- and the *R*-isomer (Scheme 2 **G**) is with 0.7 to 0.9 kcal·mol^{-1} within the typical error of DFT calculations (Figure 2). It becomes evident that the barrier for racemization is the highest for titanium ($\triangle G_{rel}$(TS) = 13.1 kcal·mol^{-1}), followed by zirconium ($\triangle G_{rel}$(TS) = 12.3 kcal·mol^{-1}) and hafnium ($\triangle G_{rel}$(TS) = 12.2 kcal·mol^{-1}). In all complexes (**2**–**4**) the transition states are characterized by an imaginary vibration, involving contrary rotations of both thiophene rings (about two C–C rotational axes (C1–C7; C8–C9)) and a loss of conjugation rather than a direct rotation around the axis formed by the two carbonyl carbon atoms (C7–C8).

Conclusions

We report on the complexation of the 1,2-diketone ligand 1,2-bis(2,5-dimethylthiophen-3-yl)ethane-1,2-dione (**1**, *DTEthane*) to MCl_4 metal precursors of group four (M=Ti, Zr, Hf). While complex **2** with a Ti center shows a monomeric structure, related complexes with a Zr (**3**) or Hf (**4**) center gave rise to dimeric scaffolds with bridging {μ^2,η^1,η^1-*O*,*O*'-DTEthane} (**1**). DFT calculations (G16, B97D3/def2-TZVP, SMD solvation model = CH_2Cl_2) suggest a general trend of dimer formation in order of Ti < Zr < Hf and reveal the carbonyl groups residing in conjugation with their adjacent thiophene substituent, that is, the carbonyl unit as well as the adjacent thiophene ring are coplanar in monomer **2** as well as in the dimers **3** and **4**. Hence the rotation about the two C–C axes (C1–C7; C8–C9) is hampered. We have identified this structural feature as decisive for the nature and number of the chiral axes with respect to the closely related complexes with a five-membered metallacycle carrying the en-diolato ligand (1,2-bis(2,5-dimethylthiophen-3-yl)ethene-1,2-diolate, Scheme 1, **B**, **a**),[18] which encompass thiophene rings that are not coplanar to their neighboring five-membered metallacycle. While the latter results in two C–C chiral axes leading to chiral helicity (Scheme 2, **E**), the former gives rise to only one chiral axis (C7–C8) thus bringing forth axial chirality as, for instance, observed for classical biaryl compounds (Scheme 2, **F**). The barriers for racemization of complex **2** and the hypothetical monomers [Zr(**1**)Cl_4] and [Hf(**1**)Cl_4] follow the trend Ti > Zr > Hf. Noteworthy, the identified transition states are characterized by an imaginary vibration, involving counter-rotations of both thiophene rings.

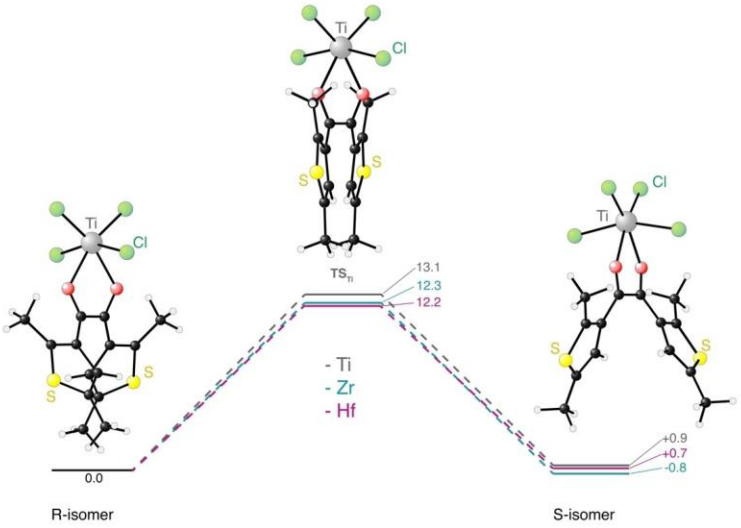

Figure 2. Calculated pathway for the racemization of **2** and the hypothetical monomers [Zr(**1**)Cl_4] and [Hf(**1**)Cl_4]. Gibbs energies based on DFT calculation (G16, B97D3/def2-TZVP) in kcal/mol^{-1}.

© 2023 The Authors. European Journal of Inorganic Chemistry published by Wiley-VCH GmbH

EurJIC
European Journal of Inorganic Chemistry

Research Article
doi.org/10.1002/ejic.202300276

Chemistry Europe
European Chemical Societies Publishing

19990682c, 0, Downloaded from https://chemistry-europe.onlinelibrary.wiley.com/doi/10.1002/ejic.202300276 by Cochrane Germany , Wiley Online Library on [17/06/2023]. See the Terms and Conditions (https://onlinelibrary.wiley.com/terms-and-conditions) on Wiley Online Library for rules of use; OA articles are governed by the applicable Creative Commons License

That is, the interconversion of the *R*- and *S*-isomer proceeds *via* loss of conjugation due to the counter-rotation about the C1–C7 and C8–C9 axis rather than *via* involvement of the rotation about the C7–C8 single bond.

In summary one may state that in contrast to the en-diolato ligand motif **a**, the direct coordination of **1** to a fully oxidized group four $M^{(IV)}$ metal fragment does not furnish a hexa-trien system, which is a prerequisite for a photo-switchable system via a pericyclic ring-opening/ring-closure reaction scheme.[40] However, the herein reported coordination motif in complex **2**–**4** gives rise to remarkable structural features with relevance to the characteristics of the chiral axes.

Experimental Section

Metal tetrachlorides were obtained commercially (Sigma Aldrich, Alfa Aesar) and used as received. Dry solvents were collected from a SPS800 mBraun solvent system. Diketone **1** was prepared following a previously reported procedure.[18] *NMR*: ^{1}H-, ^{13}C-, and 2D NMR spectra were recorded at room temperature on a Bruker Avance Neo 600 MHz and a Bruker Avance 360 MHz spectrometer. Chemical shifts (δ) are reported downfield from tetramethylsilane in parts per million (ppm). Residual solvent signals (5.32 ppm for ^{1}H, 53.84 ppm for ^{13}C in CD_2Cl_2) were used as references. ^{1}H NMR coupling constants (J) are reported in Hertz (Hz), multiplicity is appointed as follows: s (singlet), m (multiplet). Assignments of ^{1}H and ^{13}C resonance signals were based on COSY, HSQC and HMBC spectra. *UV/VIS Spectroscopy*: Experiments were carried out at 298 K on a Varian Cary 50 UV/VIS-spectrophotometer. Cuvettes: 10 mm, synthetic quartz (QS) with Teflon cap. Samples were prepared under an inert atmosphere of argon.

Complex 2: (80 mg, 0.29 mmol, 1.1 eq.) was dissolved in 5 mL toluene and treated with $TiCl_4$ (29 μL, ϱ = 1.73 g/cm^3, 0.26 mmol, 1.0 eq.). Instantly a dark red precipitate occurred. The suspension was stirred at rt for 2 h before removal of the solvent under reduced pressure and washing the crude product with small portions of *n*-hexane led to **2** as dark red to black solid. Crystals suitable for X-ray crystallography were obtained *via* slow diffusion of *n*-hexane into a saturated solution of **2** in DCM. **Yield**: 110 mg (0.23 mmol, 89%); **Mp:** > 200 °C dec.; **^{1}H NMR**: (360 MHz, CD_2Cl_2): δ 6.90 (s, 2H, c), 2.96 (s, 6H, a), 2.42 (s, 6H, b) ppm; **^{13}C NMR**: (90 MHz, CD_2Cl_2): δ 186.5 (g), 169.9 (b), 138.7 (c), 130.6 (a), 127.9 (d), 18.8 (e), 15.2 (f) ppm; **UV/Vis** (CH_2Cl_2): λ_{max} = 270 nm; $\lambda_{shoulder}$ = 314 nm.–

Complex 3: (80 mg, 0.29 mmol, 1.1 eq.) was dissolved in 5 mL toluene and treated with $ZrCl_4$ (60 mg, 0.26 mmol, 1.0 eq.). Instantly a dark red precipitate occurred. The suspension was stirred at rt for 2 h before removal of the solvent under reduced pressure and washing the crude product with small portions of *n*-hexane led to **3** as orange to brown solid. Crystals suitable for X-ray crystallography were obtained *via* slow diffusion of *n*-hexane into a saturated solution of **3** in DCM. **Yield**: 120 mg (0.12 mmol, 90%), **Mp**: > 75 °C dec.; **^{1}H NMR**: (600 MHz, CD_2Cl_2): δ 7.00–6.90 (m, 4H, thienyl), 3.02–2.84 (m, 12H, thienyl-Me), 2.47–2.38 (m, 12H, thienyl-Me) ppm; **^{13}C NMR**: (150 MHz, CD_2Cl_2): δ 188.1, 179.4, 171.2, 167.5, 155.8, 148.2, 138.7, 138.1, 132.8, 131.2, 129.4, 128.0, 124.7, 121.8, 121.3, 120.1, 39.1, 38.6, 32.0, 30.1, 26.9, 26.0, 23.1, 19.8, 16.6, 15.2, 14.3, 13.9 ppm; **UV/Vis** (CH_2Cl_2): λ_{max} = 273, 459 nm; $\lambda_{shoulder}$ = 318 nm.

Complex 4: **1** (80 mg, 0.29 mmol, 1.1 eq.) was dissolved in 5 mL toluene and treated with $HfCl_4$ (80 mg, 0.26 mmol, 1.0 eq.). Instantly a dark red precipitate occurred. The suspension was stirred at rt for 2 h before removal of the solvent under reduced pressure and washing the crude product with small portions of *n*-hexane led to **4** as orange to brown solid. Crystals suitable for X-ray crystallography were obtained *via* slow diffusion of *n*-hexane into a saturated solution of **4** in DCM. **Yield**: 141 mg (0.12 mmol, 90%), **Mp:** > 80 °C dec.; **^{1}H NMR**: (600 MHz, CD_2Cl_2): δ 7.00–6.90 (m, 4H, thienyl), 3.11–2.90 (m, 12H, thienyl-Me), 2.48–2.39 (m, 12H, thienyl-Me) ppm; **^{13}C NMR**: (150 MHz, CD_2Cl_2): δ 187.5, 174.5, 172.3, 168.3, 139.3, 138.2, 134.8, 132.7, 131.5, 131.2, 129.5, 128.9, 128.3, 120.0, 39.3, 32.3, 32.0, 30.1, 29.6, 26.0, 23.1, 20.7, 20.0, 19.6, 16.6, 15.2, 14.3, 13.9 ppm; **UV/Vis** (CH_2Cl_2): λ_{max} = 273, 518 nm; $\lambda_{shoulder}$ = 318 nm.

CCDC Deposition Numbers 2256655(for **2**), 2256654(for **3**), 2256653(for **4**) contain the supplementary crystallographic data for this paper. These data are provided free of charge by the joint Cambridge Crystallographic Data Centre and Fachinformationszentrum Karlsruhe Access Structures service.

Supporting Information

The Supporting Information is available free of charge.

DFT-optimized geometries (XYZ).

NMR spectra, UV/Vis spectra and Cyclic voltammograms (PDF).

Acknowledgements

M.V. wants to acknowledge the generous financial support by the Fonds der Chemischen Industrie (FCI) and the Central Research and Development Fund (CRDF) of the University of Bremen. Open Access funding enabled and organized by Projekt DEAL.

Conflict of Interests

The authors declare no conflict of interest.

Data Availability Statement

The data that support the findings of this study are available in the supplementary material of this article.

Keywords: atropisomerism · chiral axes · carbonyl ligands · dithienylethene · titanium

[1] M. Irie, *Chem. Rev.* **2000**, *100*, 1685–1716.
[2] K. Szaciłowski, *Chem. Rev.* **2008**, *108*, 3481–3548.
[3] S. Pu, D. Jiang, W. Liu, G. Liu, S. Cui, *J. Mater. Chem.* **2012**, *22*, 3517–3526.
[4] G. Jiang, S. Wang, W. Yuan, L. Jiang, Y. Song, H. Tian, D. Zhu, *Chem. Mater.* **2006**, *18*, 235–237.
[5] J. Andréasson, S. D. Straight, T. A. Moore, A. L. Moore, D. Gust, *J. Am. Chem. Soc.* **2008**, *130*, 11122–11128.
[6] H. Tian, *Angew. Chem. Int. Ed.* **2010**, *49*, 4710–4712.
[7] S.-Z. Pu, Q. Sun, C.-B. Fan, R.-J. Wang, G. Liu, *J. Mater. Chem. C.* **2016**, *4*, 3075–3093.
[8] H.-H. Liu, Y. Chen, *Dyes Pigm.* **2011**, *89*, 212–216.
[9] C. P. Harvey, J. D. Tovar, *Polym. Chem.* **2011**, *2*, 2699–2706.
[10] S. Cui, G. Liu, S. Pu, B. Chen, *Dyes Pigm.* **2013**, *99*, 950–956.

© 2023 The Authors. European Journal of Inorganic Chemistry published by Wiley-VCH GmbH

EurJIC
European Journal of Inorganic Chemistry

Research Article
doi.org/10.1002/ejic.202300276

Chemistry Europe
European Chemical Societies Publishing

19990682c, 0, Downloaded from https://chemistry-europe.onlinelibrary.wiley.com/doi/10.1002/ejic.202300276 by Cochrane Germany , Wiley Online Library on [17/06/2023]. See the Terms and Conditions (https://onlinelibrary.wiley.com/terms-and-conditions) on Wiley Online Library for rules of use; OA articles are governed by the applicable Creative Commons License

[11] D. Frath, S. Yokoyama, T. Hirose, K. Matsuda, *J. Photochem. Photobiol. C* **2018**, *34*, 29–40.
[12] T. Hirose, K. Matsuda, *Org. Biomol. Chem.* **2013**, *11*, 873–880.
[13] C. Xiao, W.-Y. Zhao, D.-Y. Zhou, Y. Huang, Y. Tao, W.-H. Wu, C. Yang, *Chin. Chem. Lett.* **2015**, *26*, 817–824.
[14] M. Choudhari, J. Xu, A. I. McKay, C. Guerrin, C. Forsyth, H. Z. Ma, L. Goerigk, R. A. J. O'Hair, A. Bonnefont, L. Ruhlmann, S. Aloise, C. Ritchie, *Chem. Sci.* **2022**, *13*, 13732–13740.
[15] S. Kobatake, S. Takami, H. Muto, T. Ishikawa, M. Irie, *Nature* **2007**, *446*, 778–781.
[16] K. Uchida, S. Sukata, Y. Matsuzawa, M. Akazawa, J. J. de Jong, N. Katsonis, Y. Kojima, S. Nakamura, J. Areephong, A. Meetsma, B. L. Feringa, *Chem. Commun.* **2008**, 326–328.
[17] B. M. Neilson, V. M. Lynch, C. W. Bielawski, *Angew. Chem. Int. Ed.* **2011**, *50*, 10322–10326.
[18] D. Schlüter, F. Kleemiss, M. Fugel, E. Lork, K. Sugimoto, S. Grabowsky, J. R. Harmer, M. Vogt, *Chem. Eur. J.* **2020**, *26*, 1335–1343.
[19] J. Wang, L. X. Shi, J. Y. Wang, J. X. Chen, S. H. Liu, Z. N. Chen, *Dalton Trans.* **2017**, *46*, 2023–2029.
[20] Z. Xu, Y. Cao, B. O. Patrick, M. O. Wolf, *Chem. Eur. J.* **2018**, *24*, 10315–10319.
[21] B. L. Feringa, W. R. Browne, *Molecular Switches*, Wiley-VCH, Weinheim, **2011**.
[22] T. J. Wigglesworth, D. Sud, T. B. Norsten, V. S. Lekhi, N. R. Branda, *J. Am. Chem. Soc.* **2005**, *127*, 7272–7273.
[23] J. E. Smyth, N. M. Butler, P. A. Keller, *Nat. Prod. Rep.* **2015**, *32*, 1562–1583.
[24] M. Öki, *Top. Stereochem.* **1983**, *14*, 1–81.
[25] G. H. Christie, J. Kenner, *J. Chem. Soc. Trans.* **1922**, *121*, 614–620.
[26] A. Miyashita, A. Yasuda, H. Takaya, K. Toriumi, T. Ito, T. Souchi, R. Noyori, *J. Am. Chem. Soc.* **1980**, *102*, 7932–7934.
[27] L. Pu, *Chem. Rev.* **1998**, *98*, 2405–2494.
[28] R. Noyori, *Angew. Chem. Int. Ed.* **2002**, *41*, 2008–2022.
[29] K. Mikami, M. Yamanaka, *Chem. Rev.* **2003**, *103*, 3369–3400.
[30] E. Kumarasamy, R. Raghunathan, M. P. Sibi, J. Sivaguru, *Chem. Rev.* **2015**, *115*, 11239–11300.
[31] P. W. Glunz, *Bioorg. Med. Chem. Lett.* **2018**, *28*, 53–60.
[32] J. Clayden, W. J. Moran, P. J. Edwards, S. R. LaPlante, *Angew. Chem. Int. Ed.* **2009**, *48*, 6398–6401.
[33] S. Erbas-Cakmak, D. A. Leigh, C. T. McTernan, A. L. Nussbaumer, *Chem. Rev.* **2015**, *115*, 10081–10206.
[34] G. W. Gribble, J. A. Joule, *Progress in Heterocyclic Chemistry* Elsevier, UK, **2009**, Vol. 30.
[35] P. Pakulski, D. Pinkowicz, *CSD Private Communication CCDC1895209* **2019**, 1–3.
[36] Note that we have observed facile dissociation of **1** in the presence of coordinating solvents such as thf. For NMR spectral details see Figure S9.
[37] F. Weigend, R. Ahlrichs, *Phys. Chem. Chem. Phys.* **2005**, *7*, 3297–3305.
[38] S. Grimme, S. Ehrlich, L. Goerigk, *J. Comput. Chem.* **2011**, *32*, 1456–1465.
[39] F. Weigend, *Phys. Chem. Chem. Phys.* **2006**, *8*, 1057–1065.
[40] Note that we also tried to react complexes **2–4** with potassium metal or KC_8 aiming for the two-electron-reduction of the ligand, which could allow for the formation of a hexa-trien motif in **1**. However, our attempts did not result in defined reaction products. A cyclic voltammetry study concerning this matter is included in the SI (Table S3, Figure S12).

Manuscript received: May 11, 2023
Revised manuscript received: May 22, 2023
Accepted manuscript online: May 24, 2023

© 2023 The Authors. European Journal of Inorganic Chemistry published by Wiley-VCH GmbH

19990682c, 0, Downloaded from https://chemistry-europe.onlinelibrary.wiley.com/doi/10.1002/cjoc.202300276 by Cochrane Germany , Wiley Online Library on [17/06/2023]. See the Terms and Conditions (https://onlinelibrary.wiley.com/terms-and-conditions) on Wiley Online Library for rules of use; OA articles are governed by the applicable Creative Commons License

RESEARCH ARTICLE

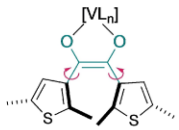

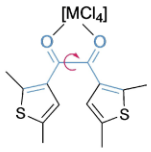

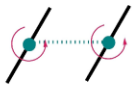

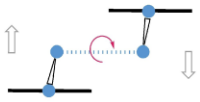

The complexation of 1,2-bis(2,5-dimethylthiophen-3-yl)ethane-1,2-dione to MCl_4 metal precursors furnishes for M=Ti monomeric – and for M=Zr or Hf dimeric complexes.

The conjugation of the carbonyl groups with the adjacent thiophene substituents determines the nature and number of the chiral axes in the ligand scaffold.

*D. Schlüter, D. Duvinage, Prof. Dr. R. Langer, Dr. M. Vogt**

1 – 8

Hexacoordinated M^{IV} (M=Ti, Zr, Hf) Tetrachlorido Complexes with Chelating Dithienylethane Based 1,2 Diketone Ligand – π-Conjugation as Decisive Factor for Axial Chirality Mode

2.4 Investigation of Re/Mn Complexes

Although experiments of a stepwise two-electron reduction of α-diketone ligand **90** or α-diimine ligand **91** to form their corresponding DTE-structure in various complexes turned out unsuccessful (cf. *Chapter 2.2*; ligands shown in *Figure 60*), another attempt in achieving this goal was undertaken, inspired by the findings of Walensky *et al*.[201]

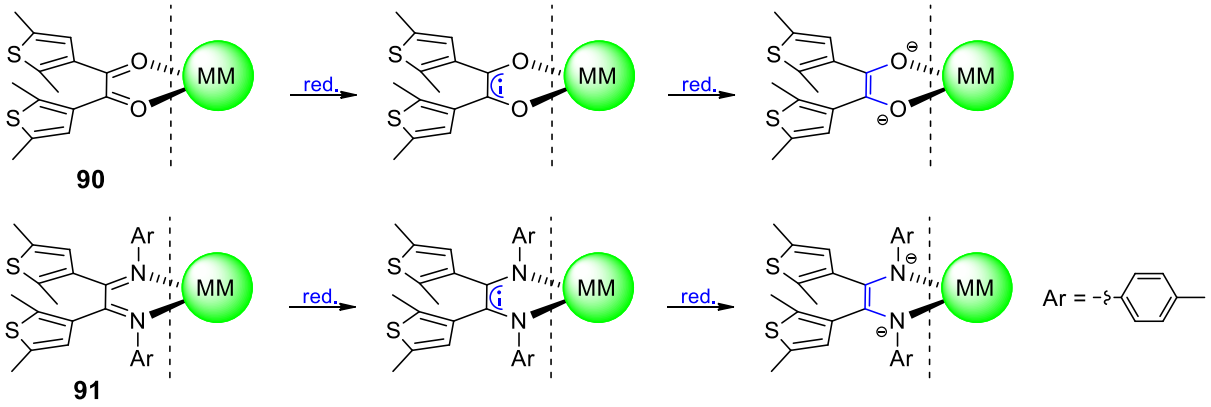

Figure 60: *α-Diketone ligand **90** and α-diimine ligand **91** used in this work and their hypothetical stepwise reduction to form a DTE-structure. MM = metal moiety.*

They reported on a rhenium(I) α-diimine complex (**103**), which they were able to reduce in two steps *via* KC_8 (*Figure 61*).

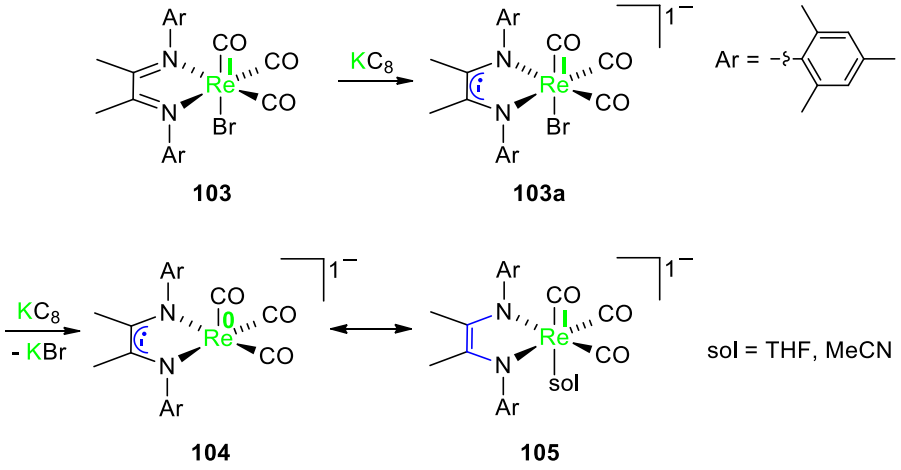

Figure 61: *Stepwise reduction of a Re(I) α-diimine complex, leading to formation of a double bond between the C-atoms of the former imine groups.*[201]

The first reduction takes place on the α-diimine ligand, leading to its corresponding radical anion **103a**. The second reduction takes place on the rhenium, changing its oxidation state from (I) to (0) with bromide simultaneously being cleaved off (**104**). When exposed to polar solvents such as THF or MeCN, an equilibrium forms between **104** and **105**, the latter being a solvent adduct where a THF or MeCN molecule is coordinated in trans position relative to one carbon monoxide. Upon coordination with a

solvent molecule, one electron from the rhenium atom gets passed on to the α-diimine ligand, leading to formation of a double bond between the C-atoms of the former imine groups. Rhenium changes its oxidation state from 0 to +1 in this process.

Stepwise reduction of a rhenium complex analogue to **103** build up with α-diimine ligand **91** (**106**) could lead to complex **108**, which, due to its photoswitchable DTE backbone, might be able to undergo reversible photocyclization (*Figure 62*).

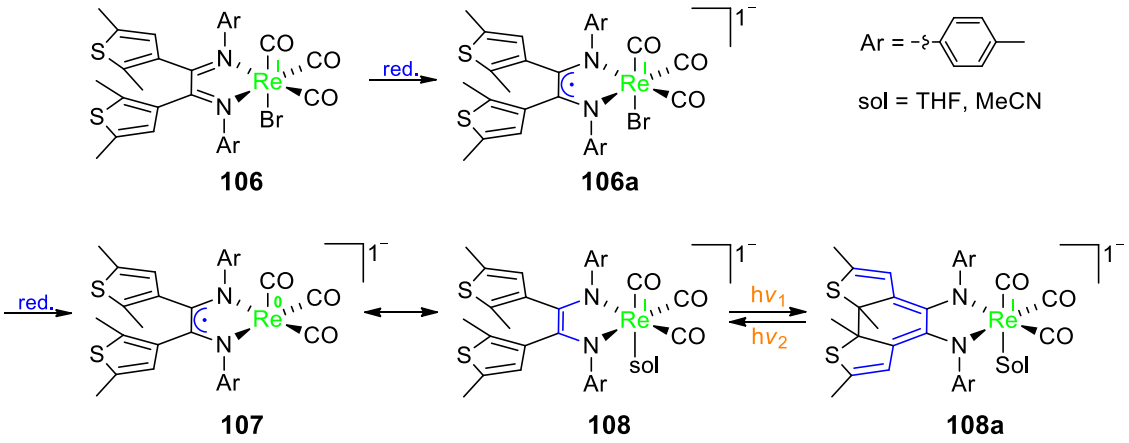

Figure 62: *Proposed stepwise reduction of* ***106****, leading to complex* ***108*** *containing a DTE structure suitable for reversible photocyclization to* ***108a****.*

2.4.1 Synthesis and Characterization of (α-Diimine)Re(CO)$_3$Br (**106**)

2.4.1.1 Synthesis of (α-Diimine)Re(CO)$_3$Br (**106**)

Synthesis of (α-diimine)Re(CO)$_3$Br (**106**) was carried out using a modified procedure reported by Vrieze *et al*.[202] with Re(CO)$_5$Br as precursor: a solution of α-diimine ligand **91** and Re(CO)$_5$Br in toluene was heated up to 100 °C to form product **106** upon release of CO of the rhenium precursor (*Figure 63*).

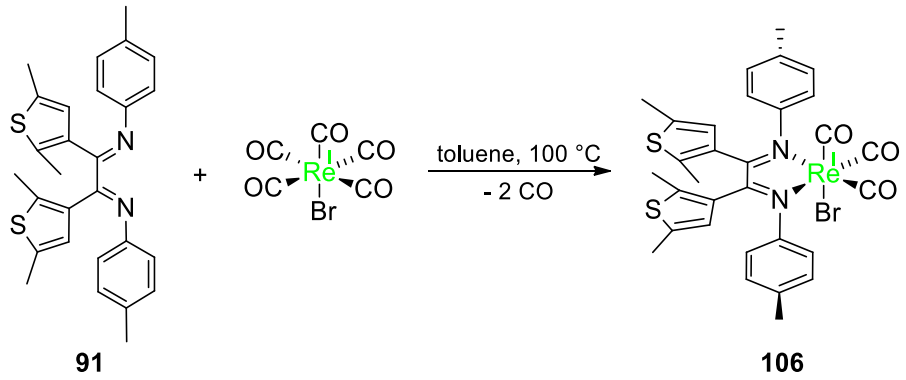

Figure 63: *Synthesis of (α-diimine)Re(CO)$_3$Br (**106**).*

2.4.1.2 NMR Investigation of (α-Diimine)Re(CO)$_3$Br (**106**)

Like the other complexes described in *Chapter 2.2* containing α-diimine ligand **91**, **106** comprises of two atropisomers bearing axial chirality and a non-helical atropisomer, as can be seen by the two sets of signals in the NMR spectra (cf SI, *Figure 64*). Larger changes when compared to free ligand **91** include the signals in *meta*- and especially in *ortho*-position of the phenyl rings to be shifted towards lower field to convergent to one multiplet and the protons of the thienyl rings to be shifted towards higher field.

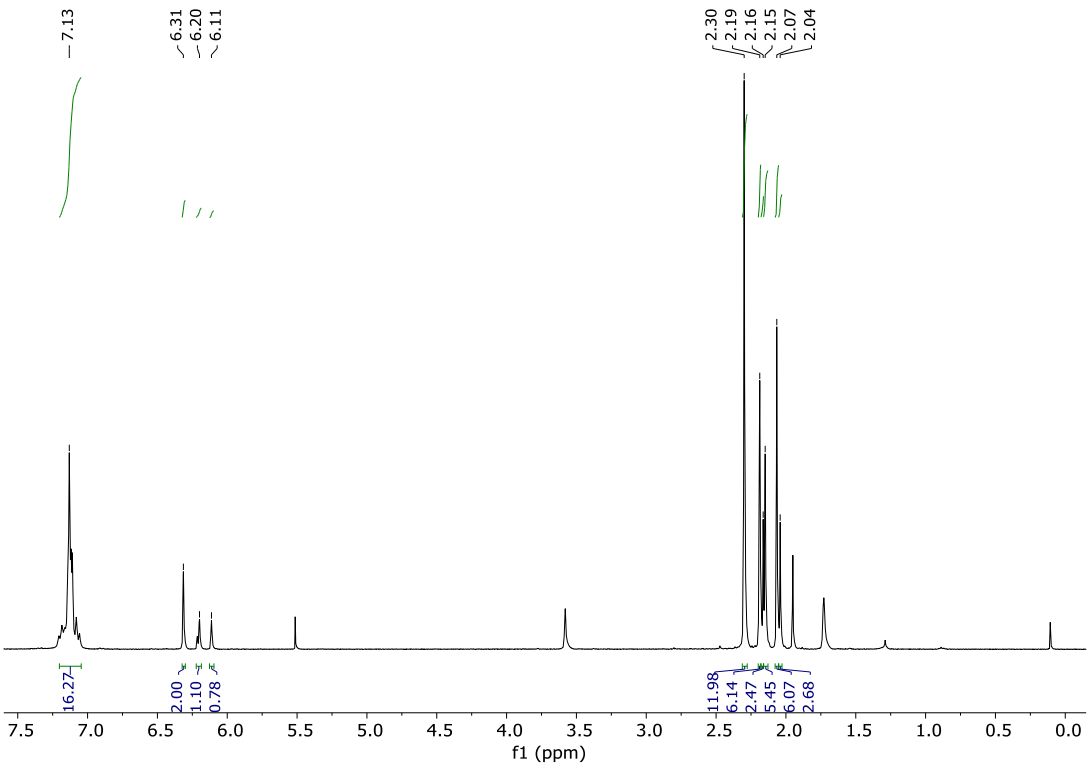

Figure 64: *^{1}H NMR spectrum (360 MHz, THF-d_8) of* ***106****.*

The ^{13}C NMR spectrum also shows two sets of signals (cf. SI).

2.4.1.3 Crystal Structure of (α-Diimine)Re(CO)$_3$Br (**106**)

Compound **106** crystallizes in the space group P2$_1$/n with α-diimine ligand **91** forming, together with the COs and bromide, a slightly distorted octahedral structure around the rhenium atom. The phenyl- as well as the thienyl rings are tilted against the plain formed by N1-C7-C8-N2 in order to reduce steric strain among them (*Figure 65*).

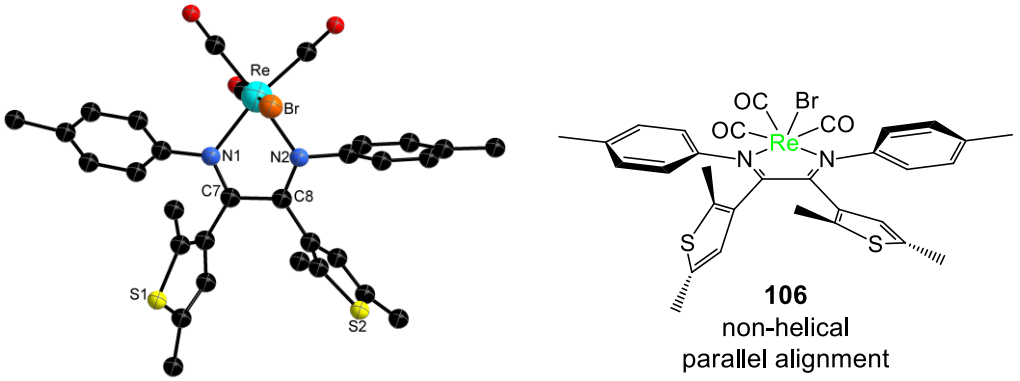

Figure 65: *X-ray crystal structure of* ***106*** *at 50% ellipsoid probability. Hydrogen atoms are omitted for clarity. Selected bond lengths [Å]: C7-C8 = 1.492(1), C7-N1: 1.314(1), N1-Re: 2.166(8), C8-N2: 1.314(1), N2-Re: 2.122(9).*

2.4.1.4 Cyclovoltammogram of (α-Diimine)Re(CO)$_3$Br (**106**)

In order to gain electrochemical information regarding the desired reduction of complex **106**, cyclovoltammetric measurements were carried out. *Figure 66* shows the corresponding cyclic voltammogram (CV), the obtained data is listed in *Table 4*.

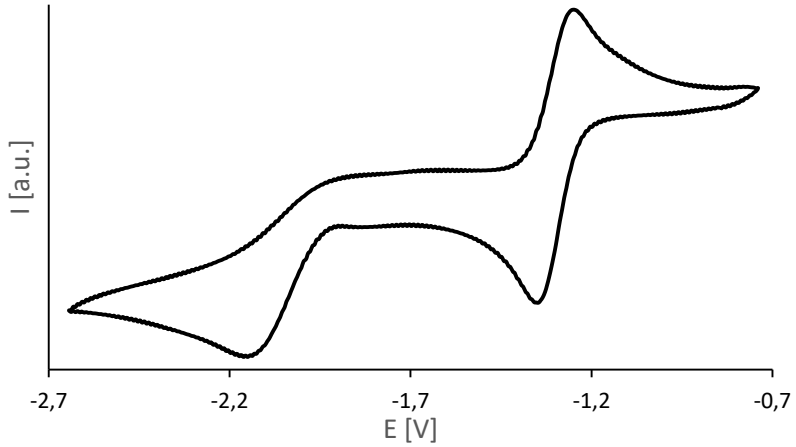

Figure 66: *Cyclic voltammogram of **106** (THF, [TBA]PF_6/0.1 M), scan rate 200 mV/s, potentials plotted vs Fc/Fc^+).*

Table 4: *Voltammetric data for **106** and **91**.*

	E^c_p (V)	E^a_p (V)	$E_{1/2}^{red}$ (V)
(α-diimine)Re(CO)$_3$Br **106** (THF)	E^c_{p1} = -1.35	E^a_{p1} = -1.23	-1.29
	E^c_{p2} = -2.15	E^a_{p2} = -1.99	
α-diimine ligand **91** (MeCN)	E^c_{p1} = -2.01		
	E^c_{p2} = -2.66	E^a_{p1} = -2.33	

Compound **106** shows a reversible half-wave potential at -1.29 V for the first reduction and an electrochemical irreversible behavior for a second reduction step around -2.07 V. The first reduction step can be associated with the formation of radical anion **106a**, the second with formation of **107**, which could explain its irreversible character due to elimination of bromide.

The CV of **106** looks well defined in comparison to the CV of **91** (cf. *Chapter 2.2.1.5*, *Figure 58,* upper right), likely caused by the same reasons described before (cf. *Chapter 2.2.1.5*).

Although measured in different solvents, it can clearly be seen that the α-diimine ligand in complex **106** is much more prone for a reduction than free α-diimine **91** (E^c_{p1} = -1.29 V vs E^c_{p1} = -2.01 V) due to interaction with the metal center (which is in agreement with observations described in *Chapter 2.2.1.5*).

2.4.1.5 UV/Vis Spectra of (α-Diimine)Re(CO)$_3$Br (**106**)

Solutions of **106** in THF or MeCN are deep red in color. Their absorption spectra are depicted in *Figure 67*.

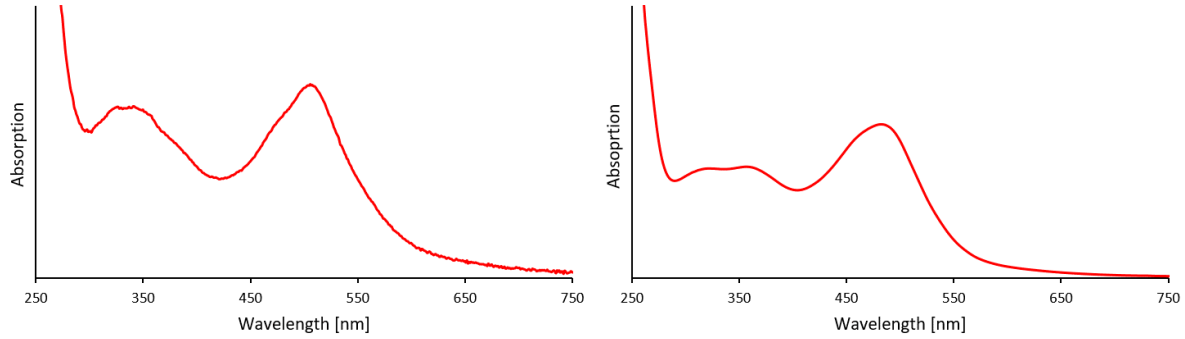

Figure 67: *UV/Vis spectrum of* ***106*** *in THF (left) and MeCN (right).*

The spectra differ only slightly due to solvatochromism with **106** in THF showing broad absorption maxima around 340 nm and 510 nm; in MeCN two maxima can be observed in the area around 340 nm and a maximum around 483 nm. The intense lowest-energy absorption bands can be assigned to MLCT (d_π(Re) → π* (α-diimine)) and/or LLCT transition(s), as they occur regularly for α-diimine-Re(CO)$_3$X complexes (X = inter alia Cl, Br I); the intense absorption bands starting at around 300 nm and below are caused by intraligand transitions within the α-diimine.[203-210] Absorption bands at around 340 can also likely be assigned to MLCT and/or LLCT transition(s).

2.4.2 Reduction of (α-Diimine)Re(CO)$_3$Br (**106**)

Reduction of **106** was first carried out with KC_8, which is easy to handle and could be weighed in a stoichiometric amount. In later experiments pure potassium as reducing agent was used since an excess of the latter had no effect on the outcome of the reduction. To keep consistency, the following described procedure only mentions potassium as reducing agent. All steps were performed under an inert atmosphere of argon and in dry solvents.

In a typical experiment potassium was added to a solution of **106** in THF and the vessel containing the mixture was placed into an ultrasonic bath. After about 40 minutes the deep red opaque solution turned into a transparent orange (*Figure 68*), pointing towards formation of radical anion **106a**.

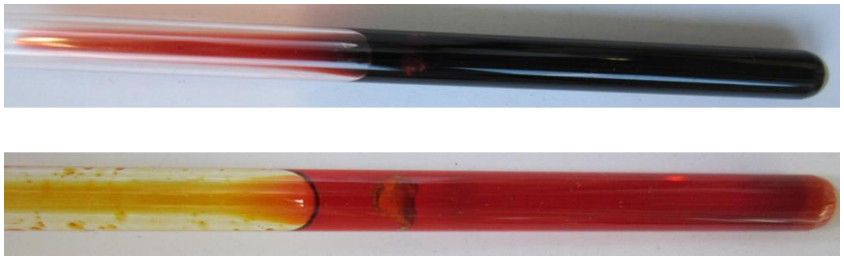

Figure 68: *A Solution of* ***106*** *in THF before (top) and after reduction (bottom).*

Consistent with a single unpaired spin, the ^{1}H NMR spectrum of the orange solution was indicating a paramagnetic species, which was confirmed *via* EPR studies (*Figure 69*).

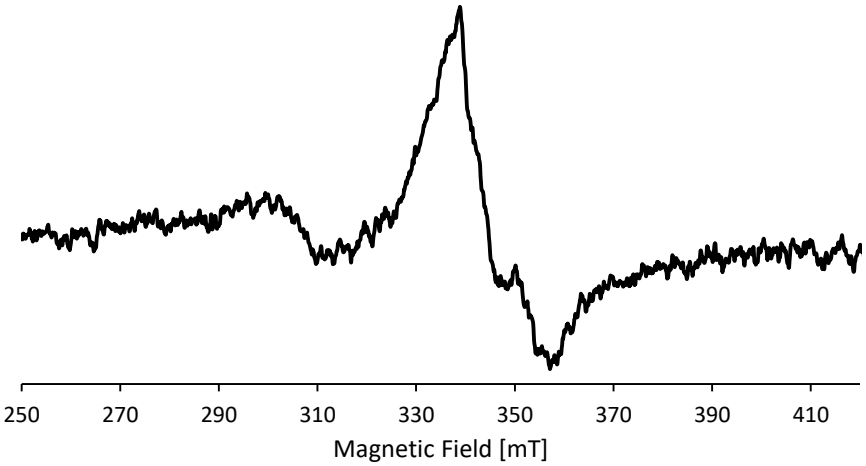

Figure 69: *EPR spectrum of* ***106*** *after reduction with potassium. Experimental parameters: microwave frequency 9.232 GHz, 273.15 K, g-value: 2.005, measured in toluene.*

The evaluated *g*-value (2.005) is in good agreement with a ligand centered radical.[201, 211, 212] However, the signal is broadened and does not show a defined fine pattern as could be expected,[213] which might be caused by the presence of more than one radical (**106a**), due to simultaneous formation of **107**. In accordance with this assumption, a fine white precipitate could be observed as soon as the solution turned transparent. Prolonged treatment in ultrasonic bath led to an increase of this precipitate, indicating the formation of KBr that forms during the second reduction step. Nonetheless no significant change in the EPR spectrum could be observed even after prolonged treatment, thus still indicating a mixture of paramagnetic compounds.

The orange solution that slightly turned murky was then filtered to remove KBr and unreacted potassium. *Figure 70* shows the UV/Vis spectrum of the orange THF solution.

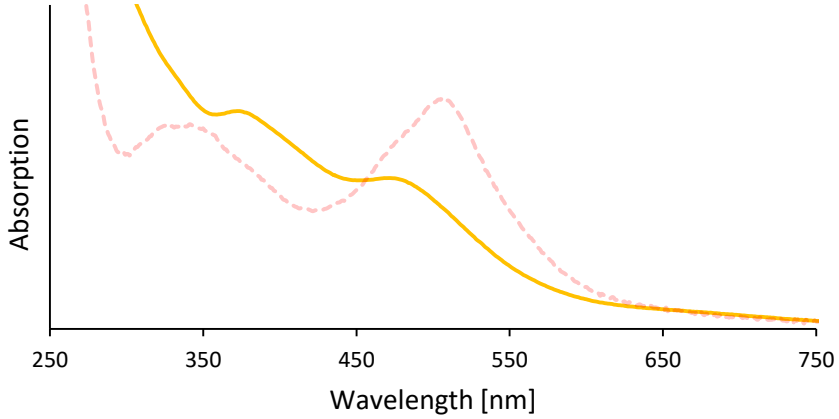

Figure 70: *UV/Vis spectrum of* ***106*** *in THF after reduction with potassium (orange).* ***106*** *in THF (red dashed line) is added for visualization of the changes occurring upon reduction. Note: the spectra show two separately recorded samples and therefore differ in concentration.*

The maxima around 340 nm and 510 nm disappear while two new maxima, not as concise as the ones before, appear at around 480 nm and 381 nm. This is in excellent agreement with the *α*-diimine-$Re(CO)_3X$ complex (X = inter alia Cl, Br) reported by Kaim et al.,[214] which, upon reduction, show a drastic decrease of the intense lowest-energy absorption bands while two new maxima with rising absorption (viewed from long to short wavelength) built up.

To verify if product **108** was formed as a result of the expected equilibrium reaction of **107** with the solvent, various methods to grow crystals suitable for X-ray crystallography, including those used by Walensky *et al.* for **105** and similar products,[201, 215, 216] were tried out; unfortunately without success.

Nonetheless UV/Vis experiments were carried out as a drastic change of color of the solution upon irradiation with UV and its reversal upon irradiation with visible light would indicate photocyclization and could therefore be accounted as indirect proof for the presence of **108**.

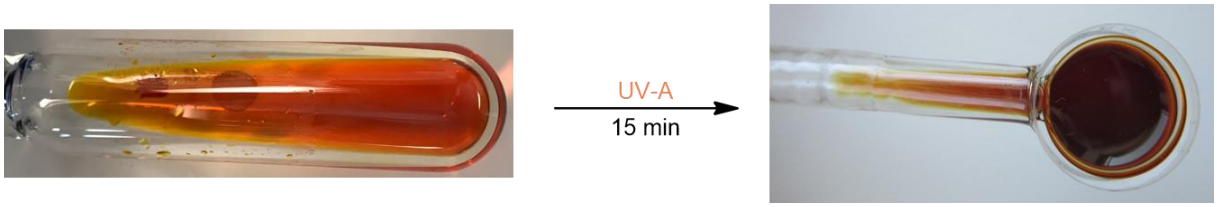

Figure 71*: Filtered orange THF solution before (left) and after irradiation with UV-A for 15 min (right).*

Upon irradiation with UV-A a significant change of color from orange to brown was observed (*Figure 71*). However, the UV/Vis spectra indicated only a slight shift of the absorption maxima to lower energy while the overall intensity of the absorption decreased (*Figure 72*).

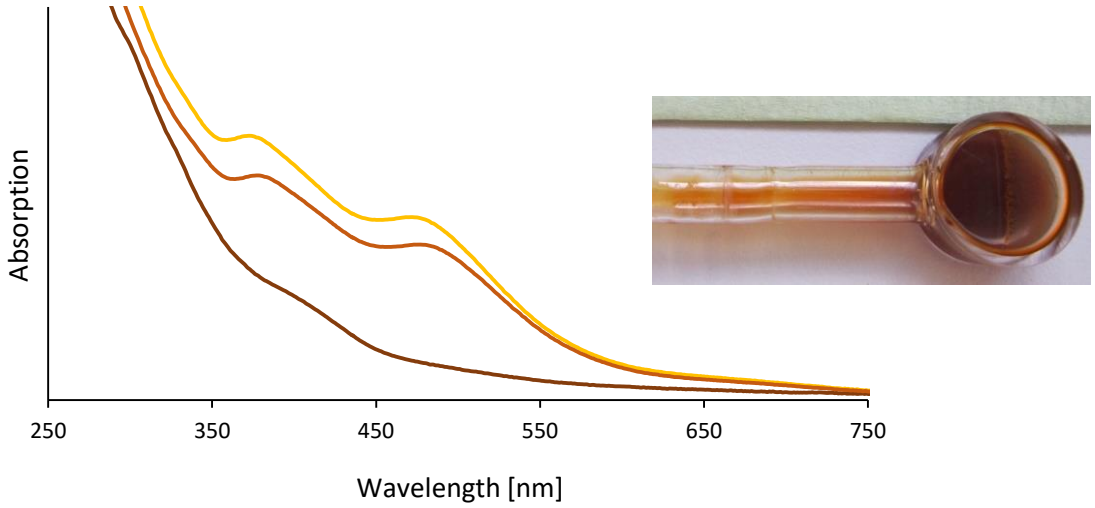

Figure 72: *Left: UV/Vis spectra of the orange THF solution before (orange), after 15 min (tan) and after 180 min (brown) of irradiation with UV-A. Right: THF solution after 180 min irradiation with UV-A showing formation of a precipitate.*

This process was not reversible, as irradiation with visible light of the sample showed no changes in the UV/Vis spectrum. Furthermore, prolonged irradiation with UV-A led to a complete decrease of the prior present maxima in the visible region while formation of a fine colorless precipitate could be observed.

The same result could be monitored for the reduced mixture in MeCN, as irradiation with UV-A also led to a small shift of the absorption maxima to lower energy while the overall intensity of the absorption decreased (*Figure 73*). This was also accompanied by an irreversible change of color from orange to brown.

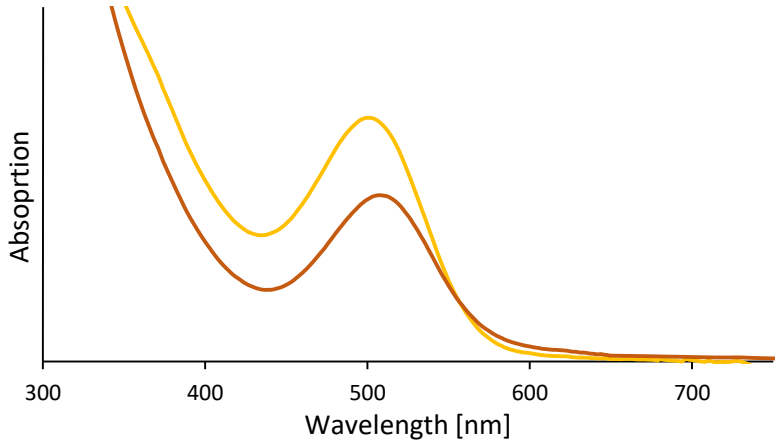

Figure 73: *UV/Vis spectra of the orange MeCN solution before (orange) and after 15 min irradiation with UV-A (tan).*

These results together with the uncertainty if **108** even has formed in the process led to the decision to not further pursue this project.

2.5 Investigation of (α-Diimine)Mn(CO)$_3$Br (**109**)

Walensky *et al*. not only reported on (α-diimine)Re(CO)$_3$Br complexes, but also on the corresponding (α-diimine)Mn(CO)$_3$Br complexes.[201] Since **108** could not be isolated and no evidence for a possible photocyclization upon irradiation with UV-A was observed, it was obvious to aim for preparation and investigation of its manganese analogue in order to see if the desired reduction sequence could be achieved with **109** (*Figure 74*).

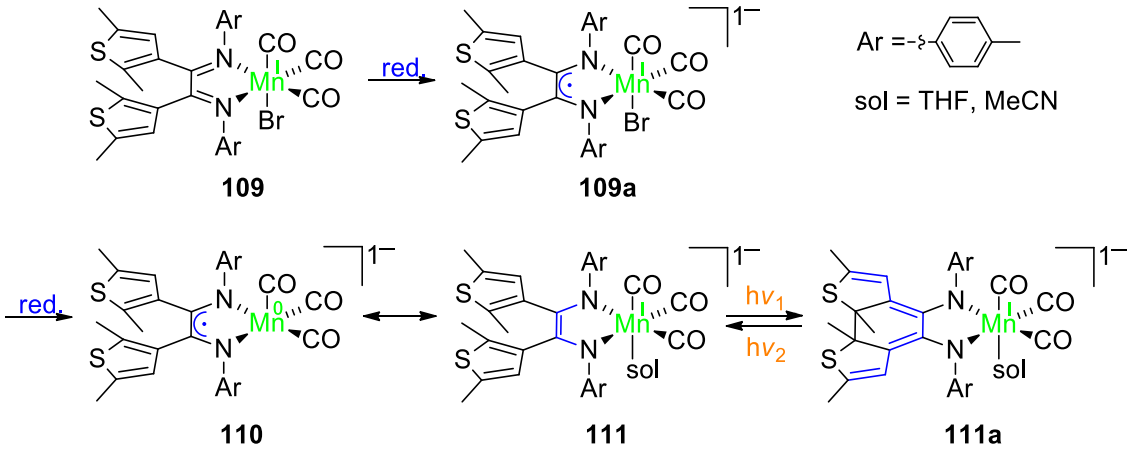

Figure 74: *Proposed stepwise reduction of* ***109****, leading to complex* ***111*** *containing a DTE-structure suitable to undergo reversible photocyclization to* ***111a****.*

2.5.1 Attempted Synthesis of (α-Diimine)Mn(CO)$_3$Br (**109**)

Synthesis of (α-diimine)Mn(CO)$_3$Br **109** was also attempted using a modified procedure reported by Vrieze *et al*.[202] with Mn(CO)$_5$Br as precursor: a mixture of α-diimine ligand **91** and Mn(CO)$_5$Br in toluene was heated up to 60 °C to form product **109** upon release of CO of the manganese precursor (*Figure 75*).

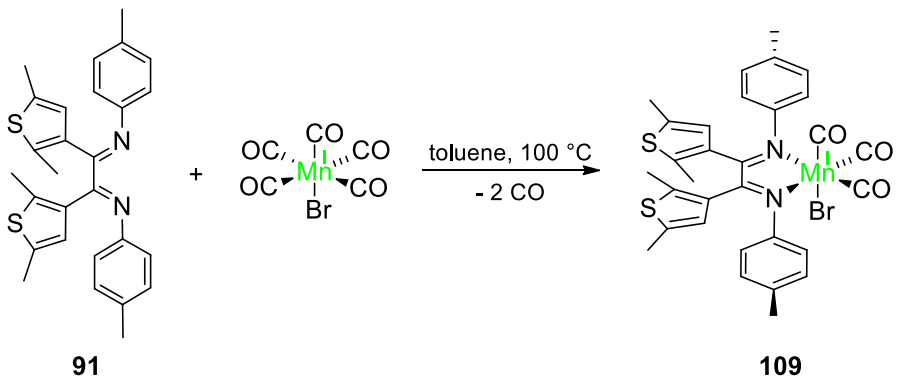

Figure 75: *Proposed synthesis of (α-diimine)Mn(CO)₃Br (****109****).*

After about 20 min of heating the solution turned green, then successively darkened and became deep purple in color. Stirring overnight at room temperature finally led to a brown-red solution (*Figure 76*).

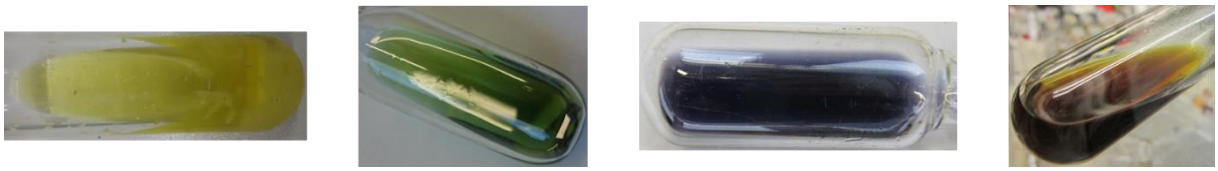

Figure 76: *Solution's color changes during reaction of α-diimine ligand* ***91*** *and* $Mn(CO)_5Br$ *from left to right.*

Surprisingly the obtained crude product was indicative of a paramagnetic species according to ^{1}H and ^{13}C NMR. X-ray crystallography and MS spectrometry revealed the cause of this observation: instead of the expected Mn(I) complex **109**, Mn(II) complex **112** was formed. *Figure 77* shows its corresponding (crystal) structure.

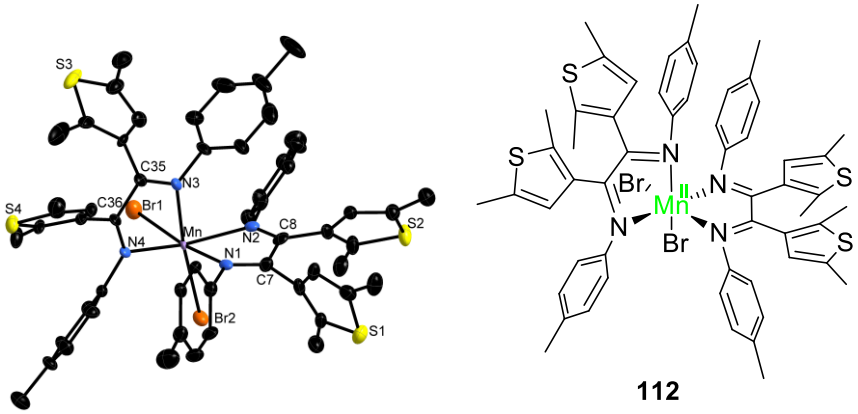

Figure 77: *X-ray crystal structure of* ***112****; 50% ellipsoid probability, hydrogen atoms are omitted for clarity. Selected bond lengths [Å]: C7-C8 = 1.513(1), C7-N1: 1.290(9), N1-Mn: 2.320(6), C8-N2: 1.280(9), N2-Mn: 2.290(6), C35-C36 = 1.502(10), C35-N3: 1.282(9), N3-Mn: 2.316(7), C36-N4: 1.285(9), N4-Mn: 2.293(6), Mn-Br1: 2.582(2), Mn-Br2: 2.592(1).*

The manganese atom is connected to two bromines and coordinated by two *α*-diimine **91** ligands, forming altogether the *cis*-isomer of a distorted octahedral complex with an angle of 105° for Br-Mn-Br. The *cis*-isomer is likely favored over the *trans*-isomer to avoid steric strain between the phenyl rings of the *α*-diimine ligands.

Attempts to crystallize other species from the green and purple solution or from the brown solution after crystallization of **112** turned out unsuccessful. Altering of the reaction conditions, e.g. stirring without heating, led to the same result as the green solution changed color upon standing for a prolonged time. It can therefore be assumed that one or more dynamic equilibriums during the reaction take place, leading to multiple species present in the respective mixtures. From the final reaction mixture (brown-red) it was possible to isolate **112** in a yield of 34%. Its formation supposedly occurred *via* a disproportionation reaction with dimanganese decacarbonyl as side product:

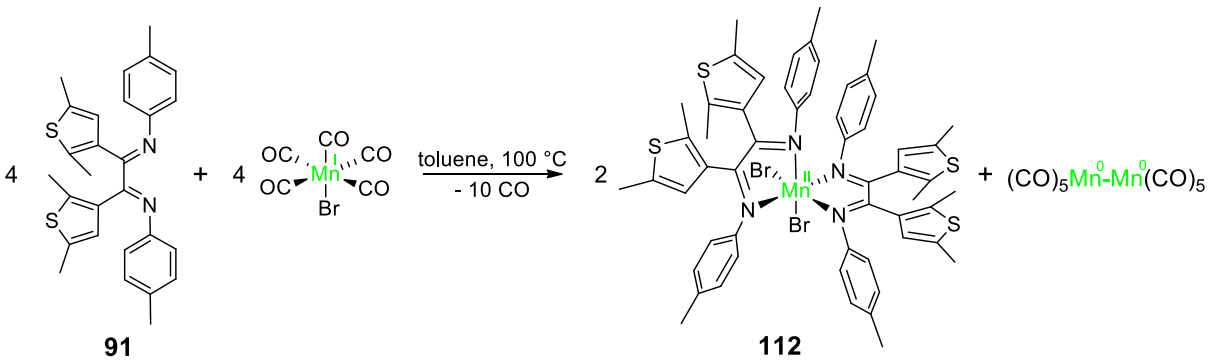

Figure 78: *Proposed disproportionation reaction leading to complex* ***112****.*

Although **109** could have formed during the reaction, it seemed unlikely being able to isolate it from the complex mixtures. Furthermore, due to the occurring disproportionation reaction, **109** could be present only as a minor side product.

Why formation of **112** is favored over **109** remains unclear. Compound **109**, like **106**, is a 18 electron complex, **112** a 17 electron complex. Formation of 17 electron complexes is not unusual for early transition metals though[217] and **112** consists of manganese's most stable oxidation state (+2).[60] Formation of **112** is therefore not surprising, however the fact that Walensky *et al*.[201] obtained their corresponding Mn(I) complexes is as **91** shows high similarity with the ligands used by that working group (*Figure 79*).

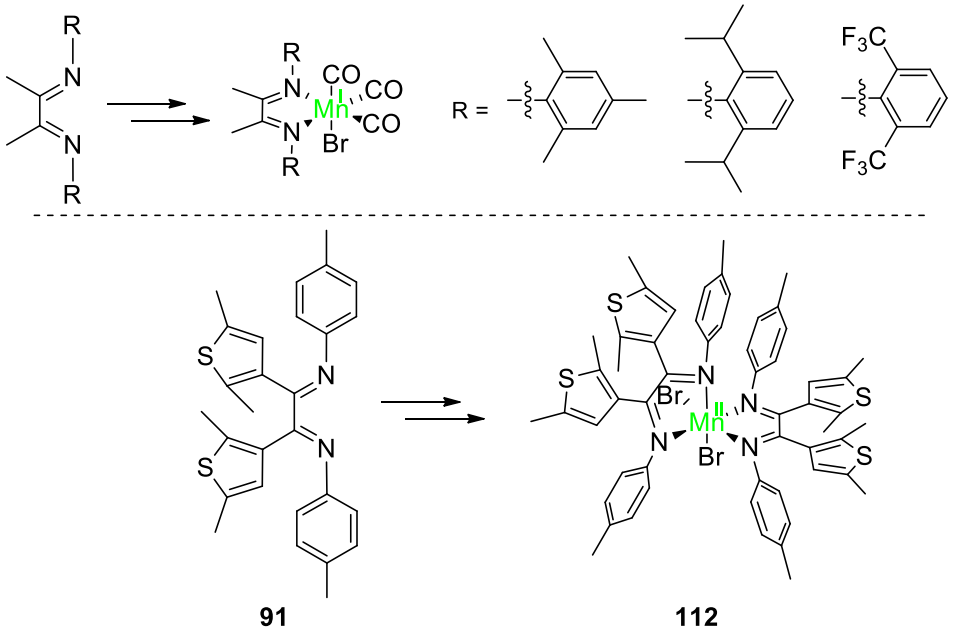

Figure 79: *Ligands used by Walensky et al.*[201] *to obtain the corresponding Mn(I) complexes (upper part); ligand* ***91****, although being similar, leads to formation of Mn(II) complex* ***112*** *(lower part).*

One possibility for the deviating behavior of **91** could be caused by its larger conjugated π-system, leading to a better stabilization of the Mn(II) center. However, the most likely reason is that Walensky

et al.'s ligands are more sterically demanding as their benzene rings are substituted in *ortho*-positions. This would be in good agreement with the observations of H. t. Dieck. He reported on the complexation of Cu(I) halides with several DAB-ligands (DAB = 1,4-diazabuta-1,3-diene): when the DAB contains sterically demanding groups at the nitrogen it is unlikely that it forms complexes of the composition $[(DAD)_2Cu]^+ [CuX_2]^-$, but rather of the composition (DAD)CuX (X = Cl, Br).[218]

Since complex **112** 1) bears two ligands, making it unlikely to reduce one of them twice to form the desired DTE structure and 2) consists of a Mn(II) species being unable to donate an electron to the ligand, it was of no interest for continued studies.

2.6 Investigation of $[(\alpha\text{-Diimine})_2CuCl]^+ [CuCl_2]^-$ (**113**)

Like mentioned in the previous chapter, H. T. Dieck investigated the formation of complexes of DABs and copper(I) halides and reported that, depending on the sterically demand of the groups at the nitrogen, complexes of different composition form (*Figure 80*).[218, 219]

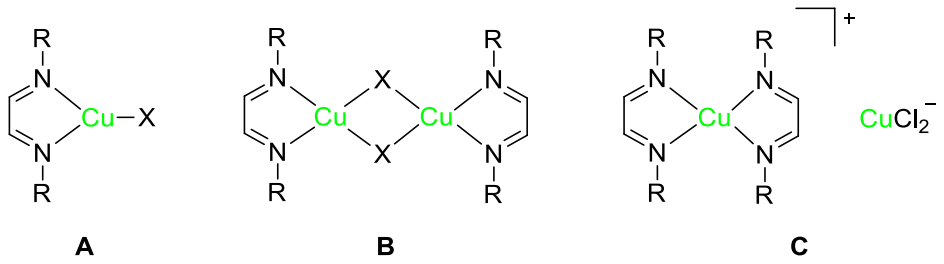

Figure 80: *Compositions of complexes of DAB and copper(I) halides (X = Cl, Br).*[218, 219]

Sterically demanding groups ((*i*Pr)$_2$-CH, 2,6-(*i*Pr)$_2$-C_6H_3) lead preferably to compositions of type **A** or **B**, while groups sterically less demanding lead to formation of type **C**. Dieck also mentioned a special case in which two compositions, namely **A** and **C**, were present in the unit cell in a ratio of 2:1.[218]

In order to see if ligand **91** would only form a complex of type **C** or also complexes of type **A** and/or **B** it was brought to reaction with copper(I) chloride in toluene at 60 °C.

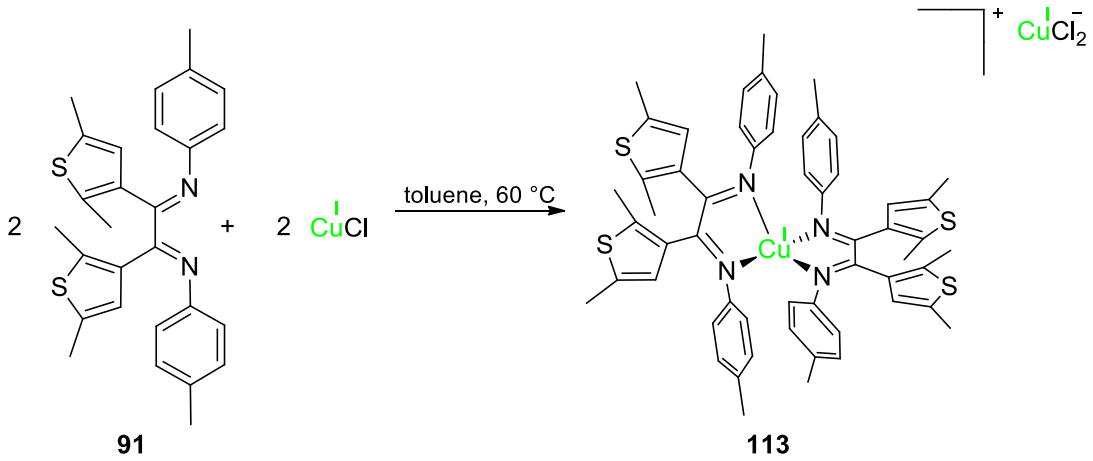

Figure 81: *Reaction of α-diimine **91** with copper(I) chloride leading to formation of **113** and $CuCl_2^-$.*

As anticipated a copper complex of composition **C** formed; *Figure 82* shows the corresponding crystal structure.

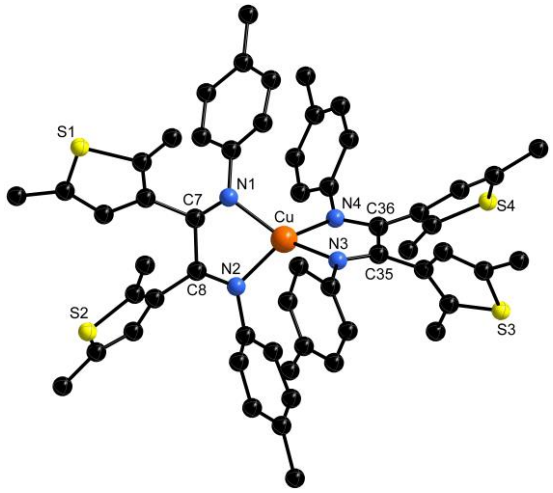

Figure 82: *X-ray crystal structure of **113** shown without $CuCl_2^-$. Due to insufficient data collection in search for crystal structures of other compositions only an image is given here.*

In search for crystal structures of the composition **A** or **B**, several crystals were measured. Since type **C** was of no interest for further intense studies, measurements of this composition were interrupted and no full data set was obtained.

Nonetheless do the collected data allow for a sufficient description of **113**, which crystallizes in the orthorhombic space group $P2_1/n$. The planes consisting of copper and the *α*-diimine units are twisted against each other by about 60°, so that the phenyl units of one ligand are in almost parallel alignment with those of the other ligand. At first sight it seems possible that π-stacking effects could play a role; however distances between the centers of the phenyl rings only measure about 3.5 Å – 4.5 Å, a distance too short for π-stacking effects as physical constraints, namely Van der Waals contacts, are more dominant.[220]

Like complex **112**, **113** bears two *α*-diimine ligands, making it unlikely to reduce one of them twice to form the desired DTE structure necessary for a photocyclization. It can furthermore be assumed that the positive copper(I) center would withdraw electron density from the ligands. Without evidence of formation of the more interesting compositions **A** or **B** the project was not continued further.

2.7 Synthesis of DTE-Metallacycles by Use of Al-/Ga-FLP Precursors

This project was inspired by the studies of Uhl and his working group on their frustrated Lewis pairs (FLP) containing aluminium or gallium (*Figure 83*).[221-223]

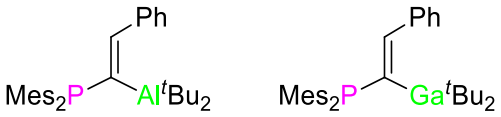

Figure 83: *Synthesized and investigated FLPs by Uhl's working group.*[221-223]

One finding was that when brought to reaction with several substrates, e.g. azides, CO_2, SO_2, alkines, *α,β*-unsaturated carbonyl compounds, the FLPs act as an efficient two electron reductant. In course of the reaction a metallacycle forms with the substrate being reduced while phosphorous changes its oxidation state from +3 to +5 (*Figure 84*).[221-223]

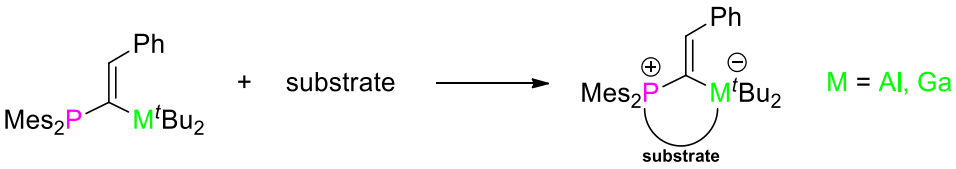

Figure 84: *Simple scheme of Uhl's working group's FLPs reactions with the above stated substrates.*

Attention was especially drawn by the reported reaction of Al-FLP with benzil, which shows a high structural correlation to *α*-diketone ligand **90** (*Figure 85*).

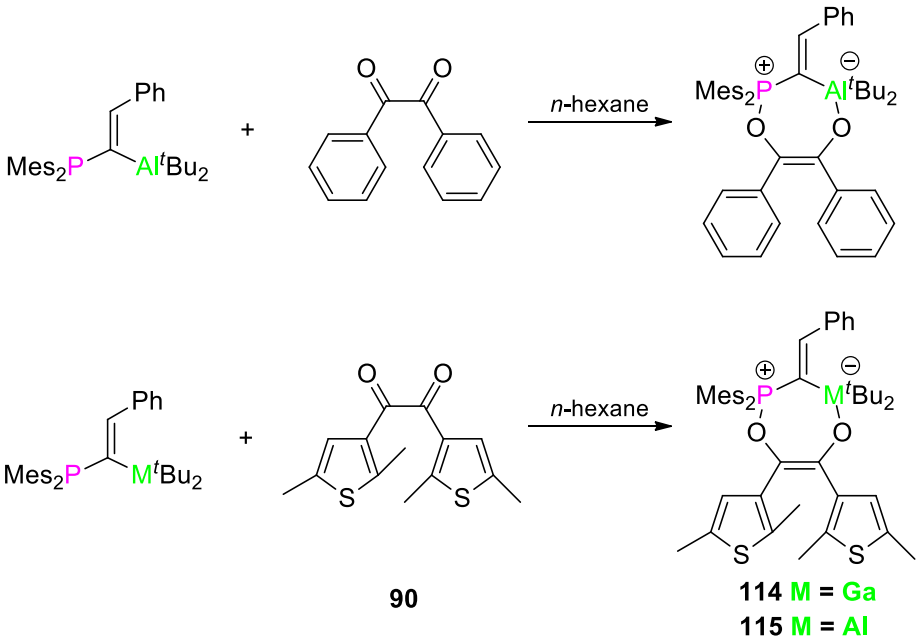

Figure 85: *Reported reaction of Al-FLP with benzil[222] (upper part); postulated reaction of α-diketone* ***90*** *with the Al/Ga-FLPs (lower part).*

This reaction therefore indicated a suitable pathway to not only build the metallacycle, but also to form the desired DTE-structure *via* a concerted reduction.

With the Al/Ga-FLPs, provided by the working group of Prof. Dr. Uhl, the proposed reactions could be carried out. Due to gallium's lower Lewis acidity in comparison to aluminium's[224], which might play an important role for a possible photocyclization, synthesis of **114** was prioritized.

2.7.1 Synthesis of (Endiolato)Ga-FLP Adduct (**114**)

Synthesis of **114** was carried out by stirring a mixture of Ga-FLP and **90** in *n*-hexane overnight at room temperature with a yield of 80%. In later experiments *n*-pentane was used as solvent, as higher yields could be obtained (up to 91%). The product was identified *via* X-ray crystallography, ^{1}H, ^{13}C, ^{13}P NMR and MS.

2.7.2 Crystal Structure of (Endiolato)Ga-FLP Adduct (**114**)

Compound **114** crystallizes in the triclinic space group P-1 with gallium and phosphorous being coordinated in a distorted tetrahedral arrangement. The seven-membered ring is bend in a way that Pitzer strain is reduced and the adjacent sterically demanding groups are able to create space between them (*Figure 86*).

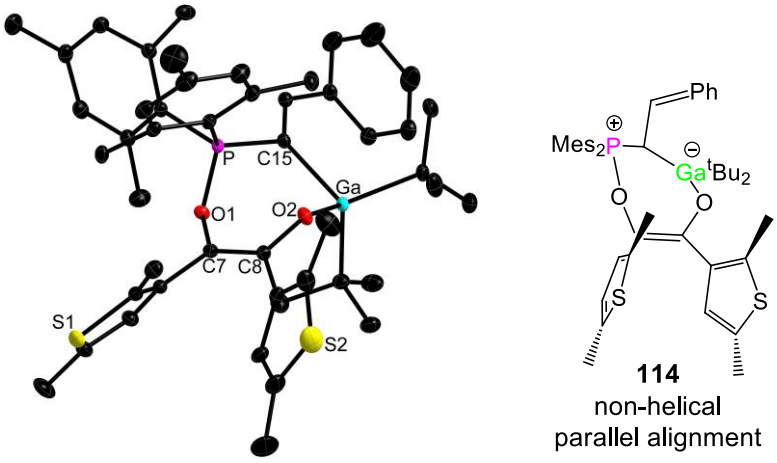

Figure 86: *X-ray crystal structure of* ***114*** *at 50% ellipsoid probability. Hydrogen atoms are omitted for clarity. Selected bond lengths [Å]: C7-C8 = 1.3535(1), C7-O1: 1.4340(1), O1-P: 1.5944(1), C8-O2: 1.3314(1), O2-Ga: 1.9414(1).*

The bond length between C7 and C8 amounts to 1.3535(1) Å, which comes close to the reported bond length for the ethene unit (1.342 Å) of the benzil adduct [222] and is in overall good agreement for a C=C double bond.[8] The thienyl rings stand in parallel alignment.

Due to absence of a mirror plane, a pair of enantiomers is present in the unit cell as shown in *Figure 87*.

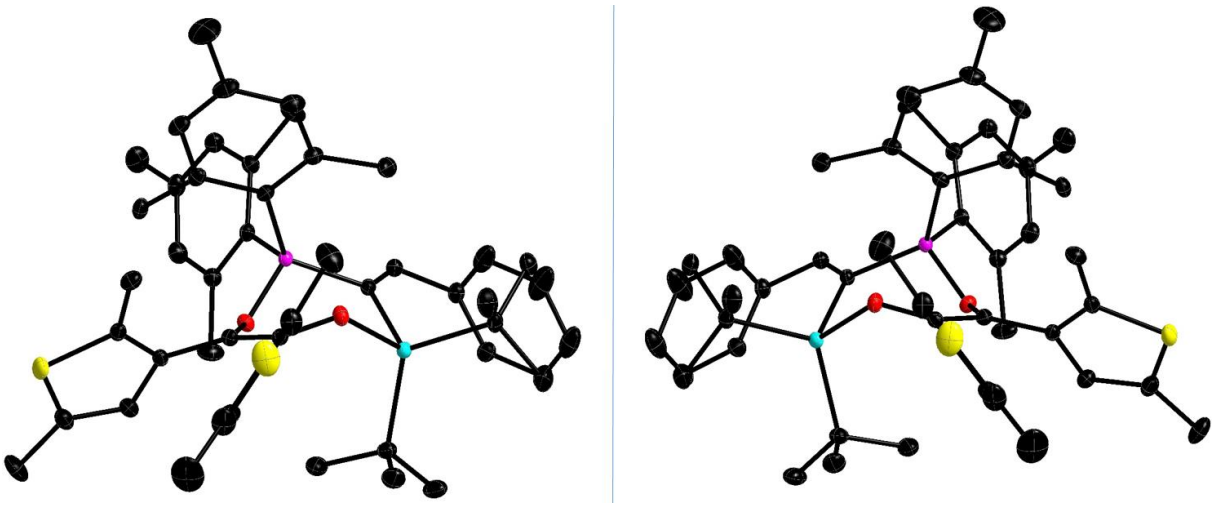

Figure 87: *Enantiomeric pair of* ***114*** *present in the unit cell.*

2.7.3 Photoirradiation Experiments of (Endiolato)Ga-FLP Adduct (**114**)

Compound **114** comprises of the reduced form of *α*-diketone ligand **90**, a DTE that could undergo photocyclization. A solution of **114** therefore was irradiated with UV-A in order to see if a response could be observed. The result is shown in *Figure 88*.

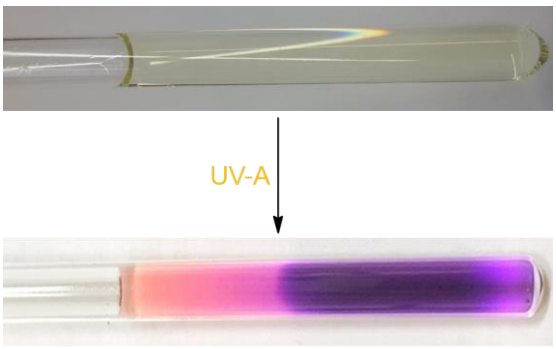

Figure 88: *Irradiation of **114** in d_6-benzene before and after punctual irradiation with an UV-A emitting pointer for 10 seconds.*

Upon irradiation a drastic change of color from pale yellow to deep purple took place immediately, indicating a photoinduced reaction.

2.7.3.1 UV/Vis Experiments of (Endiolato)Ga-FLP Adduct (**114**)

For a more detailed insight into the changes regarding **114**'s photochemical properties during irradiation, several UV/Vis experiments were carried out. First a diluted solution of **114** in toluene was irradiated with UV-A and a UV/Vis spectrum recorded every five minutes (*Figure 89*).

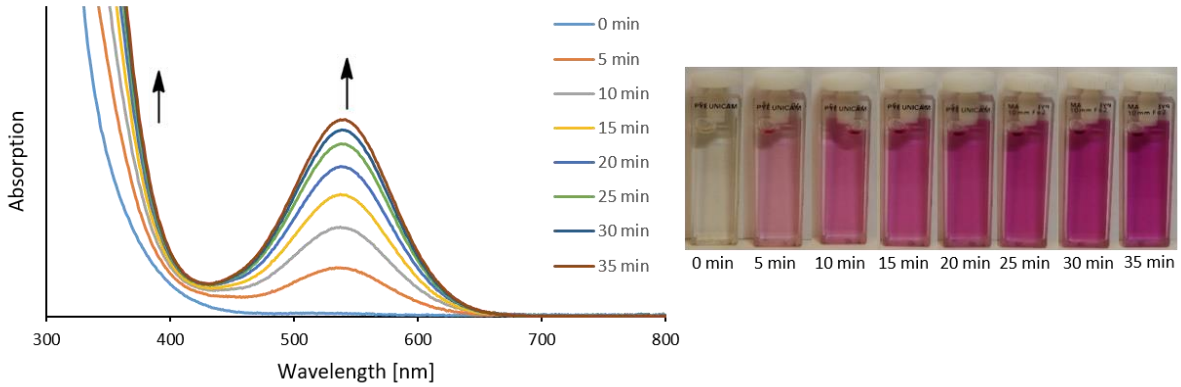

Figure 89: *Irradiation of **114** in toluene with UV-A. A UV/Vis spectrum was taken every five minutes.*

While **114** shows almost no absorption in the area of 470 nm – 650 nm, an absorption maximum forms (λ_{max} = 544 nm) upon irradiation with UV-A. Absorption in the area below 425 nm also intensifies. This

pattern can normally be observed for the ring-closed isomer of DTEs due to n → π* and π → π* transitions of the formed prolonged conjugated π-system.[150, 190, 191, 225-230]

In expectation to see a reverse of the colorization process due to ring-opening the purple sample was exposed to visible light (λ > 450 nm) for several minutes. However, despite overall slightly lower absorptions only a small decrease of the absorption maximum at 544 nm could be observed, implying that the initial photoreaction was irreversible (*Figure 90*).

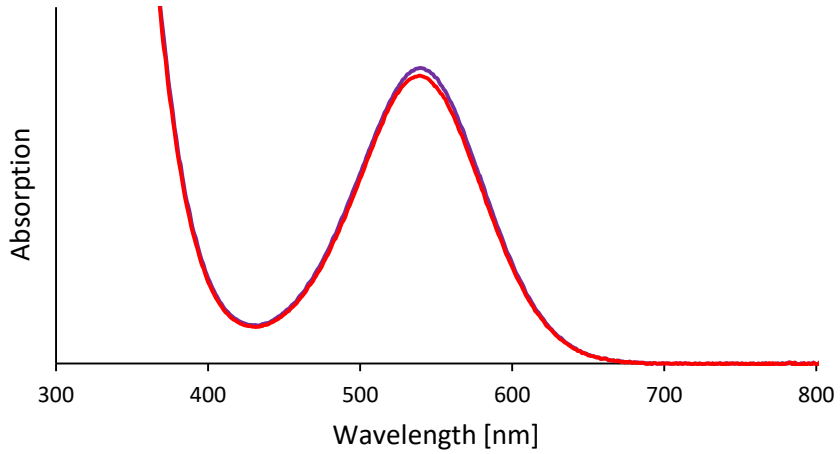

Figure 90: *UV/Vis spectra of purple solution of **114** before (purple line) and after (red line) irradiation with visible light for 10 min.*

Heck et al. reported on a similar observation with some of their DTE-linked biscobaltocenes, which would undergo an irreversible photocyclization.[231] One major difference though is that those DTEs also had a poor yield of the ring closure reaction.

Over the course of several days under normal light conditions the purple solution became completely colorless with no absorption above 400 nm to be observed. Irradiation with UV-A showed – as expected – no effect, indicating a decomposition of the initially formed purple species instead of a reconversion to starting material **114**.

2.7.3.2 NMR Experiments of (Endiolato)Ga-FLP Adduct (**114**)

NMR experiments were carried out to monitor the changes during irradiation with UV-A. *Figure 91* shows the ^{31}P NMR spectra recorded in chronological order.

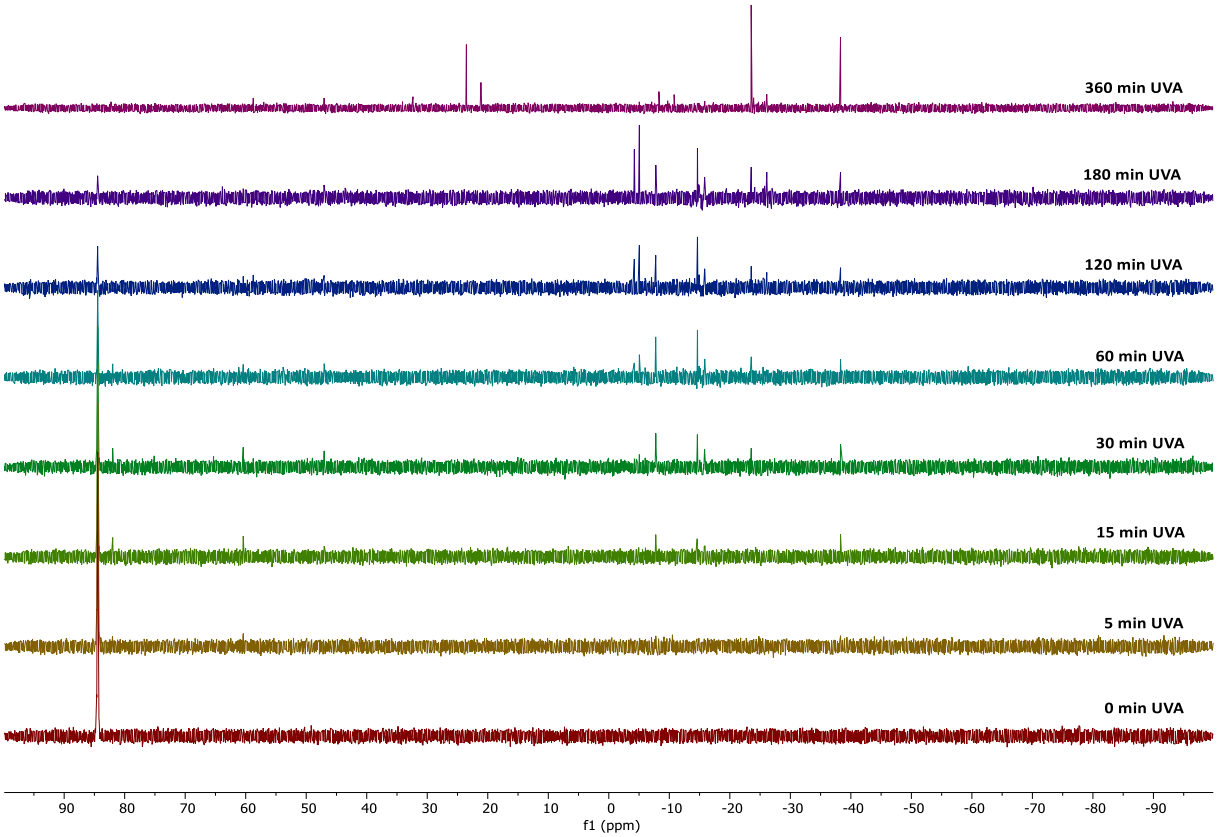

Figure 91: *Chronologically ordered $^{31}P\{^{1}H\}$ NMR spectra (240 MHz, C_6D_6) of* ***114*** *after irradiation with UV-A (bottom to top).*

Before irradiation with UV-A, only one peak for **114** at 84.5 ppm is present (red). After 5 min of irradiation, with the solutions' color already changed (see also *Figure 89*), a small peak at around 60 ppm occurs (ocher). With irradiation progressing, more signals appear in the region of 82 ppm to 47 ppm and -7 ppm to -40 ppm (lime and green). The signals in the higher field area then mostly become more intense and additional peaks evolve while signals in the lower field area, including the peak at 60 ppm, decrease and disappear almost completely (turquois, blue, purple). The final spectrum was taken after another 180 minutes of irradiation. As can be seen, several peaks in the higher field area disappeared, the peaks at -23.6 ppm and -38.3 ppm became more intense. Furthermore two signals appeared at 23.5 ppm and 21.3 ppm (wine red).

Figure 91 verifies that **114** responds to UV-A (even complete conversion). However, not one distinct product peak evolves, as could be expected due to a ring-closure reaction. Instead numerous peaks can be observed over the course of irradiation with some becoming more intense while some disappear again. This indicates formation of several complex equilibriums and irreversible reactions.

In order to gain further insight, ^{1}H and ^{13}C NMR spectra were recorded along. Unexpectedly, those were indicative of a paramagnetic species, wherefore EPR experiments were carried out. *Figure 92* shows an EPR spectrum of **114** in toluene before and directly after irradiation with UV-A.

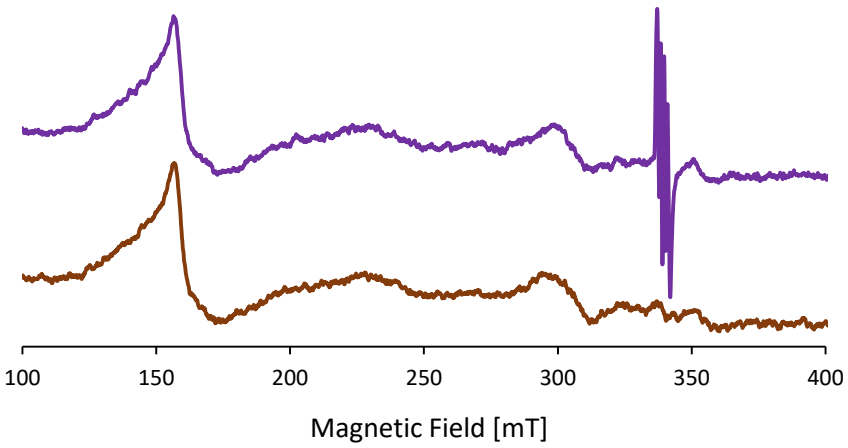

Figure 92: *EPR spectra of* ***114*** *before (brown) and after 10 seconds of irradiation with UV-A (purple). Experimental parameters: microwave frequency 9.403 GHz, 273.15 K, g-value: 2.004, measured in toluene.*

Efforts spent to characterize whether the formed radical contains an organo- or metal centered character failed, as the obtained close up spectrum was of no good enough quality to identify a distinct fine coupling (*Figure 93*).

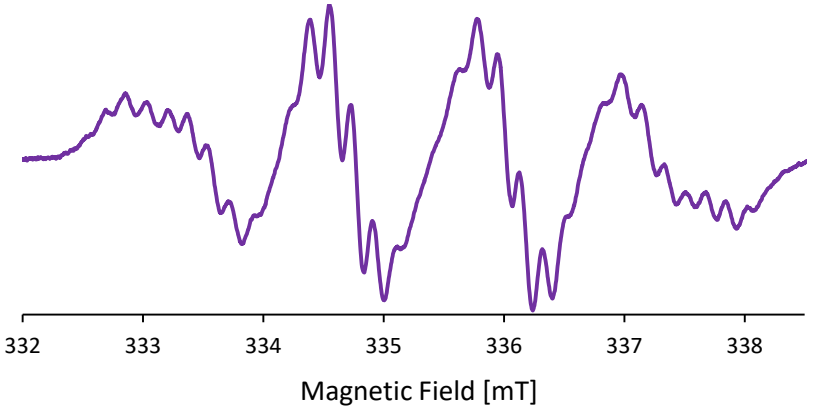

Figure 93: *EPR close-up spectrum of* ***114*** *in toluene. Experimental parameters: microwave frequency 9.403 GHz, 273.15 K, g-value: 2.004, measured in toluene.*

Although possible, no investigation to find a signal of the radical in the $^{31}P\{^{1}H\}$ NMR was undertaken, as such alone could not provide enough details to clearly identify the structure of the radical. Besides, a search for this signal could proof difficult due to the extremely large and unusual range it could fall into.[232, 233] Furthermore the radical species was no longer of high interest, as an additional experiment revealed that it was *not* responsible for the intense purple color: when an irradiated solution of **114** was stored away for several days with exclusion of light, its color barely changed. Nonetheless, EPR measurements of this solution showed that no radical species was present anymore, implying that it was only another side product occurring during photoreaction.

While drastic changes can be observed in the $^{31}P\{^{1}H\}$ NMR spectra during irradiation with UV-A, also significant changes occur thereafter. *Figure 94* shows the decolorization process of the purple solution

of fully converted **114** and the corresponding $^{31}P\{^{1}H\}$ NMR spectra. The solution was kept under inert conditions in a Young NMR tube under normal light conditions.

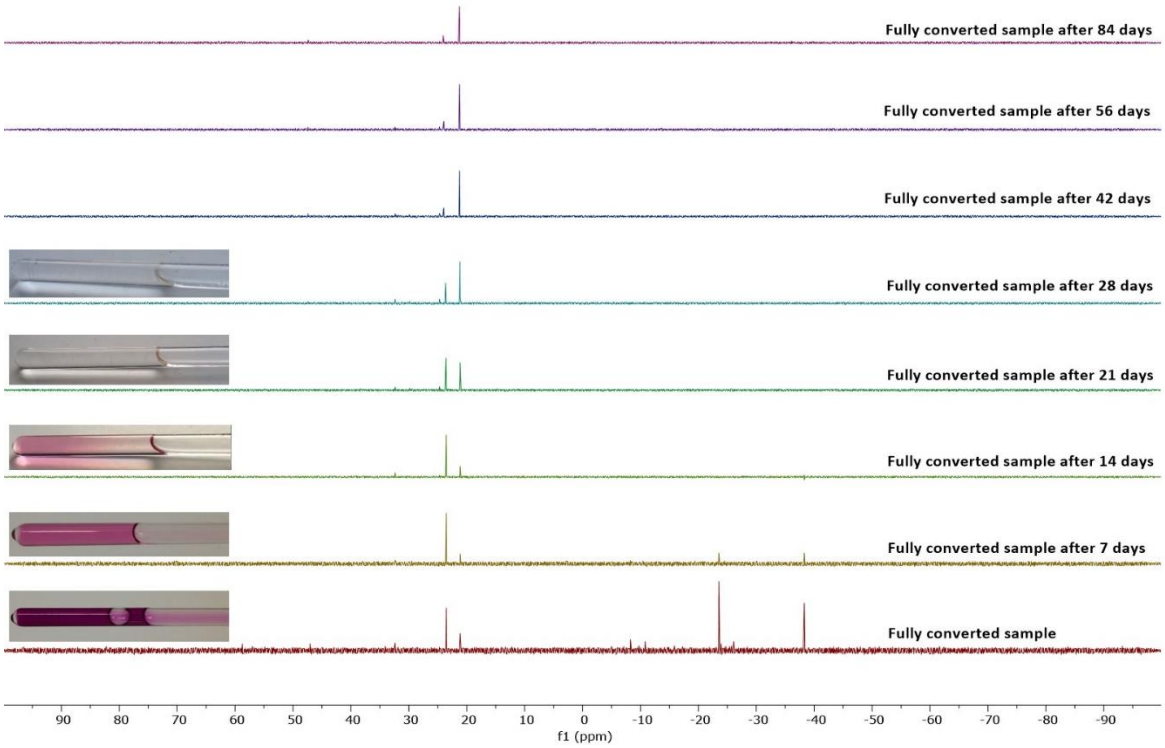

Figure 94: *Chronologically ordered $^{31}P\{^{1}H\}$ NMR spectra (240 MHz, C_6D_6) of fully converted **114** after corresponding past days (bottom to top).*

After seven days, the signals at -23.6 ppm and -38.3 ppm almost disappeared, while the signal at 23.5 ppm became more intense; the signal at 21.3 ppm slightly decreased. The solution turned from deep purple to light purple. In the following an interesting switch of intensity occurred between the signals at 23.5 ppm and 21.3 ppm with parity being reached approximately after 21 days, indicating conversion of one species into the other. During this time the solution became more and more pale. The signals in the area below 0 ppm completely disappeared.

With the solution turned colorless and a ratio of the signals at 23.5 ppm and 21.3 ppm of 1:6 reached, no further changes could be observed. As expected, irradiation of the colorless solution with UV-A showed no effect, since no reconversion of **114** (84.5 ppm) occurred.

Although the radical species disappeared and the $^{31}P\{^{1}H\}$ NMR spectra look much more refined after the described processes, recorded ^{1}H NMR spectra were of no use obtaining more information about the formed species due to massively overlapping signals. Signals in the ^{13}C NMR spectra were, even after prolonged measuring, barely visible. This indicates that, beside the phosphorous contagious species, various species without phosphorous could be present as well, forming a complex mixture.

The respective compounds could therefore be present in a dilution too great to receive pertinent signals.

Nonetheless were several attempts carried out to crystallize the main phosphorous containing species; without success. One major problem was to produce the final mixture in a large scale, as solutions set up for irradiation had to be diluted in order to achieve full conversion of **114**. Even when stored at exposure to sunlight afterwards it took several weeks to obtain the final mixture. Therefore only several mg of **114** could be converted; the final phosphorous containing species likely making up merely a fraction of it.

Attempts to crystallize the purple species shared similar problems, as, in order to avoid formation of crystals of **114**, thorough irradiation of diluted solutions was necessary. Also, even when stored in darkness and cold, a continuous transformation of the purple species could not completely be prevented. Obtaining large amounts of a 'mostly pure' purple solution therefore was not possible.

2.7.3.3 Irradiation Experiments of Crystals of (Endiolato)Ga-FLP Adduct (**114**)

As mentioned in the introduction, DTEs are capable of undergoing photocyclization not only in solution, but also in solid state[159-163]. In order to see if the observed photoreaction of **114** in solution would occur in solid state alike, crystals of **114** were irradiated with UV-A.

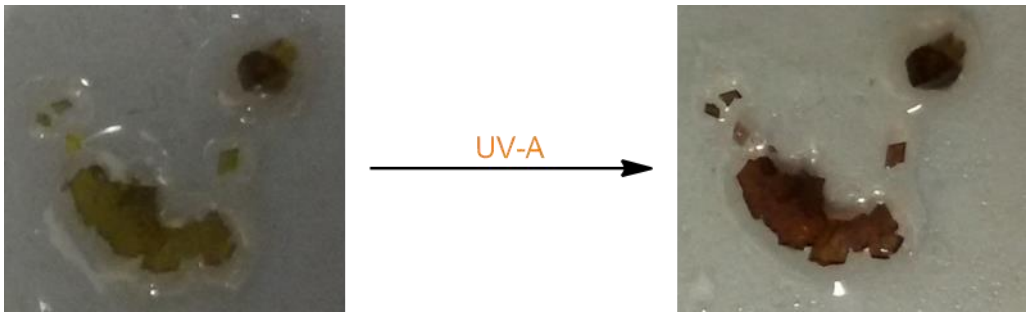

Figure 95: *Crystals of **114** before (left) and after irradiation with UV-A for 5 minutes (right).*

Figure 95 shows that those readily undergo likely the same photoinduced reaction as observed for **114** in solution. Unfortunately, measurements of prolonged irradiated purple crystals showed no transformation when compared to starting material **114**, possibly indicating a photoreaction occurring solely on the crystal's surface. Recrystallization of apparently purple crystals only led to formation of crystals of starting material **114**.

While the responsive nature of **114** accompanied by the strong change of color point towards a photocyclization reaction, the crystal structure itself is not in good agreement with this thesis: a photocyclization of DTEs only is possible in an antiparallel alignment, a requirement which is not

fulfilled by the crystals of **114** where a parallel alignment is present (*Figure 86*). Several crystals of **114** were investigated with all of them showing parallel alignment. However, the thesis of a photocyclization cannot be ruled out entirely, as eventually the applied irradiation was contagious of sufficient energy to induce a change of the structural alignment.

2.7.4 Synthesis of (Endiolato)Al-FLP Adduct (**115**)

Compound **115** was synthesized similar to **114**, with *n*-pentane as solvent due to higher yields (up to 85%) by stirring a mixture of Al-FLP and **90** in *n*-pentane overnight at room temperature (*Figure 96*).

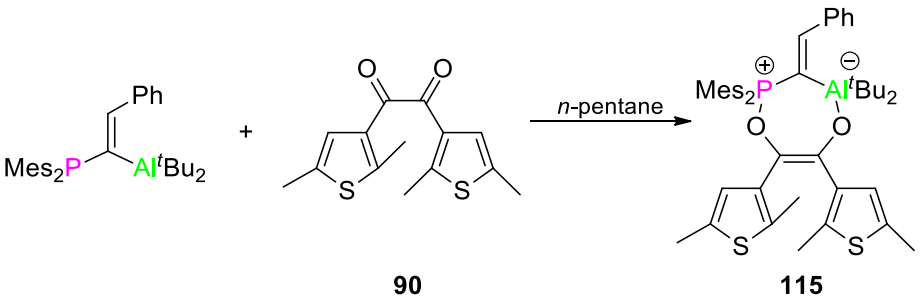

Figure 96: *Synthesis of **115** with Al-FLP precursor.*

Compound **115** was identified *via* X-ray crystallography, ^{1}H, ^{13}C, ^{13}P NMR and MS.

2.7.5 Crystal Structure of (Endiolato)Al-FLP Adduct (**115**)

Like **114**, **115** crystallizes in the triclinic space group P-1 with aluminium and phosphorous being coordinated in a distorted tetrahedral arrangement. The seven-membered ring is also bend in a way that Pitzer strain is reduced and the adjacent sterically demanding groups are able to create space between them (*Figure 97*).

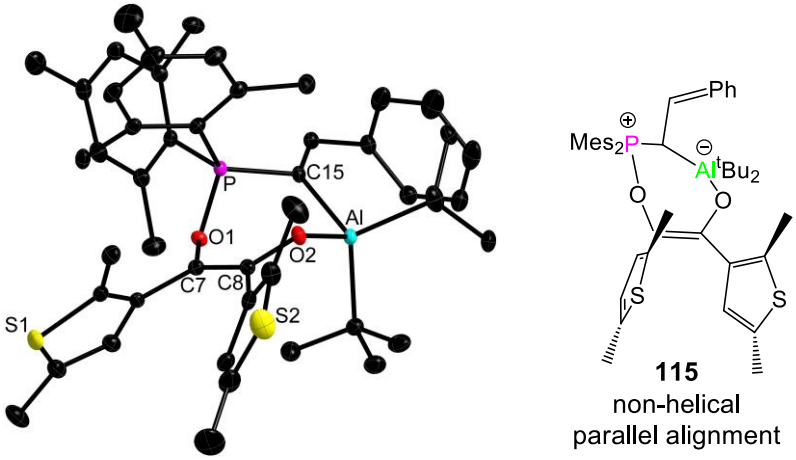

Figure 97: *X-ray crystal structure of* ***115*** *at 50% ellipsoid probability. Hydrogen atoms are omitted for clarity. Selected bond lengths [Å]: C7-C8 = 1.3461(2), C7-O1: 1.4334(1), O1-P: 1.5963(1), C8-O2: 1.383(1), O2-Al: 1.7994(1).*

The bond length of C7-C8 (1.3461(2) Å) is in good agreement for the reported double bond length of the reported derivate formed by Al-FLP and benzyl.[222] Compared to **114**, the O2-M bond of **115** is much shorter (1.7994(1) Å (Al) vs 1.9414(1) Å (Ga)) due to aluminium's smaller atom radius. All other bond lengths show no significant deviation.

Like **114**, due to absence of a mirror plane, a pair of enantiomers is present in the unit cell (not shown).

2.7.6 UV/Vis Experiments of (Endiolato)Al-FLP Adduct (**115**)

Compound **115** behaves in regard of irradiation with UV-A in the same way as **114** by showing a rapid response to the stimulus. One difference is that a solution of **115** in toluene displays a deeper purple color upon irradiation, which is reflected in slightly shifted absorption areas and a maximum absorption peak at 558 nm (vs 544 nm of **114**).

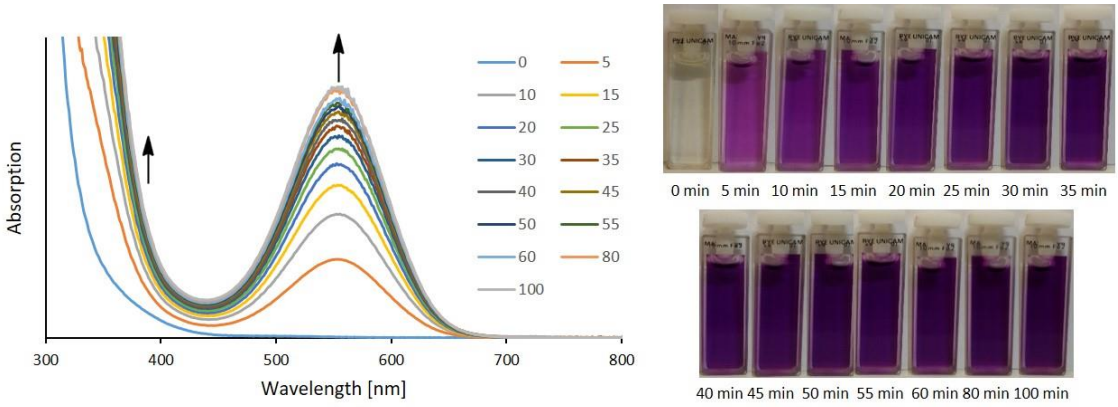

Figure 98: *Irradiation of* ***115*** *in toluene with UV-A. UV/Vis spectra were taken after different time intervals.*

The overall pattern is the same, with absorption in the area below 450 nm and 450 – 655 nm drastically increasing upon irradiation. While this points towards formation of the ring closed isomer of the DTE unit due to n → π* and π → π* transitions of the formed prolonged conjugated π-system,[150, 190, 191, 225-229] **115** also shows no reverse reaction when exposed to visible light (λ > 450 nm), implying an irreversible photoreaction.

2.7.7 NMR Experiments of (Endiolato)Al-FLP Adduct (**115**)

$^{31}P\{^{1}H\}$ NMR spectra of **115** during irradiation and thereafter also show many parallels to those of **114**. *Figure 99* shows the $^{31}P\{^{1}H\}$ NMR spectra of **114** and **115** before and after full conversion.

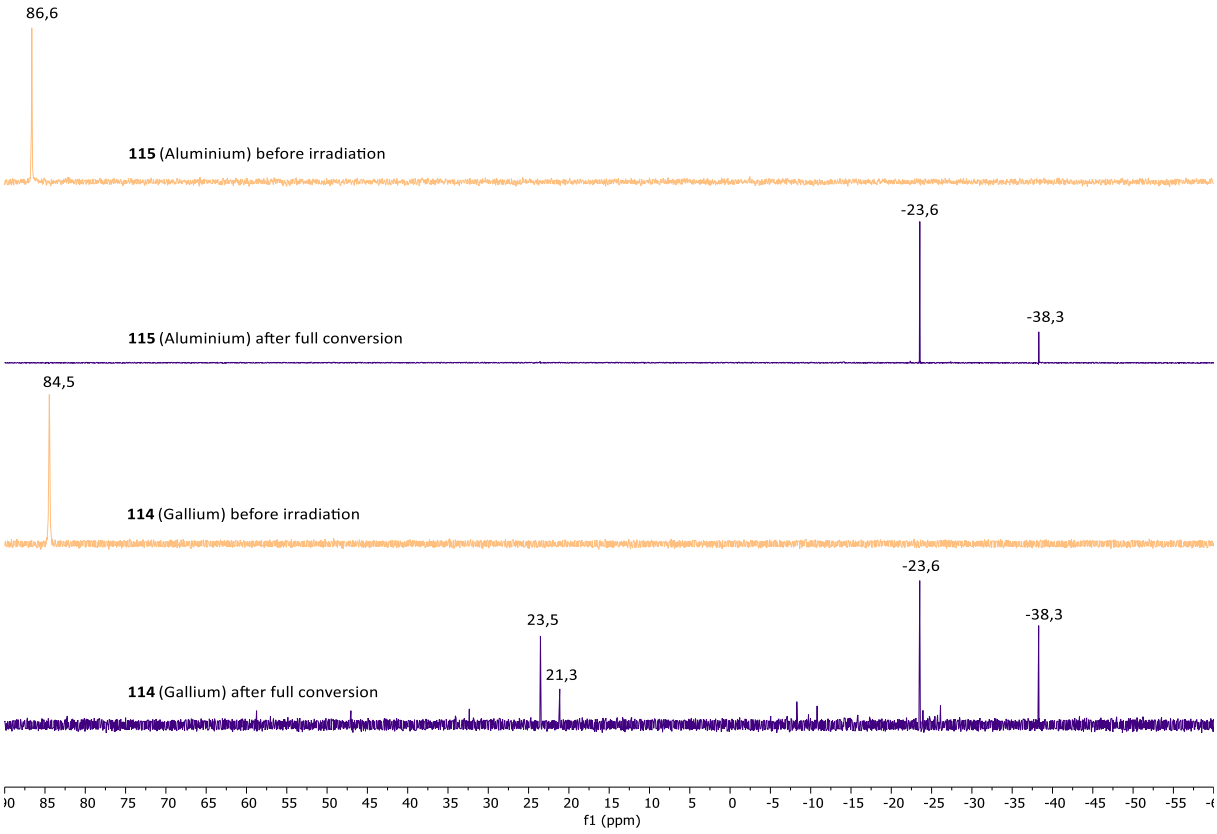

Figure 99: *$^{31}P\{^{1}H\}$ NMR spectra (240 MHz, C_6D_6) of **115** (upper part) and **114** (lower part) before and after full conversion.*

In both cases the evolved main peaks are located at -23.6 ppm and -38.3 ppm. The spectrum of **115** looks more refined, whereas **114** displays several other peaks, including those at 23.5 ppm and 21.3 ppm. Nonetheless, with time passing, those also appear in the spectra of **115** and a similar pattern of intensity shifts and signals occurring/disappearing can be observed (*Figure 94* and *Figure 100*).

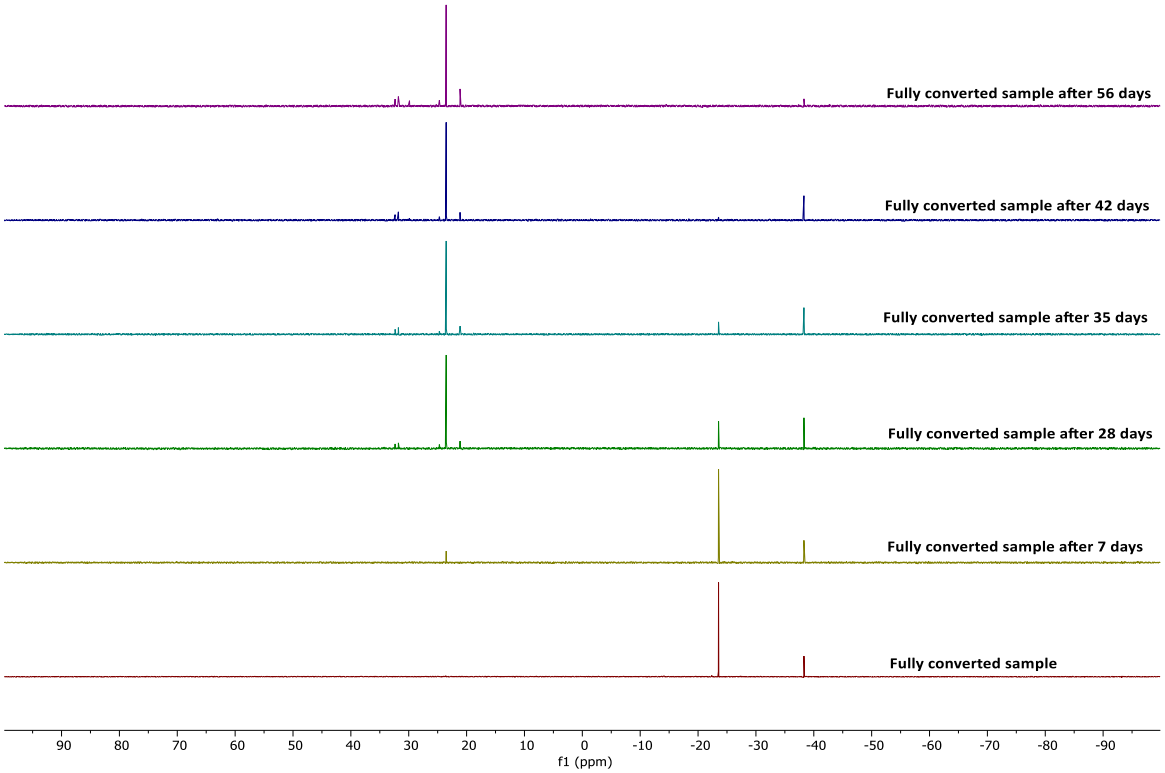

Figure 100: *Chronologically ordered $^{31}P\{^{1}H\}$ NMR spectra (240 MHz, C_6D_6) of fully converted **115** after corresponding past days (bottom to top).*

One difference is that conversion of the species seems to occur faster for **114**. *Figure 101* shows that in the spectrum of **114** both peaks in the higher field area completely disappeared after 56 days, while in the spectrum of **115** the peak at -38.3 ppm is still present.

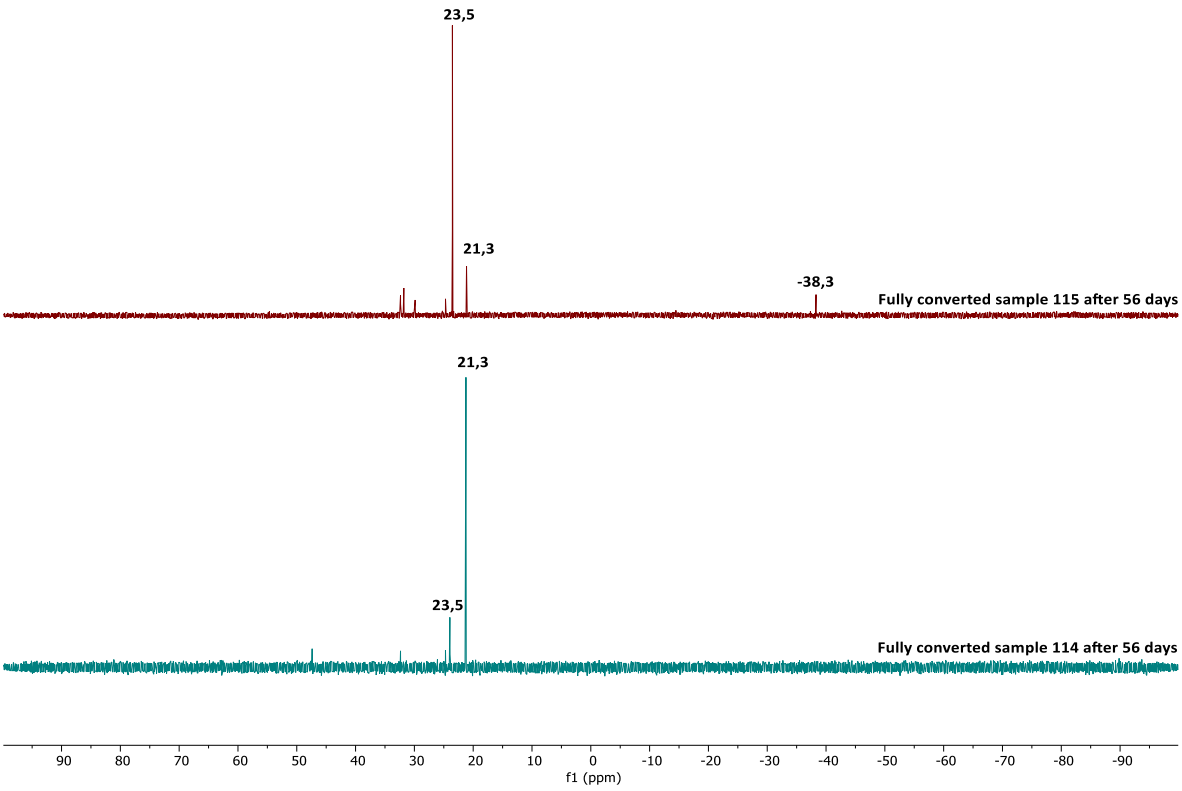

Figure 101: *Comparison of $^{31}P\{^{1}H\}$ NMR spectra (240 MHz, C_6D_6) of fully converted **115** (upper part) and **114** (lower part) after 56 days.*

Furthermore the change of intensity between the peaks at 23.5 ppm and 21.3 ppm is almost completed for **114**, while it seems to be yet at the beginning for **115**. (Unfortunately the Young NMR tube of sample **115** broke after measurement of 56 days passed; however a clear tendency for an increase of the peak at 21.3 ppm could be observed between days 42 and 56, accompanied by a decrease of the peak at 23.5 ppm, *Figure 100*).

This $^{31}P\{^{1}H\}$ NMR monitoring implies 1) that the photoreaction of **114** and **115** and the occurring reactions thereafter proceed in a similar way and 2) that the species formed differ only in regard of the metal (and therefore exhibit a very similar chemical shift) or even are, in case of decomposition, the same.

While all described spectroscopic measurements of **115** resemble those of **114** so far, one major difference is that no EPR signal and hence no radical species could be observed upon irradiation, suggesting that gallium plays an important role in formation of this species.

Of more importance though was the fact that ^{1}H NMR monitoring of **115**'s photoconversion was possible due to the absence of such radical species.

Figure 102 shows the ^{1}H NMR of **115** before and after full conversion.

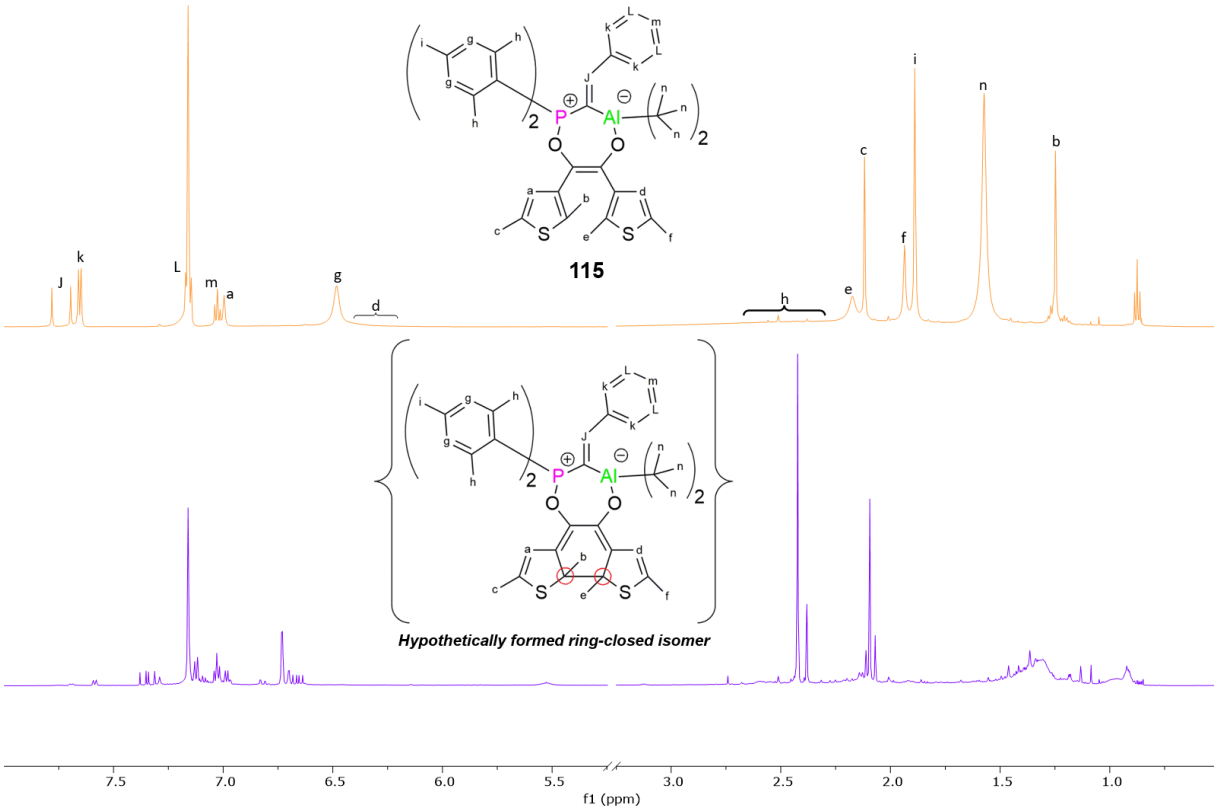

Figure 102: *^{1}H NMR spectra (600 MHz, C_6D_6) of **115** before (upper part) and after full photoconversion (lower part) via UV-A.*

Of particular interest was to observe the signal's changes of the thienyl protons and the CH_3-groups of the thienyl ring, which could give clues about a possible photocyclization: in the open-ring isomer of DTEs, the thienyl protons are part of an aromatic system. Upon ring-closure they lose their aromatic character and become shifted towards higher field. At the same time the protons of the methyl groups attached to the carbon atoms involved in the ring-closure reaction become shifted towards lower field.[234, 235]

Applied to the spectra of **115** strong chemical shifts of *a* (thienyl-H, 7.00 ppm), *d* (thienyl-H, 6.34 ppm), *b* (thienyl-CH_3, 1.25 ppm) and *e* (thienyl-CH_3, 2.17 ppm) could be expected. Unfortunately disappearance of *d* could hardly be observed, as the broad singulet was barely visible before; *a, b* and *e* completely disappeared and new signals formed in the aliphatic area at 5.53 ppm and around 2.40 ppm. However, while this might point towards a photocylization, also almost all other signals were affected by significant changes, e.g. in the aromatic area *J*, *k* and *g* disappeared with many new signals appearing. This observation is quite uncommon for photocylization reactions of DTEs, where, besides the named protons directly affected by formation of the six membered ring, only minor changes for chemical shifts of the other protons can be observed,[234, 235] hence pointing towards decomposition and formation of new fragments (as the $^{31}P\{^{1}H\}$ NMR spectra suggested).

Due to the likely presence of several species, integration of the signals and investigation *via* ^{13}C NMR and 2D NMR revealed no further insights regarding the occurred photoreaction.

2.7.8 Irradiation of Crystals of (Endiolato)Al-FLP Adduct (**115**)

Like **114**, **115** is responsive to UV-A in the solid state (*Figure 103*).

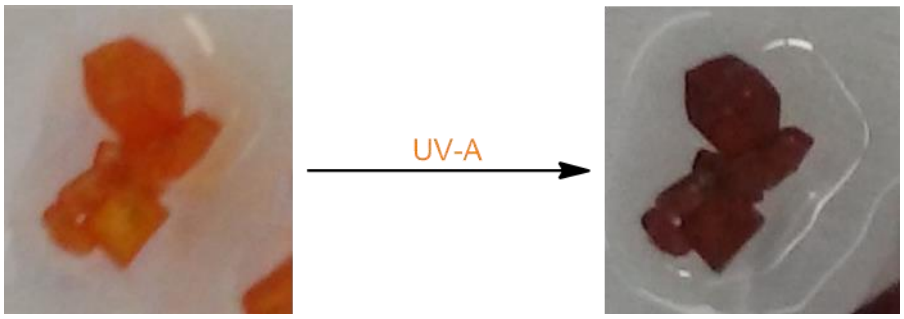

Figure 103: *Crystals of **115** before (left) and after irradiation with UV-A for 5 minutes (right).*

Unfortunately the same problems regarding crystallization of the purple species obtained *via* irradiation with UV-A applied as described in Chapter 2.7.3.3.

2.7.9 Conclusion and Outlook on (Endiolato)Ga-FLP Adduct (**114**) and (Endiolato)Al-FLP Adduct (**115**)

Synthesis of **114** and **115** was a success and showed that DTEs directly connected to a metal center can be obtained pure and in high yield by attachment of dithienylethane ligands to a metal containing precursor *via* concerted reduction of the ligand. Like other DTEs, **114** and **115** responded to irradiation with UV light rapidly accompanied by a drastic change of color, even in solid state. Unfortunately, it remains unclear whether photocyclization followed by decomposition or direct photoconversion to other (unidentifiable) species occurred, as ^{1}H and $^{31}P\{^{1}H\}$ NMR spectra suggested formation of several species. The original photoreaction proofed to be irreversible.

For further investigations in regard of the photoreaction taking place, it could be useful to alter either the outer methyl groups of the dithienylethane precursor and/or those groups attached to phosphorous and aluminium/gallium. Electron withdrawing groups could hamper a photocyclization reaction and it would be interesting to see if a photoreaction could still be observed. If so, additional phosphorous or other with NMR easy to track atoms, especially on the dithienylethane unit, could provide for valuable insights of the occurring photoreaction.

2.8 Investigation of (Endiolato)$ReCl_2(PPh_3)_2$ (**118**)

Inspired by the results described in the previous chapters, focus was laid again on forming a DTE structure *via* a concerted reaction instead of stepwise reduction of the dithienylethane.

Sokolov *et al.*[236] reported on the synthesis of rhenium(V) complexes through reaction of $ReCl_3(CH_3CN)(PPh_3)_2$ as precursor with *β*-lapachone or benzil. The reaction with benzil was already described by Rouschias and Wilkinson[237] as early as in 1967 (*Figure 104*).

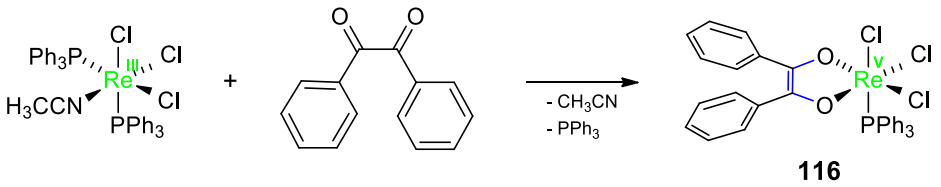

Figure 104: *Reaction of $ReCl_3(CH_3CN)(PPh_3)$ with benzil leads to 1:1 complex **116** upon release of CH_3CN and one PPh_3 group.*[236, 237]

The 1:1 complex **116** forms upon release of CH_3CN and PPh_3 of the Re(III) precursor. Simultaneously rhenium changes its oxidation state from +3 to +5, benzil becomes reduced and the carbon atoms of the former carbonyl groups form a double bond between them.

Figure 105 shows the expected analogue reaction of **90** with $ReCl_3(CH_3CN)(PPh_3)_2$:

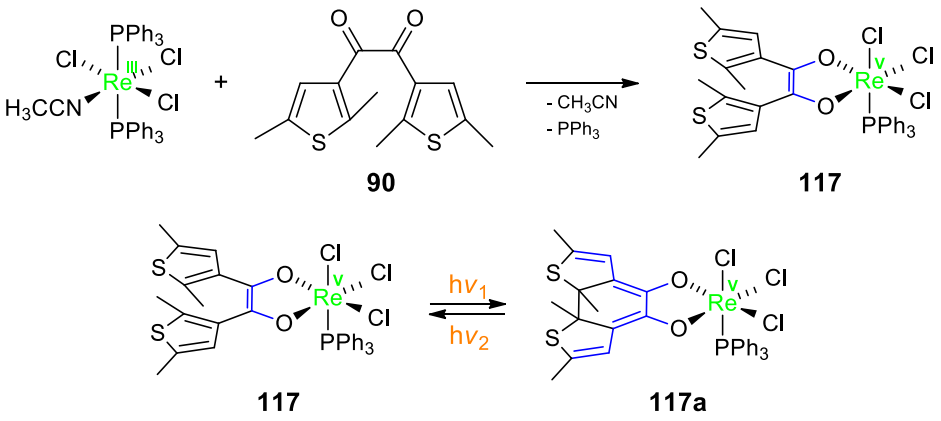

Figure 105: *Proposed reaction of **90** with $ReCl_3(CH_3CN)(PPh_3)_2$ to form **117** with DTE backbone (upper part) and possible photocyclization of **117** (lower part).*

With the DTE backbone formed during reduction of **90**, complex **117** could be capable of undergoing reversible photocyclization (**117a**).

2.8.1 Attempted Synthesis of (Endiolato)$ReCl_3(PPh_3)$ (**117**)

The attempted synthesis of **117** was carried out in a slightly modified procedure of the one described by Rouschias and Wilkinson[237] for synthesis of **116**: α-diketone **90** was dissolved in toluene and treated with $ReCl_3(CH_3CN)(PPh_3)_2$ in a ratio of 1:1. The brown suspension was then heated to reflux for 2 h, upon which a fast conversion to a purple solution could be observed (*Figure 106*).

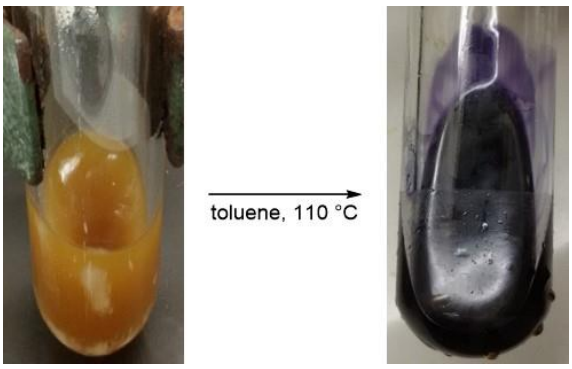

Figure 106: *Observed color change during reaction of* ***90*** *and* $ReCl_3(CH_3CN)(PPh_3)_2$ *in toluene.*

The solvent was removed under reduced pressure, the crude residue dissolved in a small portion of DCM and the resulting solution overlayered with *n*-hexane. Over the course of a few days dark brown to red crystals could be obtained and were examined *via* X-ray crystallography. The examined crystals turned out to be $ReCl_4(PPh_3)_2$, a rhenium(IV) complex known in literature that forms by reaction of several rhenium compounds with triphenylphosphine.[238-240] The presence of this rhenium(IV) species pointed towards an unforeseen course of reaction and possibly formation of other rhenium species as well. Therefore the solvent mixture, now blue-green in color, was decanted, the solvents evaporated under reduced pressure and the remainder again dissolved in a small amount of DCM and overlayered with *n*-hexane.

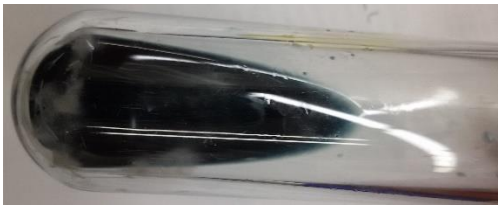

Figure 107: *In DCM dissolved residue with blue-green color after crystallization of* $ReCl_4(PPh_3)_2$.

Yet again dark brown to red crystals of $ReCl_4(PPh_3)_2$ formed; however also two other crystal types could be identified: a brown 'Hinkelstein' (2) and a light brown rod (3) (*Figure 108*).

Figure 108: *The three obtained crystal types after 2nd crystallization cycle: 1) literature known $ReCl_4(PPh_3)_2$; 2) starting material $ReCl_3(CH_3CN)(PPh_3)_2$; 3) (endiolato)$ReCl_2(PPh_3)_2$ (**118**).*

The 'Hinkelstein' crystal type (2) turned out to be rhenium precursor $ReCl_3(CH_3CN)(PPh_3)_2$, the rod type could be identified as (endiolato)$ReCl_2(PPh_3)_2$ (3) **118**. The net reaction could therefore be postulated as follows:

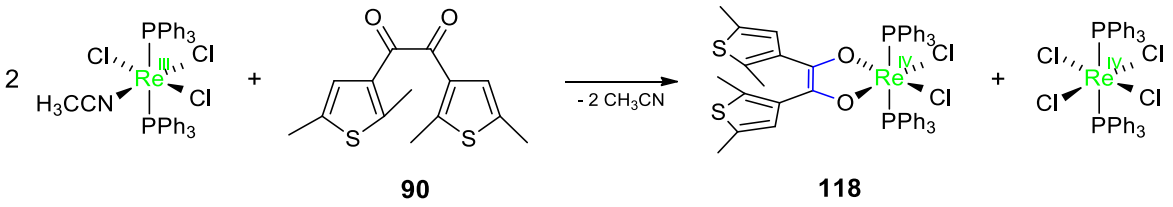

Figure 109: *Net reaction of reaction of **90** and $ReCl_3(CH_3CN)(PPh_3)_2$.*

The exact mechanism and what intermediates formed during the reaction remain unclear. Nonetheless, the unexpectedly obtained Re(IV) species **118** was of high interest for further investigations since 1) a photocyclization could be possible due to the formed DTE-structure and 2) such photocyclization could pave the way for non-innocent behavior of the DTE and a possible switching between the physical oxidation states +4 and +5 of rhenium:

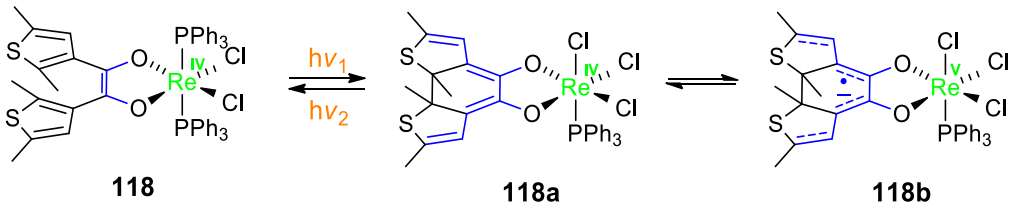

Figure 110: *Possible photocyclization of **118** and non-innocent behavior of DTE, leading to a change of rhenium's physical oxidation state from +4 to +5.*

Effort was therefore spent to isolate **118** in pure form.

After the third crystallization cycle, large amounts of **118** were present, though crystals of the other two species still grew along (*Figure 111*).

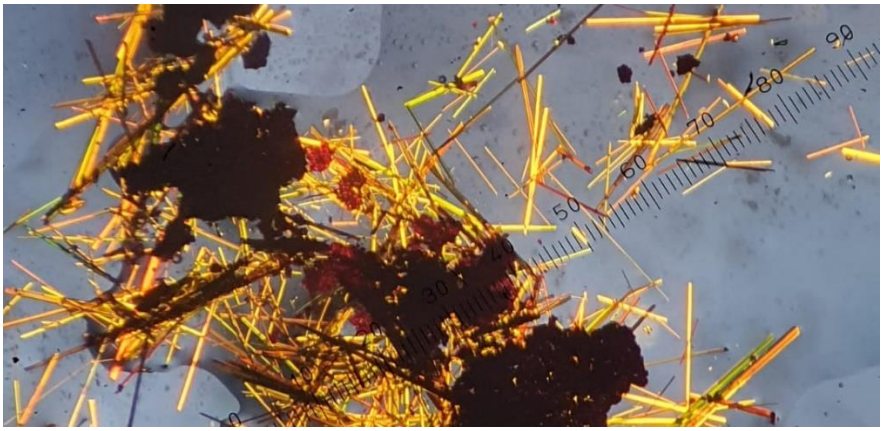

Figure 111: *Formation of greater amounts of* ***118*** *(orange rods) could be observed after the 3rd crystallization cycle.*

As a valid method for a clean separation of **118** the following procedure could be established (under an inert atmosphere of argon): after crystallization, the formed crystals of all types turned out to be extremely sticky to the glass surface of the reaction vessel. Through addition of a small amount of *n*-hexane and gentle shaking only crystals of **118** were able to break loose. (This is because **118** is soluble to a small extend in *n*-hexane. Experiments to extract **118** before crystallization with *n*-hexane from the reaction mixture failed though, as $ReCl_4(PPh_3)_2$, when not in crystalline form, was extracted along.) The suspension with crystals of **118** was then transferred into another vessel. Decantation and washing with small portions of cold *n*-hexane led to pure product **118**.

The structure of **118** was also verified *via* HR-MS. Due to paramagnetic Re(IV), no signals could be observed in NMR for ^{1}H, ^{13}C and ^{31}P; however, NMR spectroscopy revealed that no (non-paramagnetic) impurities were present. Compound **118** is readily soluble in DCM, toluene and to a small extend in *n*-hexane, showing a green-blue color when dissolved (*Figure 112*).

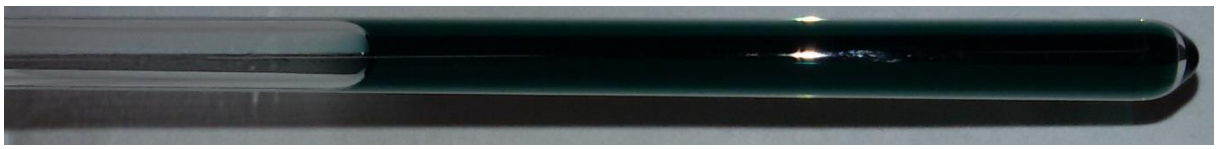

Figure 112: Green-blue solution of ***118*** *in* CD_2Cl_2.

2.8.2 Crystal Structure of (Endiolato)$ReCl_2(PPh_3)_2$ (**118**)

Compound **118** crystallizes in the triclinic space group P-1. The rhenium atom is connected to the oxygens of former α-diketone ligand **90**, two chlorides and two phosphorous atoms of the triphenylphospine units, forming a distorted octahedral structure (*Figure 113*).

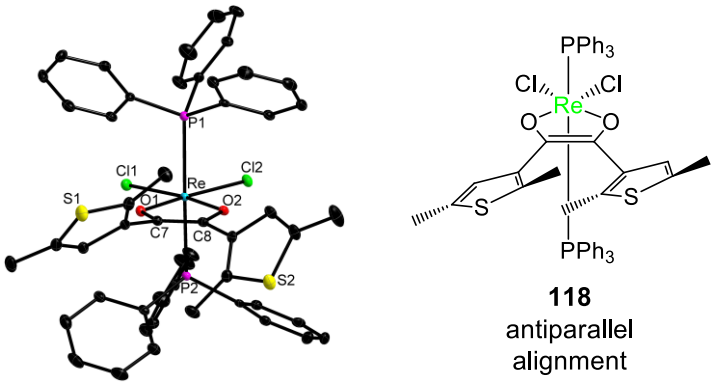

Figure 113: *X-ray crystal structure of* ***118*** *at 50% ellipsoid probability. Hydrogen atoms are omitted for clarity. Selected bond lengths [Å]: C7-C8 = 1.369(3), C7-O1: 1.345(3), O1-Re: 1.995(1), C8-O2: 1.342(3), O2-Re: 1.990(1), P1-Re: 2.488(1), P2-Re: 2.491(1).*

The sterically demanding triphenylphospine units coordinate in *trans*-positions while the chlorides and oxygens are in coplanar arrangement with the rhenium center. Bond length of C7-C8 (1.369(3) Å) as well as C7-O1 (1.345(3) Å) and C8-O2 (1.342(3) Å) are clearly indicative for a formed DTE backbone. Note: the thienyl rings exhibit an antiparallel alignment.

2.8.3 UV/Vis Experiments of (Endiolato)$ReCl_2(PPh_3)_2$ (**118**)

In order to see if **118** would show a response when exposed to UV-light as result of photocyclization, a diluted solution of **118** in DCM was irradiated with UV-A and a UV/Vis spectrum recorded after certain time intervals (*Figure 114*).

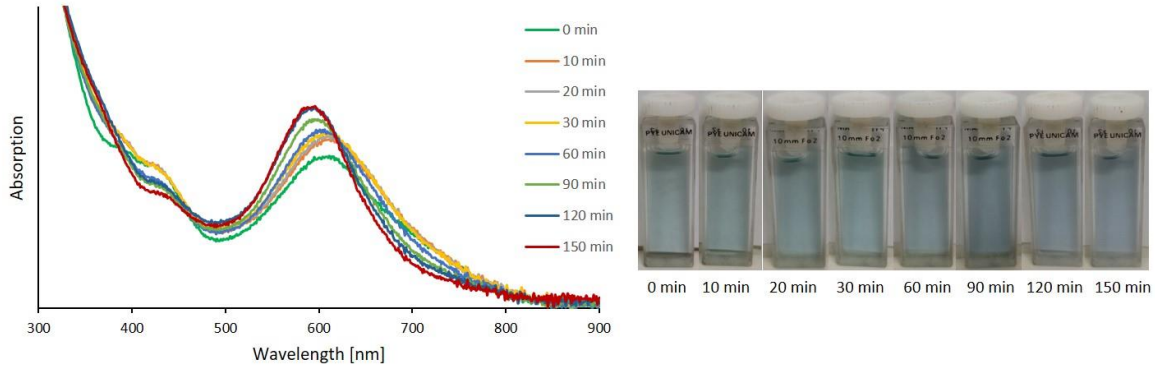

Figure 114: *Irradiation of **118** in DCM with UV-A. UV/Vis spectra were taken after different time intervals.*

Compound **118** shows significant absorption in the area of 380 nm – 490 nm and 500 nm – 850 nm (λ_{max} = 613 nm). Upon irradiation with UV-A, overall absorption in those areas first rises (up to 30 min), and then declines with exception of the area around 600 nm, where absorption becomes more intense and a shift of λ_{max} to 593 nm can be observed. This is accompanied by a slight change of color from green-blue to blue *(Figure 114*, right). This change, clearly visible in the UV/Vis spectra, likely points towards a change of conformation within the complex rather than a photocyclization as a more drastic change of color due to a formed prolonged conjugated π-system could be expected.[150, 190, 191, 225-230] Such conformational change could include the transformation of the DTE's parallel to an antiparallel alignment (and therefore a switch of *P*- or *M*-helicity to para formation) as reported in *Chapter 2.1*.[241] Irradiation with visible light (λ > 450 nm) for several minutes of the formerly with UV-A irradiated sample showed no response, the UV/Vis spectrum remained unchanged, indicating an irreversible photoreaction.

Irradiation with UV-B showed a similar, but slower process; irradiation with UV-C led to decomposition. Crystals of **118**, although comprising of DTE in parallel alignment, showed no response upon irradiation with UV-light.

2.8.4 Conclusion and Outlook on (Endiolato)$ReCl_2(PPh_3)_2$ (**118**)

Reaction of α-diketone ligand **90** with $ReCl_3(CH_3CN)(PPh_3)_2$ did not lead to expected product (endiolato)$Re(V)Cl_3(PPh_3)$ (**117**). Instead, due to an unexpected reaction with unknown intermediates, product **118**, (endiolato)$Re(IV)Cl_2(PPh_3)_2$, could be isolated. **118** comprises of a DTE backbone with parallel alignment in the measured crystals, a precondition for photocyclization. Irradiation of the crystals with UV light showed no response, while irradiation of a solution of **118** in DCM or toluene led to observable changes in the UV/Vis spectra and a change of color from green-blue to blue. Irradiation with visible light led to no reconversion, indicating an irreversible photoreaction. These observations point towards that **118** is not capable of photocyclization and rather a conformational change within the complex led to the described results. Unfortunately, due to time constraints, it was not possible to further investigate **118** and its irradiated pendant *via* EPR to verify this assumption.

Nonetheless, **118** remains a promising candidate for further investigations and modifications, e.g. substitution of the methyl groups in 5' position of the thiophene rings with more electron donating groups like phenyl rings and its derivatives, which could provide for higher electron density of the DTE backbone, possibly paving a way for photocylization.

3 Summary

This Ph.D. thesis describes the synthesis and characterization of metal complexes containing a dithienylethane or dithienylethene (DTE) moiety adjacent to the metal center and are based on the ligands 1,2-bis(2,5-dimethyl-3-thienyl)ethanedione and 1,2-bis(2,5-dimethyl-3-thienyl)ethane-*N*-*p*-tolyl-diimine.

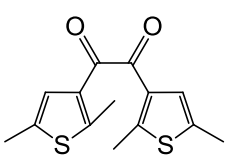

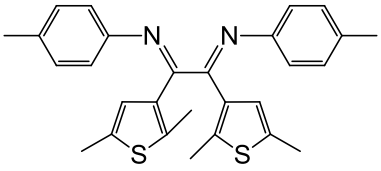

Those with a DTE unit were investigated in regards of a possible photocyclization or other geometrical changes upon irradiation with UV/Vis.

3.1 Non-Oxido-Vanadium(IV) Metalloradical Complexes with Bidentate 1,2-Dithienylethene Ligands

Within the first project the first five-membered metallacycle with an endiolato-DTE-motif to report could be obtained, achieved *via* reaction of 1,2-bis(2,5-dimethyl-3-thienyl)ethanedione with a V(II)-precursor. Present as a racemic mixture containing both DTE units either with *M*- or *P*-helicity, this non-oxido vanadium(IV) complex would convert to the corresponding diastereomer with one DTE changing its geometrical arrangement from *M*- or *P*-helicity to a parallel alignment upon irradiation with UV-A or heating to 80 °C. This irreversible conversion is accompanied by a change of color from deep blue to purple.

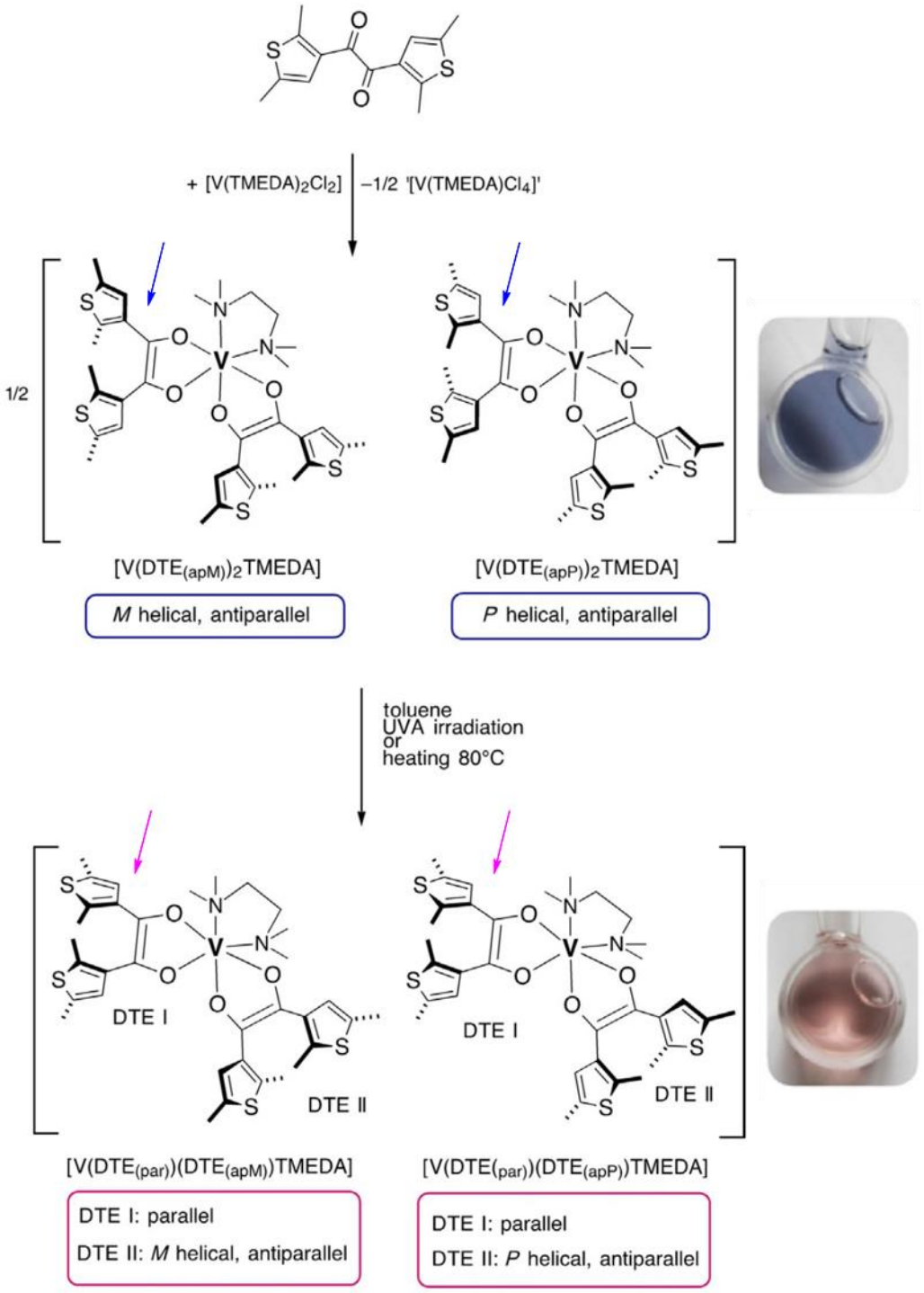

Advanced EPR studies pointed towards a dynamic reversible cyclization reaction of the blue species at ambient temperature; however, a well-defined photocyclization upon exposure to photochemical stimuli could not be observed.

3.2 M(IV) (M = Ti, Zr, Hf, Sn) Tetrachlorido Complexes based on 1,2-Bis(2,5-dimethyl-3-thienyl)ethanedione and 1,2-Bis(2,5-dimethyl-3-thienyl)ethane-*N*-*p*-tolyl-diimine

Within the second project M^{IV} tetrachlorido complexes were formed by reaction of metal precursors MCl_4 (M = Ti, Zr, Hf, Sn) and ligands 1,2-bis(2,5-dimethyl-3-thienyl)ethanedione and 1,2-bis(2,5-dimethyl-3-thienyl)ethane-*N*-*p*-tolyl-diimine.

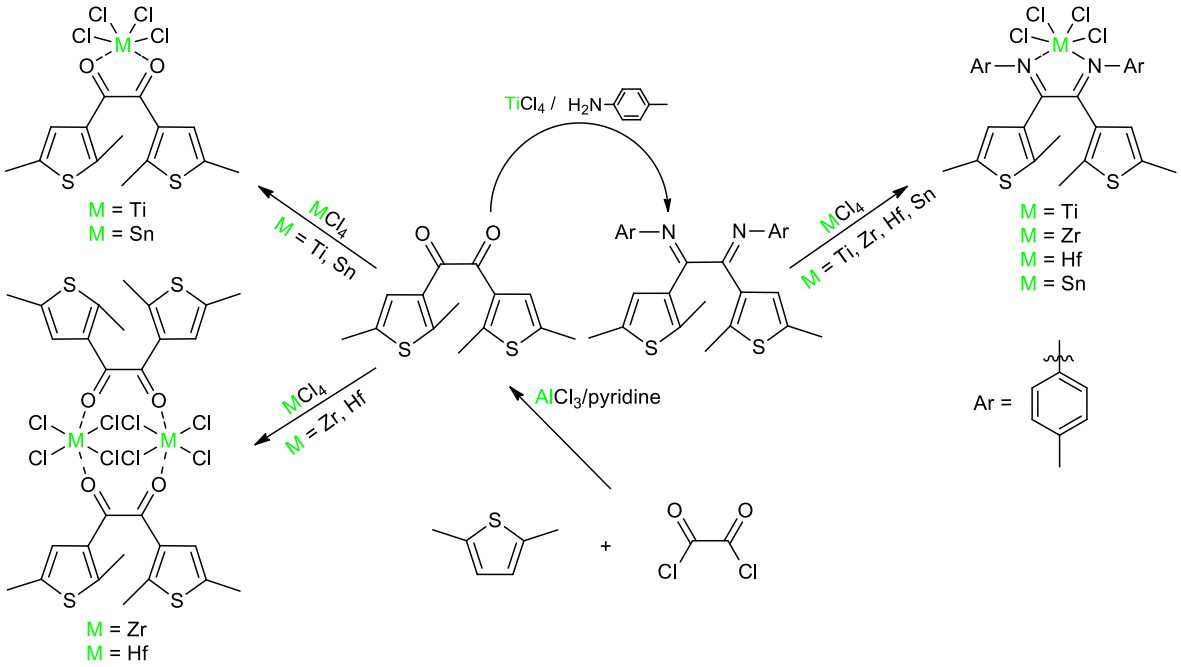

While the original idea of two one electron reductions of those to form DTE complexes with a photoswitchable hexatriene motif turned out unsuccessful, other interesting observations like formation of [2+2] complexes, the presence of atropisomers and overall in regard of stereochemical aspects were made. Further insides on the latter for complexes formed with 1,2-bis(2,5-dimethyl-3-thienyl)ethanedione are described in *Chapter 2.3*, for complexes formed with 1,2-bis(2,5-dimethyl-3-thienyl)ethane-*N*-*p*-tolyl-diimine in *Chapter 2.2*; in addition a manuscript is currently in the writing.

3.3 Hexacoordinated M(IV) (M = Ti, Zr, Hf) Tetrachlorido Complexes with Chelating Dithienylethane based 1,2 Diketone Ligand – π-Conjugation as Decisive Factor for Axial Chirality Mode

In this paper the synthesis and characterization of complexes formed by 1,2-bis(2,5-dimethyl-3-thienyl)ethanedione and MCl_4 metal precursors of group four (M= Ti, Zr, Hf) were described. Use of $TiCl_4$ led to formation of a monomeric structure, while $ZrCl_4$ and $HfCl_4$ gave rise to dimeric scaffolds with bridging {μ^2,η^1,η^1-*O*,*O'*-DTEthane}.

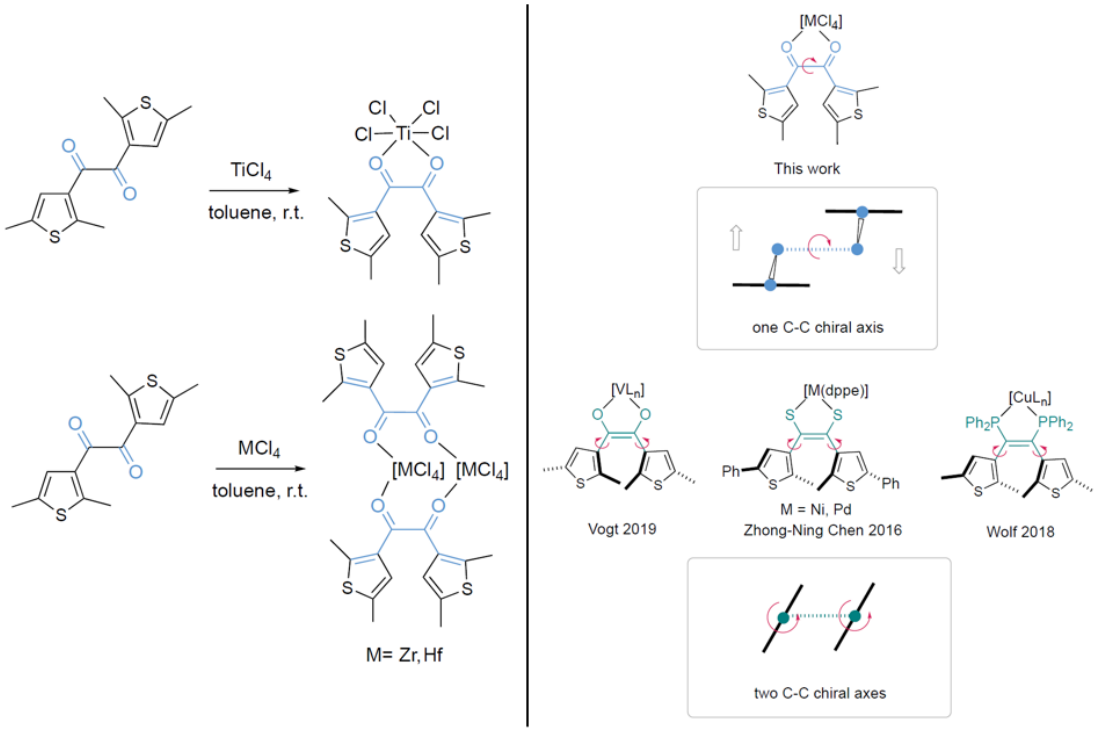

DFT calculations (G16, B97D3/def2-TZVP) pointed towards a general trend of dimer formation in order of Ti < Zr < Hf and revealed that the carbonyl groups reside in conjugation with their adjacent thiophene ring. This leads to a hampered rotation about the two C-C axes formed by the carbon atom in 3' position of the thiophene ring and the carbonyl group's carbon atoms. In comparison to the closely related complexes with a five-membered metallacycle carrying endiolato ligand (1,2-bis(2,5-dimethylthiophen-3-yl)ethene-1,2-diolate, in which no coplanarity of the thiophene rings to their neighboring five-membered metallacycle is observed, this structural feature was found to be decisive for the nature and number of the chiral axes: the latter gives rise to two C–C chiral axes leading to helicity, while the former results in only one chiral axis bringing forth axial chirality analogue to e.g. classical biaryl compounds.

3.4 Investigation of Rhenium/Manganese Complexes Bearing 1,2-Bis(2,5-dimethyl-3-thienyl)ethane-*N*-*p*-tolyl-diimine as Ligand

Although the attempt of two one-electron reduction steps turned out unsuccessful before, further effort was spent in this regard, yet with a different approach: a rhenium- and manganese complex were to be synthesized, with the first reduction step appearing on the ligand, the second on the metal, changing its oxidation state from +1 to 0. The second reduction step occurring on the ligand was supposed to be initiated by the metal center upon addition of a solvent molecule to it.

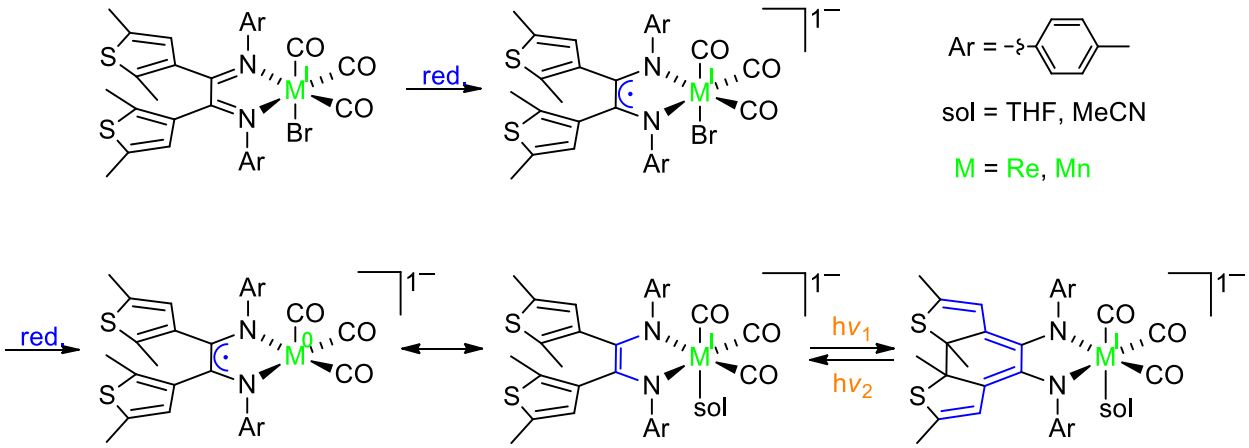

Synthesis of the rhenium complex was successful; however the reduction ended in a mixture of several (paramagnetic) species and no evidence for formation of the double reduced ligand could be found.

Synthesis of the manganese complex turned out unsuccessful, as a manganese (II) complex bearing two *α*-diimine ligands formed instead.

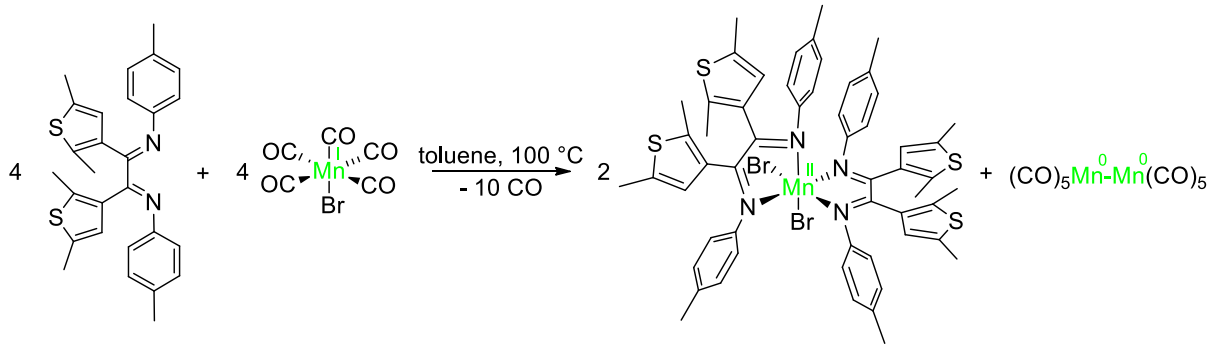

3.5 Investigation of a Copper(I) Complex with 1,2-Bis(2,5-dimethyl-3-thienyl)ethane-*N*-*p*-tolyl-diimine as Ligand

This project referred to reports that copper(I) halides form with DABs complexes of different types of composition. 1,2-bis(2,5-dimethyl-3-thienyl)ethane-*N*-*p*-tolyl-diimine was therefore brought to reaction with copper(I) chloride to investigate if highly interesting complex type **A** would form.

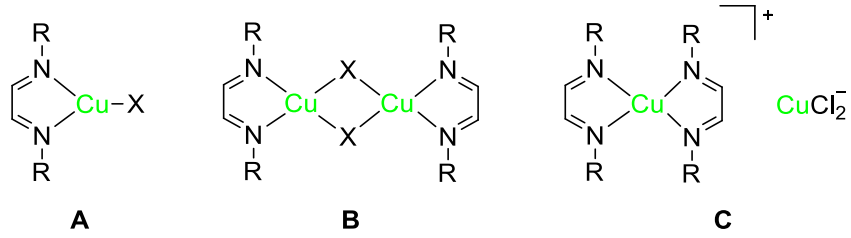

Unfortunately only complex type **C** could be isolated, which was of no interest for further studies.

3.6 DTE Complexes Formed with 1,2-Bis(2,5-dimethyl-3-thienyl)ethanedione and Al-/Ga-FLPs

In this project DTE complexes, formed *via* reaction of 1,2-bis(2,5-dimethyl-3-thienyl)ethanedione with Al-/Ga-FLPs, were investigated in regard of an occurring photoreaction: when exposed to UV-A light, a rapid change of color from ocher to purple occurred in solution and also in solid state.

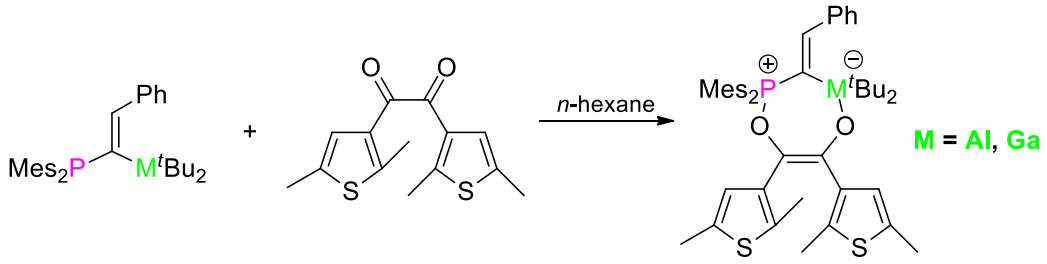

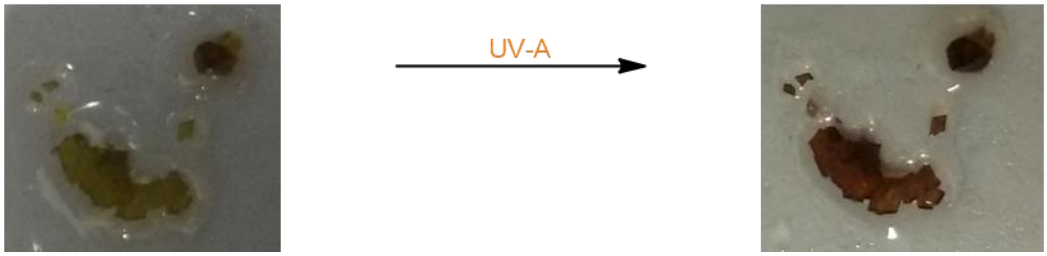

Therefore UV/Vis, ^{31}P, ^{13}C and ^{1}H NMR and other experiments were carried out. However, while some results pointed towards the desired photocyclization, other findings did not. Whether photocyclization occurred or not, the experiments clearly showed that the products of the photoconversion were not stable and complex mixtures of decomposition products evolved.

The successful synthesis of the DTE complexes suggested that a synthetic route for those should be based on metal precursors which simultaneously can act as a two-electron reducing agent.

3.7 DTE Complex Formed with 1,2-Bis(2,5-dimethyl-3-thienyl)ethanedione and $ReCl_3(CH_3CN)(PPh_3)_2$

The aim of the last project was 1) to confirm the suggestion that using a metal precursor which also acts as reducing agent would lead to the corresponding DTE complex upon reaction with 1,2-bis(2,5-dimethyl-3-thienyl)ethanedione and 2) to investigate this complex in regard of a possible photocyclization. Surprisingly, reaction of 1,2-bis(2,5-dimethyl-3-thienyl)ethanedione and $ReCl_3(CH_3CN)(PPh_3)_2$ turned out not as expected, as a different product, a Re(IV) complex, could be isolated.

expected

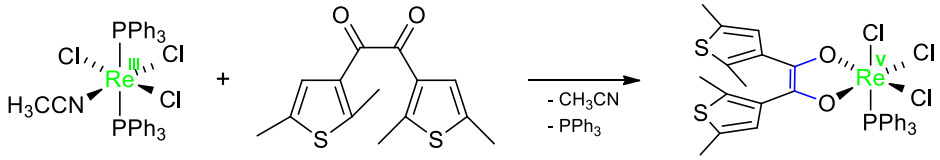

observed/suggested

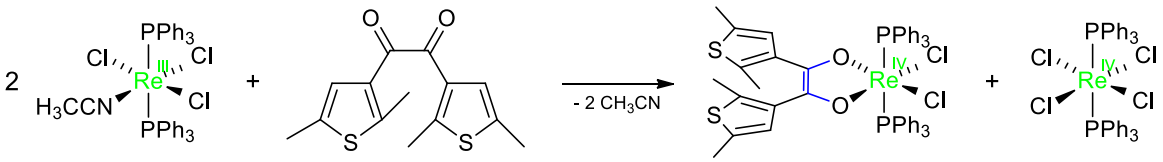

Nonetheless the isolated product was of high interest, as a possible photocyclization could also lead to non-innocent behavior of the DTE ligand. Unfortunately no evidence for occurring photocyclization could be observed upon irradiation with UV light; changes monitored in the UV/Vis spectra solely pointed towards a change of conformation within the complex.

4 Zusammenfassung

Im Rahmen dieser Promotionsarbeit wurden die Synthese und Charakterisierung von Metallkomplexen, welche eine Dithienylethan- oder Dithienylethen-Einheit in direkter Nähe zu dem Metallzentrum beinhalten, beschrieben. Als Precursor-Liganden dienten 1,2-Bis(2,5-dimethyl-3-thienyl)ethandion und 1,2-Bis(2,5-dimethyl-3-thienyl)ethan-*N*-*p*-tolyl-diimin.

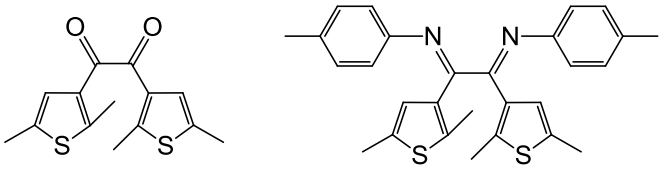

Komplexe mit einer DTE-Einheit wurden hinsichtlich einer möglichen Photozyklisierung oder anderen geometrischen Veränderungen bei Bestrahlung mit UV/Vis untersucht.

4.1 Non-Oxido-Vanadium(IV) Metalloradical Complexes with Bidentate 1,2-Dithienylethene Ligands

Im Rahmen des ersten Projekts konnten die ersten fünfgliedrigen Metallacyclen auf Basis eines Endiolato-DTE-Motivs mittels einer Reaktion aus 1,2-Bis(2,5-dimethyl-3-thienyl)ethandion und einem Vanadium(II)-Precursor erhalten werden. Dieser Non-oxido-Vanadium(IV)-Komplex liegt als ein racemisches Gemisch mit beiden DTE-Einheiten entweder in *M*- oder *P*-Helizität vor und konvertiert bei Bestrahlung mit UV-A oder Erhitzen auf 80 °C zu dem entsprechenden Diasteromer, in welchem eine DTE-Einheit seine *M*- oder *P*-Helizität verliert und in einer parallelen Anordnung vorliegt. Dieser irreversible Vorgang verläuft unter einem Farbwechsel von Dunkelblau zu Purpur.

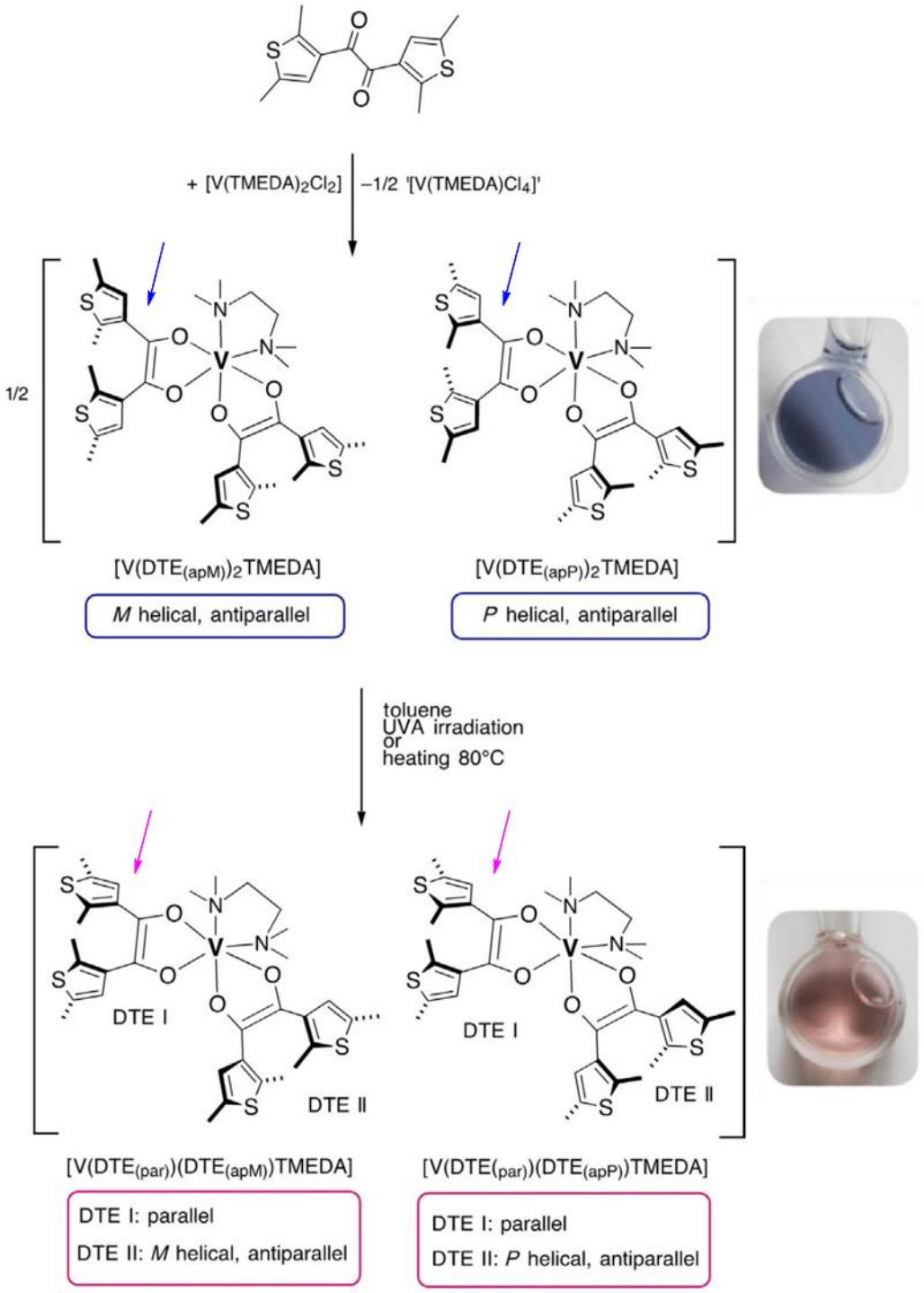

Weiterführende ESR-Untersuchungen wiesen auf eine dynamische reversible Zyklisierungsreaktion der blauen Spezies bei Raumtemperatur hin; eine genau definierte Photozyklisierung bei Einwirkung photochemischer Stimuli konnte jedoch nicht beobachtet werden.

4.2 M^{IV} (M = Ti, Zr, Hf, Sn) Tetrachlorido Complexes Based on 1,2-Bis(2,5-dimethyl-3-thienyl)ethanedione and 1,2-Bis(2,5-dimethyl-3-thienyl)ethane-*N*-*p*-tolyl-diimine

Im Rahmen des zweiten Projekts wurden M^{IV}-Tetrachloridkomplexe durch Reaktion der Precursors MCl_4 (M = Ti, Zr, Hf, Sn) und der Liganden 1,2-Bis(2,5-dimethyl-3-thienyl)ethandion und 1,2-Bis(2,5-dimethyl-3-thienyl)ethan-*N*-*p*-tolyl-diimin synthetisiert.

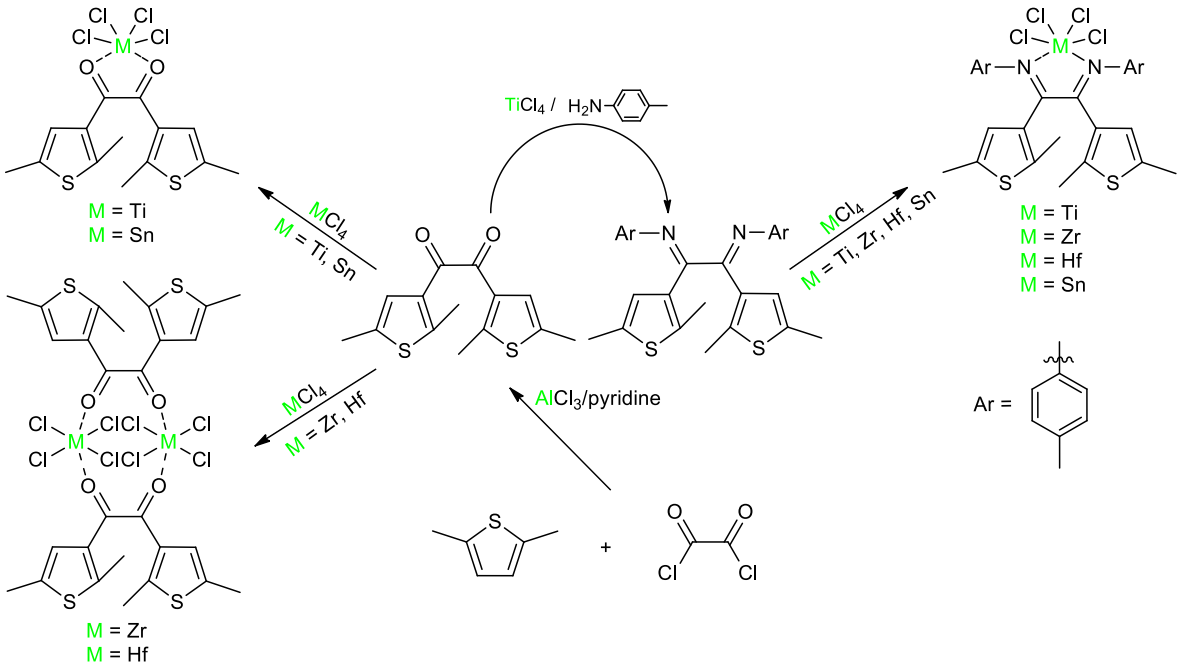

Während sich die ursprüngliche Idee von zwei Ein-Elektronenreduktionen zur Bildung von DTE-Komplexen mit einem photoschaltbaren Hexatrien-Motiv als erfolglos erwies, wurden andere interessante Beobachtungen wie die Bildung von [2+2]-Komplexen, das Vorhandensein von Atropisomeren sowie hinsichtlich stereochemischer Aspekte gemacht. Weiterführende Details zu letzteren für Komplexe mit 1,2-Bis(2,5-dimethyl-3-thienyl)ethandion sind in *Kapitel 2.3* beschrieben, für Komplexe mit 1,2-Bis(2,5-dimethyl-3-thienyl)ethan-*N*-*p*-tolyl-diimin in *Kapitel 2.2*; zusätzlich befindet sich derzeit ein Manuskript in Bearbeitung.

4.3 Hexacoordinated M(IV) (M = Ti, Zr, Hf) Tetrachlorido Complexes with Chelating Dithienylethane based 1,2 Diketone Ligand – π-Conjugation as Decisive Factor for Axial Chirality Mode

In diesem Projekt wurden die Synthese und Charakterisierung von Komplexen beschrieben, die sich aus 1,2-Bis(2,5-dimethyl-3-thienyl)ethandion und MCl_4-Precursors der vierten Nebengruppe (M = Ti, Zr, Hf) bildeten. Die Verwendung von $TiCl_4$ führte zur Entstehung einer monomeren Struktur, jene von $ZrCl_4$ und $HfCl_4$ zu einem dimeren Gerüsten mit verbrückendem {μ2,η1,η1-O,O'-DTEthan}.

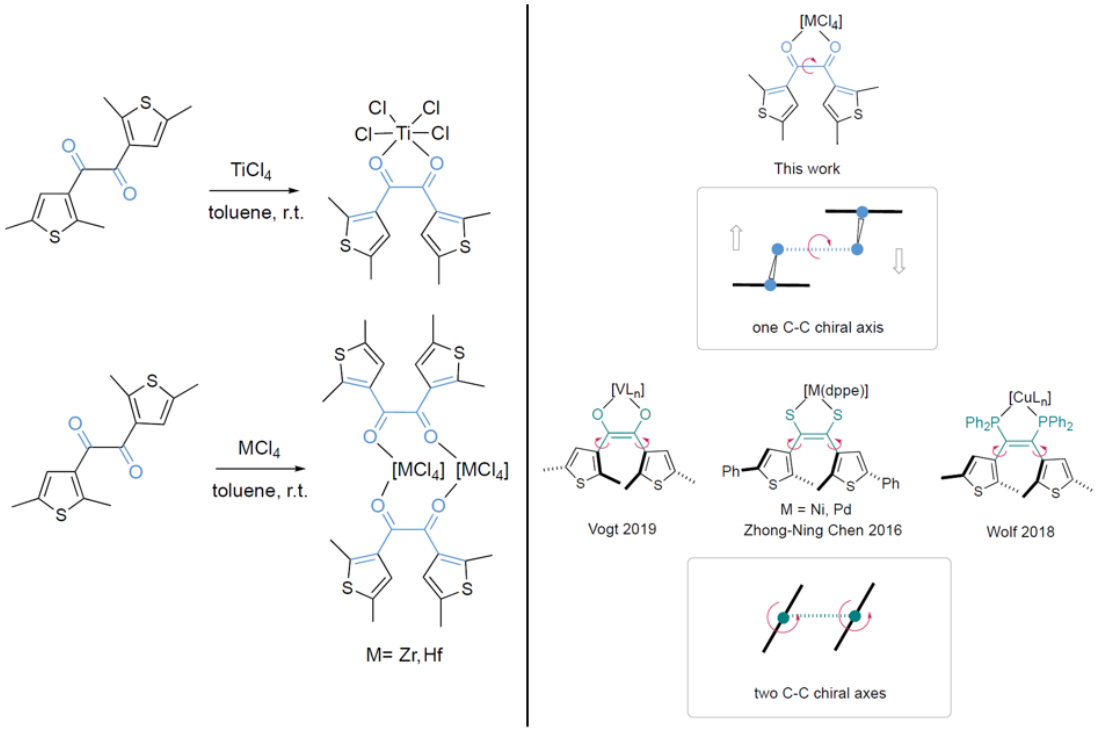

DFT-Rechnungen (G16, B97D3/def2-TZVP) deuteten auf einen allgemeinen Trend der Dimerbildung in der Reihenfolge Ti < Zr < Hf hin; des Weiteren, dass die Carbonylgruppen in Konjugation mit ihrem benachbarten Thiophenring stehen. Dies führt zu einer gehinderten Rotation um die beiden C-C-Achsen, die durch das Kohlenstoffatom in 3'-Position des Thiophenrings und das jeweilige Kohlenstoffatom der Carbonylgruppe gebildet werden. Durch Vergleich zu den strukturverwandten Komplexen mit einem fünfgliedrigen Metallzyklus, die einen en-Diolato-Liganden tragen (1,2-Bis(2,5-dimethylthiophen-3-yl)ethen-1,2-diolat) und bei denen keine Koplanarität des Thiophens zu ihrem benachbarten Metallzyklus beobachtet wird, erweist sich dieses Strukturmerkmal als entscheidend für die Art und Anzahl der chiralen Achsen: bei den letztgenannten Komplexen führt dies zu zwei C-C-Chiralitätsachsen, woraus Helizität entsteht; bei den erstgenannten Komplexen führt dies zu nur einer

chiralen Achse und damit einhergehend einer axialen Chiralität analog zu jener etwa von klassischen Biarylverbindungen.

4.4 Untersuchung von Rhenium-/Mangan-Komplexen mit 1,2-Bis(2,5-dimethyl-3-thienyl)ethan-*N*-*p*-tolyl-diimin als Ligand

Obwohl der Versuch von zwei Ein-Elektronen-Reduktionsschritten wie zuvor beschrieben erfolglos verlief, wurden weitere Anstrengungen in dieser Hinsicht unternommen, jedoch mit einem anderen Ansatz: Ein Rhenium- und Mangan-Komplex sollten synthetisiert werden, bei denen der erste Reduktionsschritt am Liganden auftritt, der zweite am Metall, begleitet von einem Wechsel der Oxidationsstufe von +1 zu 0. Der zweite am Liganden auftretende Reduktionsschritt sollte vom Metallzentrum ausgehen, sobald sich an dieses ein Lösemittelmolekül anlagert.

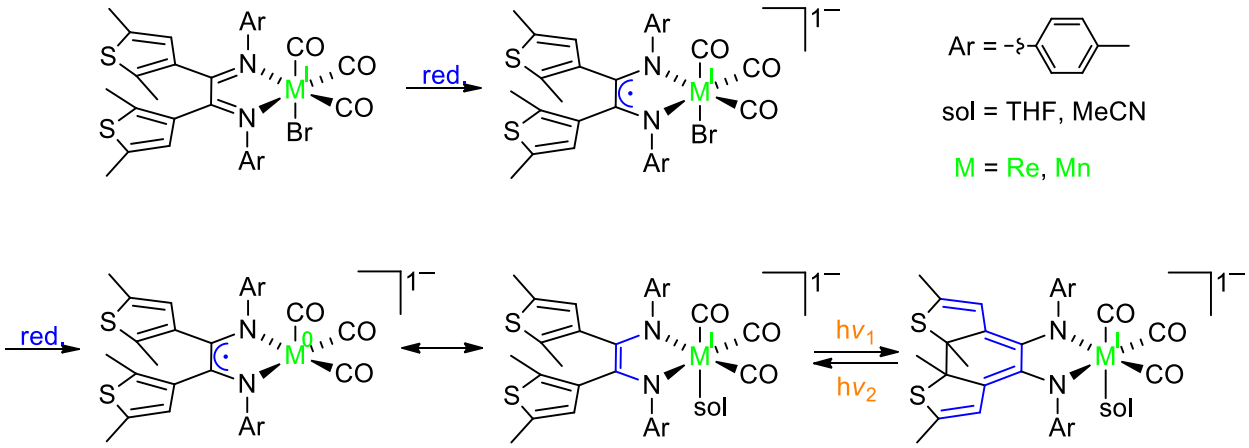

Die Synthese des Rhenium-Komplexes verlief erfolgreich; die Reduktion endete jedoch in einer Mischung mehrerer (paramagnetischer) Spezies. Für die Bildung des doppelt reduzierten Liganden konnten keine ausreichenden Hinweise gefunden werden.

Die Synthese des gewünschten Mangan-Komplexes erwies sich als erfolglos, da stattdessen ein Mangan(II)-Komplex mit zwei *α*-Diimin-Liganden gebildet wurde.

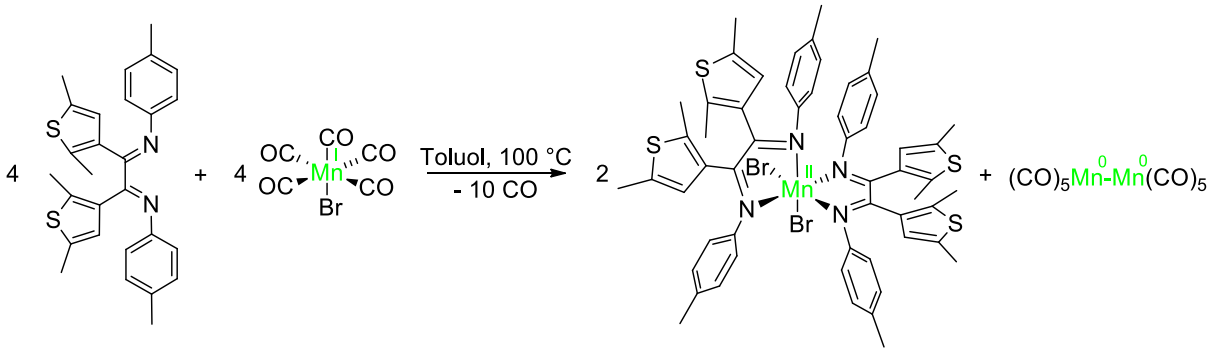

4.5 Kupfer(I)-Komplex mit 1,2-Bis(2,5-dimethyl-3-thienyl)ethan-*N*-*p*-tolyl-diimin als Ligand

Dieses Projekt entstand durch Berichte, dass Kupfer(I)-Halogenide mit DABs Komplexe unterschiedlicher Zusammensetzung bilden. Daher wurde 1,2-Bis(2,5-dimethyl-3-thienyl)ethan-*N*-*p*-tolyl-diimin mit Kupfer(I)-chlorid zur Reaktion gebracht, um herauszufinden, ob sich ein für die Zielsetzung dieser Arbeit geeigneter Komplex des Typs **A** bilden würde.

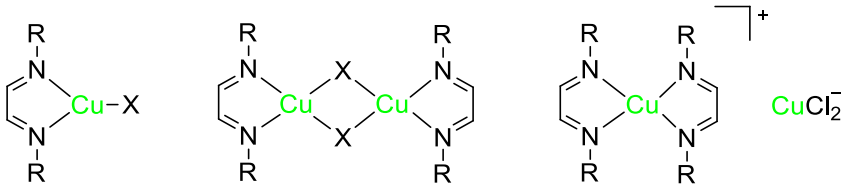

Leider konnte nur ein Komplex des Typs **C** isoliert werden, der für weitere Untersuchungen nicht von Interesse war.

4.6 Untersuchung von DTE-Komplexen Gebildet aus 1,2-Bis(2,5-dimethyl-3-thienyl)ethandion und Al-/Ga-FLPs

In diesem Projekt wurden DTE-Komplexe, die durch Reaktion von 1,2-Bis(2,5-dimethyl-3-thienyl)ethandion mit Al-/Ga-FLPs gebildet wurden, hinsichtlich einer auftretenden Photoreaktion untersucht: bei Bestrahlung mit UV-A Licht konnte, sowohl in Lösung und als auch im Feststoff, ein rascher Farbumschlag von Ocker zu Purpur beobachtet werden.

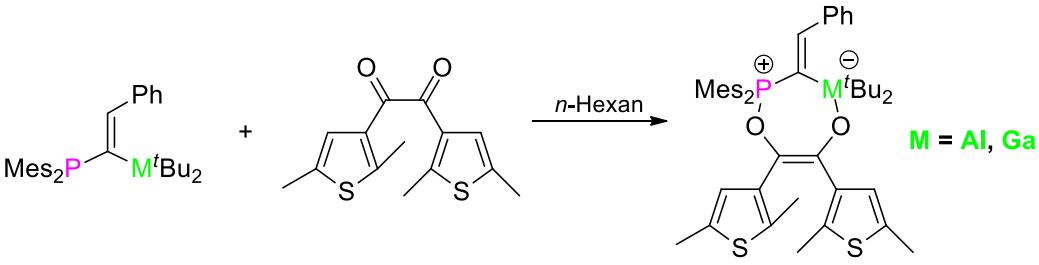

Daher wurden UV/Vis-, ^{31}P-, ^{13}C-, ^{1}H-NMR Untersuchungen und andere Experimente durchgeführt. Während einige Ergebnisse auf die gewünschte Photozyklisierung hindeuteten, ist dies bei anderen Befunden nicht der Fall. Unabhängig davon, ob eine Photozyklisierung stattfand oder nicht, zeigten die Experimente deutlich, dass die Produkte der photoinduzierten Umwandlung labil waren und sich komplexe Mischungen von Zersetzungsprodukten entwickelten.

Die erfolgreiche Synthese der DTE-Komplexe legte nahe, dass ein Syntheseweg für diese auf Metallprecursors basieren sollte, die gleichzeitig als Zwei-Elektronen-Reduktionsmittel wirken können.

4.7 Untersuchungen des DTE-Komplexes der Reaktion von 1,2-Bis(2,5-dimethyl-3-thienyl)ethandion und $ReCl_3(CH_3CN)(PPh_3)_2$

Das Ziel des letzten Projekts war 1) die Vermutung zu bestätigen, dass die Verwendung eines Metallprecursors, der auch als Zwei-Elektronen-Reduktionsmittel fungieren kann, bei der Reaktion mit 1,2-Bis(2,5-dimethyl-3-thienyl)ethandion zum entsprechenden DTE-Komplex führen würde und 2) diesen Komplex in Hinblick auf eine mögliche Photozyklisierung zu untersuchen. Die Reaktion von 1,2-Bis(2,5-dimethyl-3-thienyl)ethandion und $ReCl_3(CH_3CN)(PPh_3)_2$ verlief jedoch nicht wie erwartet, da ein anderes Produkt, ein Rh(IV)-Komplex, stattdessen isoliert wurde.

erwartet

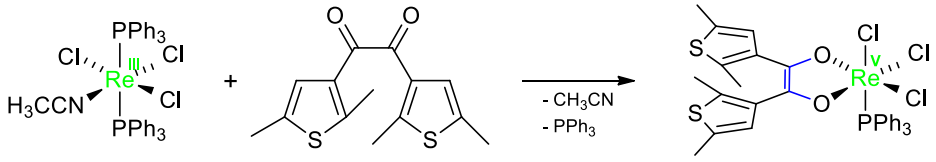

beobachtet/vermutet

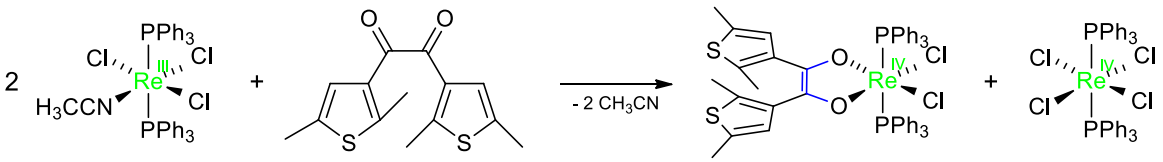

Das unerwartete Produkt war jedoch von großem Interesse, da eine Photozyklisierung zu einem non-innocent Verhalten des DTE-Liganden hätte führen können. Leider konnte bei Bestrahlung mit UV-Licht kein Hinweis auf eine auftretende Photozyklisierung gefunden werden; Unterschiede, die in den UV/Vis-Spektren beobachtet wurden, deuteten lediglich auf eine Konformationsänderung innerhalb des Komplexes hin.

References

1 https://www.acs.org/content/acs/en/greenchemistry/what-is-green-chemistry.html, 12.02.2023.
2 O. U. Press, *The Oxford New Greek Dictionary: Greek-English, English-Greek*., Penguin Putnam Inc., New York, **2008**.
3 G. Ertl, *Angew. Chem. Int. Ed.* **2009**, *48*, 6600-6606.
4 J. J. Berzelius, *Jahresberichte über die Fortschritte der physikalischen Wissenschaften* **1836**, 237-245.
5 http://www.culturevoyage.co.uk/wp-content/uploads/2013/03/Alchymist.jpg,
6 W. Ostwald, *Z. Phys. Chem. 1894* **1894**, *15*, 705-706.
7 W. Ostwald, *Phys. Z.* **1902**, *3*, 313-322.
8 M. A. Fox, J. K. Whitesell, *Organische Chemie*, Spektrum Akademischer Verlag, Heidelberg, **1995**.
9 H. Bisswanger, *Enzyme: Struktur, Kinetik und Anwendungen*, John Wiley & Sons, Weinheim, **2015**.
10 W. Reschetilowski, *Einführung in die Heterogene Katalyse*, Springer Spektrum, **2015**.
11 https://upload.wikimedia.org/wikipedia/commons/1/15/Hamburg_Museum_2010-1207-217.jpg, 12.02.2023.
12 D. Steinborn, *Grundlagen der metallorganischen Komplexkatalyse*, 3rd ed., Springer-Verlag, **2019**.
13 Numerous editors, *Ullmann's Encyclopedia of Industrial Chemistry*, **2011**.
14 R. Froböse, *Mein Auto repariert sich selbst*, John Wiley & Sons, Weinheim, **2012**.
15 https://pubs.usgs.gov/periodicals/mcs2020/mcs2020-nitrogen.pdf, 12.02.2023.
16 G. Schwedt, *Experimente rund um die Kunststoffe des Alltags*, John Wiley & Sons, Weinheim, **2013**.
17 K. Ziegler, E. Holzkamp, H. Breil, H. Martin, *Angew. Chem.* **1955**, *67*, 541-636.
18 https://www.nobelprize.org/prizes/lists/all-nobel-prizes-in-chemistry, *12.02.2023*.
19 A. M. Thayer, *Chem. Eng. News* **2013**, *91*, 68-70.
20 C. K. Jørgensen, *Coord. Chem. Rev.* **1966**, *1*, 164–178.
21 C. K. Jørgensen, *Structure and Bonding* **1966**, *1*, 234-248.
22 K. P. Butin, E. K. Beloglazkina, N. V. Zyk, *Russ. Chem. Rev.* **2005**, *74*, 531-553.
23 M. D. Ward, J. A. McCleverty, *Dalton Trans.* **2002**, 275-288.
24 A. Mukherjee, T. K. Sen, P. K. Ghorai, S. K. Mandal, *Sci. Rep.* **2013**, *3*, 2821-2831.
25 P. J. Chirik, K. Wieghardt, *Science* **2010**, *327*, 794-795.
26 P. J. Chirik, *Inorg. Chem.* **2011**, *50*, 9737-9740.
27 V. Lyaskovskyy, B. de Bruin, *ACS Catal.* **2012**, *2*, 270-279.
28 T. Tezgerevska, K. G. Alley, C. Boskovic, *Coord. Chem. Rev.* **2014**, *268*, 23-40.
29 J. A. McCleverty, *Prog. Inorg. Chem.* **1968**, *10*, 49-221.
30 G. N. Schrauzer, V. P. Mayweg, *J. Am. Chem. Soc.* **1962**, *84*, 3221.
31 H. B. Gray, R. Williams, I. Bernal, E. Billig, *J. Am. Chem. Soc.* **1962**, *84*, 3596-3597.
32 G. N. Schrauzer, V. P. Mayweg, *J. Am. Chem. Soc.* **1965**, *87*, 3585-3592.
33 G. N. Schrauzer, V. P. Mayweg, H. W. Finck, U. Müller-Westerhoff, W. Heinrich, *Angew. Chem. Int. Ed.* **1964**, *3*, 381.
34 G. N. Schrauzer, V. P. Mayweg, *Z. Naturforsch. B* **1964**, *19b*, 192-198.
35 G. N. Schrauzer, V. P. Mayweg, *J. Am. Chem. Soc.* **1965**, *87*, 1483-1489.
36 G. N. Schrauzer, V. P. Mayweg, *J. Am. Chem. Soc.* **1966**, *88*, 3235-3242.
37 G. N. Schrauzer, V. P. Mayweg, W. Heinrich, *J. Am. Chem. Soc.* **1966**, *88*, 5174-5179.
38 G. N. Schrauzer, H. N. Rabinowitz, *J. Am. Chem. Soc.* **1968**, *90*, 4297-4302.
39 H. B. Gray, E. Billig, *J. Am. Chem. Soc.* **1963**, *85*, 2019-2020.

40 E. Billig, R. Williams, I. Bernal, J. H. Waters, H. B. Gray, *Inorg. Chem.* **1964**, *3*, 663-666.
41 S. I. Shupack, E. Billig, R. J. H. Clark, R. Williams, H. B. Gray, *J. Am. Chem. Soc.* **1964**, *86*, 4594-4602.
42 E. I. Stiefel, J. H. Waters, E. Billig, H. B. Gray, *J. Am. Chem. Soc.* **1965**, *87*, 3016-3017.
43 A. Davison, N. Edelstein, R. H. Holm, A. H. Maki, *J. Am. Chem. Soc.* **1963**, *85*, 2029-2030.
44 A. Davison, N. Edelstein, R. H. Holm, A. H. Maki, *Inorg. Chem.* **1963**, *2*, 1227-1232.
45 A. H. Maki, N. Edelstein, A. Davison, R. H. Holm, *J. Am. Chem. Soc.* **1964**, *86*, 4580-4587.
46 C. K. Jørgensen, *Oxidation Numbers and Oxidation States*, Springer, Germany, **1969**.
47 F. Wöhler, *Grundriss der Chemie*, Duncker und Humblot, Berlin, **1840**.
48 L. S. Hegedus, *Transition Metals in the Synthesis of Complex Organic Molecules*, University Science Books, Sausalito, **1999**.
49 P. Chaudhuri, C. N. Verani, E. Billig, E. Bothe, T. Weyhermüller, K. Wieghardt, *J. Am. Chem. Soc.* **2001**, *123*, 2213-2223.
50 P. Day, *Nature not Mocked*, Imperial College Press, London, **2005**.
51 W. Kaim, B. Schwederski, *Coord. Chem. Rev.* **2010**, *254*, 1580-1588.
52 J. Hockertz, S. Steenken, K. Wieghardt, P. Hildebrandt, *J. Am. Chem. Soc.* **1993**, *115*, 11222-11230.
53 B. Adam, E. Bill, E. Bothe, B. Goerdt, G. Haselhorst, K. Hildenbrandt, A. Sokolowski, S. Steenken, T. Weyhermüller, K. Wieghardt, *Chem. Eur. J.* **1997**, *3*, 308-319.
54 R. Schnepf, A. Sokolowski, J. Müller, V. Bachler, K. Wieghardt, P. Hildebrandt, *J. Am. Chem. Soc.* **1998**, *120*, 2352-2364.
55 M. D. Snodin, L. Ould-Moussa, U. Wallmann, S. Lecomte, V. Bachler, E. Bill, H. Hummel, T. Weyhermüller, P. Hildebrandt, K. Wieghardt, *Chem. Eur. J.* **1999**, *5*, 2554-2565.
56 R. Gleiter, I. Hyla-Kryspin, P. Binger, M. Regitz, *Organometallics* **1992**, *11*, 177-181.
57 M.-H. Baik, T. Ziegler, C. K. Schauer, *J. Am. Chem. Soc.* **2000**, *122*, 9143-9154.
58 R. F. Winter, in *Spectroelectrochemistry*, **2008**, pp. 145-206.
59 W. I. Dzik, B. de Bruin, *Organomet. Chem.* **2011**, *37*, 46-78.
60 R. Riedel, C. Janiak, *Anorganische Chemie 7. Auflage*, De Gruyter, Berlin, **2007**.
61 C. G. Pierpont, *Coord. Chem. Rev.* **2001**, *216-217*, 99-125.
62 D. N. Hendrickson, C. G. Pierpont, *Spin Crossover in Transition Metal Compounds II* **2004**, *234*, 63-95.
63 R. M. Buchanan, C. G. Pierpont, *J. Am. Chem. Soc.* **1980**, *102*, 4951-4957.
64 C. G. Pierpont, R. M. Buchanan, *Coord. Chem. Rev.* **1981**, *38*, 45-87.
65 C. G. Pierpont, W. Lange, *Prog. Inorg. Chem.* **1994**, *41*, 331-442.
66 O. Sato, J. Tao, Y.-Z. Zhang, *Angew. Chem. Int. Ed.* **2007**, *46*, 2152-2187.
67 A. Witt, F. W. Heinemann, M. M. Khusniyarov, *Chem. Sci.* **2015**, *6*, 4599-4609.
68 J. Sedó, J. Saiz-Poseu, F. Busqué , D. Ruiz-Molina, *Adv. Mater.* **2013**, *25*, 653-701.
69 V. I. Minkin, *Russ. Chem. Bull. Int. Ed.* **2008**, *57*, 687-717.
70 A. Dei, D. Gatteschi, C. Sangregorio, L. Sorace, *Acc. Chem. Res.* **2004**, *11*.
71 A. Bencini, A. Caneschi, A. Dei, D. Gatteschi, C. Sangregorio, D. Shultz, L. Sorace, M. G. F. Vaz, *C. R. Chimie* **2003**, *6*, 663-676.
72 D. A. Schultz, S. H. Bodnar, R. K. Kumar, J. W. Kampf, *J. Am. Chem. Soc.* **1999**, *121*, 10664-10665.
73 W. P. Griffith, *Transit. Met. Chem.* **1993**, *18*, 250-256.
74 M. Nomura, T. Cauchy, M. Fourmigué, *Coord. Chem. Rev.* **2010**, *254*, 1406-1418.
75 C. V. Krishnan, C. Creutz, H. A. Schwarz, N. Sutin, *J. Am. Chem. Soc.* **1983**, *105*, 5617-5623.
76 A. Juris, V. Balzani, F. Barigelletti, S. Campagna, P. Belser, A. Zelewsky, *Coord. Chem. Rev.* **1988**, *84*, 85-277.
77 I. Hanazaki, S. Nagakura, *Bull. Chem. Soc. Jpn.* **1971**, *44*, 2312-2321.
78 M. C. Hughes, D. J. Macero, *Inorg. Chem.* **1976**, *15*, 2040-2044.
79 Y. Saito, J. Takemoto, B. Hutchinson, K. Nakamoto, *Inorg. Chem.* **1972**, *11*, 2003-2011.

80 E. König, S. Herzog, *J. Inorg. Nucl. Chem.* **1970**, *32*, 585-599.
81 S. Blanchard, E. Derat, M. Desage-El Murr, L. Fensterbank, M. Malacria, V. Mouriès-Mansuy, *Eur. J. Inorg. Chem.* **2012**, 376-389.
82 J. I. van der Vlugt, J. N. H. Reek, *Angew. Chem. Int. Ed.* **2009**, *48*, 8832-8846.
83 S. Enthaler, K. Junge, M. Beller, *Angew. Chem. Int. Ed.* **2008**, *47*, 3317-3321.
84 R. H. Crabtree, *The Organometallic Chemistry of the Transition Metals*, John Wiley & Sons, New Jersey, **2009**.
85 C. Bolm, J. Legros, J. Le Paih, L. Zani, *Chem. Rev.* **2004**, *104*, 6217-6254.
86 C. Bolm, *Nat. Chem.* **2009**, *1*, 420.
87 R. M. Wachter, M. P. Montague-Smith, B. P. Branchaud, *J. Am. Chem. Soc.* **1997**, *119*, 7743-7749.
88 P. Chaudhuri, M. Hess, U. Flörke, K. Wieghardt, *Angew. Chem. Int. Ed.* **1998**, *37*, 2217-2220.
89 B. Jazdzewski, W. B. Tolman, *Coord. Chem. Rev.* **2000**, *200-202*.
90 J. W. Whittaker, *Chem. Rev.* **2003**, *103*, 2347-2363.
91 L. Que, Jr., W. B. Tolman, *Nature* **2008**, *455*, 333-340.
92 P. Chaudhuri, M. Hess, U. Flörke, K. Wieghardt, *Angew. Chem. Int. Ed.* **1998**, *37*, 2217-2220.
93 R. M. Wing, G. C. Tustin, W. H. Okamura, *J. Am. Chem. Soc.* **1970**, *92*, 1935-1939.
94 A. Herman, R. M. Wing, *J. Organomet. Chem.* **1973**, *63*, 441-450.
95 K. Wang, E. I. Stiefel, *Science* **2001**, *291*, 106-109.
96 M. W. Bouwcamp, A. C. Bowman, E. Lobkovsky, P. J. Chirik, *J. Am. Chem. Soc.* **2006**, *128*, 13340-13341.
97 B. de Bruin, E. Bill, E. Bothe, T. Weyhermüller, K. Wieghardt, *Inorg. Chem.* **2000**, *39*, 2936-2947.
98 P. H. M. Budzelaar, B. de Bruin, A. W. Gal, K. Wieghardt, J. H. van Lenthe, *Inorg. Chem.* **2001**, *40*, 4649-4655.
99 S. K. Russell, E. Lobkovsky, P. J. Chirik, *J. Am. Chem. Soc.* **2011**, *133*, 8858-8861.
100 A. M. Tondreau, C. Milsmann, A. D. Patrick, H. M. Hoyt, E. Lobkovsky, K. Wieghardt, P. J. Chirik, *J. Am. Chem. Soc.* **2010**, *132*, 15046-15059.
101 K. T. Sylvester, P. J. Chirik, *J. Am. Chem. Soc.* **2009**, *131*, 8772-8774.
102 W. Morris, H. M. C. Stuff, *The American Heritage Dictionary of the English Language*, Houghton Mifflin Harcourt, Wilmington, **1982**.
103 M. D. Ward, *Chem. Ind. (London)* **1997**, *16*, 640-645.
104 R. H. Mitchell, T. R. Ward, Y. Wang, P. W. Dibble, *J. Am. Chem. Soc.* **1999**, *121*, 2601-2602.
105 V. Balzani, A. Credi, M. Venturi, *Molecular Devices and Machines Concepts and Perspectives for the Nanoworld*, Wiley VCH, Weinheim, **2008**.
106 B. L. Feringa, W. R. Browne, *Molecular Switches*, Wiley-VCH, Weinheim, **2011**.
107 J.-P. Launay, C. Coudret, *Ann. N. Y. Acad. Sci.* **1998**, *852*, 116-132.
108 M. D. Ward, *J. Chem. Educ.* **2001**, *78*, 321-328.
109 M. D. Ward, *Chem. Soc. Rev.* **1995**, *24*, 121-134.
110 A. P. de Silva, H. Q. N. Gunaratne, T. Gunnlaugsson, A. J. M. Huxley, C. P. McCoy, J. T. Rademacher, T. E. Rice, *Chem. Rev.* **1997**, *97*, 1515-1566.
111 E. R. Kay, D. A. Leigh, F. Zerbetto, *Angew. Chem. Int. Ed.* **2007**, *46*, 72-191.
112 G. Wittke, *J. Chem. Educ.* **1983**, *60*, 239-240.
113 P. Monk, *Physical Chemistry Understanding our Chemical World*, Wiley VCH, Chichester, **2004**.
114 J. Strähle, E. Schweda, G. Jander, E. Blasius, *Lehrbuch der analytischen und präparativen anorganischen Chemie*, S. Hirzel, Stuttgart, **2006**.
115 J. M. Berg, J. L. Tymoczko, L. Stryer, *Biochemistry*. 5th ed., W. H. Freeman, New York, **2002**.
116 D. G. Stavenga, W. J. de Grip, E. N. Pugh, *Molecular Mechanisms in Visual Transduction*, Elsevier Sciene B. V., Amsterdam, **2000**.

117 H. Dürr, H. Bouas-Laurent, *Photochromism: Molecules and Systems*, Elsevier, Amsterdam, **2003**.
118 D. Gust, T. A. Moore, A. L. Moore, *Chem. Commun.* **2006**, 1169-1178.
119 A. M. Weiner, *Ultrafast Optics*. Editor, Wiley, New Jersey, **2009**.
120 Y. Kishimoto, J. Abe, *J. Am. Chem. Soc.* **2009**, *131*, 4227-4229.
121 Y. Satoh, Y. Ishibashi, S. Ito, Y. Nagasawa, H. Miyasaka, H. Chosrowjan, S. Taniguchi, N. Mataga, D. Kato, A. Kikuchi, J. Abe, *Chem. Phys. Lett.* **2007**, *448*, 228-231.
122 J. Fritzsche, *C. R. Acad. Sci.* **1867**, *69*, 1035-1037.
123 E. Fischer, Y. Hirshberg, *J. Chem. Soc.* **1952**, 4522-4524.
124 O. Chaudé, P. Rumpf, *C. R. Acad. Sci.* **1953**, *236*, 697-699.
125 R. Heiligman-Rim, Y. Hirshberg, E. Fischer, *J. Phys. Chem.* **1962**, *66*, 2470-2477.
126 L. Kortekaas, W. R. Browne, *Chem Soc Rev* **2019**, *48*, 3406-3424.
127 Y. Hirshberg, *J. Am. Chem. Soc.* **1956**, *78*, 2304-2312.
128 R. Klajn, *Chem. Soc. Rev.* **2014**, *43*, 148-184.
129 C. J. Martin, G. Rapenne, T. Nakashima, T. Kawai, *J. Photochem. Photobiol., C* **2018**, *34*, 41-51.
130 M. Li, Q. Zhang, Y.-N. Zhou, S. Zhu, *Prog. Polym. Sci.* **2018**, *79*, 26-39.
131 P. Rivera-Fuentes, S. J. Lippard, *ChemMedChem* **2014**, *9*, 1238-1243.
132 P. Rivera-Fuentes, A. T. Wrobel, M. L. Zastrow, M. Khan, J. Georgiou, T. T. Luyben, J. C. Roder, K. Okamoto, S. J. Lippard, *Chem. Sci.* **2015**, *6*, 1944-1948.
133 E. Mitscherlich, *Ann. Phys.* **1834**, *108*, 225-227.
134 E. Mitscherlich, *Liebigs Ann.* **1834**, *12*, 305-311.
135 F. Beilstein, R. Fittig, H. Hübner, *Zeitschrift Für Chemie*, Quandt & Händel, Göttingen, **1866**.
136 G. S. Hartley, *Nature* **1937**, *140*, 281.
137 A. H. Cook, *J. Chem. Soc.* **1938**, 876-881.
138 J. M. Robertson, *J. Chem. Soc.* **1939**, 232-236.
139 S. Shinkai, T. Nakaji, T. Ogawa, K. Shigematsu, O. Manabe, *J. Am. Chem. Soc.* **1981**, *103*, 111-115.
140 S. Shinkai, T. Ogawa, Y. Kusano, O. Manabe, K. Kukukawa, T. Goto, T. Matsuda, *J. Am. Chem. Soc.* **1982**, *104*, 1960-1967.
141 S. Shinkai, O. Manabe, *Top. Curr. Chem.* **1984**, *121*, 67-104.
142 A. Laurent, *C. R. Acad. Sci.* **1843**, 856-860.
143 W. A. Miller, *Elements of Chemistry: Theoretical and Practical*, 5th ed., Longmans, Green, Reader & Dyer, London, **1880**.
144 E. L. Eliel, S. H. Wilen, *Stereochemistry of Organic Compounds*, John Wiley & Sons, INC., USA, **1994**.
145 D. C. Neckers, D. H. Volman, G. von Bünau, *Advances in Photochemistry Volume 19*, John Wiley & Sons, Inc., USA, **1995**.
146 C. Bastianelli, V. Caia, G. Cum, R. Gallo, V. Mancini, *J. Chem. Soc. Perin Trans.* **1991**, *2*, 679-683.
147 F. B. Mallory, C. W. Mallory, *Organic Reactions: Photocyclization of Stilbenes and Related Molecules*, Wiley & Sons, Inc., New York, **1984**, Vol. 30.
148 D. H. Waldeck, *Chem. Rev.* **1991**, *91*, 415-436.
149 M. Irie, *Chem. Rev.* **2000**, *100*, 1685-1716.
150 M. Irie, M. Mohri, *J. Org. Chem.* **1988**, *53*, 803-808.
151 R. M. Kellogg, M. B. Groen, H. Wynberg, *J. Org. Chem.* **1967**, *32*, 3093-3100.
152 M. Irie, *Jpn. J. Appl. Phys.* **1989**, *28*, 215-219.
153 M. Irie, T. Fukaminato, K. Matsuda, S. Kobatake, *Chem. Rev.* **2014**, *114*, 12174-277.
154 M. Irie, K. Sakemura, M. Okinaka, K. Uchida, *J. Org. Chem.* **1995**, *60*, 8305-8309.
155 H. Tian, S. Yang, *Chem. Soc. Rev.* **2004**, *33*, 85-97.
156 H. Tian, Y. Feng, *J. Mater. Chem.* **2008**, *18*, 1617-1622.
157 M. Irie, T. Fukaminato, K. Matsuda, S. Kobatake, *Chem. Rev.* **2014**, *114*, 12174-12277.

158 T. Fukaminato, S. Ishida, R. Métivier, *NPG Asia Mater.* **2018**, *10*, 859-881.
159 S. Kobatake, S. Takami, H. Muto, T. Ishikawa, M. Irie, *Nature* **2007**, *446*, 778-781.
160 S. Pu, C. Zheng, Z. Le, G. Liu, C. Fan, *Tetrahedron* **2008**, *64*, 2576-2585.
161 K. Uchida, S. Sukata, Y. Matsuzawa, M. Akazawa, J. J. de Jong, N. Katsonis, Y. Kojima, S. Nakamura, J. Areephong, A. Meetsma, B. L. Feringa, *Chem. Commun.* **2008**, 326-328.
162 M. Irie, *Photochem. Photobiol. Sci.* **2010**, *9*, 1535-1542.
163 M. Irie, *Proc. Jpn. Acad. Ser. B Phys. Biol. Sci.* **2010**, *86*, 472-483.
164 S. H. Kawai, S. L. Gilat, J.-M. Lehn, *Eur. J. Org. Chem.* **1999**, 2359-2366.
165 Y. Odo, K. Matsuda, M. Irie, *Chem. Eur. J.* **2006**, *12*, 4283-4288.
166 J.-P. Malval, I. Gosse, J.-P. Morand, R. Lapouyade, *J. Am. Chem. Soc.* **2002**, *124*, 904-905.
167 M. Takeshita, M. Irie, *J. Org. Chem.* **1998**, *63*, 6643-6649.
168 K. P. C. Vollhardt, N. E. Schore, *Organische Chemie*. 4th ed., Wiley VCH, Weinheim, **2005**.
169 R. Janoschek, *Chirality - From Weak Bosons to the α-Helix*. 1st ed., Editor, Springer, Berlin, Heidelberg, **1991**.
170 T. J. Wigglesworth, D. Sud, T. B. Norsten, V. S. Lekhi, N. R. Branda, *J. Am. Chem. Soc.* **2005**, *127*, 7272-7273.
171 T. Nakagawa, T. Ubukata, Y. Yokoyama, *J. Photochem. Photobiol., C* **2018**, *34*, 152-191.
172 Y. Inoue, R. V., *Chiral Photochemistry*, Marcel Dekker, New York, **2004**.
173 Y. Yokoyama, T. Shiozawa, Y. Tani, T. Ubukata, *Angew. Chem. Int. Ed.* **2009**, *48*, 4521-4523.
174 M. Takeshita, H. Jin-nouchi, *Chem. Commun.* **2010**, *46*, 3994-3995.
175 C. Jurissek, F. Berger, F. Eisenreich, M. Kathan, S. Hecht, *Angew. Chem. Int. Ed.* **2019**, *58*, 1945-1949.
176 J. E. Smyth, N. M. Butler, P. A. Keller, *Nat. Prod. Rep.* **2015**, *32*, 1562-1583.
177 M. Ōki, *Topics in Stereochemistry* **1983**, *14*, 1-81.
178 G. H. Christie, J. Kenner, *J. Chem. Soc., Trans.* **1922**, *121*, 614-620.
179 A. Miyashita, A. Yasuda, H. Takaya, K. Toriumi, T. Ito, T. Souchi, R. Noyori, *J. Am. Chem. Soc.* **1980**, *102*, 7932-7934.
180 L. Pu, *Chem. Rev.* **1998**, *98*, 2405-2494.
181 R. Noyori, *Angew. Chem. Int. Ed.* **2002**, *41*, 2008-2022.
182 K. Mikami, M. Yamanaka, *Chem. Rev.* **2003**, *103*, 3369-3400.
183 E. Kumarasamy, R. Raghunathan, M. P. Sibi, J. Sivaguru, *Chem. Rev.* **2015**, *115*, 11239-11300.
184 P. W. Glunz, *Bioorg. Med. Chem. Lett.* **2018**, *28*, 53-60.
185 J. Clayden, W. J. Moran, P. J. Edwards, S. R. LaPlante, *Angew. Chem. Int. Ed.* **2009**, *48*, 6398-6401.
186 S. Erbas-Cakmak, D. A. Leigh, C. T. McTernan, A. L. Nussbaumer, *Chem. Rev.* **2015**, *115*, 10081-10206.
187 G. W. Gribble, J. A. Joule, *Progress in Heterocyclic Chemistry*, Elsevier, UK, **2009**, Vol. 30.
188 P. Bamfield, M. G. Hutchings, *Chromic Phenomena: Technological Applications of Colour Chemistry*, Royal Society of Chemistry, **2010**.
189 S. H. Kawai, S. L. Gilat, J.-M. Lehn, *J. Chem. Soc., Chem. Commun.* **1994**, 1011-1013.
190 S. H. Kawai, S. L. Gilat, R. Ponsinet, J.-M. Lehn, *Chem. Eur. J.* **1995**, *1*, 285-293.
191 P. H.-M. Lee, C.-C. Ko, N. Zhu, V. W.-W. Yam, *J. Am. Chem. Soc.* **2007**, *129*, 6058-6059.
192 V. W.-W. Yam, C.-C. Ko, N. Zhu, *J. Am. Chem. Soc.* **2004**, *126*, 12734-12735.
193 A. Fernández-Acebes, J.-M. Lehn, *Adv. Mater.* **1998**, *10*, 1519-1522.
194 A. Fernández-Acebes, J.-M. Lehn, *Chem. Eur. J.* **1999**, *5*, 3285-3292.
195 R. T. F. Jukes, V. Adamo, F. Hartl, P. Balser, L. De Cola, *Inorg. Chem.* **2004**, *43*, 2779-2792.
196 B. M. Neilson, V. M. Lynch, C. W. Bielawski, *Angew. Chem. Int. Ed.* **2011**, *50*, 10322-10326.
197 V. Lemieux, M. D. Spantulescu, K. K. Baldridge, N. R. Branda, *Angew. Chem.* **2008**, *120*, 5112-5115.
198 K. M. Clark, *Inorg. Chem.* **2016**, *55*, 6443-6448.
199 J. T. Price, P. J. Ragogna, *Chem. Eur. J.* **2013**, *19*, 8473-8477.

200 R. Bautista, P. Bernal, R. Herrera, B. M. Santoyo, J. M. Lazcano-Seres, F. Delgado, J. Tamariz, *J. Org. Chem.* **2011**, *76*, 7901-7911.
201 M. V. Vollmer, C. W. Machan, M. L. Clark, W. E. Antholine, J. Agarwal, H. F. Schaefer, 3rd, C. P. Kubiak, J. R. Walensky, *Organometallics* **2015**, *34*, 3-12.
202 L. H. Staal, A. Oskan, K. Vrieze, *J. Organomet. Chem.* **1979**, 235-245.
203 R. W. Balk, D. J. Stufkens, A. Oskam, *J. Chem. Soc., Dalton Trans.* **1981**, 1124-1133.
204 W. K. Smothers, M. S. Wrighton, *J. Am. Chem. Soc.* **1983**, *105*, 1067-1069.
205 K. Kalyanasundaram, *J. Chem. Soc., Faraday Trans.* **1986**, *2*, 2401-2415.
206 R. R. AndréaWim, W. G. J. De Lange, D. J. Stufkens, A. Oskam, *Inorganica Chimica Acta* **1988**, 77-84.
207 D. J. Stufkens, *Coord. Chem. Rev.* **1990**, *104*, 39-112.
208 B. D. Rossenaar, C. J. Kleverlaan, M. C. E. van de Ven, D. J. Stufkens, A. Oskam, J. Fraanje, K. Goubitz, *J. Organomet. Chem.* **1995**, *493*, 153-162.
209 B. D. Rossenaar, D. J. Stufkens, J. Vlček, A., *Inorg. Chem.* **1996**, *35*, 2902-2909.
210 A. M. B. Rodríguez, A. Gabrielsson, M. Motevalli, P. Matousek, M. Towrie, J. Šebera, S. Záliš, A. Vlček, *J. Phys. Chem. A* **2005**, *109*, 5016-5025.
211 J. C. Waltin, *in: Encyclopedia of Radicals in Chemistry, Biology and Materials*, John Wiley & Sons, Online, **2012**.
212 R. J. Baker, R. D. Farley, C. Jones, D. P. Mills, M. Kloth, D. M. Murphy, *Chem. Eur. J.* **2005**, *11*, 2972-2982.
213 W. R. Hagen, *Dalton trans.* **2006**, 4415-4434.
214 A. Grupp, M. Bubrin, F. Ehret, H. Kvapilová, S. Záliš, W. Kaim, *J. Org. Chem.* **2014**, *751*, 678-685.
215 J. M. Smieja, E. E. Benson, B. Kumar, K. A. Grice, C. S. Seu, A. J. Miller, J. M. Mayer, C. P. Kubiak, *Proc. Natl. Acad. Sci. USA* **2012**, *109*, 15646-15650.
216 J. M. Smieja, M. D. Sampson, K. A. Grice, E. E. Benson, J. D. Froehlich, C. P. Kubiak, *Inorg. Chem.* **2013**, *52*, 2484-2491.
217 F. Breher, in *Anorganische Chemie - Prinzipien von Struktur und Reaktivität*, 4th ed., De Gruyter, Berlin, **2012**.
218 H. t. Dieck, L. Stamp, *Z. Naturforsch. B* **1990**, *45*, 1369-1382.
219 H. t. Dieck, I. W. Renk, *Chem. Ber.* **1971**, *104*, 92-109.
220 S. K. Burley, G. A. Petsoko, *Science* **1985**, *229*, 23-28.
221 J. Backs, M. Lange, J. Possart, A. Wollschlager, C. Muck-Lichtenfeld, W. Uhl, *Angew. Chem. Int. Ed.* **2017**, *56*, 3094-3097.
222 M. Lange, J. C. Tendyck, P. Wegener, A. Hepp, E. U. Wurthwein, W. Uhl, *Chem. Eur. J.* **2018**, *24*, 12856-12868.
223 J. Possart, W. Uhl, *Organometallics* **2018**, *37*, 1314-1323.
224 S. Aldrige, in *The Group 13 Metals Aluminium, Gallium, Indium and Thallium: Chemical Patterns and Peculiarities*, John Wiley & Sons, **2011**, Chap. 2, pp. 75 - 147.
225 S. Xiao, T. Yi, F. Li, C. Huang, *Tetrahedron Letters* **2005**, *46*, 9009-9012.
226 J. T. van Herpt, M. C. Stuart, W. R. Browne, B. L. Feringa, *Chem. Eur. J.* **2014**, *20*, 3077-3083.
227 E. Feng, R. Lu, C. Fan, C. Zheng, S. Pu, *Tetrahedron Letters* **2017**, *58*, 1390-1394.
228 N. R. Branda, A. J. Myles, *Adv. Funct. Mater.* **2002**, *12*, 167-173.
229 B. M. Neilson, V. M. Lynch, C. W. Bielawski, *Angew. Chem. Int. Ed.* **2011**, *50*, 10322-10326.
230 G. Duan, N. Zhu, V. W. Yam, *Chem. Eur. J.* **2010**, *16*, 13199-13209.
231 A. Escribano, T. Steenbock, C. Stork, C. Herrmann, J. Heck, *Chemphyschem.* **2017**, *18*, 596-609.
232 A. Flambard, L. Ruhlmann, J. Canny, R. Thouvenot, *C. R. Chimie* **2008**, *11*, 415-422.
233 J. C. Ott, E. A. Suturina, I. Kuprov, J. Nehrkorn, A. Schnegg, M. Enders, L. H. Gade, *Angew. Chem. Int. Ed.* **2021**, *60*, 22856-22864.
234 A. J. Teator, H. Shao, G. Lu, P. Liu, C. W. Bielawski, *Organometallics* **2017**, *36*, 490-497.

235 J. Boixel, A. Colombo, F. Fagnani, P. Matozzo, C. Dragonetti, *Eur. J. Inorg. Chem.* **2022**, e202200034.
236 M. N. Sokolov, N. E. Fyodorova, R. Paetow, D. Fenske, A. G. Ravelo, D. Y. Naumov, V. E. Fedorov, *Inorg. Chim. Acta* **2007**, *360*, 2192-2196.
237 G. Rouschias, G. Wilkinson, *J. Chem. Soc. A* **1967**, 993-1000.
238 G. Rouschias, G. Wilkinson, *J. Chem. Soc. A* **1966**, 465-472.
239 G. Wilkinson, *Comprehensive Coordination Chemistry*, Pergamon Press, **1987**, Vol. 4.
240 H. Kraudelt, U. Schilde, E. Uhlemann, *Z. anorg. allg. Chem.* **1995**, *621*, 1797-1799.
241 D. Schlüter, F. Kleemiss, M. Fugel, E. Lork, K. Sugimoto, S. Grabowsky, J. R. Harmer, M. Vogt, *Chem. Eur. J.* **2020**, *26*, 1335-1343.

Supporting Information

Table of Contents

General Information

All reagents, except the FLPs, were obtained commercially (Sigma Aldrich, Alfa Aesar) and used as received. Anhydrous solvents were collected from a SPS800 mBraun solvent system and stored over 3 Å molecular sieves under an inert argon atmosphere after being degassed.

NMR: ^{1}H, ^{13}C, ^{31}P, ^{119}Sn NMR spectra were recorded at room temperature, unless stated otherwise, with a Bruker Avance Neo 600 MHz or a Bruker Avance 360 MHz spectrometer. ^{1}H and ^{13}C NMR Chemical shifts (δ) are reported downfield from tetramethylsilane, those of ^{31}P NMR were referenced to 85% H_3PO_4 in H_2O, those of ^{119}Sn NMR to 90% Me_4Sn 90% in C_6D_6; signals in parts per million (ppm). Residual solvent signals (5.32 ppm for ^{1}H, 53.84 ppm for ^{13}C in CD_2Cl_2; 7.26 ppm for ^{1}H, 77.16 for ^{13}C in CD_3Cl; 3.58 ppm for ^{1}H, 67.21 for ^{13}C in *d*-THF; 7.16 ppm for ^{1}H, 128.06 ppm for ^{13}C in *d*-benzene) were used as references. ^{1}H NMR coupling constants (J) are reported in hertz (Hz), multiplicity is appointed as follows: s (singlet), d (doubled), t (triplet), m (muliplet). Assignments of ^{1}H and ^{13}C resonance signals were made based on COSY, HSQC and HMBC spectra. *High resolution MS (HRMS):* Electrospray ionization mass spectrometry (ESI-MS) was carried out on a Bruker Impact II. A MeCN solution or a mixture of a MeCN/DCM solution was directly injected into the spectrometer at a flow rate of 3 µL min^{-1}. Nitrogen served as both, drying gas and nebulizer with flow rates of 4 L min^{-1} and a pressure of 0.4 bar. Spectra were collected for 30 seconds and averaged. *UV/Vis Spectroscopy***:** Experiments were carried out at 298 K on a Varian Cary 50 UV/Vis-spectrophotometer. Cuvettes: 10 mm, synthetic quartz (QS) with Teflon cap. Probes were prepared under an inert atmosphere of argon. *Cyclic Voltammetry:* Experiments were carried out at 298 K with a Metrohm potentiostat running the NOVA 2.1 software package using a RHD Instruments electrochemical cell TSC 1600 closed. Solvent: DCM, MeCN; Electrolyte: $[TBA]PF_6$; Electrodes: Pt working electrode, Ag/AgCl pseudo reference electrode, Pt counter electrode.

Synthesis and Characterization of α-Diketone Ligand (90)

In a three neck flask $AlCl_3$ (9.39 g, 70.42 mmol, 1.00 eq.) was suspended in DCM (40 mL), cooled to -15 °C and treated with pyridine (2.8 mL, ρ = 0.978 g/cm^3, 35.21 mmol, 0.50 eq.) and 2,5-dimethylthiophene (8.0 mL, ρ = 0.985 g/cm^3, 70.42 mmol, 1.00 eq.), each dissolved in DCM (40 mL). Over a time period of 40 minutes oxalyl chloride (3.6 mL, ρ = 1.48 g/cm^3, 42.25 mmol, 0.60 eq.), dissolved in DCM (40 mL), was added to the red solution. After stirring for 40 minutes at -5 °C and 1 h at 5-10 °C, the mixture was poured onto ice. The organic layer was separated and the aqueous layer extracted with chloroform. The combined organic phases were then washed with water, sodium carbonate solution and saturated NaCl solution subsequently. Filtering through hot cotton and removal of the solvent under reduced pressure followed by a flash chromatography (cyclohexane/ethyl acetate, 100:3) of the viscous oil led to pure orange-brown product. **Yield:** 4.12 g (14.80 mmol, 42%); **Mp:** 65 °C; **R_f** = 0.38 (cyclohexane/ethyl acetate, 100:3); **^{1}H NMR:** (360 MHz, CD_2Cl_2) δ 6.90-6.88 (m, 2H, c), 2.70 (s, 6H, a), 2.39-2.36 (m, 6H, b) ppm; **^{13}C{1H} NMR:** (90 MHz, CD_2Cl_2) δ 189.7 (g), 151.9 (b), 136.9 (c), 132.1 (a), 127.1 (d), 16.1 (e), 15.0 (f) ppm; **^{1}H NMR:** (600 MHz, CD_3CN) δ 6.90 (s, 2H, c), 2.67 (s, 6H, a), 2.37 (s, 6H, b) ppm; **^{13}C{1H} NMR:** (150 MHz, CD_3CN) δ 190.5 (g), 152.4 (b), 138.1 (c), 132.6 (a), 127.4 (d), 16.0 (e), 14.8 (f) ppm; **^{1}H NMR:** (600 MHz, C_6D_6) δ 7.03-7.02 (m, 2H, c), 2.56 (s, 6H, a), 1.84-1.83 (m, 6H, b) ppm; **^{13}C{1H} NMR:** (150 MHz, C_6D_6) δ 189.5 (g), 151.2 (b), 136.3 (c), 132.7 (a), 127.6 (d), 15.8 (e), 14.4 (f) ppm; **^{1}H NMR:** (600 MHz, THF-d_8) δ 6.92-6.91 (m, 2H, c), 2.68 (s, 6H, a), 2.37-2.35 (m, 6H, b) ppm; **^{13}C{1H} NMR:** (150 MHz, THF-d_8) δ 189.5 (g), 151.2 (b), 136.9 (c), 132.8 (a), 127.6 (d), 15.6 (e), 14.5 (f) ppm; **UV/Vis** (CH_2Cl_2): λ_{max} = 271 nm; $\lambda_{shoulder}$ = 317 nm; **HRMS** (ESI) *m/z*: $[M+Na]^+$ calculated for $C_{14}H_{14}NaO_2S_2^+$, 301.03274, found 301.03296; CV (referenced to Fc/Fc^+, MeCN) $E_{1/2}^{red1}$ = -1.94 V, $E_{1/2}^{red2}$ = -2.91 V, (referenced to Fc/Fc^+, DCM) $E_{1/2}^{red}$ = -2.13 V.-

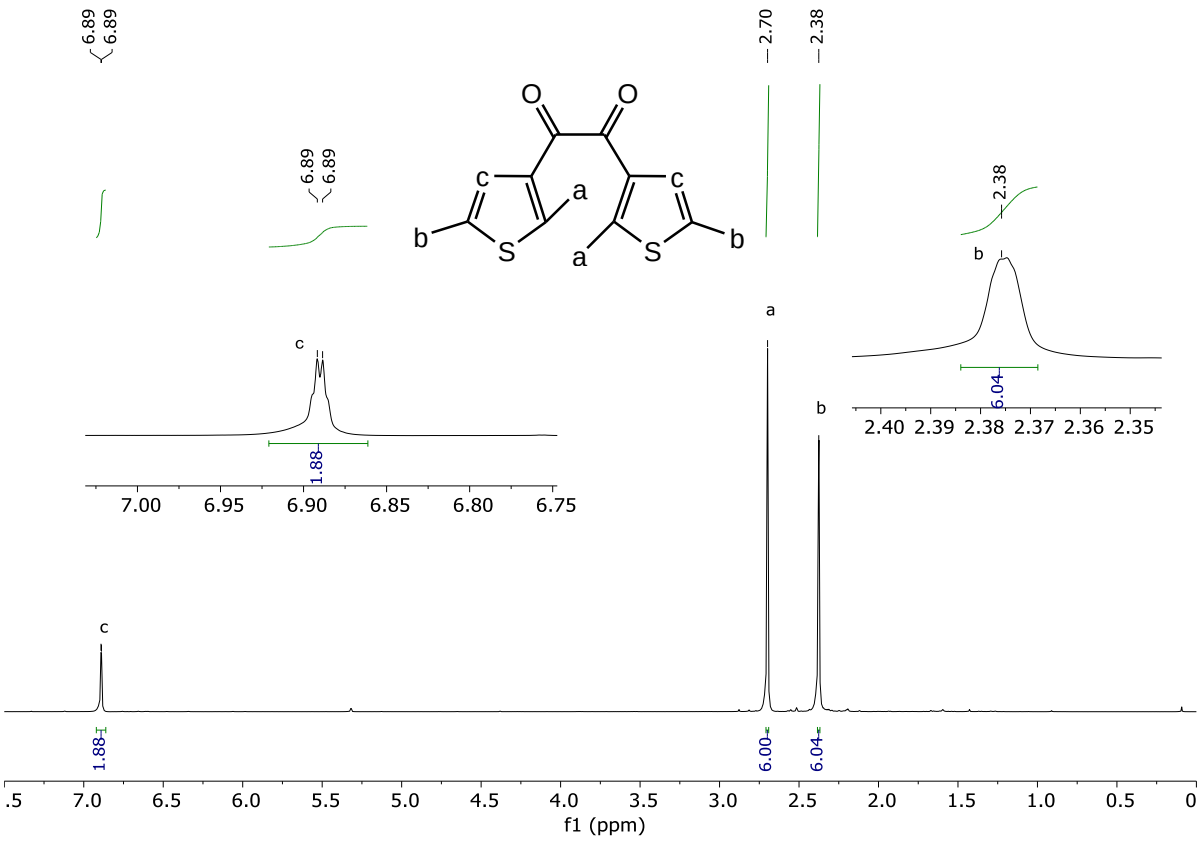

Figure S1: *^{1}H NMR spectrum (360 MHz, CD_2Cl_2) of* ***90****.*

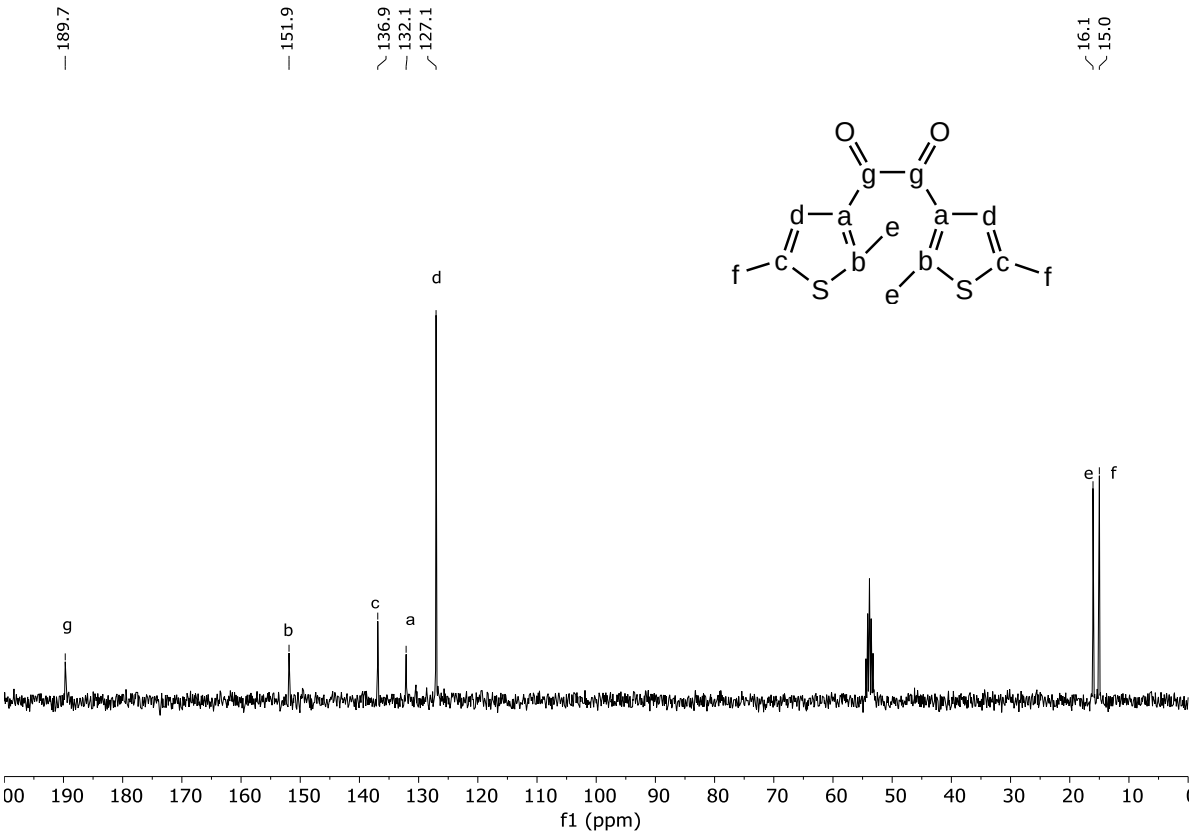

Figure S2: *$^{13}C\{^{1}H\}$ spectrum NMR (90 MHz, CD_2Cl_2) of* ***90****.*

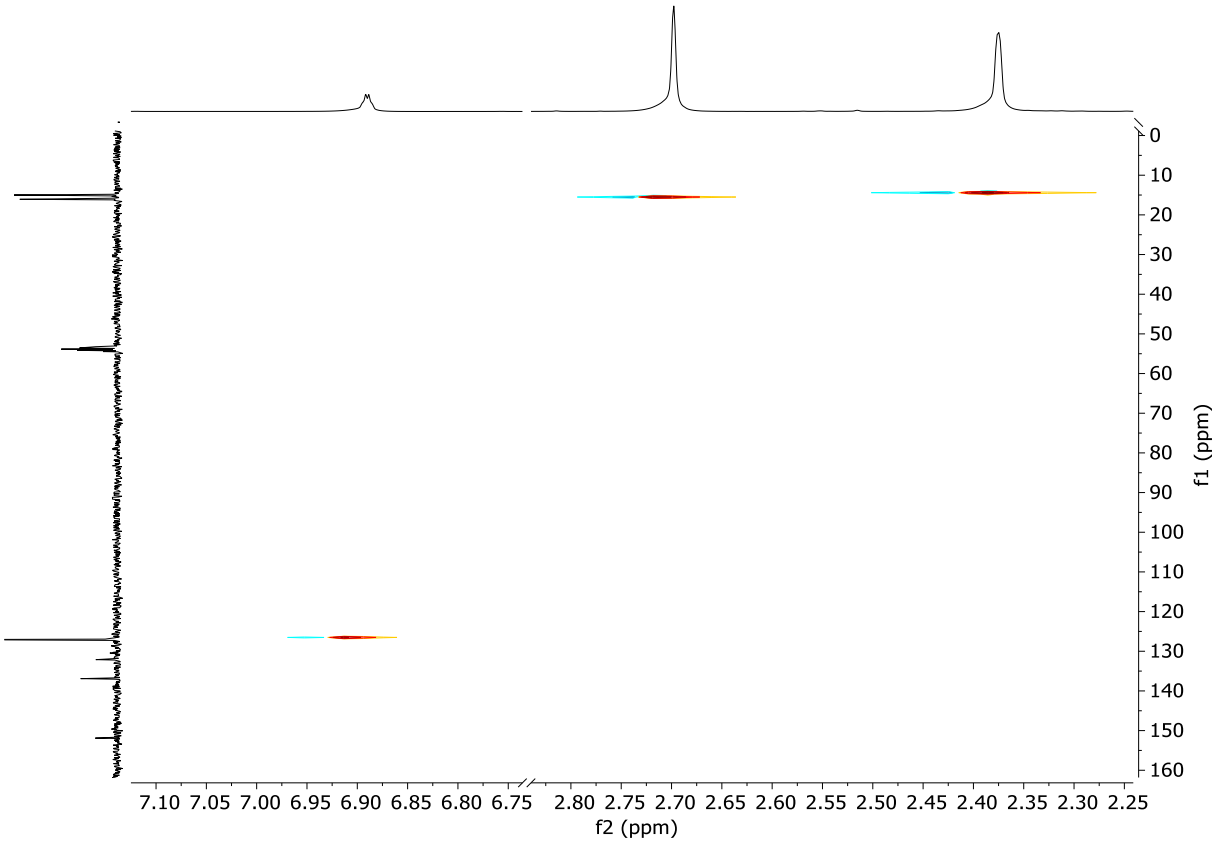

Figure S3: *HSQC spectrum (360/90 MHz, CD_2Cl_2) of* ***90****.*

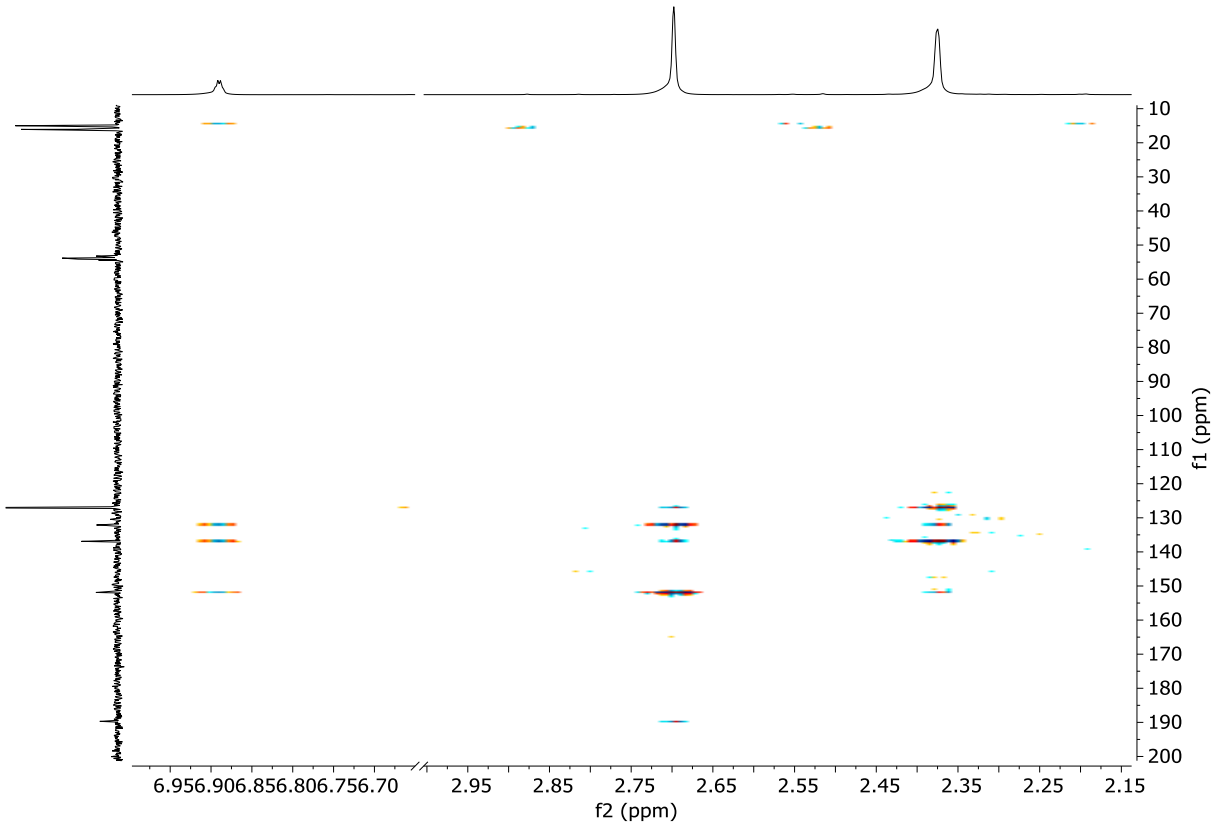

Figure S4: *HMBC spectrum (360/90 MHz, CD_2Cl_2) of* ***90****.*

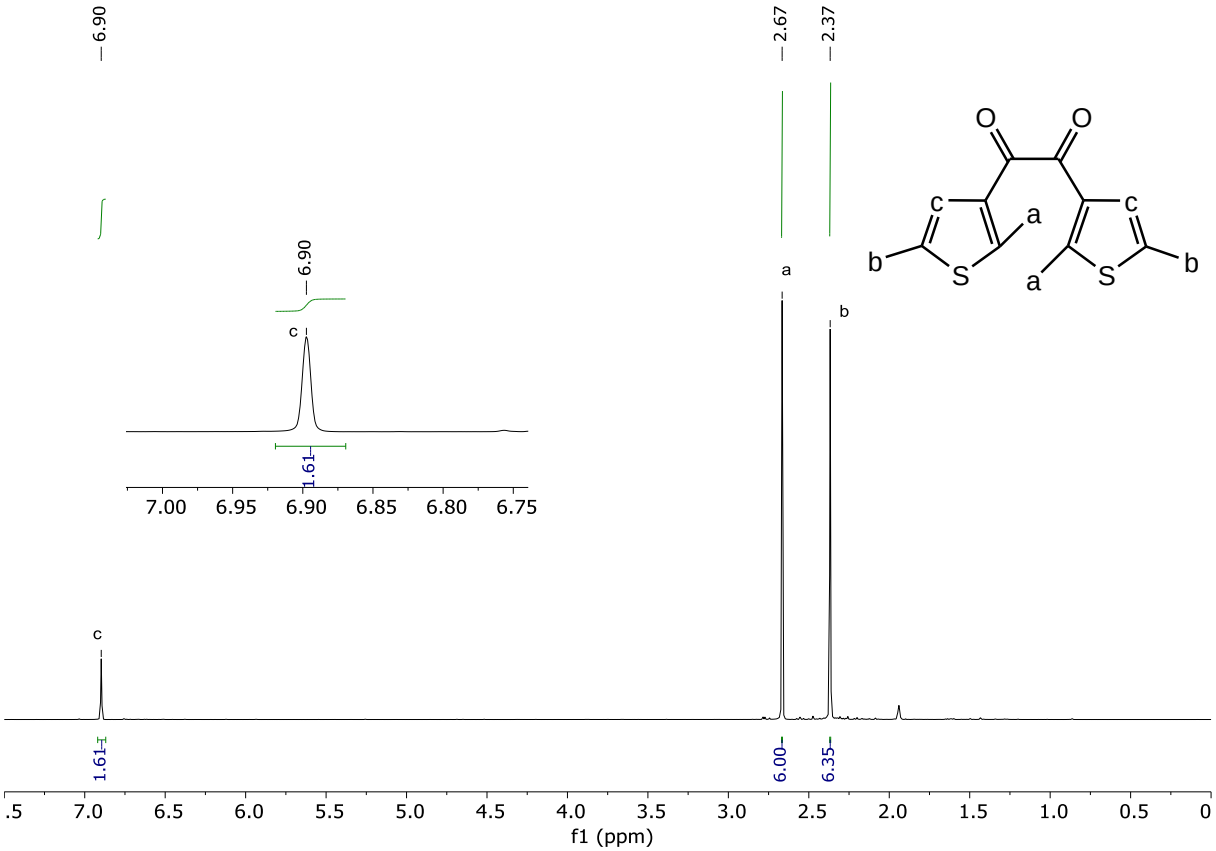

Figure S5: *^{1}H NMR spectrum (600 MHz, CD_3CN) of **90**.*

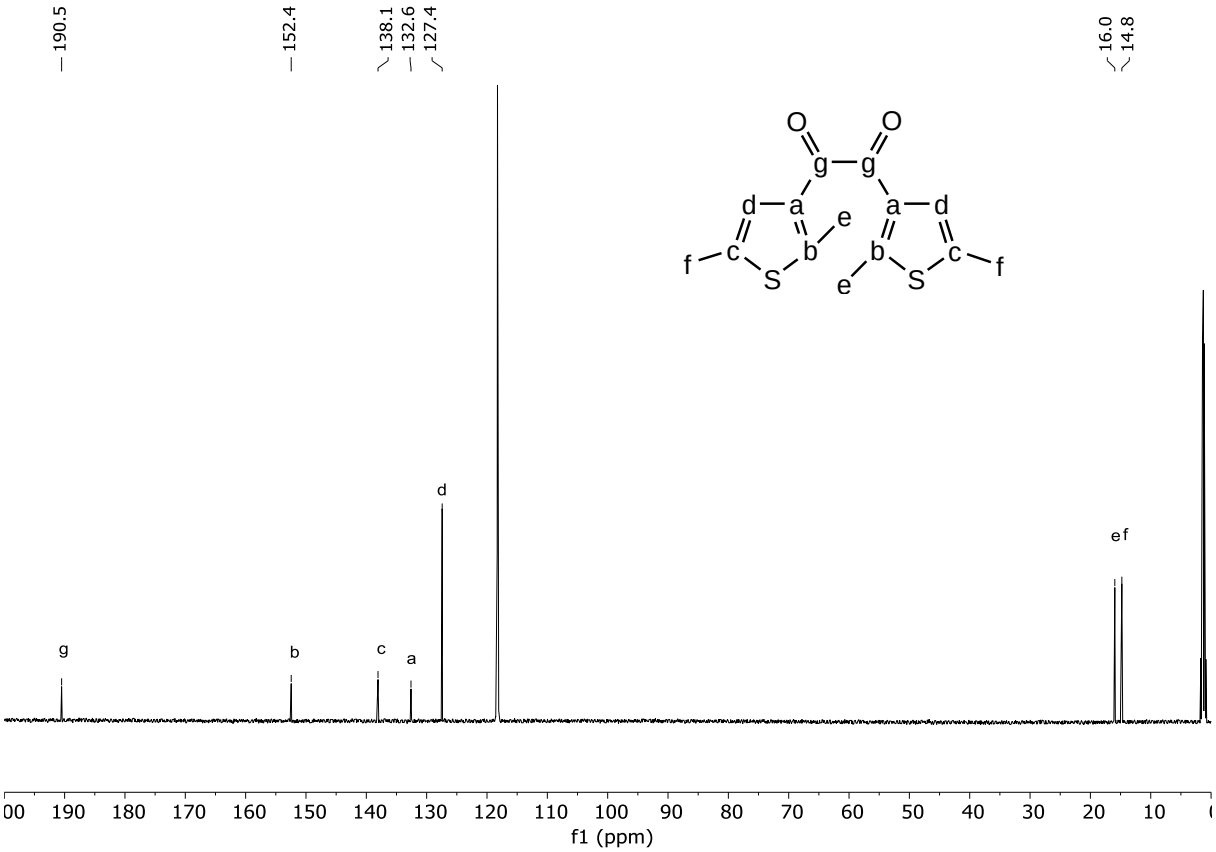

Figure S6: *$^{13}C\{^{1}H\}$ NMR spectrum (150 MHz, CD_3CN) of **90**.*

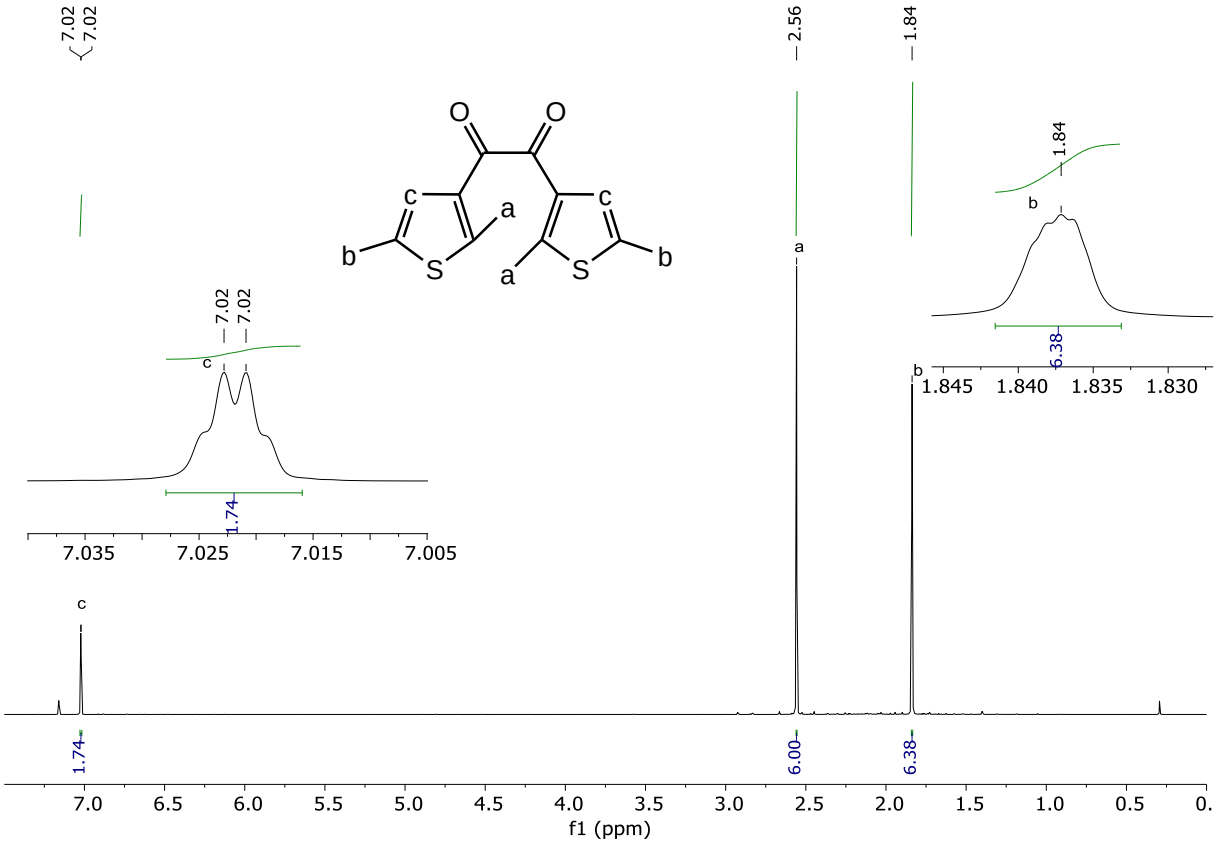

Figure S7: *^{1}H NMR spectrum (600 MHz, C_6D_6) of* ***90****.*

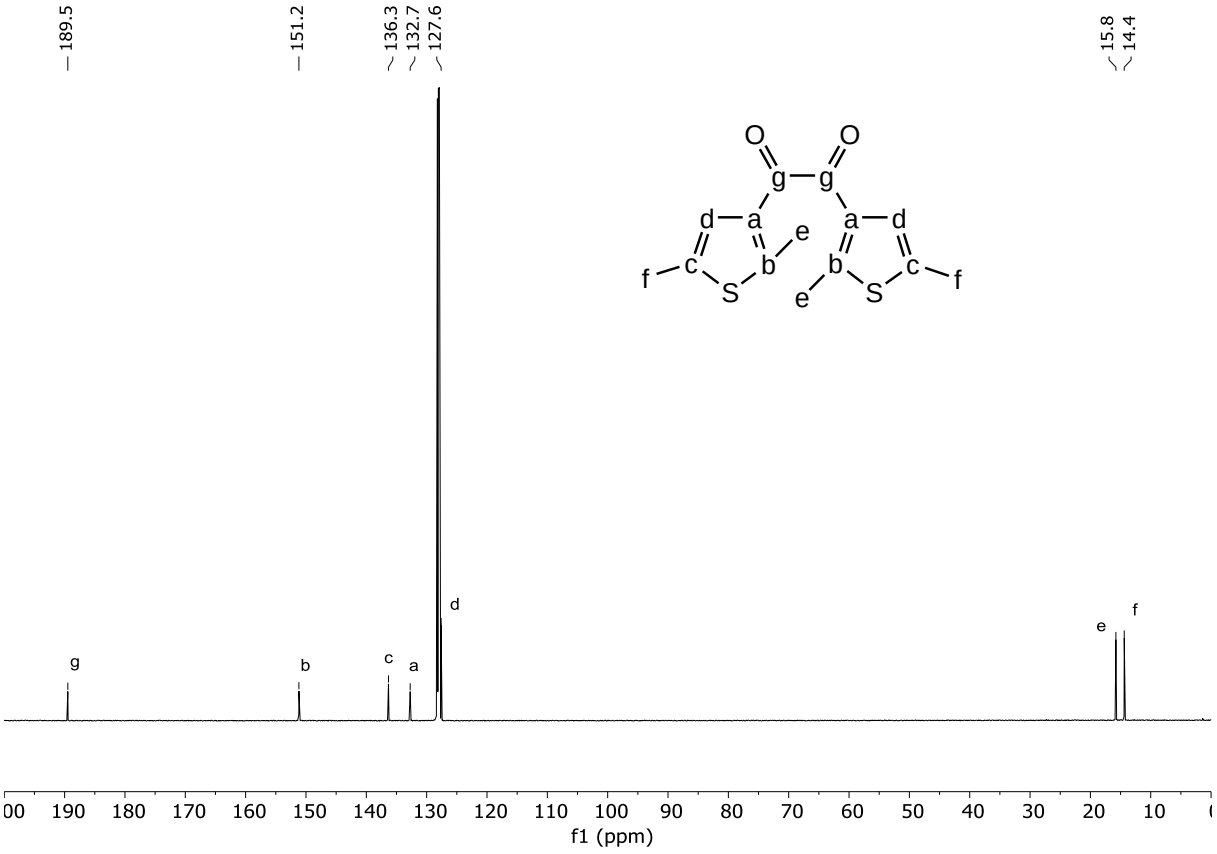

Figure S8: *$^{13}C\{^{1}H\}$ NMR spectrum (150 MHz, C_6D_6) of* ***90****.*

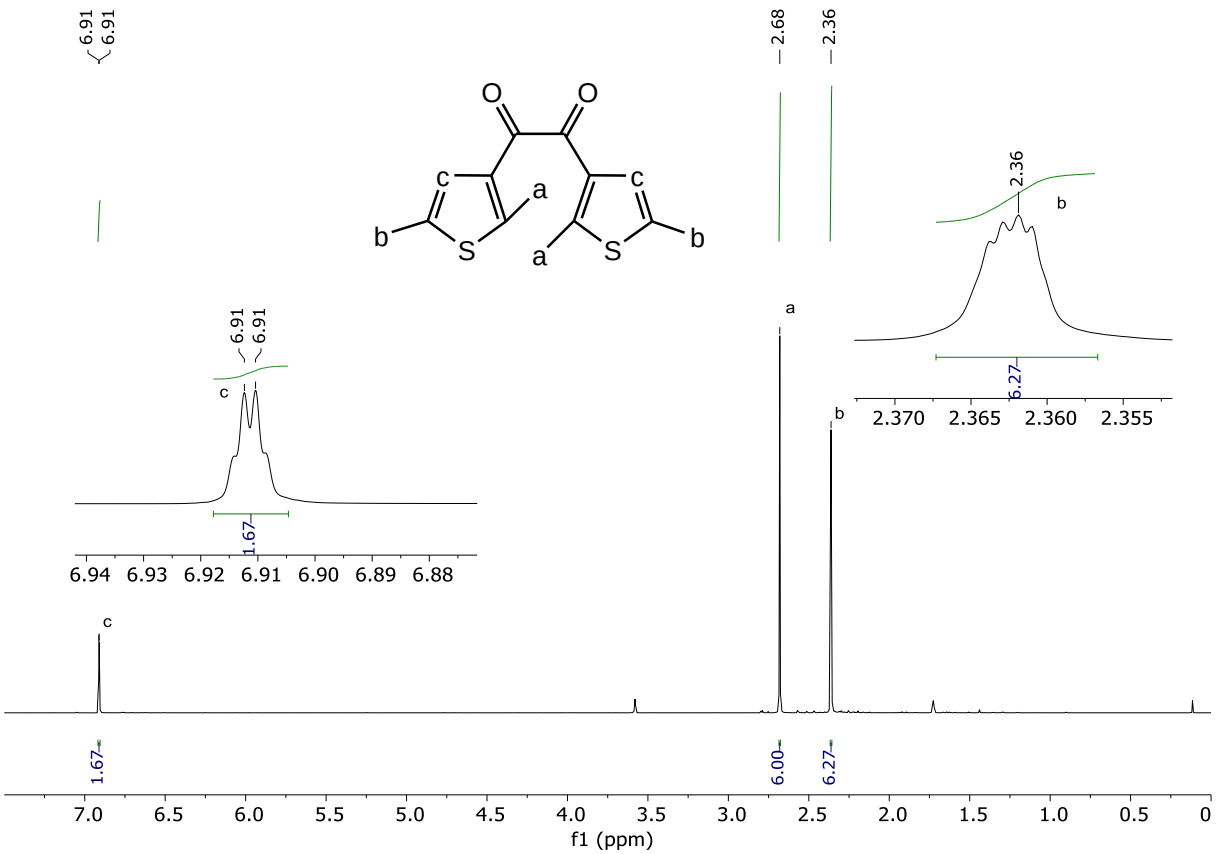

Figure S9: *^{1}H NMR spectrum (600 MHz, THF-d_8) of* ***90****.*

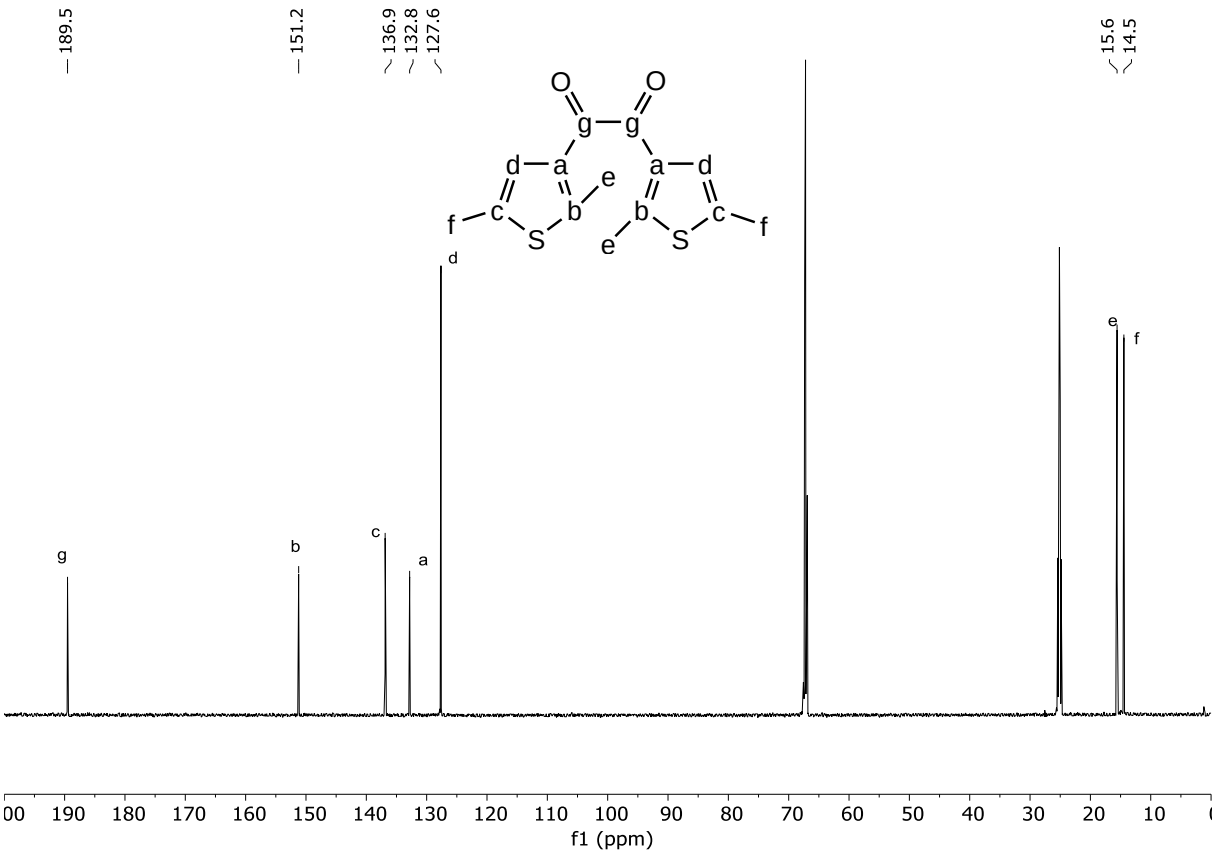

Figure S10: *$^{13}C\{^{1}H\}$ NMR spectrum (150 MHz, THF-d_8) of* ***90****.*

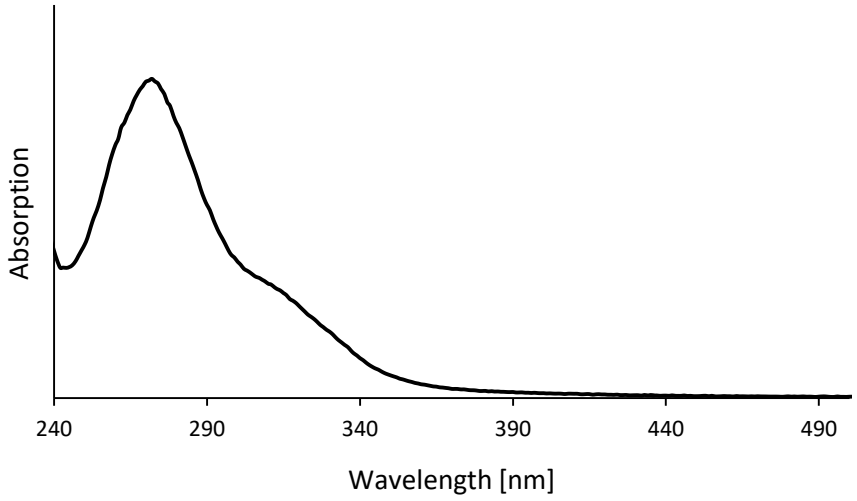

Figure S11: *UV/Vis spectrum of* ***90*** *in DCM.*

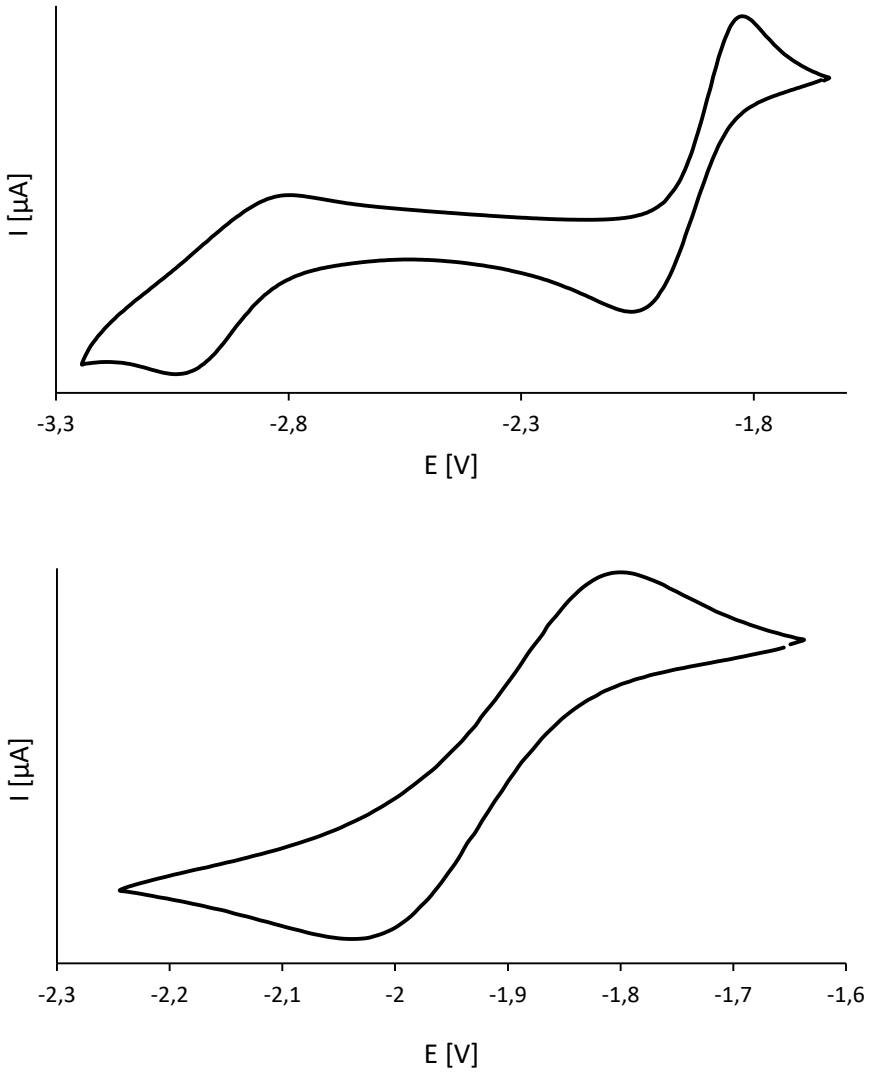

Figure S12: *Cyclic voltammograms of* ***90*** *(MeCN, [TBA]PF_6/0.1 M, scan rate 200 mV/s, potentials plotted vs Fc/Fc^+).*

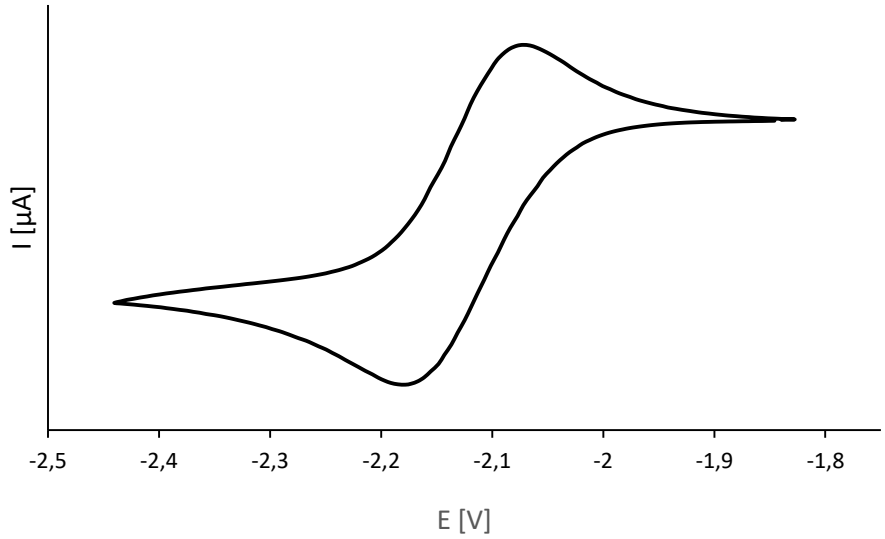

Figure S13: *Cyclic voltammogram of* ***90*** *(DCM, [TBA]PF_6/0.1 M, scan rate 200 mV/s, potentials plotted vs Fc/Fc^+).*

Synthesis and Characterization of *α*-Diimine Ligand (91)

α-Diketone **90** (0.41 g, 1.47 mmol, 1.0 eq.) was dissolved in 15 mL DCM and treated with $TiCl_4$ (194 µL, ρ = 1.73 g/cm^3, 1.77 mmol, 1.2 eq.). The immediately turned red solution was stirred for 1.5 h before *p*-toluidine (1.26 g, 11.78 mmol, 8.0 eq.) was added. After stirring for 72 h at rt a small amount of water was added and the occurring precipitate was filtered off. The phases were separated and the aqueous one was extracted with DCM. The organic layers were combined and dried over hot cotton before a column chromatography (cyclohexane/ethyl acetate, 100:2.5) was carried out. Subsequently the received product was dissolved in ethanol and crystallized by evaporation of the solvent. Washing the obtained orange crystals with small portions of *n*-hexane led to pure yellow product. Crystals suitable for X-ray crystallography were obtained from a solution of **91** in ethanol *via* slow evaporation of the solvent. **Yield:** 0.44 g (0.96 mmol, 65%); **Mp:** 107-110 °C; $\mathbf{R_f}$ = 0.15 (cyclohexane/ethyl acetate, 100:2.5); **^{1}H NMR:** (360 MHz, CD_2Cl_2): δ 6.92 (d, ^3J=8.2 Hz, 4H, e), 6.83 (s, 2H, c), 6.46 (d, ^3J=8.2 Hz, 4H, d), 2.50 (s, 6H, a), 2.36 (s, 6H, b), 2.26 (s, 6H, f) ppm; **^{13}C{1H} NMR:** (90 MHz, CD_2Cl_2): δ 161.2 (g), 147.3 (h), 141.7 (a/b), 135.6 (c), 135.0 (a/b), 134.4 (k), 129.2 (J), 127.1 (d), 120.7 (i), 21.0 (L), 15.8 (e), 15.2 (f) ppm; **^{1}H NMR:** (600 MHz, THF-d_8): δ 6.88 (d, ^3J=7.9 Hz, 4H, e), 6.86 (s, 2H, c), 6.44 (d, ^3J=8.3 Hz, 4H, d), 2.50 (s, 6H, a), 2.33 (s, 6H, b), 2.22 (s, 6H, f) ppm; **^{13}C{1H} NMR:** (150 MHz, THF-d_8): δ 161.5 (g), 148.0 (h), 141.6 (a/b), 135.6 (a/b), 135.5 (c), 134.2 (k), 129.2 (J), 127.7 (d), 121.1 (i), 20.8 (L), 15.8 (e), 14.7 (f) ppm; **UV/Vis** (CH_2Cl_2): λ_{max} = 275 nm; $\lambda_{shoulder}$ = 339 nm **HRMS** (ESI) *m/z*: $[M+H]^+$ calculated for $C_{28}H_{29}N_2S_2^+$, 457.17667, found 457.17690.-

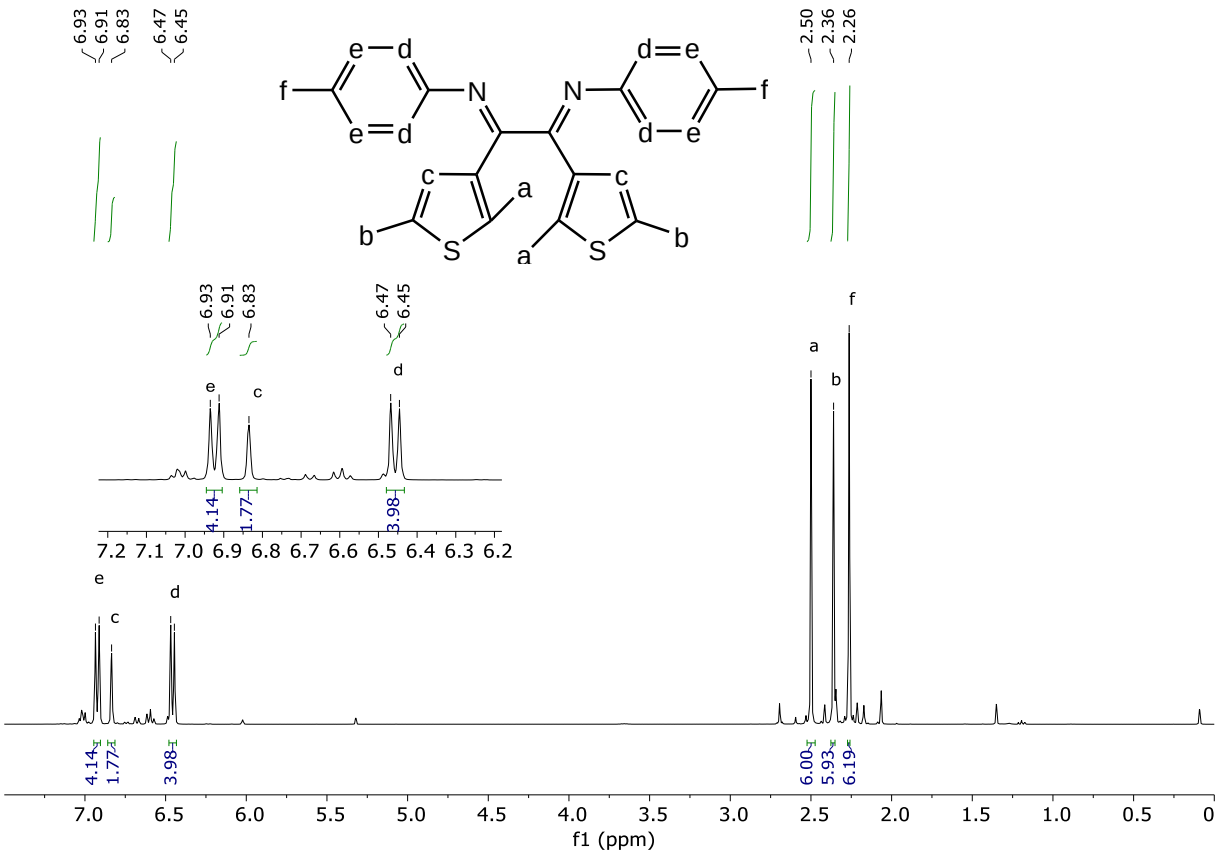

Figure S14: *^{1}H NMR spectrum (360 MHz, CD_2Cl_2) of* ***91****.*

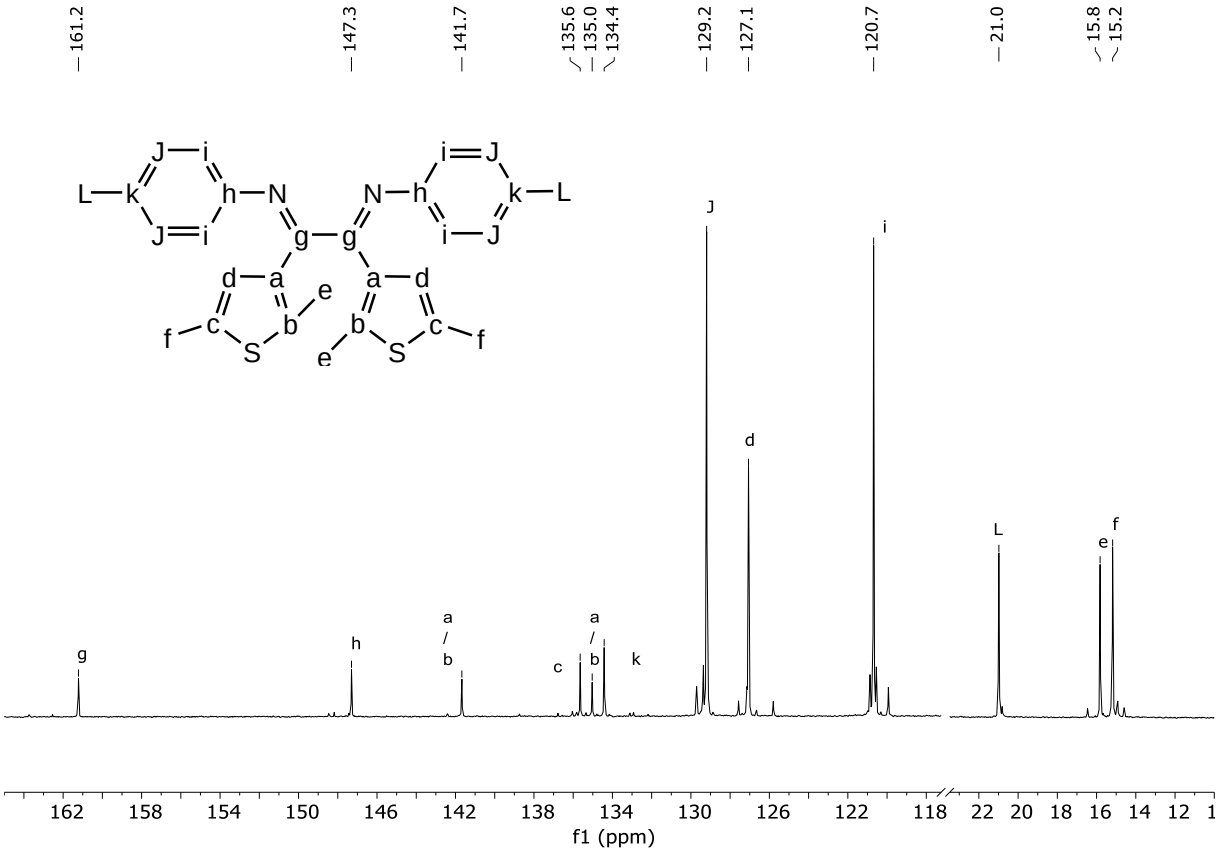

Figure S15: *$^{13}C\{^{1}H\}$ NMR spectrum (90 MHz, CD_2Cl_2) of* ***91****.*

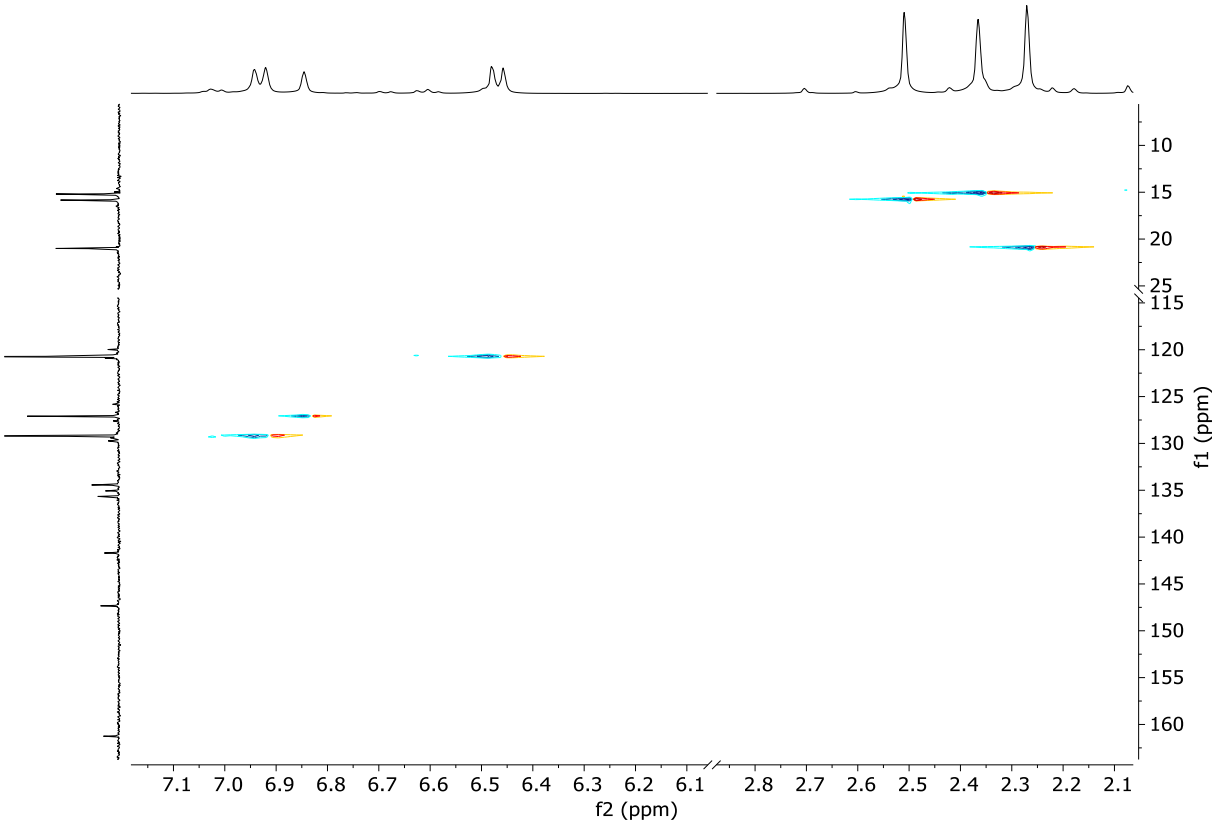

Figure S16: *HSQC spectrum (360/90 MHz, CD_2Cl_2) of* ***91****.*

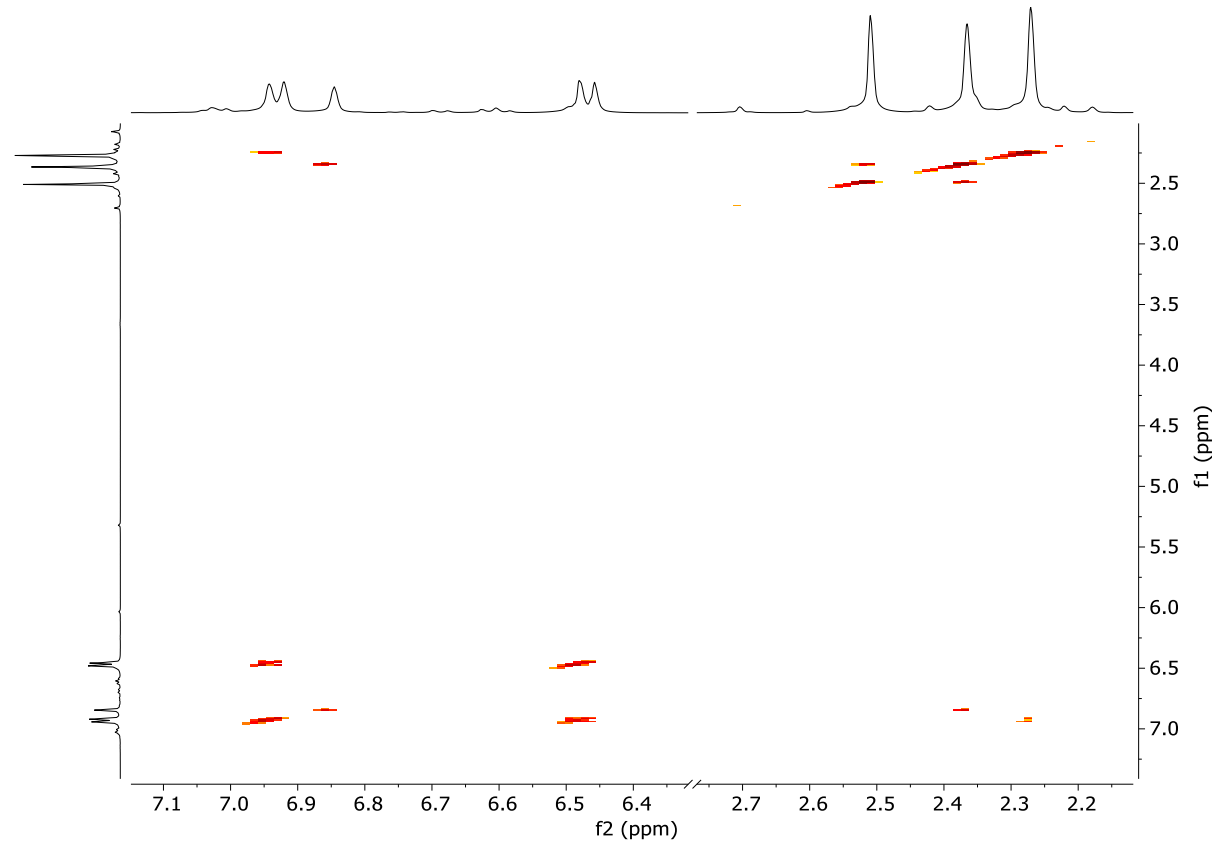

Figure S17: *H,H-COSY spectrum (360 MHz, CD_2Cl_2) of* ***91****.*

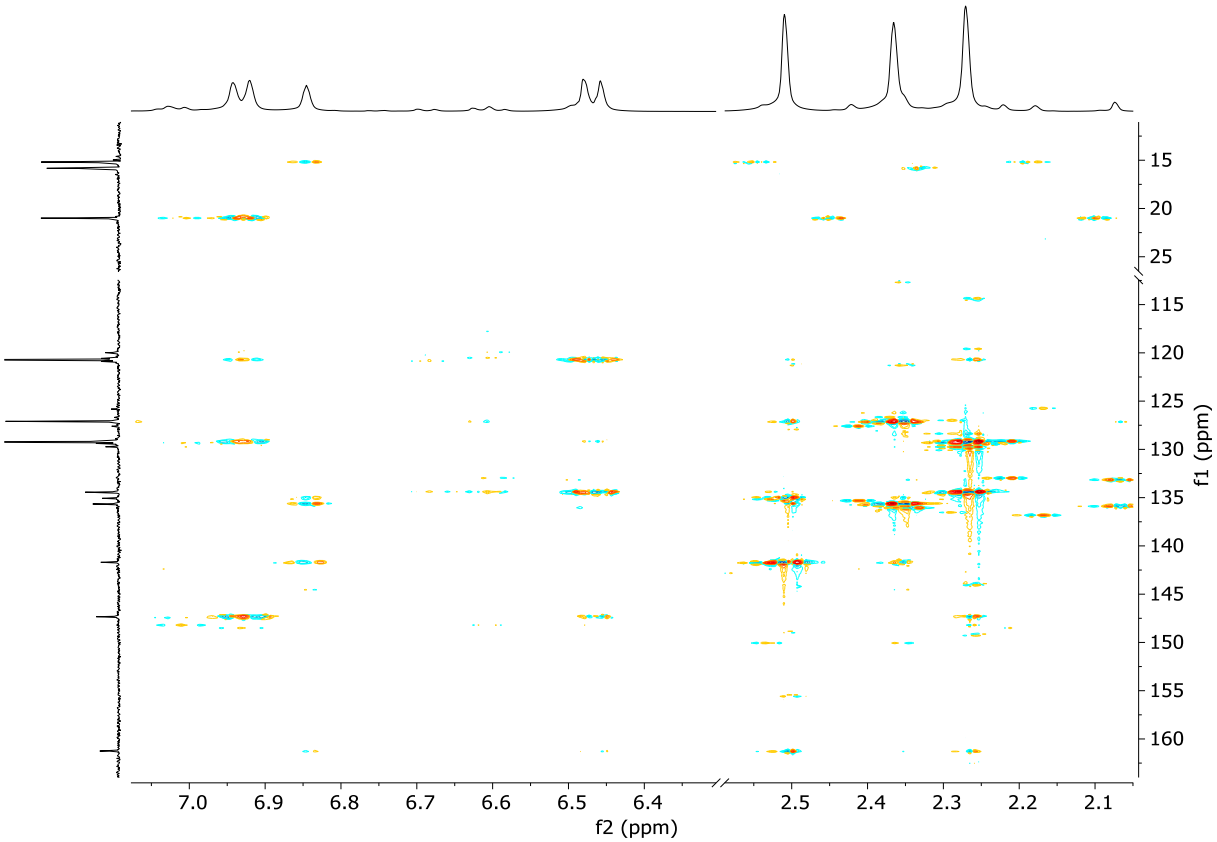

Figure S18: *HMBC spectrum (360/90 MHz, CD_2Cl_2) of* ***91****.*

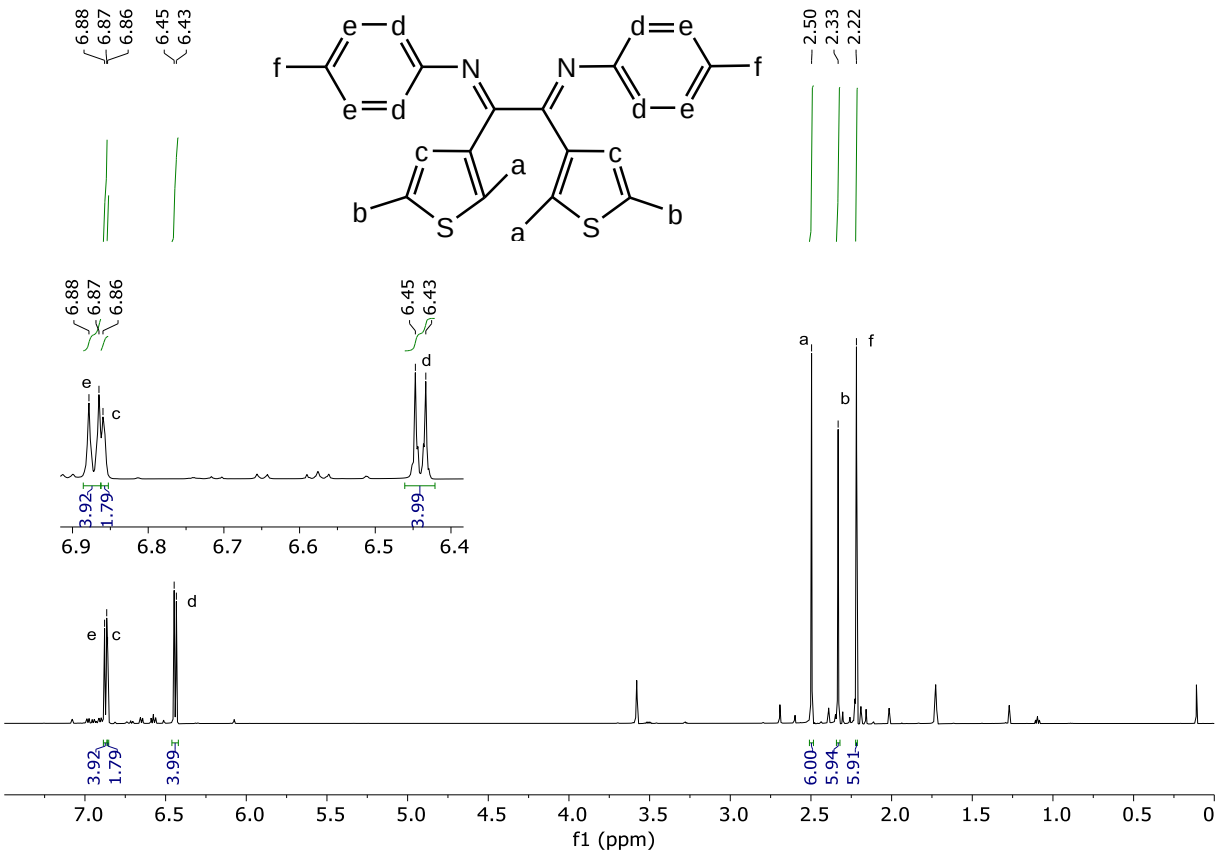

Figure S19: *^{1}H NMR spectrum (600 MHz, THF-d_8) of* ***91****.*

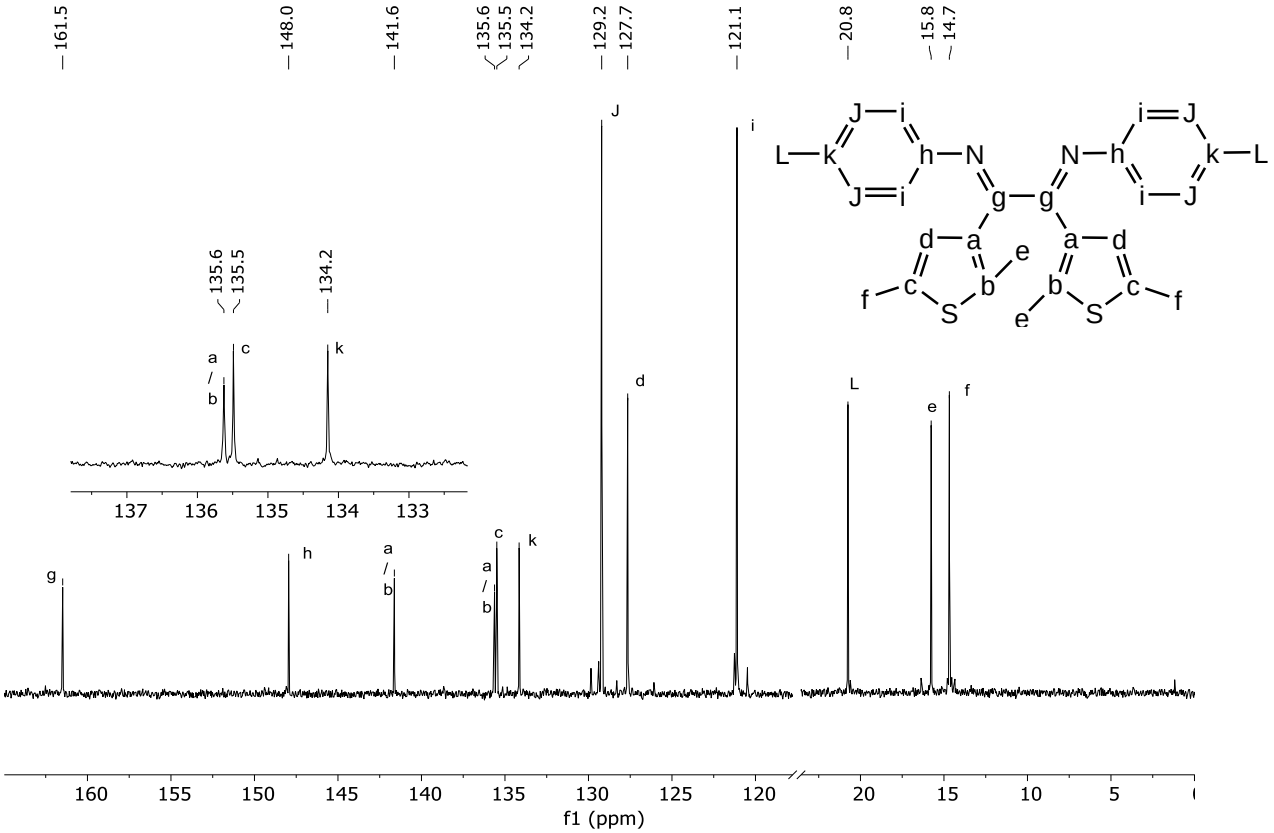

Figure S20: *$^{13}C\{^{1}H\}$ NMR spectrum (150 MHz, THF-d_8) of* ***91****.*

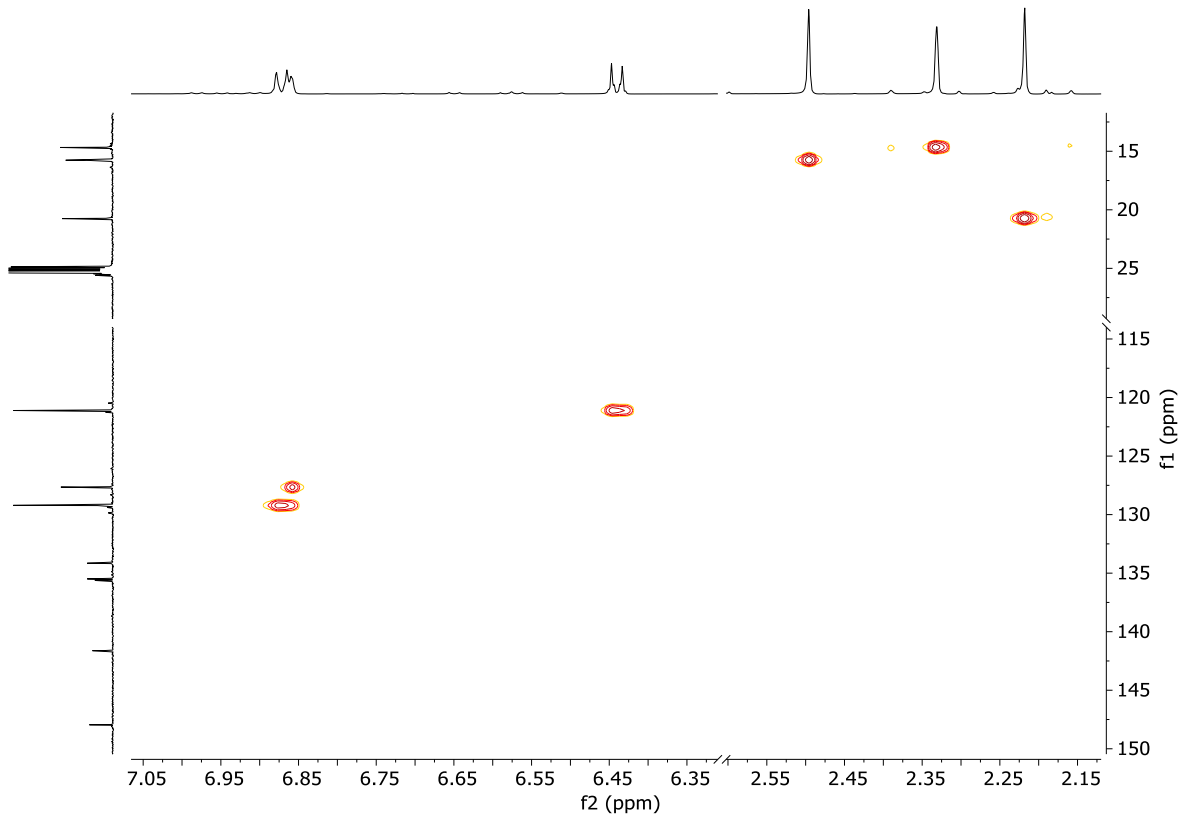

Figure S21: *HSQC spectrum (600/150 MHz, THF-d_8) of* ***91****.*

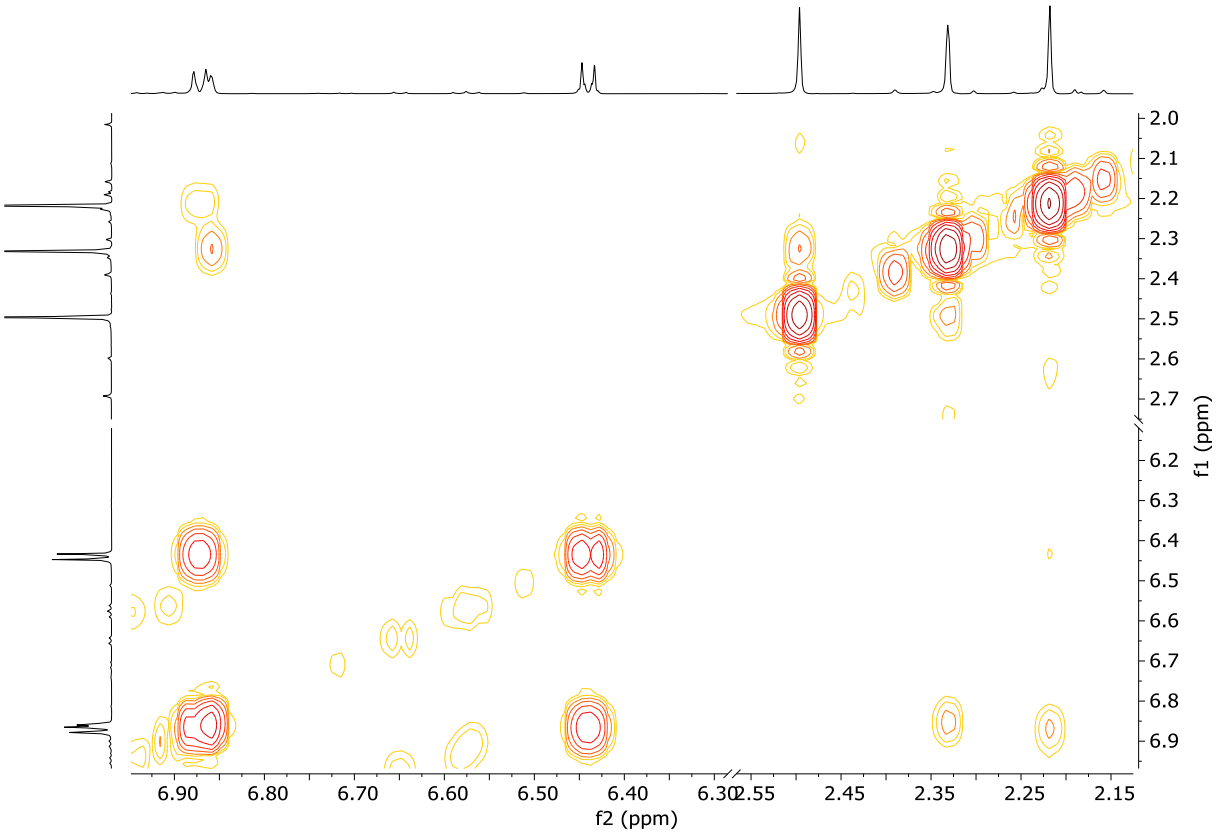

Figure S22: *H,H-COSY spectrum (600 MHz, THF-d_8) of* ***91****.*

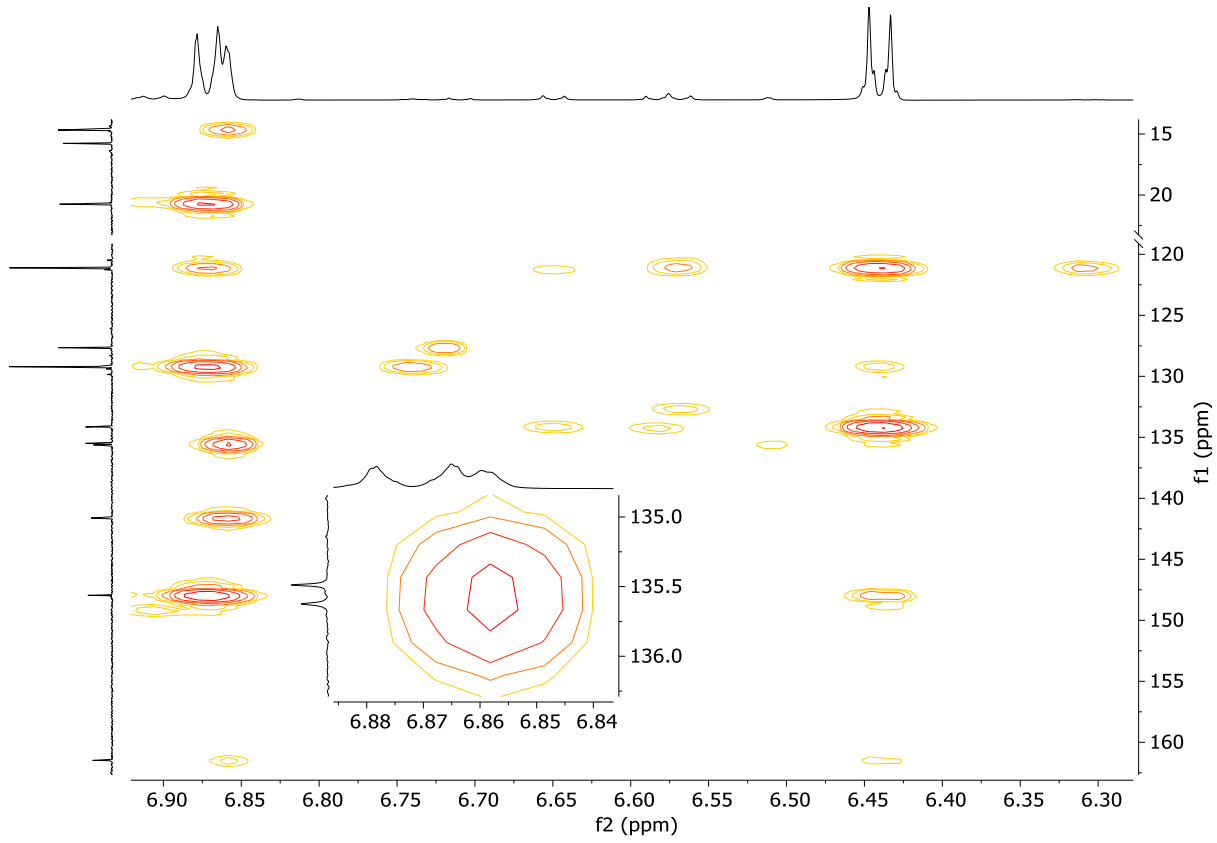

Figure S23: *HMBC aromatic area spectrum (600/150 MHz, THF-d_8) of* ***91****.*

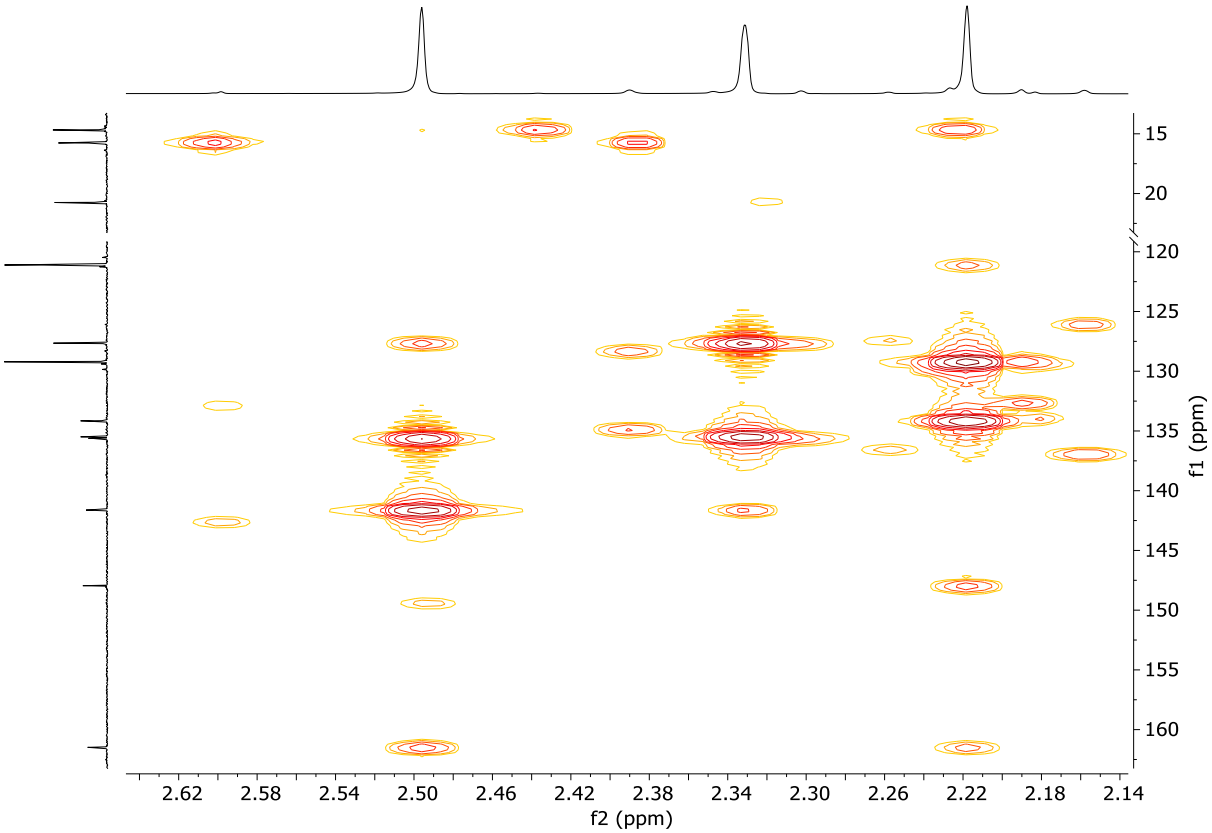

Figure S24: *HMBC aliphatic area spectrum (600/150 MHz, THF-d_8) of* ***91****.*

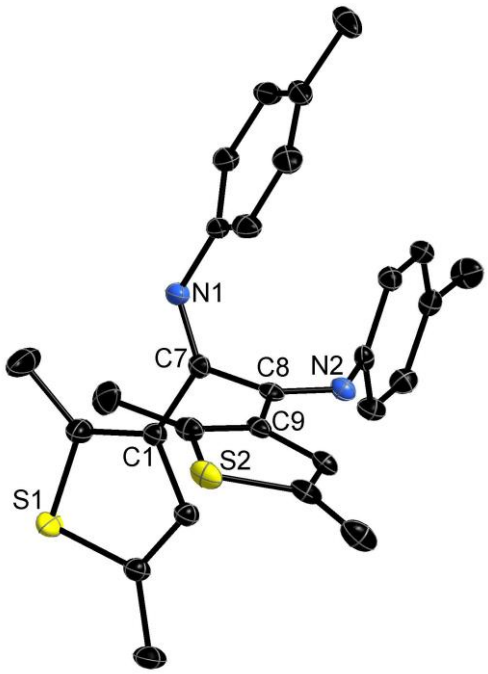

Figure S25: *X-ray crystal structure of* ***91*** *at 50% ellipsoid probability. Hydrogen atoms are omitted for clarity. Selected bond lengths [Å]: C1-C7 = 1.475(2), C7-C8 = 1.519(2), C7-N1: 1.284(2), C8-N2: 1.276(2), C8-C9 = 1.479(2).*

Table S1: *Crystal data for α-diimine ligand (**91**).*

	α-diimine ligand (**91**)
Formula	$C_{28}H_{28}N_2S_2$
Formula weight, g mol^{-1}	456.64
Crystal system	Triclinic
Space group	$P\bar{1}$
a, Å	9.6310 (3)
b, Å	15.9114 (4)
c, Å	16.1640 (4)
α, º	86.502 (1)
β, º	86.612 (2)
γ, º	81.265 (1)
V, Å^3	2440.60 (12)
Z	4
ρ_{calcd}, Mg m^{-3}	1.243
μ (Mo *Kα*), mm^{-1}	0.236
F(000)	968
θ range, deg	2.4 – 27.5
Index ranges	$-12 \leq h \leq 12$
	$-20 \leq k \leq 20$
	$-21 \leq l \leq 21$
No. of reflns collected	101886
Completeness to θ_{max}	99.9%
No. indep. Reflns	11265
No. obsd reflns with($I>2\sigma(I)$)	9179
No. refined params	589
GooF (F^2)	1.052
R_1 (F) ($I > 2\sigma(I)$)	0.0464
wR_2 (F^2) (all data)	0.1157
Largest diff peak/hole, e Å^{-3}	1.255 / -0.393

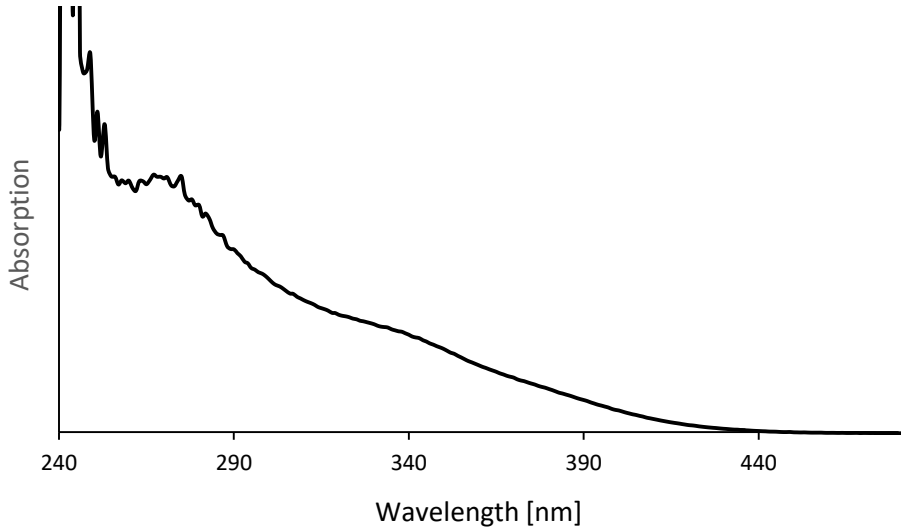

Figure S26: *UV/Vis spectrum of* ***91*** *in DCM.*

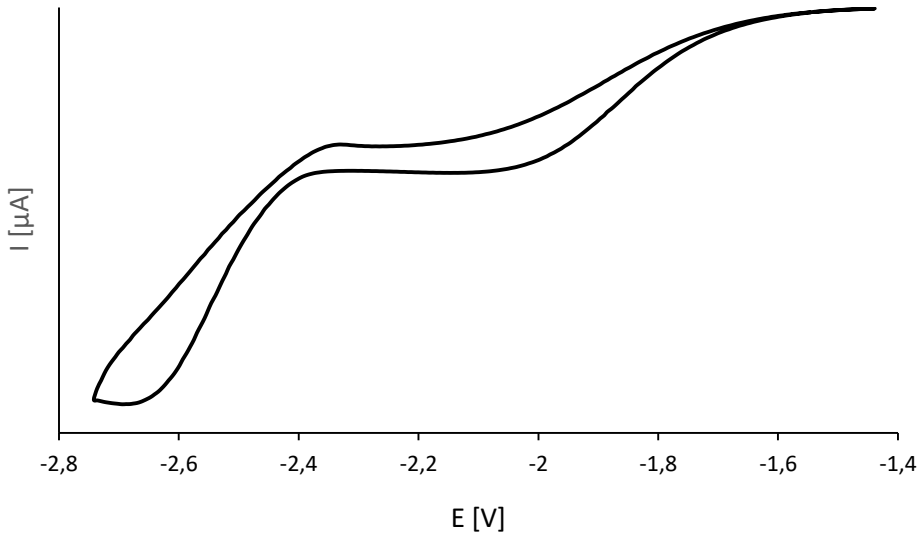

Figure S27: *Cyclic voltammogram of* ***91*** *(MeCN, [TBA]PF_6/0.1 M, scan rate 200 mV/s, potentials plotted vs Fc/Fc^+).*

Synthesis and Characterization of (α-Diimine)$TiCl_4$ (92)

α-Diimine **91** (0.08 g, 0.17 mmol, 1.1 eq.) was dissolved in 5 mL toluene and treated with $TiCl_4$ (17 µL, ρ = 1.73 g/cm^3, 0.16 mmol, 1.0 eq.). The instantly turned red solution was stirred at rt for 24 h. Removal of the solvent under reduced pressure and washing the crude product with small portions of *n*-hexane led to **92** as dark red to black solid. Crystals suitable for X-ray crystallography were obtained *via* slow diffusion of *n*-hexane into a saturated solution of **92** in DCM. **Yield:** 0.10 g (0.15 mmol, 97%); **Mp:** 170-172 °C; **^{1}H NMR:** (600 MHz, CD_2Cl_2): δ 7.30-7.00 (m, 16H, phenyl), 6.19-6.17 (m, 2H, b-thienyl) 6.04-6.02 (m, 2H, a-thienyl), 2.32 (s, 12H, phenyl-Me), 2.20 (s, 6H, a-thienyl-Me), 2.20 (s, 6H, b-thienyl-Me), 2.15 (s, 6H, a-thienyl-Me), 2.07 (s, 6H, b-thienyl-Me) ppm; **^{13}C{1H} NMR:** (150 MHz, CD_2Cl_2): δ 171.2 (b-C=N), 171.1 (a-C=N), 148.4 (C-N), 139.9 (b-thienyl), 139.1 (a-thienyl), 139.1 (a-thienyl), 138.8 (b-thienyl), 138.5 (C-phenyl-Me), 138.4 (C-phenyl-Me), 129.9 (a-thienyl), 129.6 (b-thienyl), 129.4 (phenyl), 124.8 (b-C-thienyl-H), 124.2 (a-C-thienyl-H), 122.9 (phenyl), 122.8 (phenyl), 21.3 (phenyl-Me), 15.1 (a-thienyl-Me), 15.1 (b-thienyl-Me), 14.9 (b-thienyl-Me), 14.8 (a-thienyl-Me) ppm; **^{1}H NMR:** (600 MHz, C_6D_6): δ 7.61-7.35 (m, 8H, phenyl), 6.84 (d, 8H, ^3J=8.3 Hz, phenyl), 6.01-6.02 (m, 2H, b-thienyl) 5.91-5.89 (m, 2H, a-thienyl), 2.07 (s, 6H, a-thienyl-Me), 1.90 (s, 6H, b-thienyl-Me), 1.87 (s, 6H, phenyl-Me), 1.87 (s, 6H, phenyl-Me), 1.71 (s, 6H, b-thienyl-Me), 1.63 (s, 6H, a-thienyl-Me) ppm; **^{13}C{1H} NMR:** (150 MHz, C_6D_6): δ 170.4 (a-C=N), 170.2 (b-C=N), 148.7 (C-N), 148.7 (C-N), 139.0 (b-thienyl), 138.5 (a-thienyl), 138.2 (b-thienyl), 138.2 (a-thienyl), 137.9 (C-phenyl-Me) 137.9 (C-phenyl-Me), 130.4 (a-thienyl), 130.2 (b-thienyl), 129.4 (phenyl), 129.4 (phenyl), 125.0 (b-C-thienyl-H), 124.2 (a-C-thienyl-H), 123.1 (phenyl), 122.9 (phenyl), 21.0 (phenyl-Me), 14.9 (a-thienyl-Me), 14.8 (b-thienyl-Me), 14.5 (b-thienyl-Me) 14.4 (a-thienyl-Me) ppm; **UV/Vis** (CH_2Cl_2): λ_{max} = 300 nm, $\lambda_{shoulder}$ = 337, 444 nm; CV (referenced to Fc/Fc$^+$, MeCN) $E_{1/2}^{red1}$ = -0.50 V.-

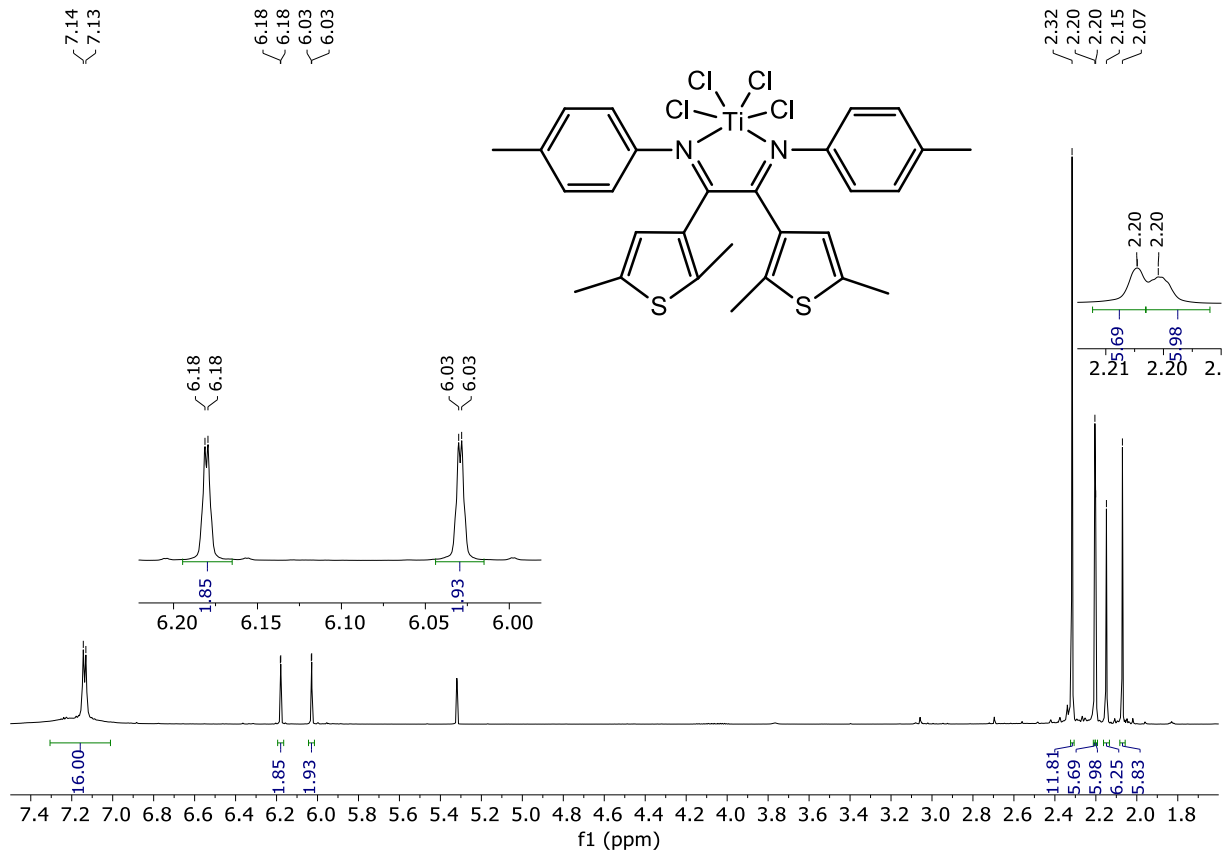

Figure S28: *^{1}H NMR spectrum (600 MHz, CD_2Cl_2) of* ***92****.*

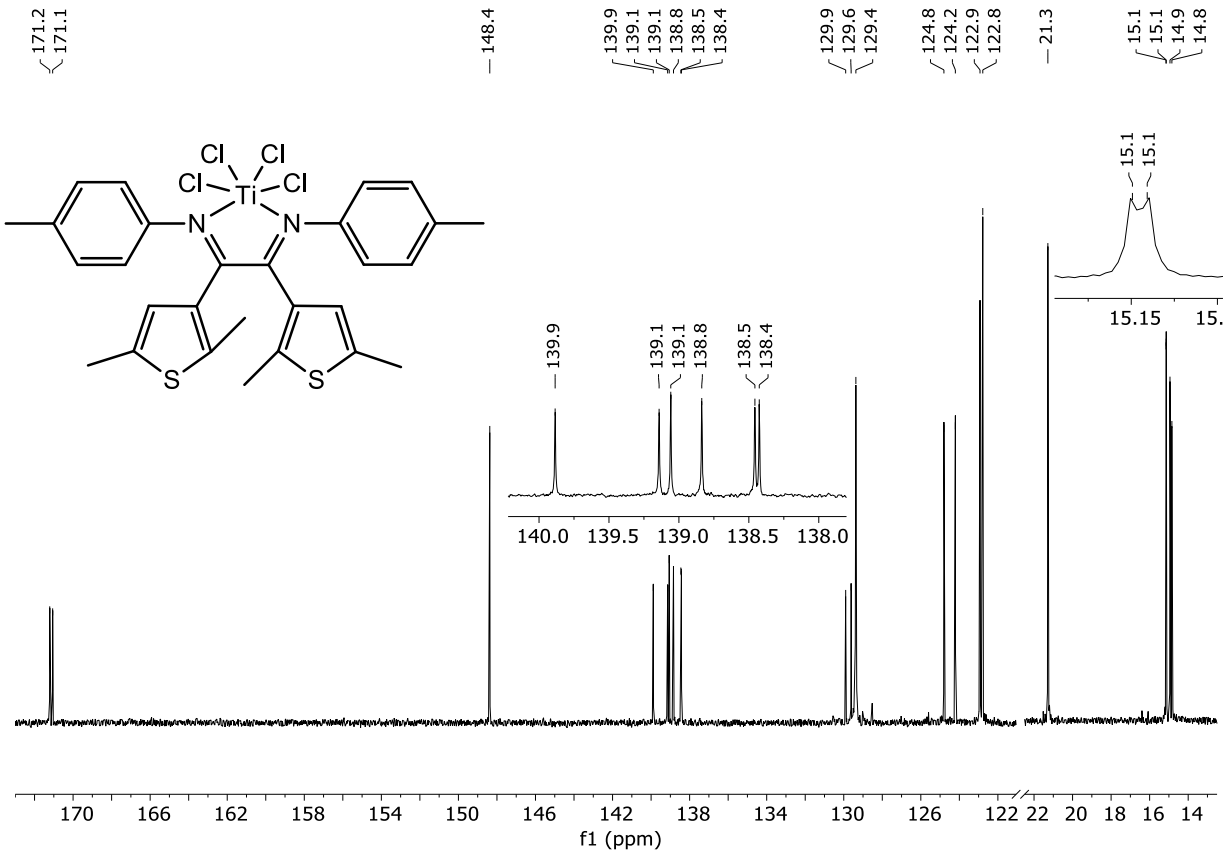

Figure S29: *$^{13}C\{^{1}H\}$ NMR spectrum (150 MHz, CD_2Cl_2) of* ***92****.*

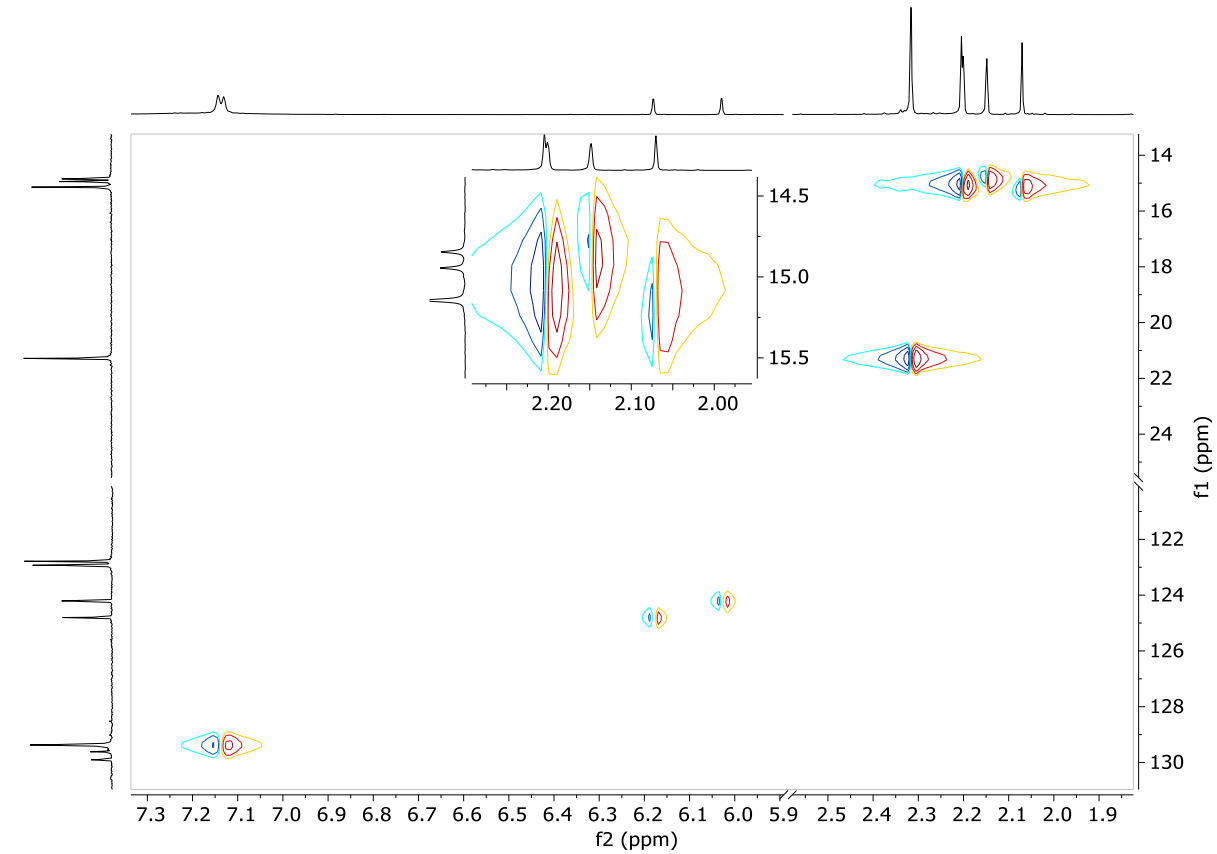

Figure S30: *HSQC spectrum (600/150 MHz, CD_2Cl_2) of* ***92****.*

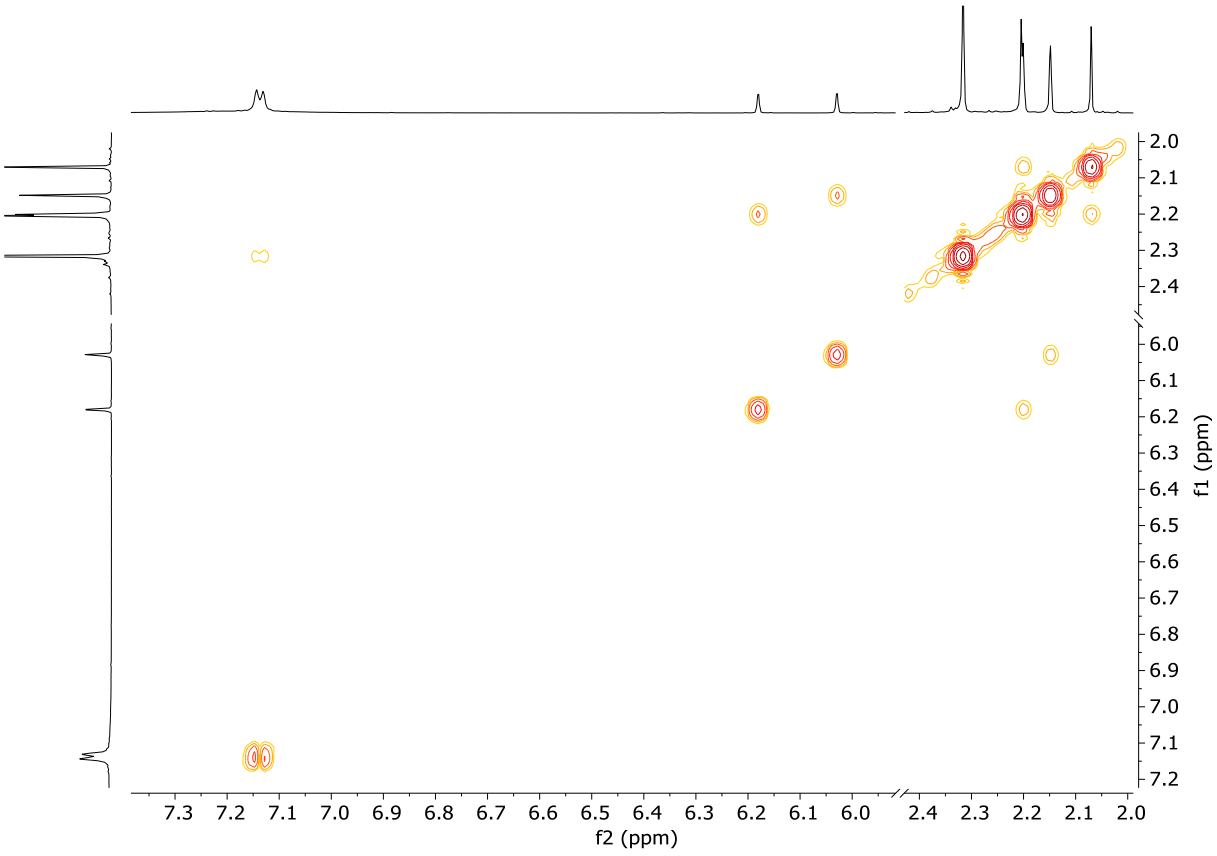

Figure S31: *H,H-COSY spectrum (600 MHz, CD_2Cl_2) of* ***92****.*

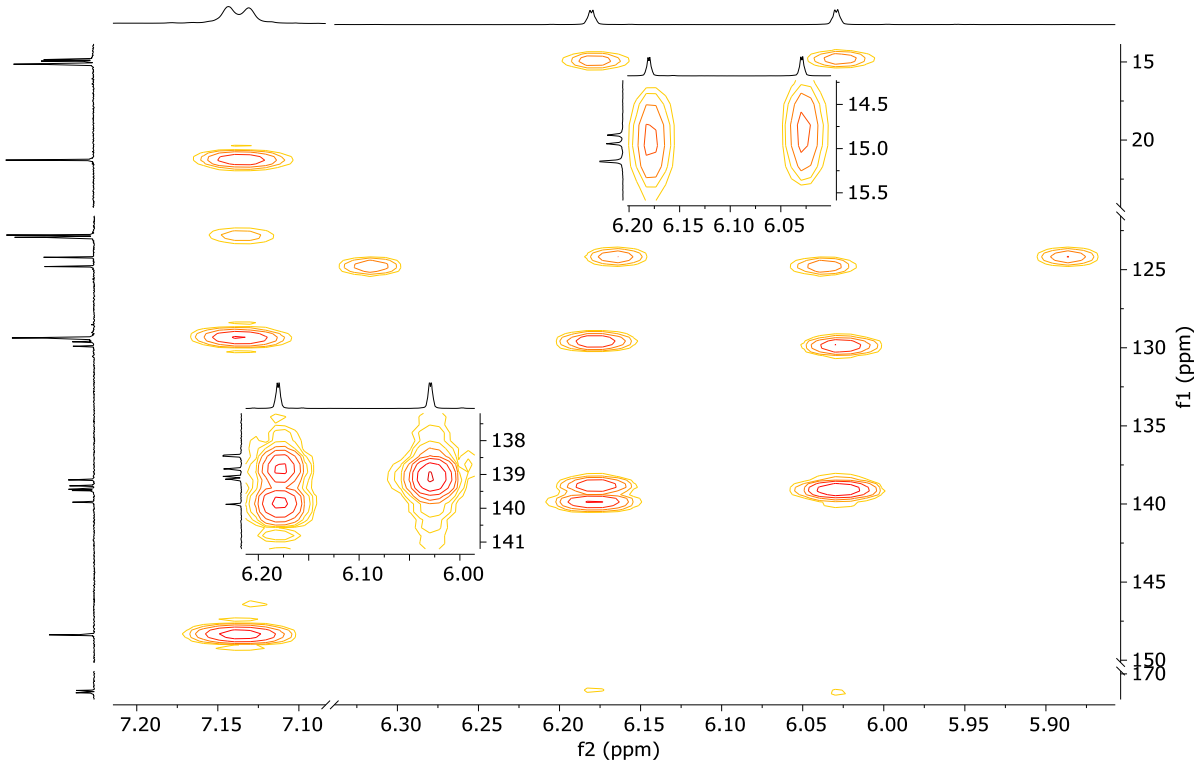

Figure S32: *HMBC aromatic area spectrum (600/150 MHz, CD_2Cl_2) of* ***92****.*

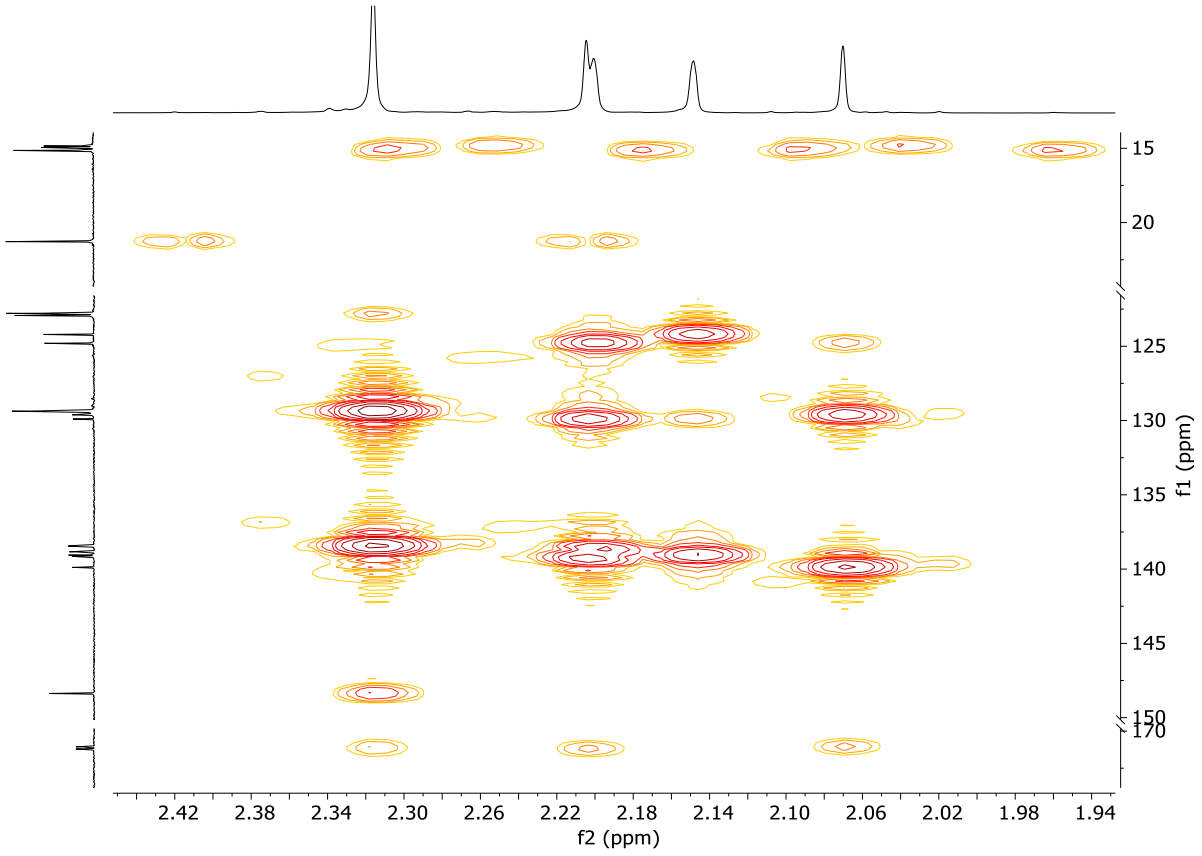

Figure S33: *HMBC aliphatic area spectrum (600/150 MHz, CD_2Cl_2) of* ***92****.*

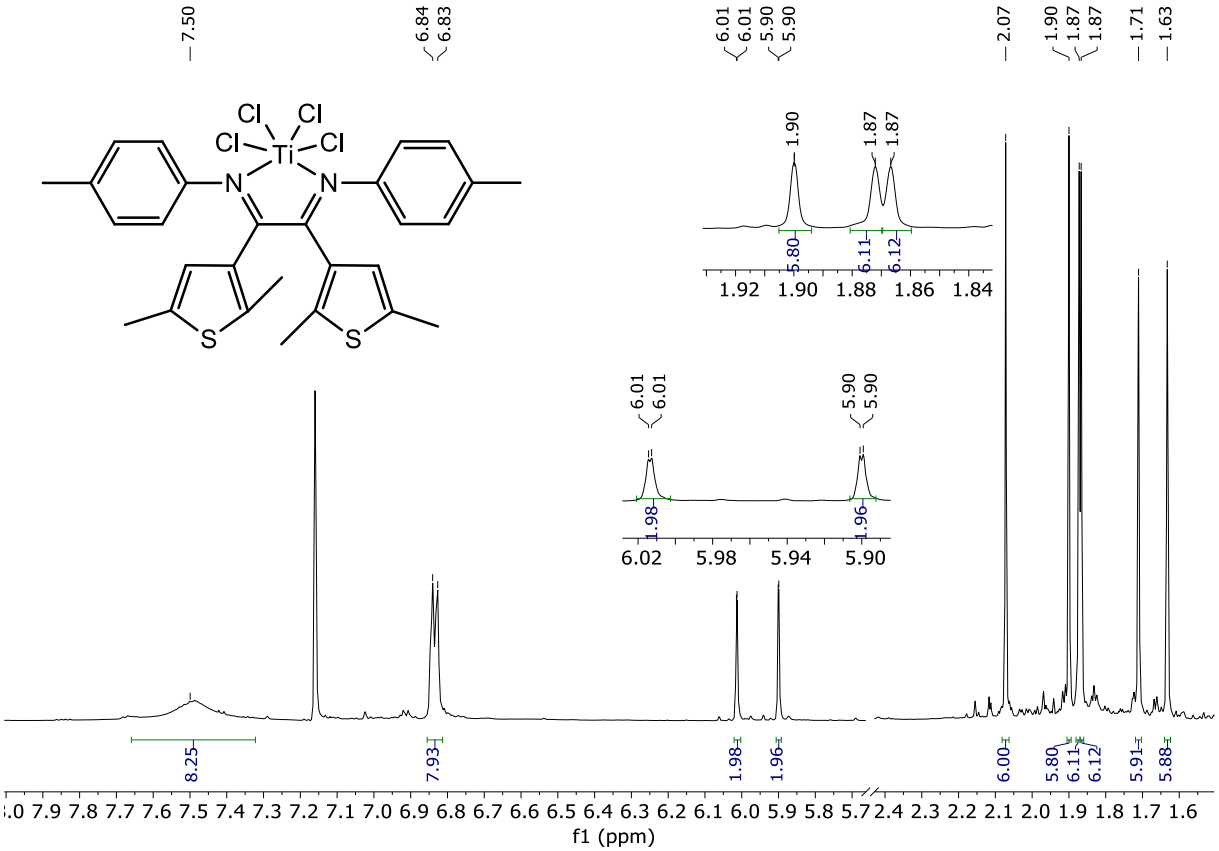

Figure S34: *^{1}H NMR spectrum (600 MHz, C_6D_6) of* ***92****.*

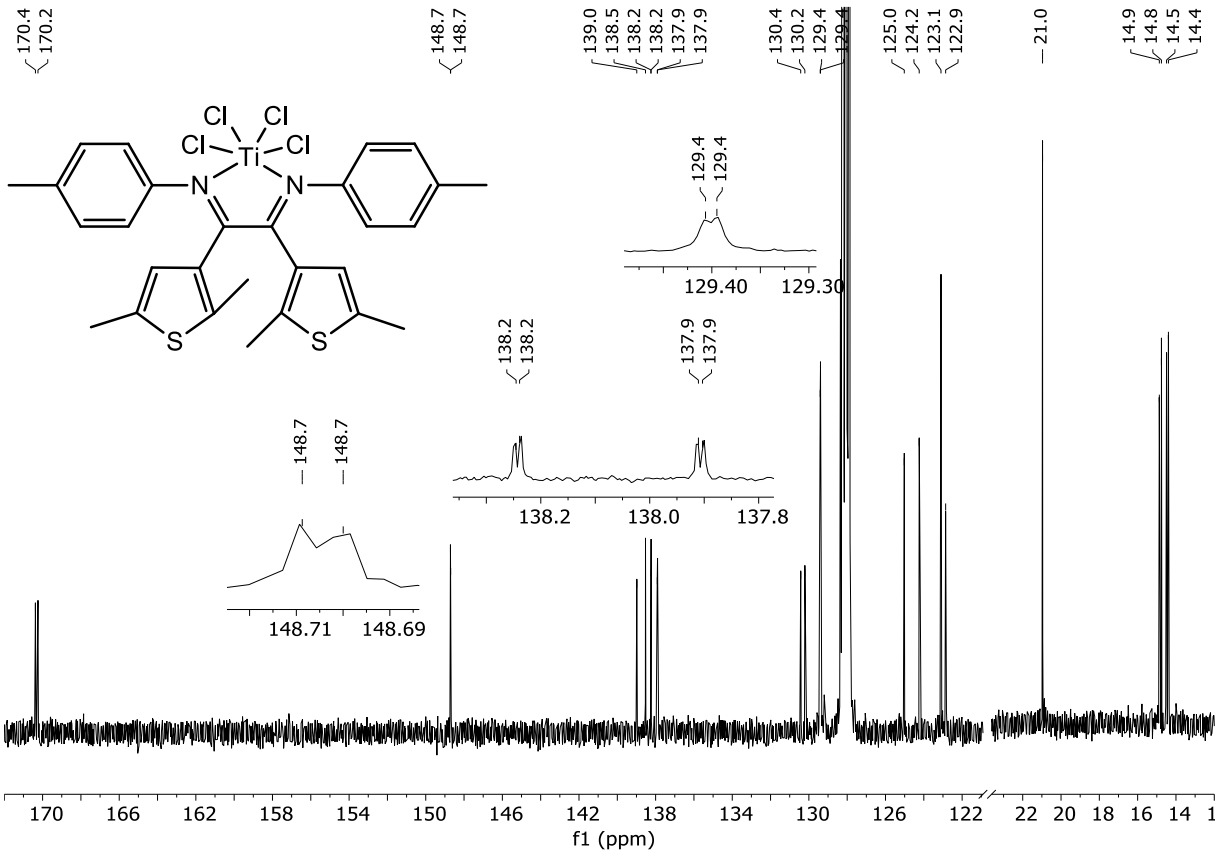

Figure S35: *$^{13}C\{^{1}H\}$ NMR spectrum (150 MHz, C_6D_6) of* ***92****.*

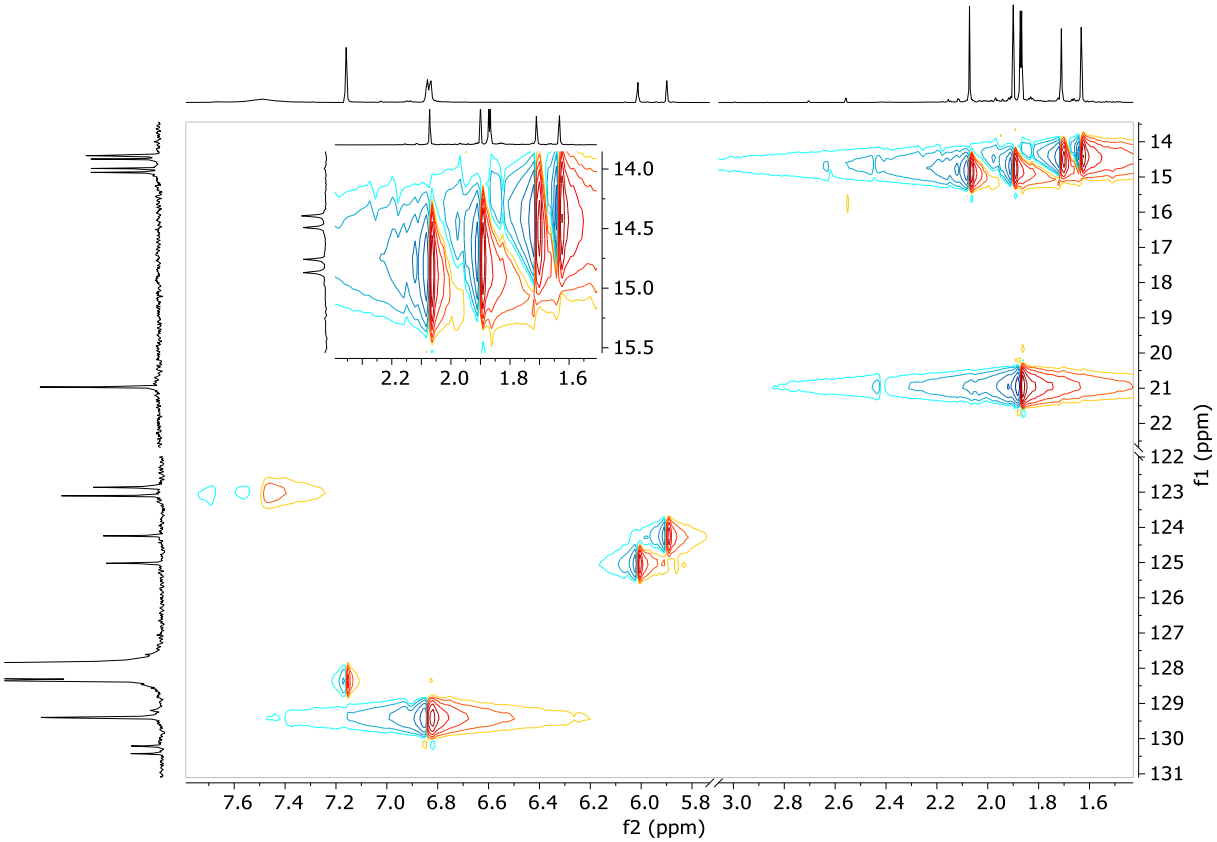

Figure S36: *HSQC spectrum (600/150 MHz, C_6D_6) of* ***92****.*

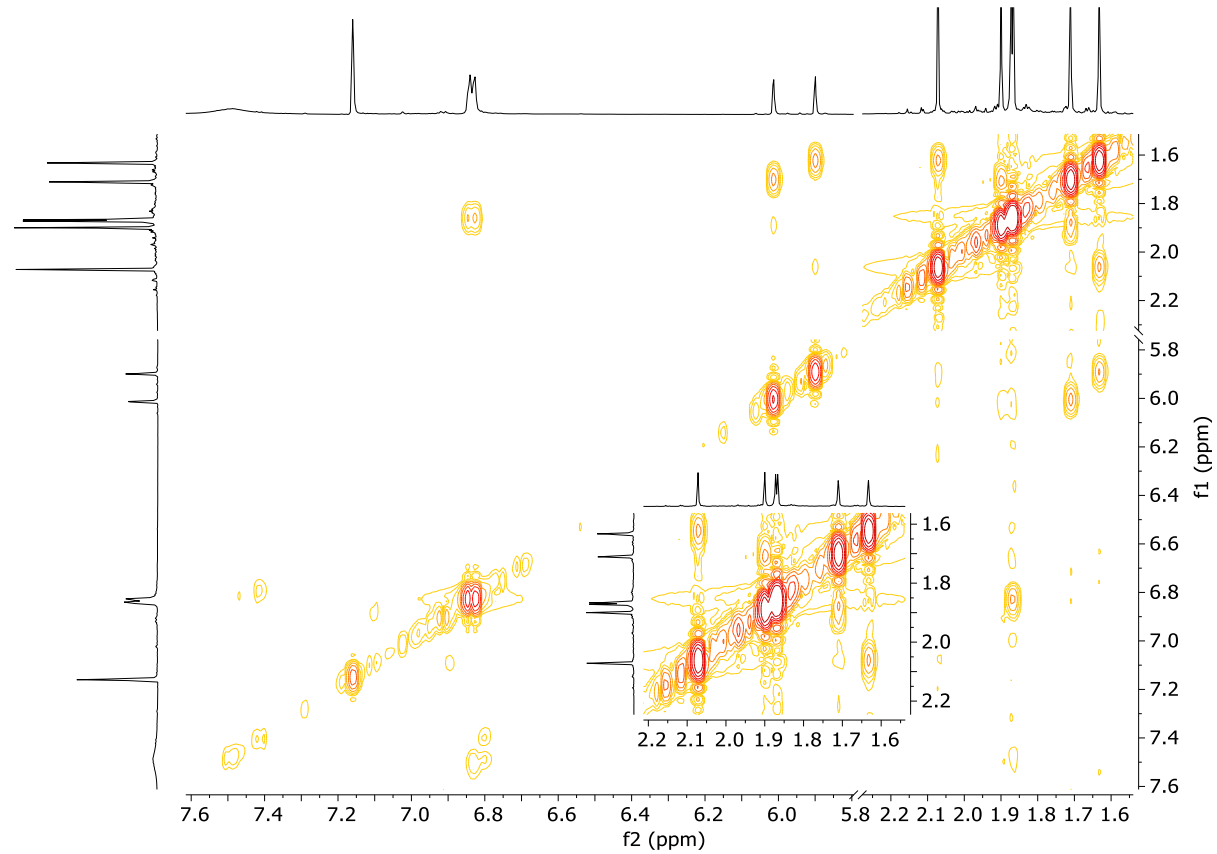

Figure S37: *H,H-COSY spectrum (600 MHz, C_6D_6) of* ***92****.*

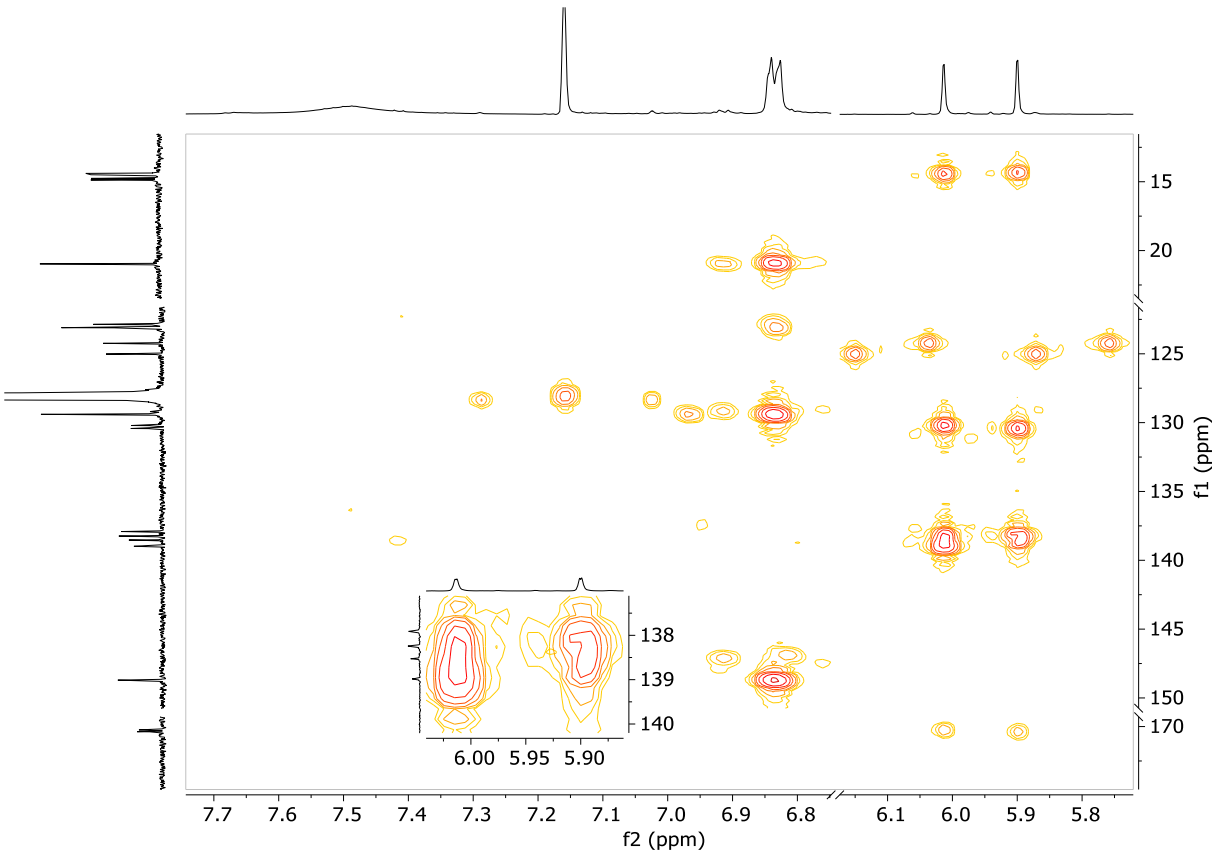

Figure S38: *HMBC aromatic area spectrum (600/150 MHz, C_6D_6) of* ***92****.*

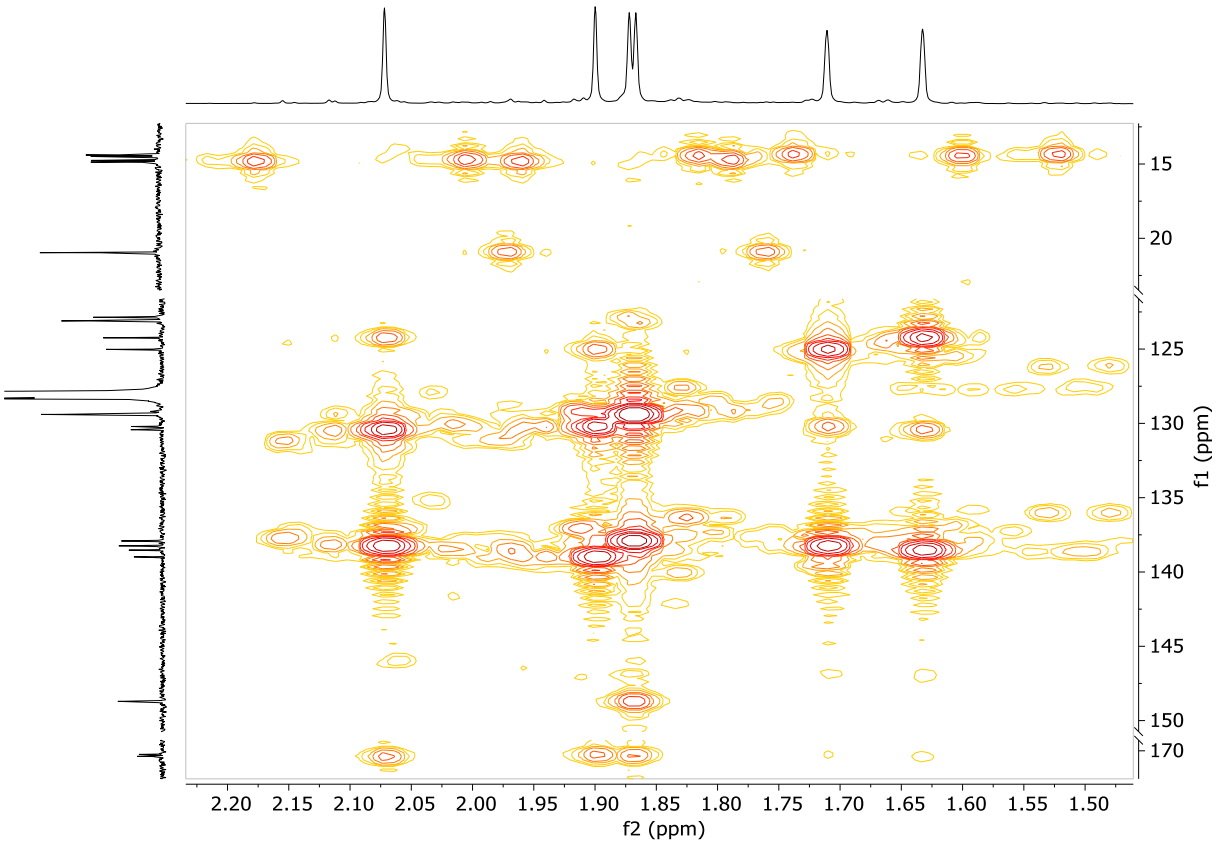

Figure S39: *HMBC aliphatic area spectrum (600/150 MHz, C_6D_6) of* ***92****.*

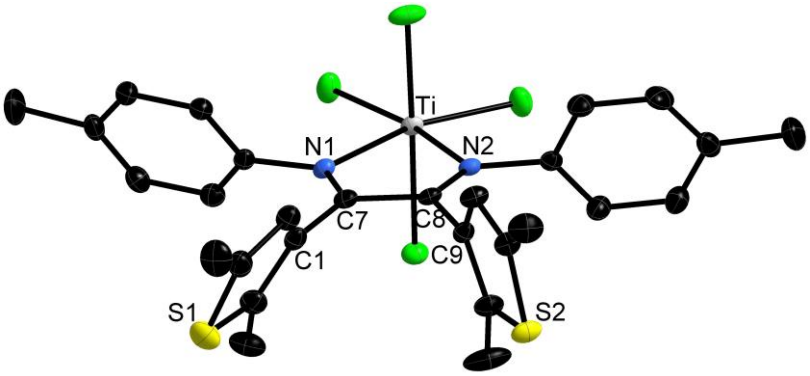

Figure S40: *X-ray crystal structure of* ***92*** *at 50% ellipsoid probability. Hydrogen atoms are omitted for clarity. Selected bond lengths [Å]: C1-C7 = 1.479(2), C7-C8 = 1.499(2), C7-N1: 1.287(2), C8-N2: 1.283(2), C8-C9 = 1.482(2), N1-Ti: 2.225(2), N2-Ti: 2.213(2).*

Table S2: *Crystal data for (α-diimine)$TiCl_4$ (**92**).*

	(α-diimine)$TiCl_4$ (**92**)
Formula	$C_{28}H_{28}Cl_4N_2S_2Ti$
Formula weight, g mol^{-1}	646.34
Crystal system	Monoclinic
Space group	$P2_1/n$
a, Å	11.2553 (2)
b, Å	18.5022 (4)
c, Å	14.6441 (3)
α, º	90
β, º	96.423 (1)
γ, º	90
V, Å^3	3030.46 (11)
Z	4
ρ_{calcd}, Mg m^{-3}	1.417
μ (Mo *Kα*), mm^{-1}	0.794
F(000)	1328
θ range, deg	2.4 – 34.2
Index ranges	$-14 \le h \le 14$
	$-24 \le k \le 24$
	$-19 \le l \le 19$
No. of reflns collected	189802
Completeness to θ_{max}	100%
No. indep. Reflns	7323
No. obsd reflns with($I>2\sigma(I)$)	6418
No. refined params	340
GooF (F^2)	1.053
R_1 (F) ($I > 2\sigma(I)$)	0.0332
wR_2 (F^2) (all data)	0.0852
Largest diff peak/hole, e Å^{-3}	0.650 / -0.389

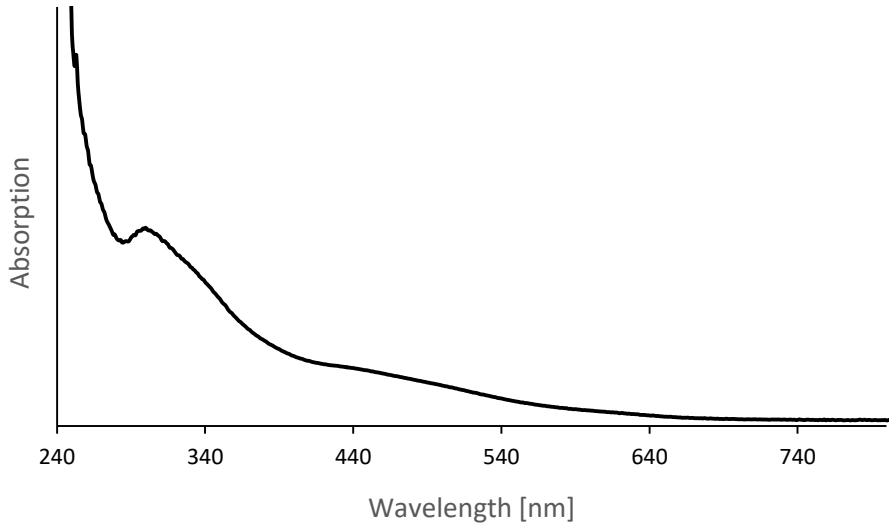

Figure S41: *UV/Vis spectrum of* ***92*** in DCM.

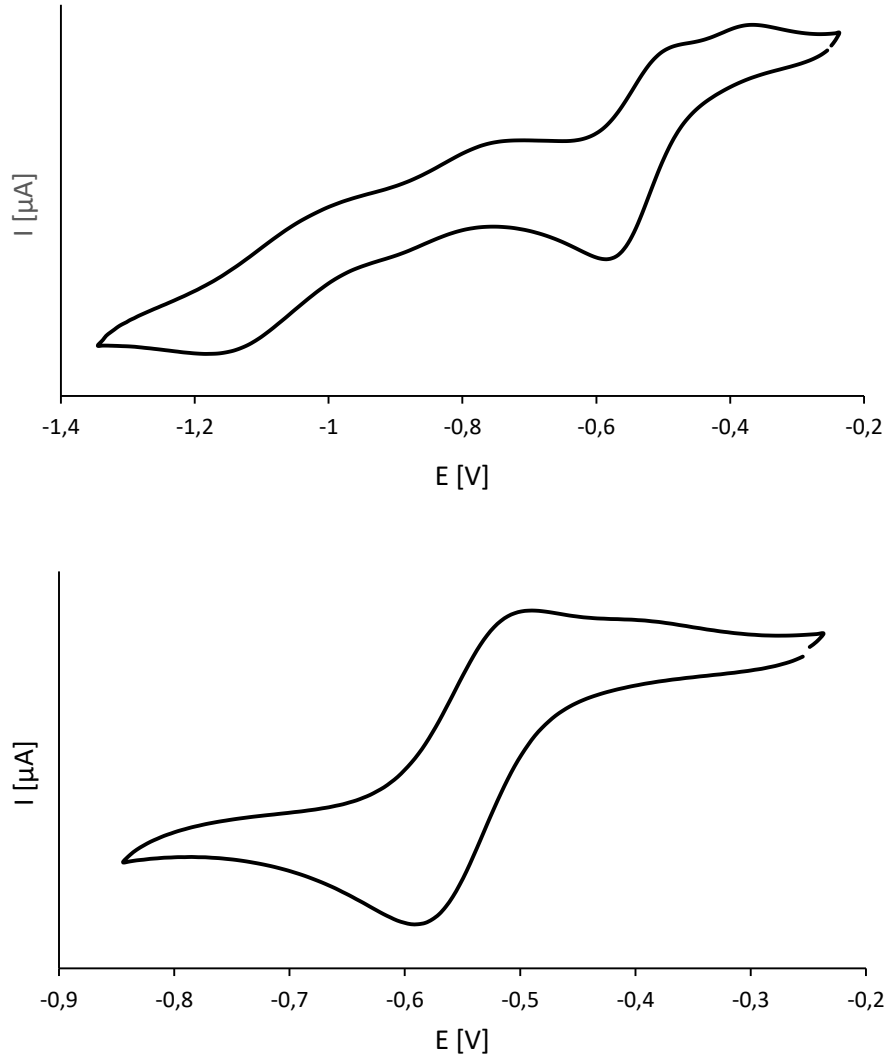

Figure S42: *Cyclic voltammograms of* ***92*** *(MeCN, [TBA]PF_6/0.1 M, scan rate 200 mV/s, potentials plotted vs Fc/Fc^+).*

Synthesis and Characterization of (α-Diimine)$ZrCl_4$ (96)

α-Diimine **91** (0.08 g, 0.18 mmol, 1.1 eq.) was dissolved in 5 mL toluene and treated with $ZrCl_4$ (0.04 g, 0.16 mmol, 1.0 eq.). The instantly turned orange solution was stirred at rt for 24 h. Removal of the solvent under reduced pressure and washing the crude product with small portions of *n*-hexane led to **96** as red to brown solid. Crystals suitable for X-ray crystallography were obtained *via* slow diffusion of *n*-hexane into a saturated solution of **96** in DCM. **Yield:** 0.11 g (0.16 mmol, 98%); **Mp:** 195-198 °C; **^{1}H NMR:** (600 MHz, CD_2Cl_2): δ 7.22-7.14 (m, 16H, phenyl), 6.18-6.17 (m, 2H, b-thienyl), 6.01-6.00 (m, 2H, a-thienyl), 2.36 (s, 12H, phenyl-Me), 2.22 (s, 6H, b-thienyl-Me), 2.17 (s, 6H, a-thienyl-Me), 2.15 (s, 6H, a-thienyl-Me), 2.02 (s, 6H, b-thienyl-Me) ppm; **^{13}C{1H} NMR:** (150 MHz, CD_2Cl_2): δ 161.2 (a-C=N), 161.1 (b-C=N), 141.8 (b-thienyl), 140.8 (a-thienyl), 140.1 (a-thienyl), 140.0 (C-N), 140.0 (C-N), 139.7 (b-thienyl), 139.2 (C-phenyl-Me), 139.1 (C-phenyl-Me), 129.7 (phenyl), 129.7 (phenyl), 128.4 (a-thienyl), 128.0 (b-thienyl), 124.7 (b-C-thienyl-H), 124.6 (phenyl), 124.5 (phenyl), 124.2 (a-C-thienyl-H), 21.4 (phenyl-Me), 15.4 (b-thienyl-Me), 15.3 (a-thienyl-Me), 15.0 (b-thienyl-Me), 14.9 (a-thienyl-Me) ppm; **UV/Vis** (CH_2Cl_2): λ_{max} = 340, 412 nm.-

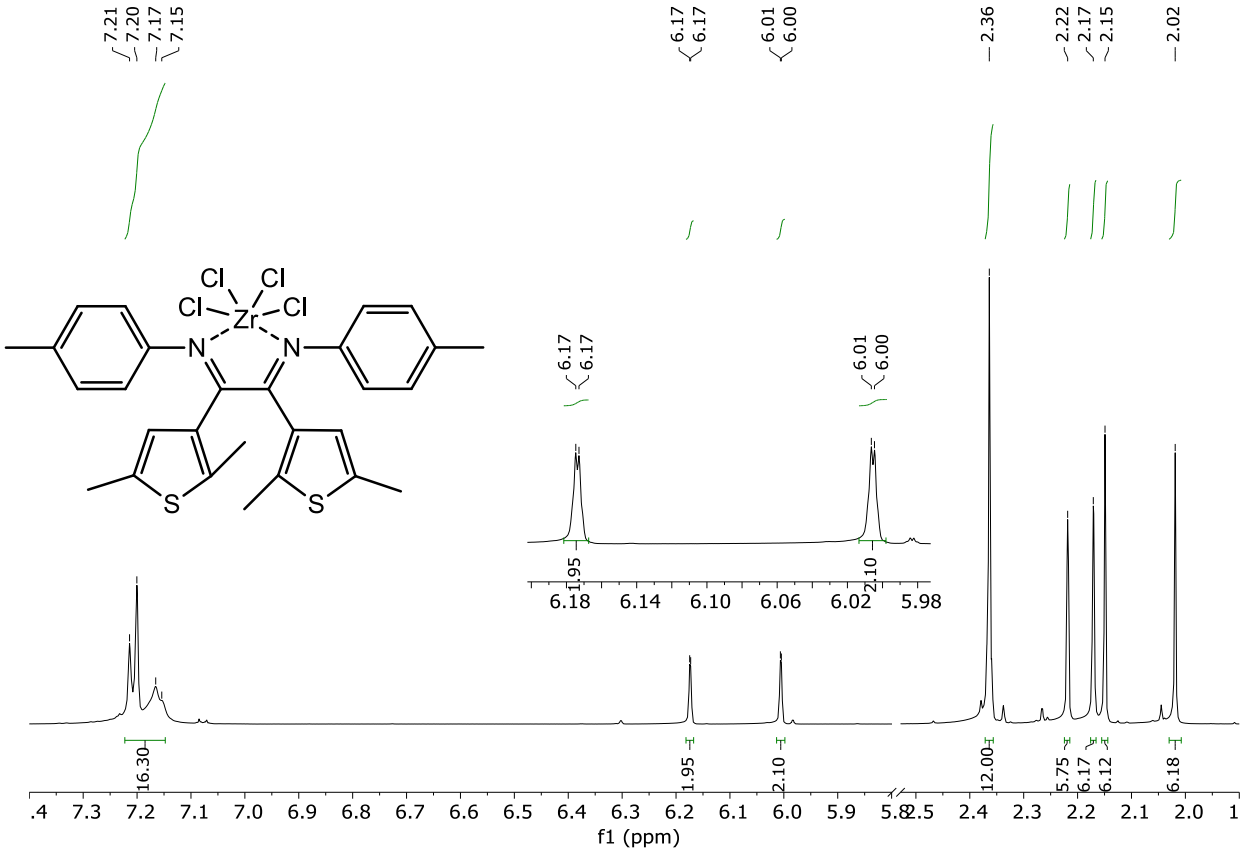

Figure S43: *^{1}H NMR spectrum (600 MHz, CD_2Cl_2) of **96**.*

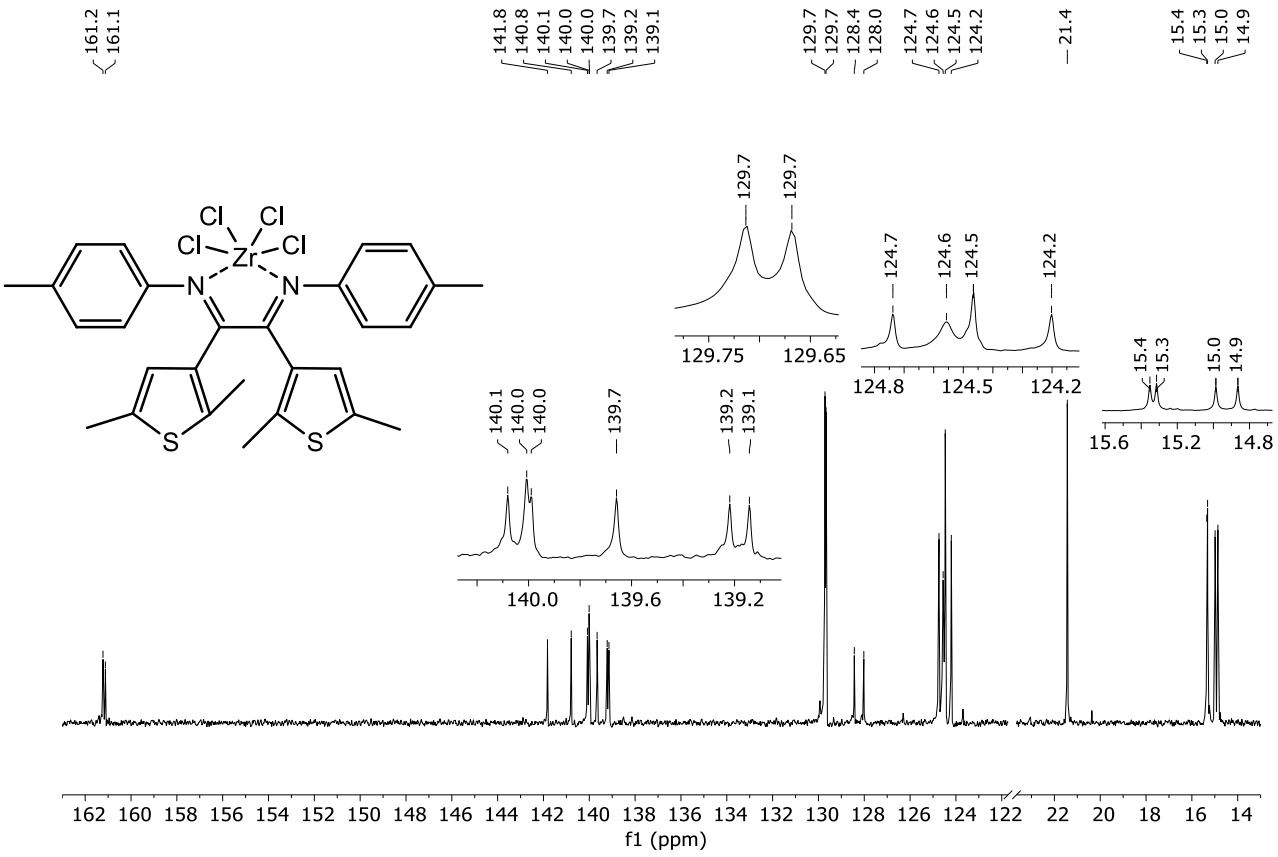

Figure S44: *$^{13}C\{^{1}H\}$ NMR spectrum (150 MHz, CD_2Cl_2) of **96**.*

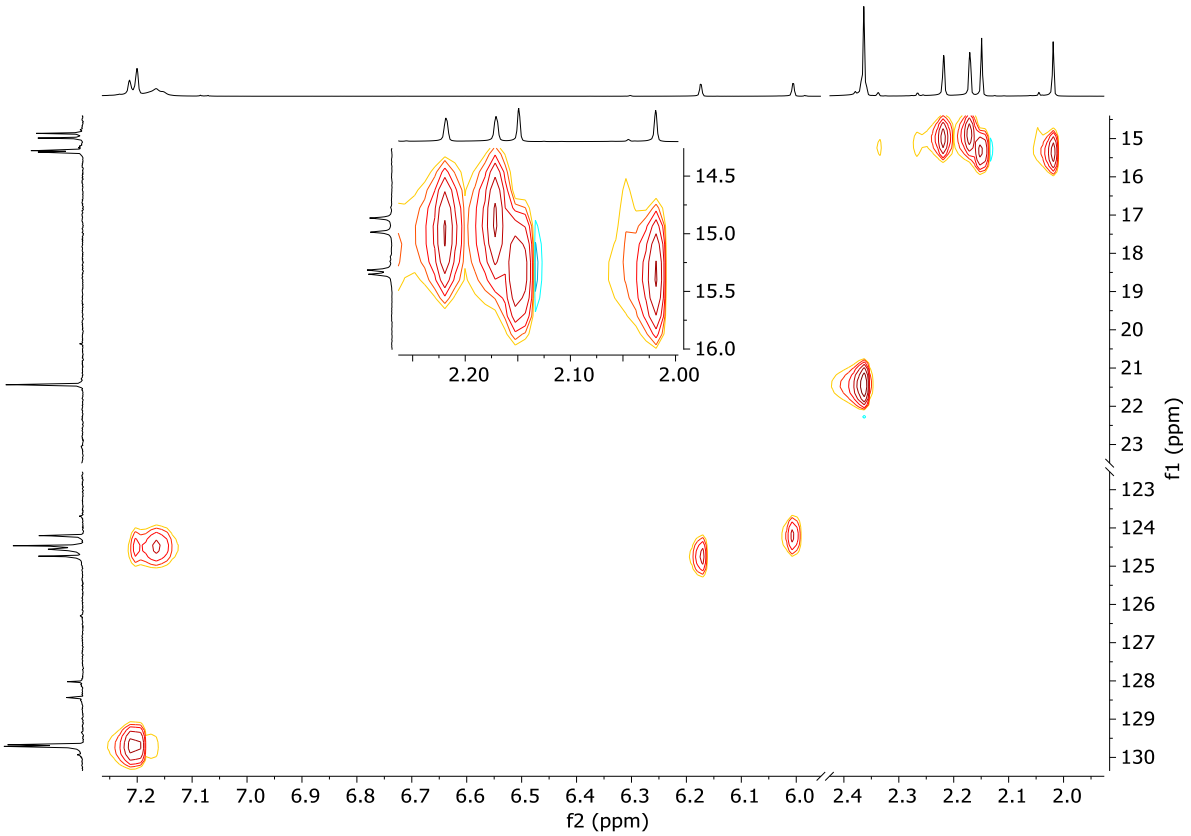

Figure S45: *HSQC spectrum (600/150 MHz, CD_2Cl_2) of **96**.*

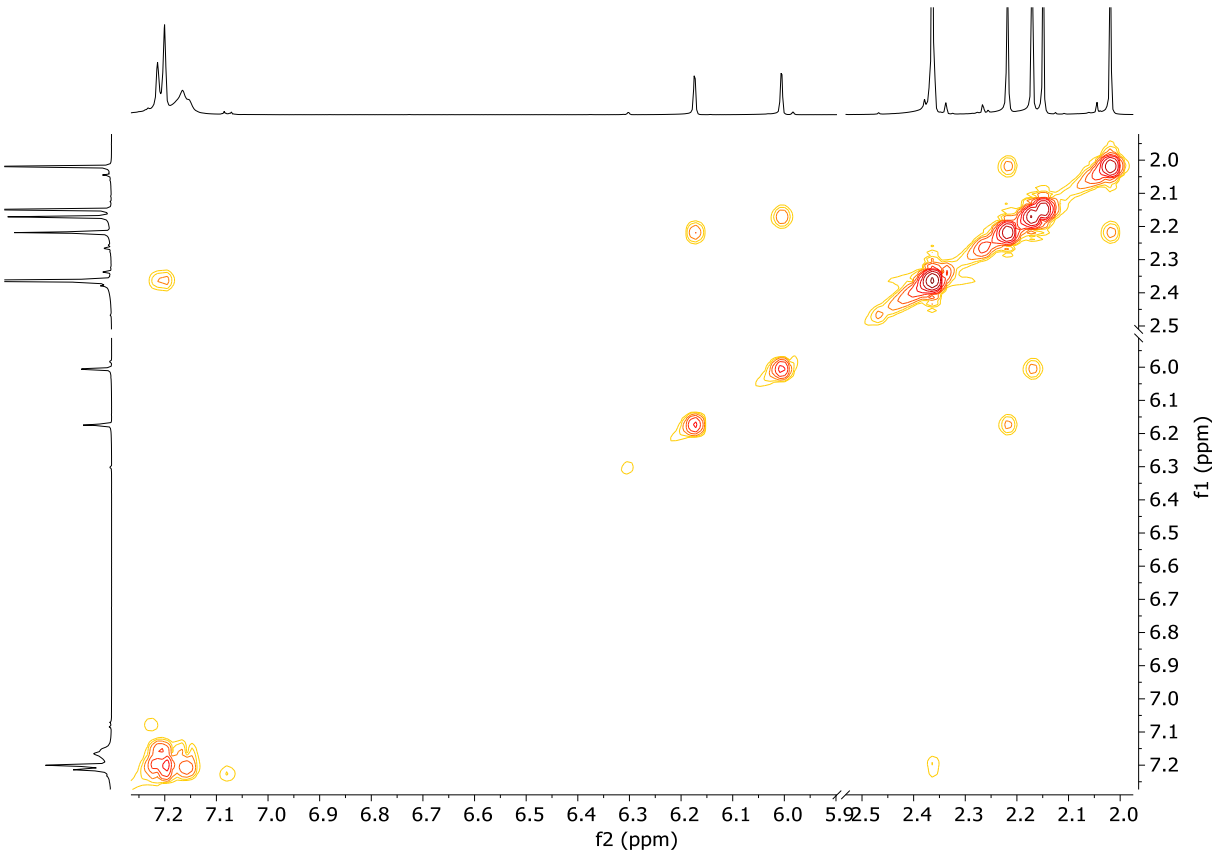

Figure S46: *H,H-COSY spectrum (600 MHz, CD_2Cl_2) of* ***96****.*

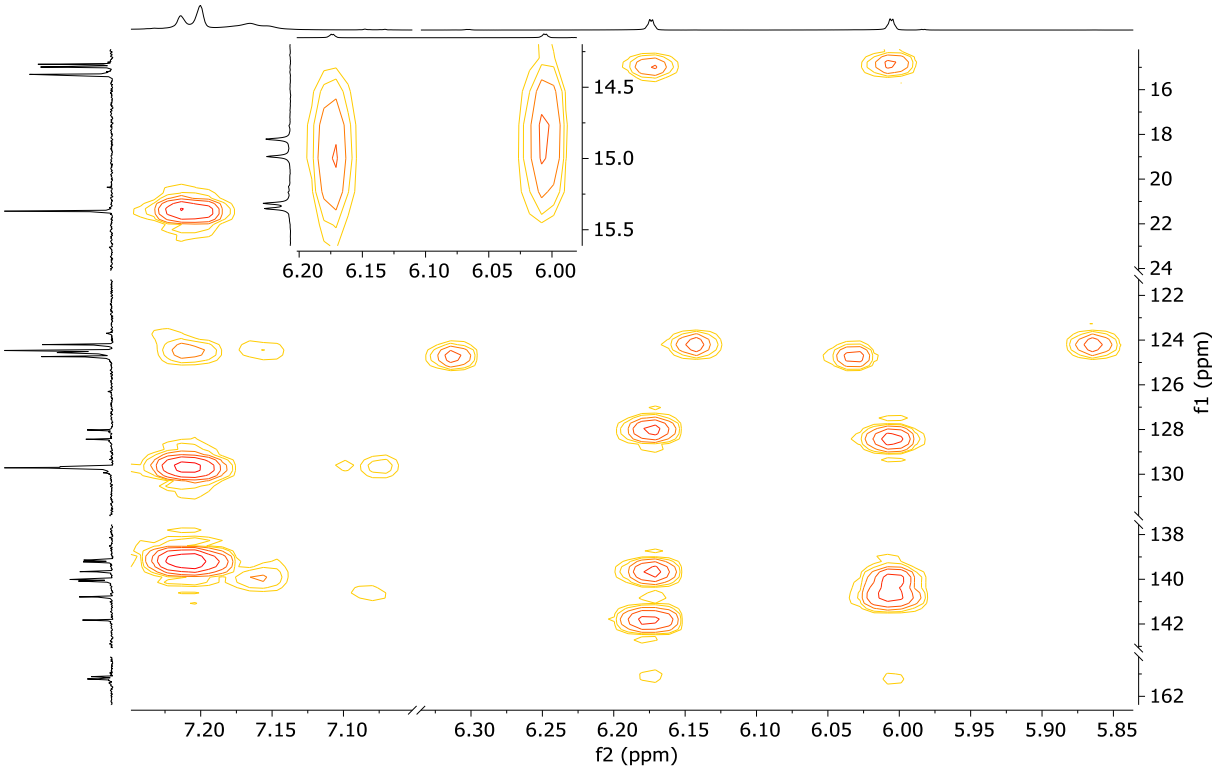

Figure S47: *HMBC aromatic area spectrum (600/150 MHz, CD_2Cl_2) of* ***96****.*

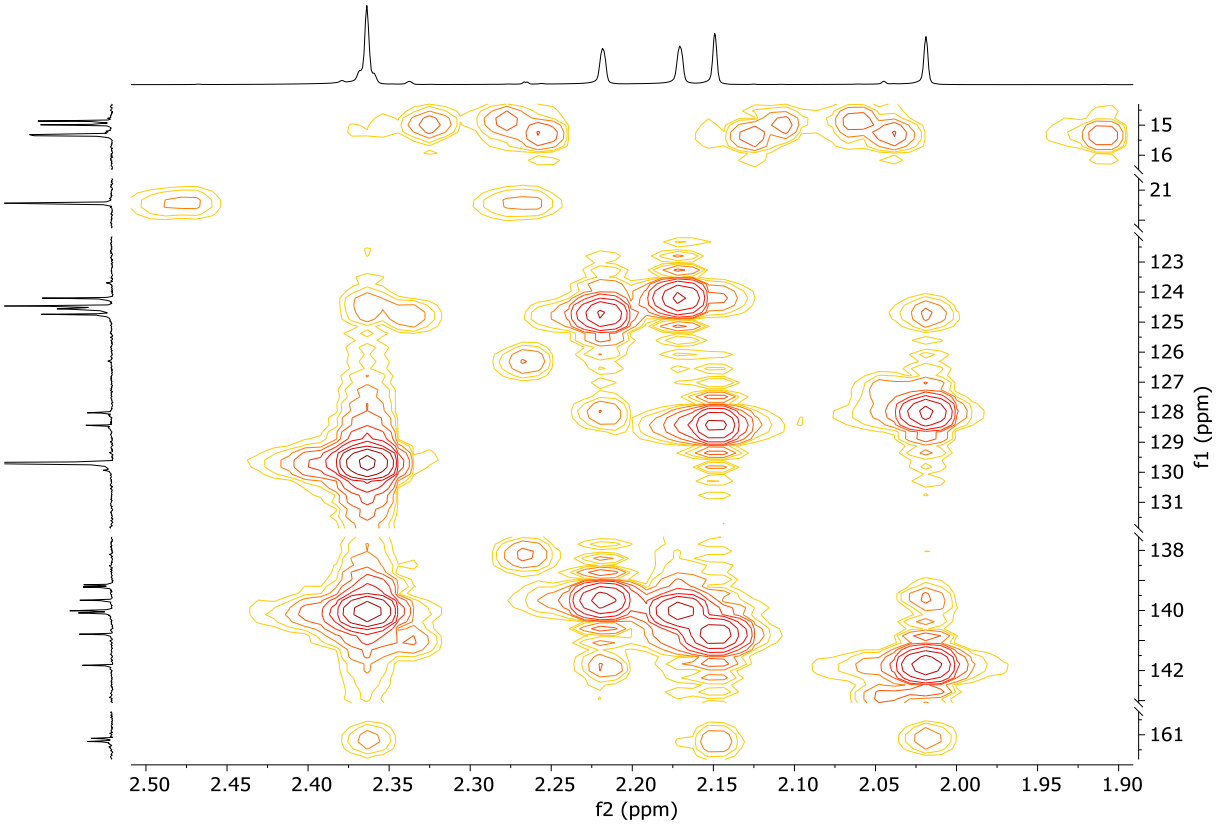

Figure S48: *HMBC aliphatic area spectrum (600/150 MHz, CD_2Cl_2) of* ***96****.*

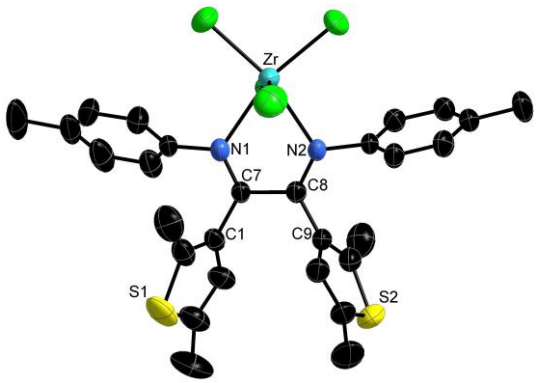

Figure S49: *X-ray crystal structure of* ***96*** *at 50% ellipsoid probability. Hydrogen atoms are omitted for clarity. Selected bond lengths [Å]: C1-C7 = 1.476(5), C7-C8 = 1.503(5), C7-N1: 1.284(4), C8-N2: 1.283(4), C8-C9 = 1.470(5), N1-Zr: 2.358(3), N2-Zr: 2.349(3).*

Table S3: *Crystal data for (α-diimine)$ZrCl_4$ (**96**).*

	(α-diimine)$ZrCl_4$ (**96**)
Formula	$C_{28}H_{28}Cl_4N_2S_2Zr$
Formula weight, g mol^{-1}	689.66
Crystal system	Monoclinic
Space group	$P2_1/n$
a, Å	12.8667 (4)
b, Å	14.2644 (5)
c, Å	17.3727 (5)
α, º	90
β, º	92.138 (1)
γ, º	90
V, Å^3	3186.29 (18)
Z	4
ρ_{calcd}, Mg m^{-3}	1.438
μ (Mo *Kα*), mm^{-1}	0.832
F(000)	1400
θ range, deg	2.4 – 24.7
Index ranges	$-15 \le h \le 15$
	$-16 \le k \le 16$
	$-20 \le l \le 20$
No. of reflns collected	86083
Completeness to θ_{max}	99.8%
No. indep. Reflns	5485
No. obsd reflns with($I>2\sigma(I)$)	4457
No. refined params	340
GooF (F^2)	1.045
R_1 (F) ($I > 2\sigma(I)$)	0.0469
wR_2 (F^2) (all data)	0.1177
Largest diff peak/hole, e Å^{-3}	1.124 / -0.766

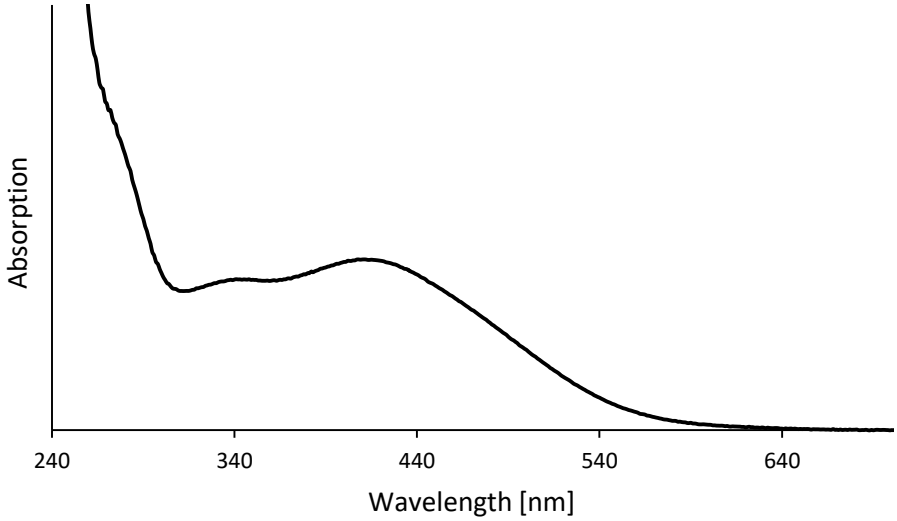

Figure S50: *UV/Vis spectrum of* ***96*** *in DCM.*

Synthesis and Characterization of (α-Diimine)$HfCl_4$ (97)

α-Diimine **91** (0.08 g, 0.18 mmol, 1.1 eq.) was dissolved in 5 mL toluene and treated with $HfCl_4$ (0.05 g, 0.16 mmol, 1.0 eq.). The solution was stirred at rt for 24 h upon which a color change from orange to brown occurred. Removal of the solvent under reduced pressure and washing the crude product with small portions of *n*-hexane led to **97** as red to brown solid. Crystals suitable for X-ray crystallography were obtained *via* slow diffusion of *n*-hexane into a saturated solution of **97** in DCM. **Yield:** 0.12 g (0.15 mmol, 97%), **Mp:** 205-207 °C; **^{1}H NMR:** (600 MHz, CD_2Cl_2): δ 7.20-7.14 (m, 16H, phenyl), 6.17-6.15 (m, 2H, b-thienyl-H), 6.01-5.99 (m, 2H, a-thienyl-H), 2.34 (s, 12H phenyl-Me), 2.21 (s, 6H, b-thienyl-Me), 2.16 (s, 6H, a-thienyl-Me), 2.16 (s, 6H, a-thienyl-Me), 2.03 (s, 6H, b-thienyl-Me) ppm; **^{13}C{1H} NMR:** (150 MHz, CD_2Cl_2): δ 173.2 (a-C=N), 173.1 (b-C=N), 144.4 (C-N), 144.3 (C-N), 140.9 (b-thienyl), 140.0 (a-thienyl), 139.5 (a-thienyl), 139.2 (b-thienyl), 139.1 (C-phenyl-Me), 139.0 (C-phenyl-Me), 130.0 (a-thienyl), 129.7 (phenyl), 129.7 (phenyl), 129.7 (b-thienyl), 124.9 (b-C-thienyl-H), 124.3 (a-C-thienyl-H), 123.5 (phenyl), 123.5 (phenyl), 21.3 (phenyl-Me), 15.3 (b-thienyl-Me), 15.3 (a-thienyl-Me), 15.0 (b-thienyl-Me), 14.8 (a-thienyl-Me) ppm; **UV/Vis** (CH_2Cl_2): λ_{max} = 416 nm; $\lambda_{shoulder}$ = 274, 332 nm.-

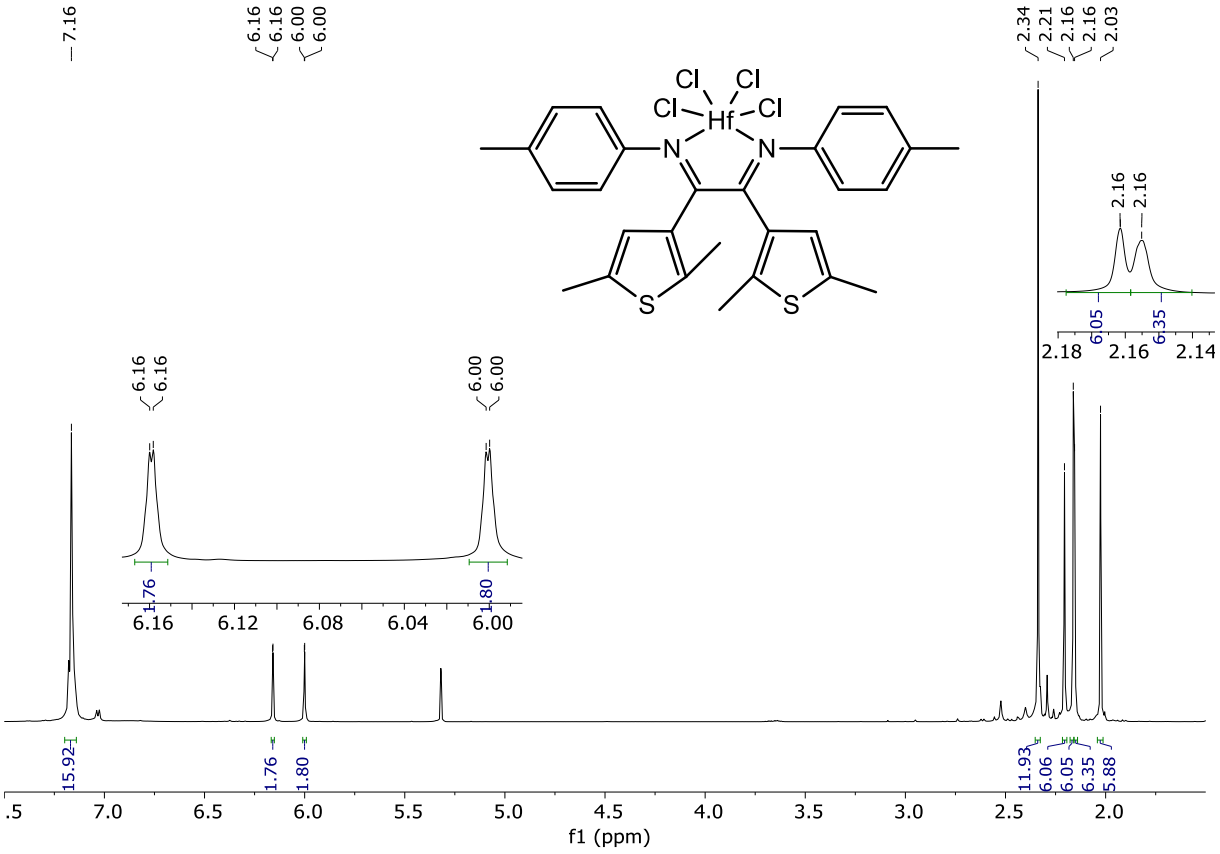

Figure S51: *^{1}H NMR spectrum (600 MHz, CD_2Cl_2) of **97**.*

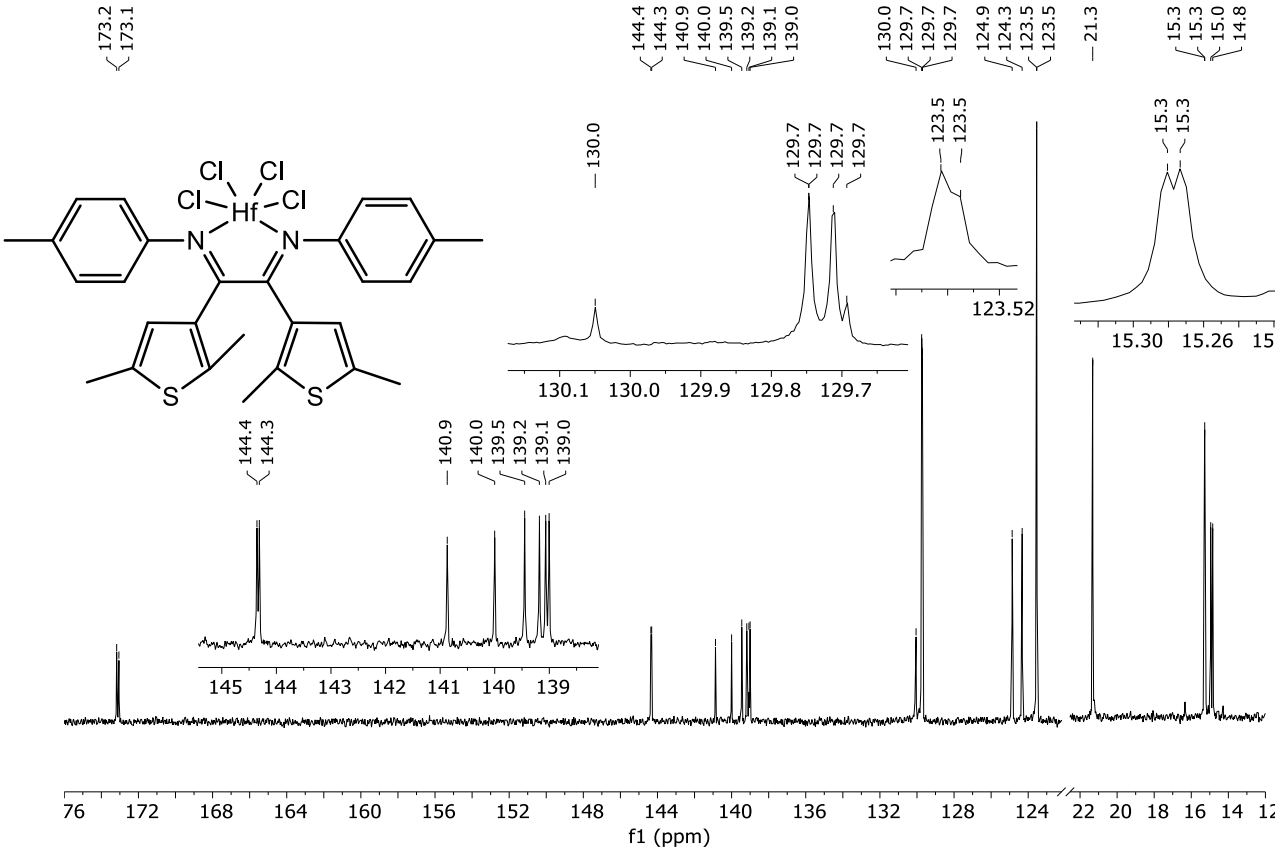

Figure S52: *$^{13}C\{^{1}H\}$ NMR spectrum (150 MHz, CD_2Cl_2) of* ***97****.*

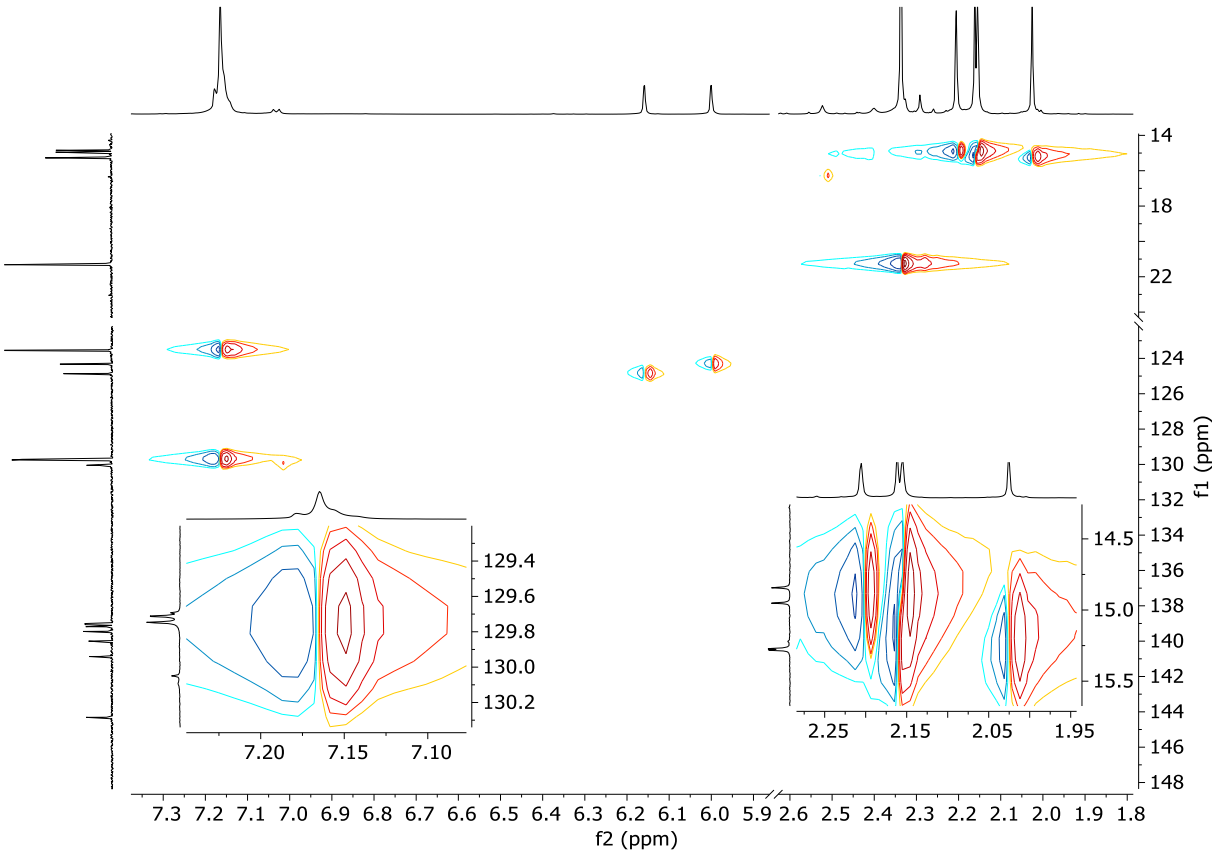

Figure S53: *HSQC spectrum (600/150 MHz, CD_2Cl_2) of* ***97****.*

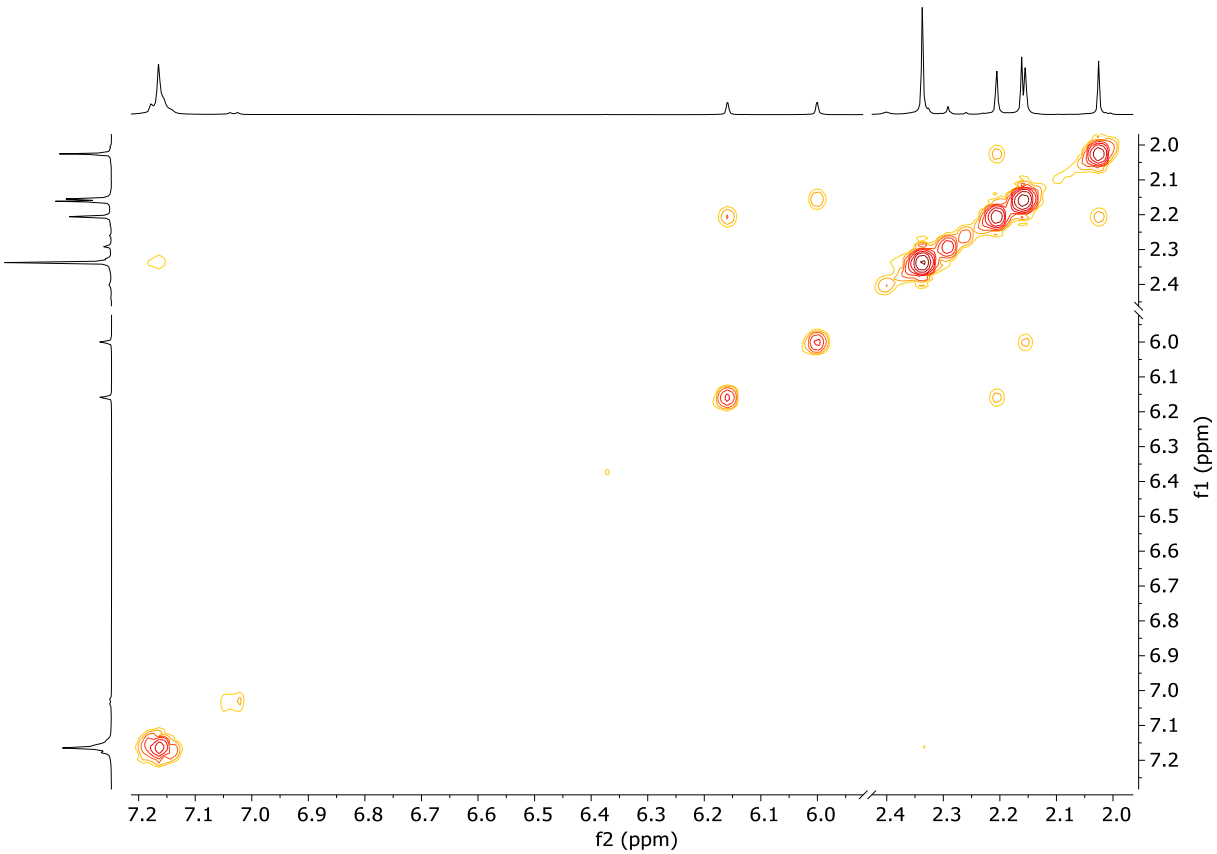

Figure S54: *H,H-COSY spectrum (600 MHz, CD_2Cl_2) of* ***97****.*

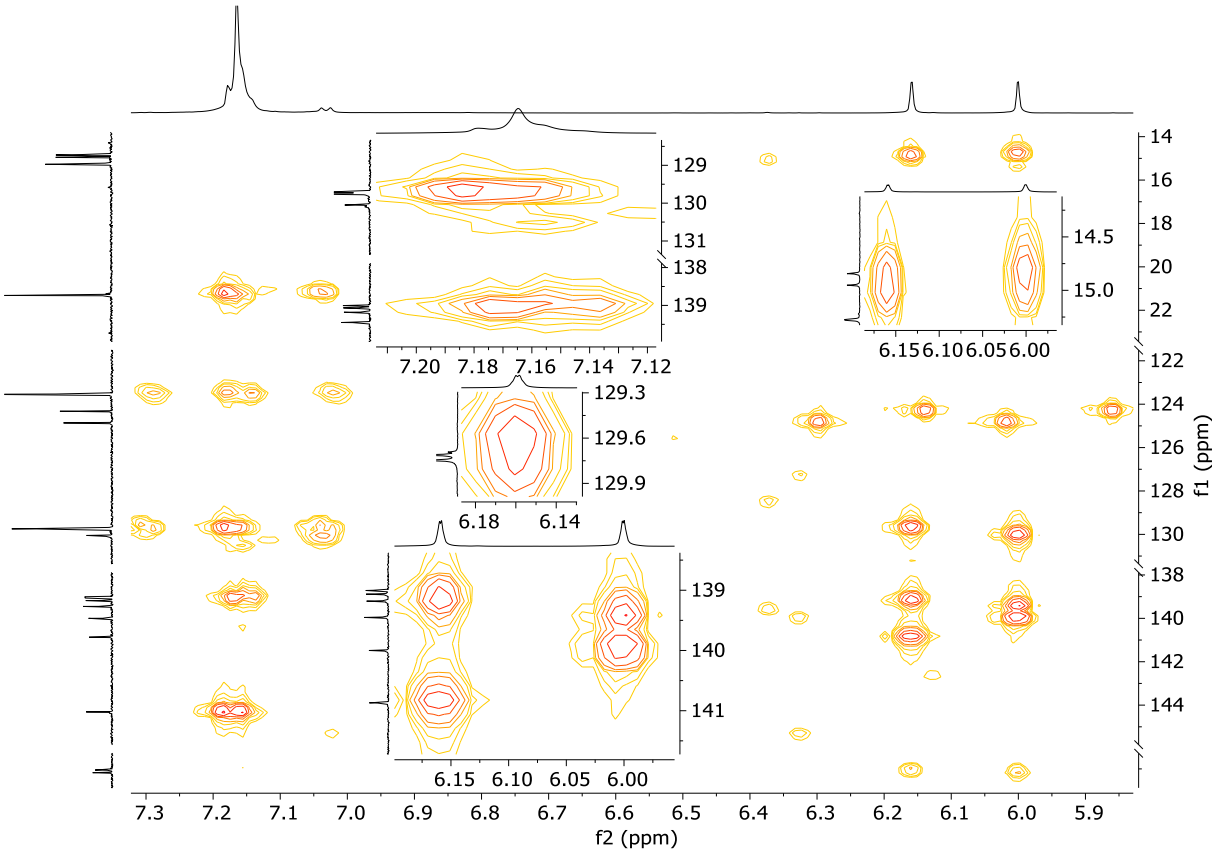

Figure S55: *HMBC aromatic area spectrum (600/150 MHz, CD_2Cl_2) of* ***97****.*

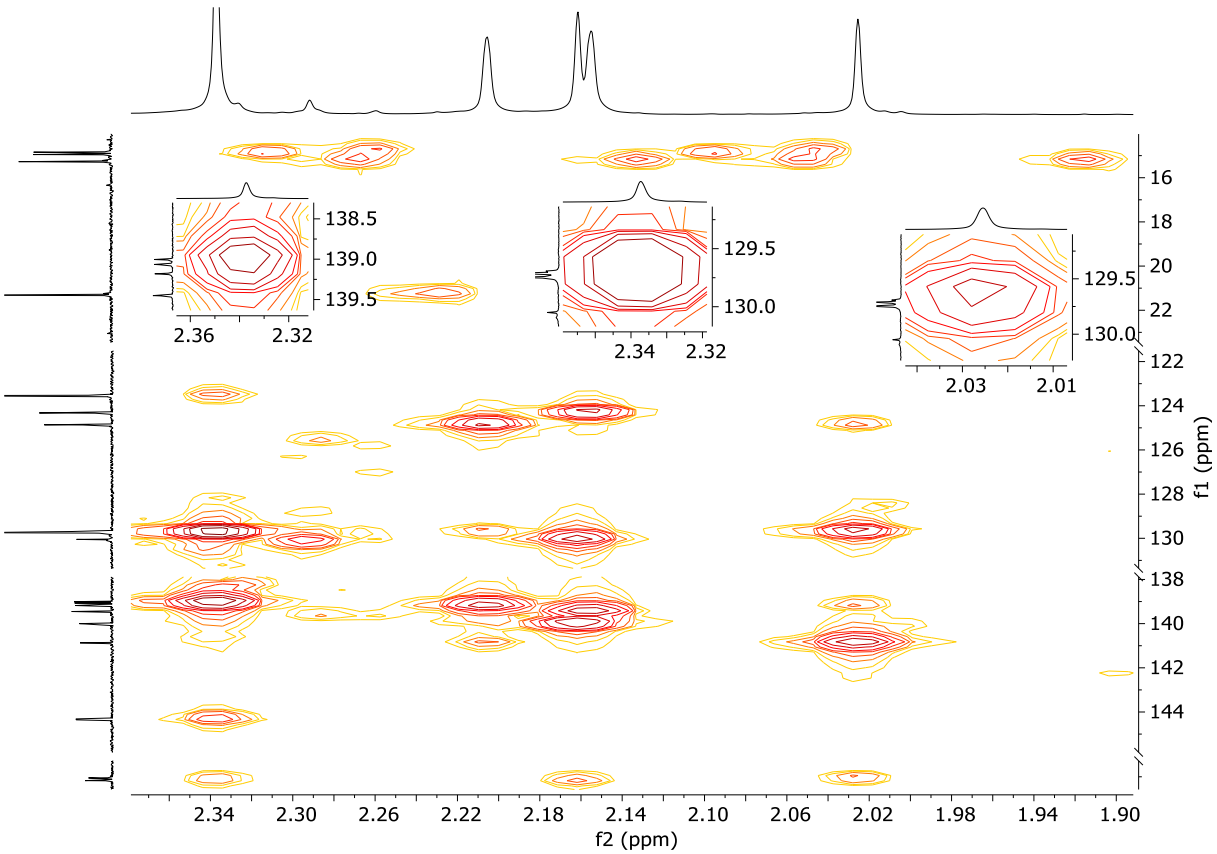

Figure S56: *HMBC aliphatic area spectrum (600/150 MHz, CD_2Cl_2) of* ***97****.*

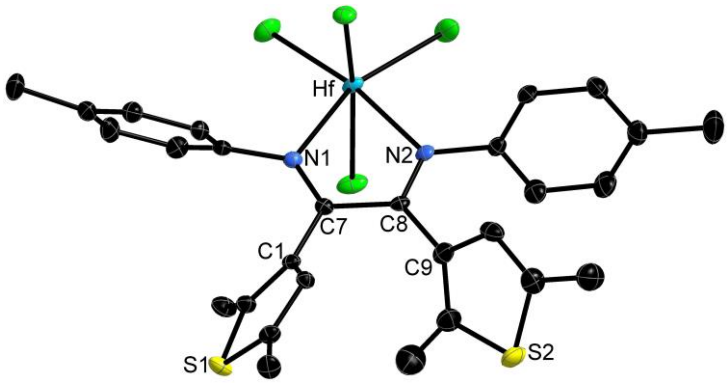

Figure S57: *X-ray crystal structure of* ***97*** *at 50% ellipsoid probability. Hydrogen atoms are omitted for clarity. Selected bond lengths [Å]: C1-C7 = 1.476(6), C7-C8 = 1.501(6), C7-N1: 1.294(6), C8-N2: 1.298(6), C8-C9 = 1.482(6), N1-Hf: 2.331(4), N2-Hf: 2.338(4).*

Table S4: *Crystal data for (α-diimine)$HfCl_4$ (**97**).*

	(α-diimine)$HfCl_4$ (**97**)
Formula	$C_{28}H_{28}Cl_4N_2S_2Hf$
Formula weight, g mol^{-1}	776.93
Crystal system	Monoclinic
Space group	$P2_1/n$
a, Å	11.7205 (6)
b, Å	12.9508 (7)
c, Å	20.3397 (10)
α, º	90
β, º	95.926 (2)
γ, º	90
V, $Å^3$	3030.46 (11)
Z	4
ρ_{calcd}, Mg m^{-3}	1.680
μ (Mo *Kα*), mm^{-1}	3.902
F(000)	1528
θ range, deg	2.4 – 28.4
Index ranges	$-14 \le h \le 14$
	$-15 \le k \le 15$
	$-24 \le l \le 21$
No. of reflns collected	56968
Completeness to θ_{max}	99.9%
No. indep. Reflns	5727
No. obsd reflns with($I>2\sigma(I)$)	5326
No. refined params	340
GooF (F^2)	1.258
R_1 (F) ($I > 2\sigma(I)$)	0.0333
wR_2 (F^2) (all data)	0.0675
Largest diff peak/hole, e $Å^{-3}$	0.930 / -1.739

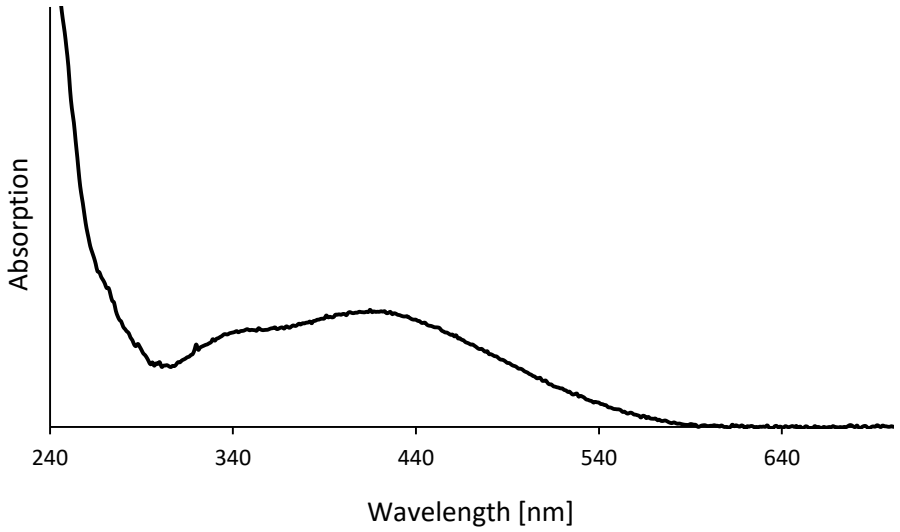

Figure S58: *UV/Vis spectrum of* ***97*** *in DCM.*

Synthesis and Characterization of (α-Diimine)$SnCl_4$ (101)

α-Diimine **91** (0.08 g, 0.17 mmol, 1.1 eq.) was dissolved in 5 mL toluene and treated with $SnCl_4$ (18 µL, ρ = 2.23 g/cm^3, 0.16 mmol, 1.0 eq.). The instantly turned orange solution was stirred at rt for 24 h. Removal of the solvent under reduced pressure and washing the crude product with small portions of *n*-hexane led to **101** as red solid. **Yield:** 0.11 g (0.15 mmol, 96%); **Mp:** >170 °C decomposition; **^{1}H NMR:** (600 MHz, CD_2Cl_2): δ 7.22-7.15 (m, 16H, phenyl), 6.19-6.18 (m, 2H, b-thienyl-H), 6.02-6.01 (m, 2H, a-thienyl-H), 2.36 (s, 12H, phenyl-Me), 2.22 (s, 6H, b-thienyl-Me), 2.17 (s, 6H, a-thienyl-Me), 2.15 (s, 6H, b-thienyl-Me), 2.02 (s, 6H, a-thienyl-Me) ppm; **^{13}C{1H} NMR:** (150 MHz, CD_2Cl_2): δ 161.3 (b-C=N), 161.2 (a-C=N), 141.8 (b-thienyl), 140.8 (a-thienyl), 140.1 (a-thienyl), 140.0 (C-N), 140.0 (C-N), 139.7 (b-thienyl), 139.2 (phenyl-C-Me), 139.2 (phenyl-C-Me), 129.7 (phenyl), 129.7 (phenyl), 128.4 (a-thienyl), 128.0 (b-thienyl), 124.8 (b-C-thienyl-H), 124.6 (phenyl), 124.5 (phenyl), 124.2 (a-C-thienyl-H), 21.4 (phenyl-Me), 15.4 (a-thienyl-Me), 15.3 (b-thienyl-Me), 15.0 (b-thienyl-Me), 14.9 (a-thienyl-Me) ppm; **^{119}Sn NMR:** (150 MHz, $CDCl_3$): δ -555.6, -556.2 ppm; **^{1}H NMR:** (600 MHz, THF-d_8): δ 7.24-7.15 (m, 16H, phenyl), 6.37-6.36 (m, 2H, b-thienyl-H), 6.21-6.20 (m, 2H, a-thienyl-H), 2.32 (s, 12H, phenyl-Me), 2.21 (s, 6H, b-thienyl-Me), 2.19 (s, 6H, a-thienyl-Me), 2.16 (s, 6H, a-thienyl-Me), 2.05 (s, 6H, b-thienyl-Me) ppm; **^{13}C{1H} NMR:** (150 MHz, THF-d_8): δ 161.3 (a-C=N), 161.2 (b-C=N), 141.1 (b-thienyl), 140.2 (a-thienyl), 140.1 (C-N), 140.1 (C-N), 139.8 (a-thienyl), 139.6 (phenyl-C-Me), 139.6 (phenyl-C-Me), 139.5 (b-thienyl), 129.7 (phenyl), 129.6 (phenyl), 129.4 (a-thienyl), 128.9 (b-thienyl), 125.7 (b-C-thienyl-H), 125.0 (a-C-thienyl-H), 124.9 (phenyl), 124.9 (phenyl), 21.1 (phenyl-Me), 14.9 (b-thienyl-Me), 14.8 (a-thienyl-Me), 14.4 (b-thienyl-Me), 14.3 (a-thienyl-Me) ppm; **^{1}H NMR:** (600 MHz, C_6D_6): δ 7.53-7.41 (m, 8H, phenyl), 6.87-6.82 (m, 8H, phenyl), 5.98-5.96 (m, 2H, b-thienyl-H), 5.83-5.81 (m, 2H, a-thienyl-H), 1.96 (s, 6H, a-thienyl-Me), 1.88 (s, 6H, phenyl-Me), 1.87 (s, 6H, phenyl-Me), 1.78 (s, 6H, b-thienyl-Me) 1.68 (s, 6H, b-thienyl-Me), 1.61 (s, 6H, a-thienyl-Me) ppm; **^{13}C{1H} NMR:** (150 MHz, C_6D_6): δ 160.5 (C=N), 160.4 (C=N), 140.4 (b-thienyl), 139.8 (C-N), 139.8 (C-N), 139.5 (a-thienyl), 139.4 (phenyl-C-Me), 139.3 (phenyl-C-Me), 139.2 (a-thienyl), 138.9 (b-thienyl), 129.7 (phenyl), 129.6 (phenyl), 129.0 (a-thienyl), 128.6 (b-thienyl), 125.0 (b-C-thienyl-H), 124.6 (phenyl), 124.6 (phenyl), 124.2 (a-C-thienyl-H), 21.1 (phenyl-Me), 14.9 (a-thienyl-Me), 14.8 (b-thienyl-Me), 14.5 (b-thienyl-Me), 14.4 (a-thienyl-Me) ppm; **^{119}Sn NMR:** (150 MHz, C_6D_6): δ -544.2, -545.2 ppm **UV/Vis** (CH_2Cl_2): λ_{max} = 420 nm; $\lambda_{shoulder}$ = 347 nm.-

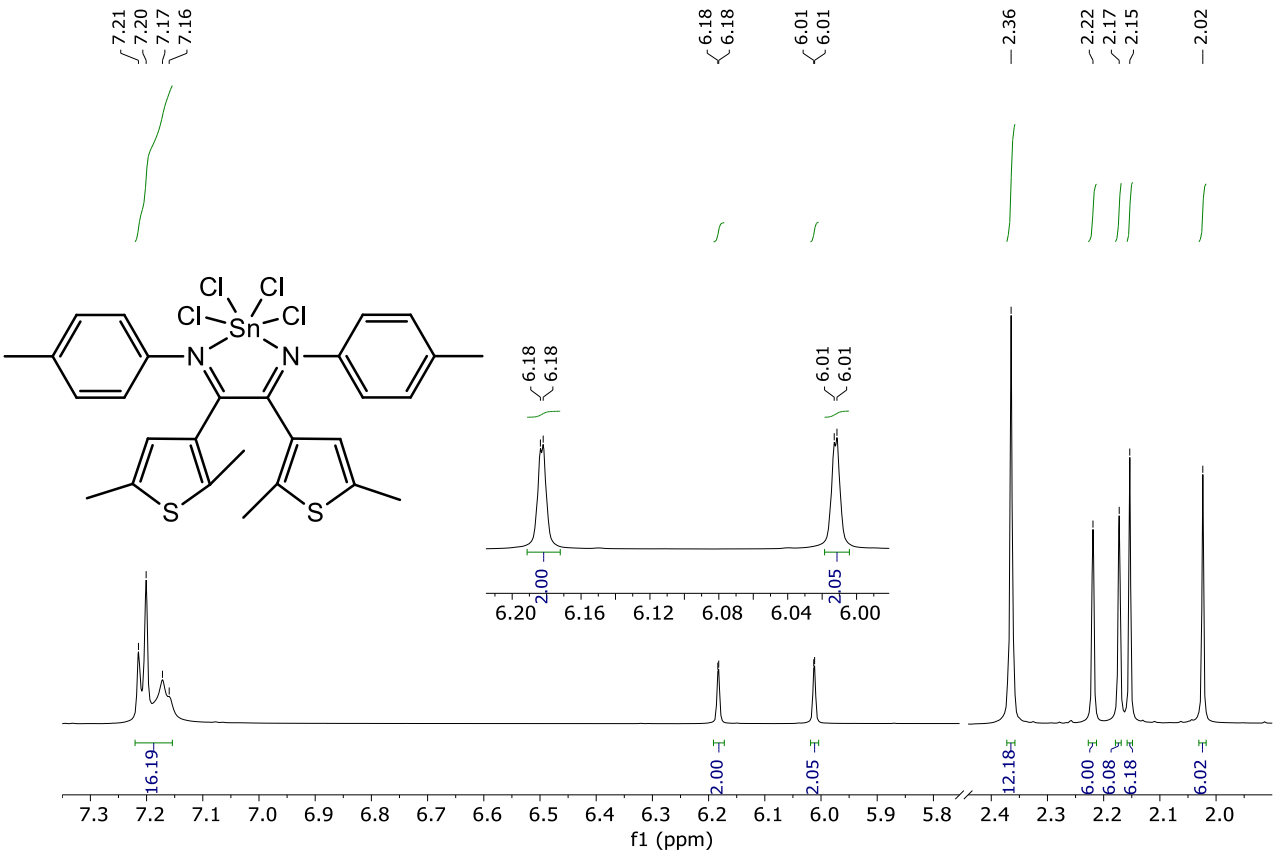

Figure S59: *^{1}H NMR spectrum (600 MHz, CD_2Cl_2) of* ***101****.*

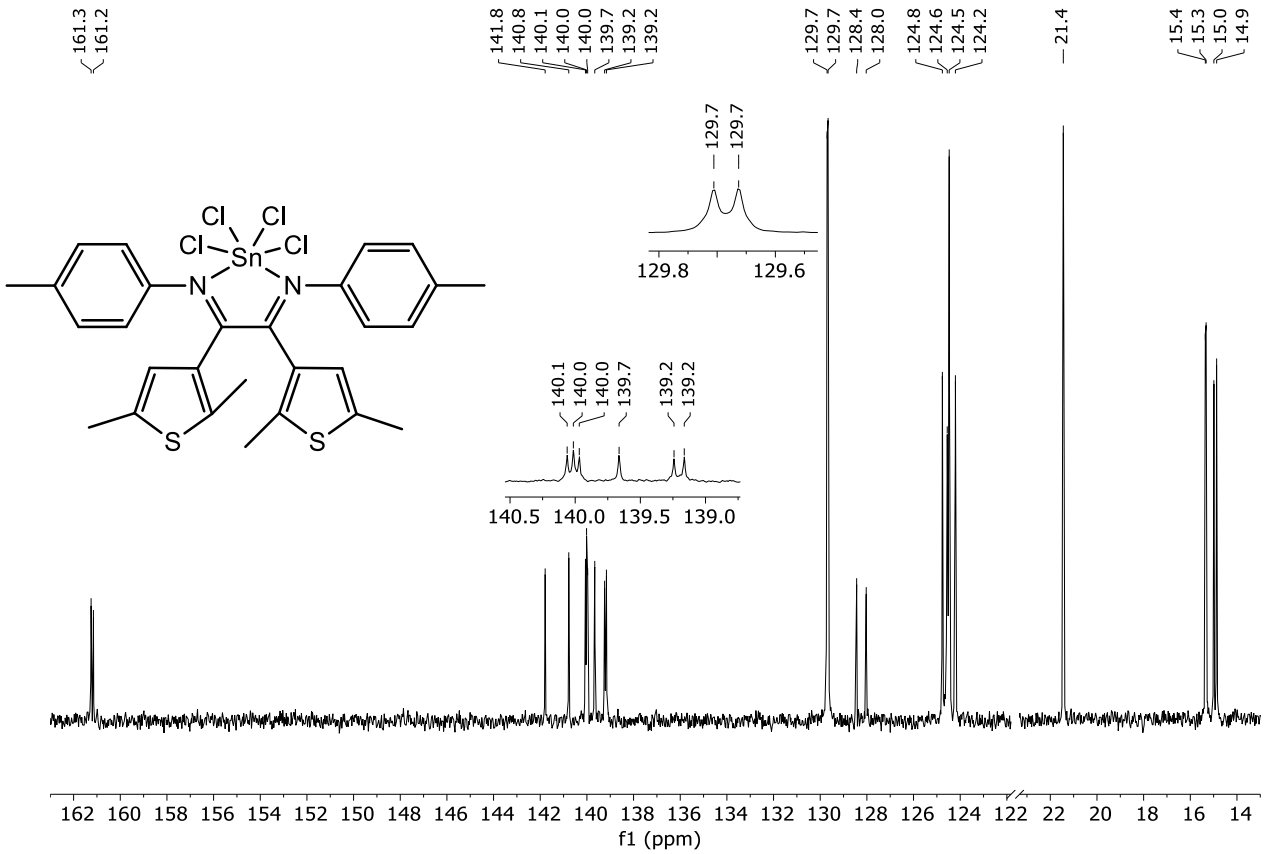

Figure S60: *$^{13}C\{^{1}H\}$ NMR spectrum (150 MHz, CD_2Cl_2) of* ***101****.*

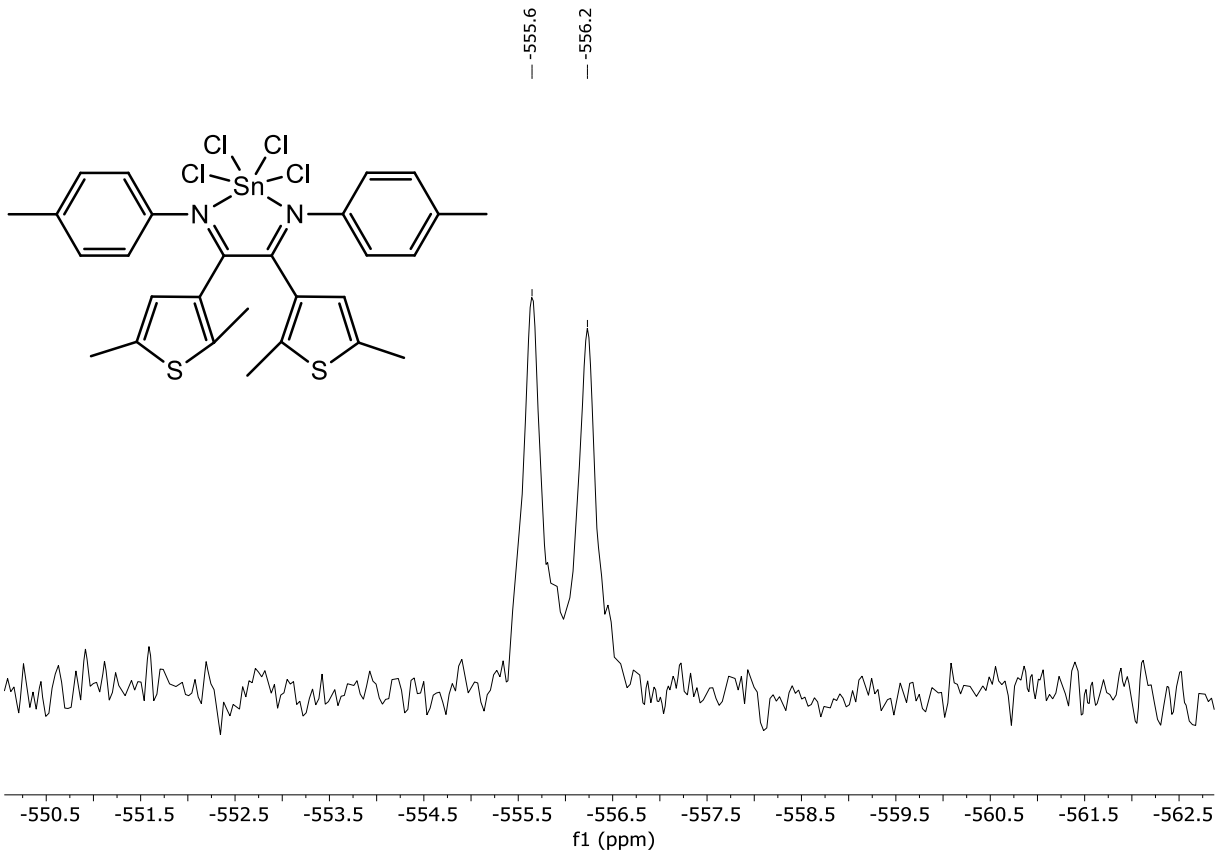

Figure S61: *^{119}Sn NMR spectrum (150 MHz, $CDCl_3$) of* ***101****.*

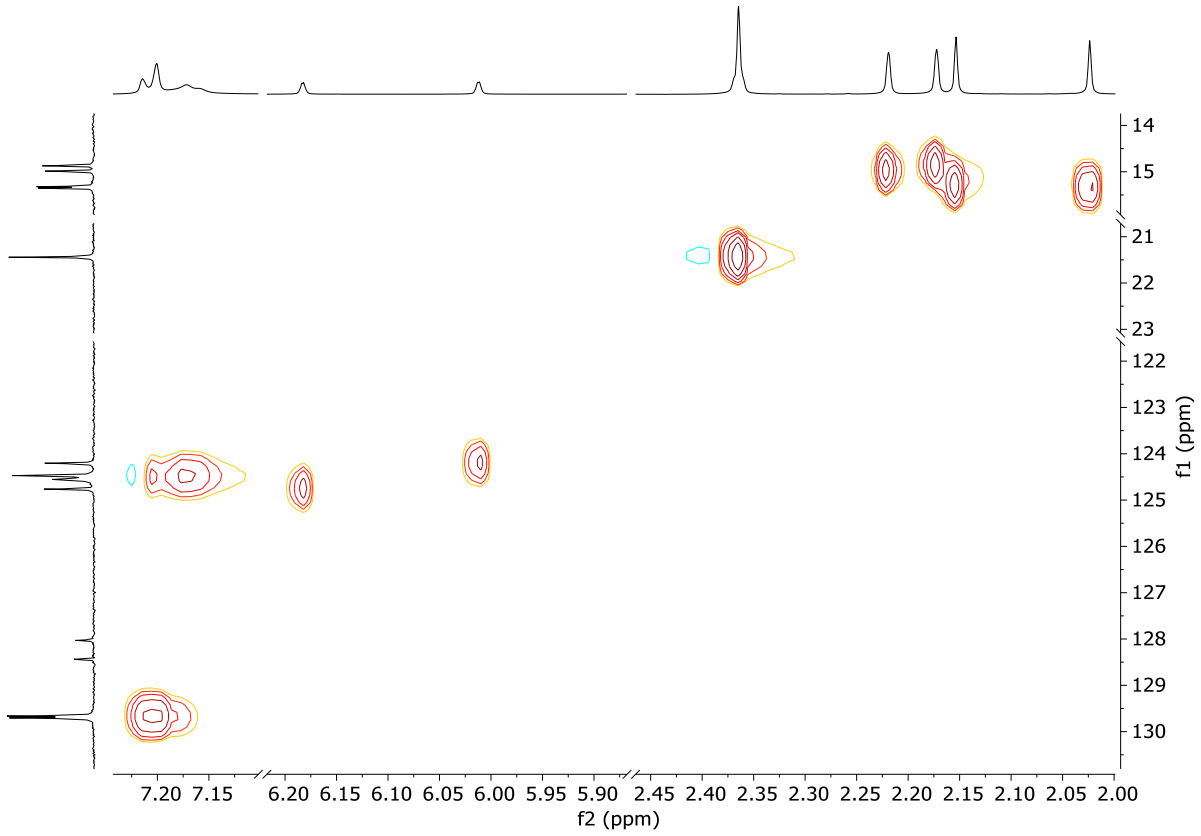

Figure S62: *HSQC spectrum (600/150 MHz, CD_2Cl_2) of* ***101****.*

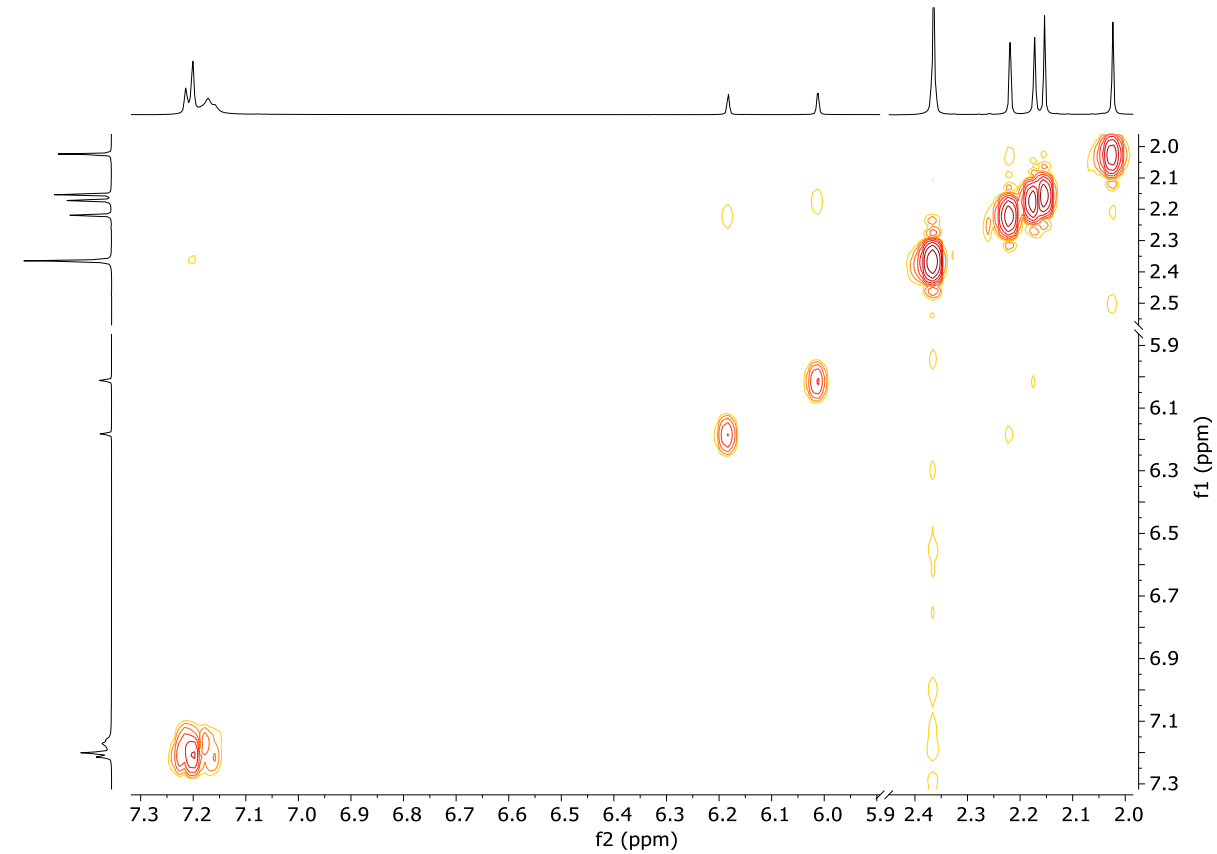

Figure S63: *H,H-COSY spectrum (600 MHz, CD_2Cl_2) of* ***101****.*

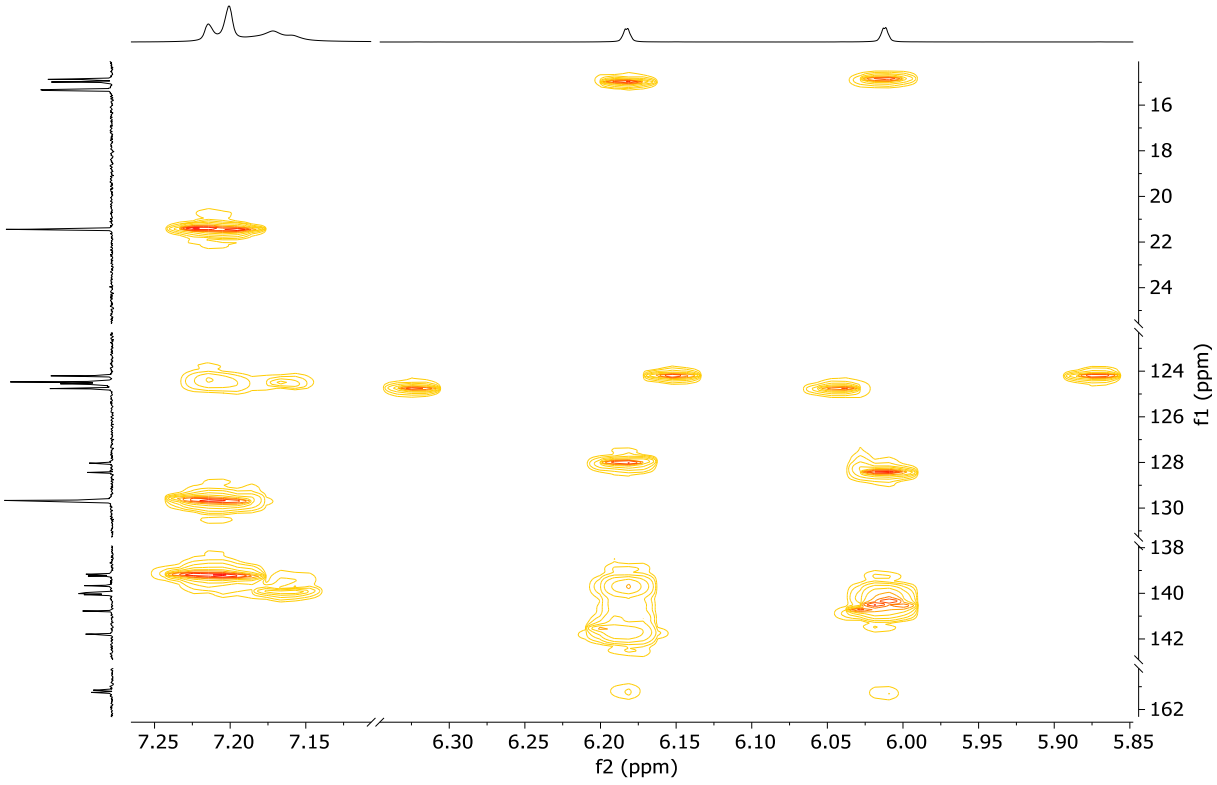

Figure S64: *HMBC aromatic area spectrum (600/150 MHz, CD_2Cl_2) of* ***101****.*

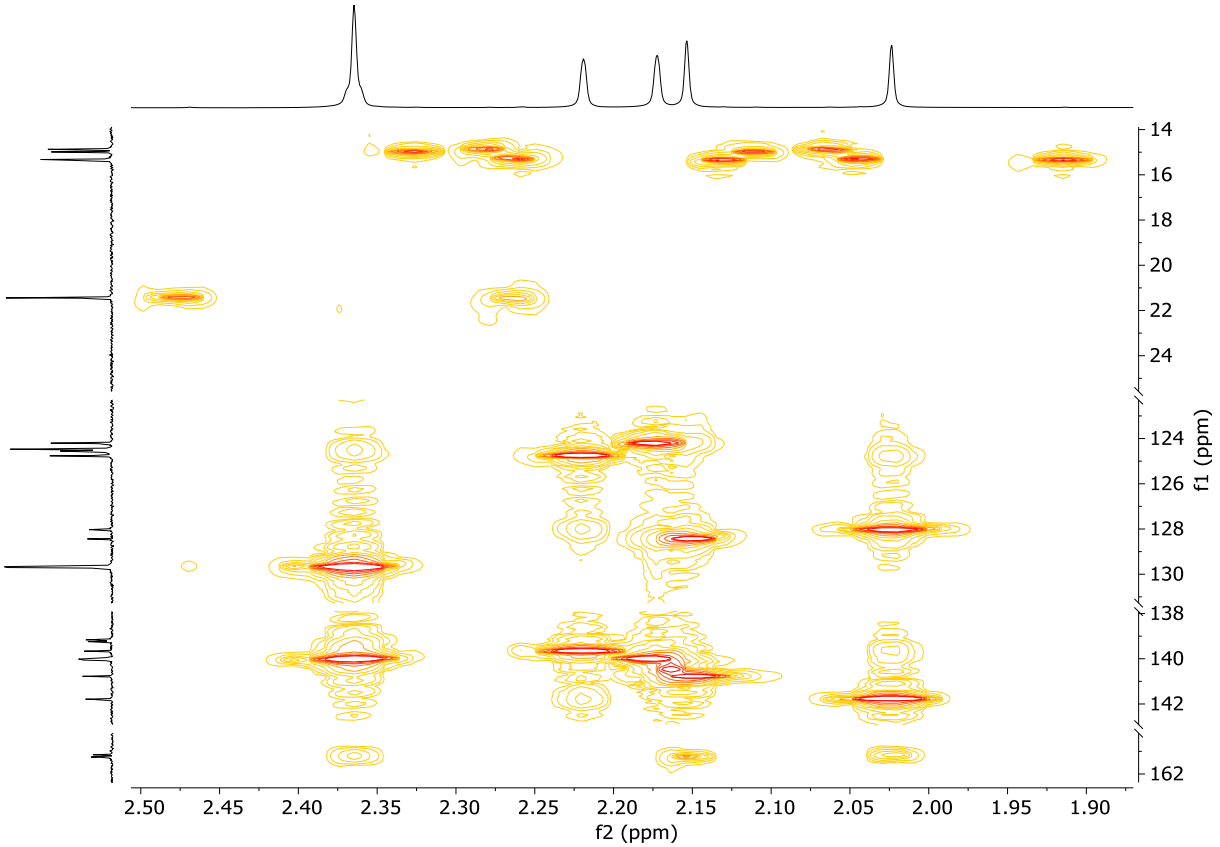

Figure S65: *HMBC aliphatic area spectrum (600/150 MHz, CD_2Cl_2) of* ***101****.*

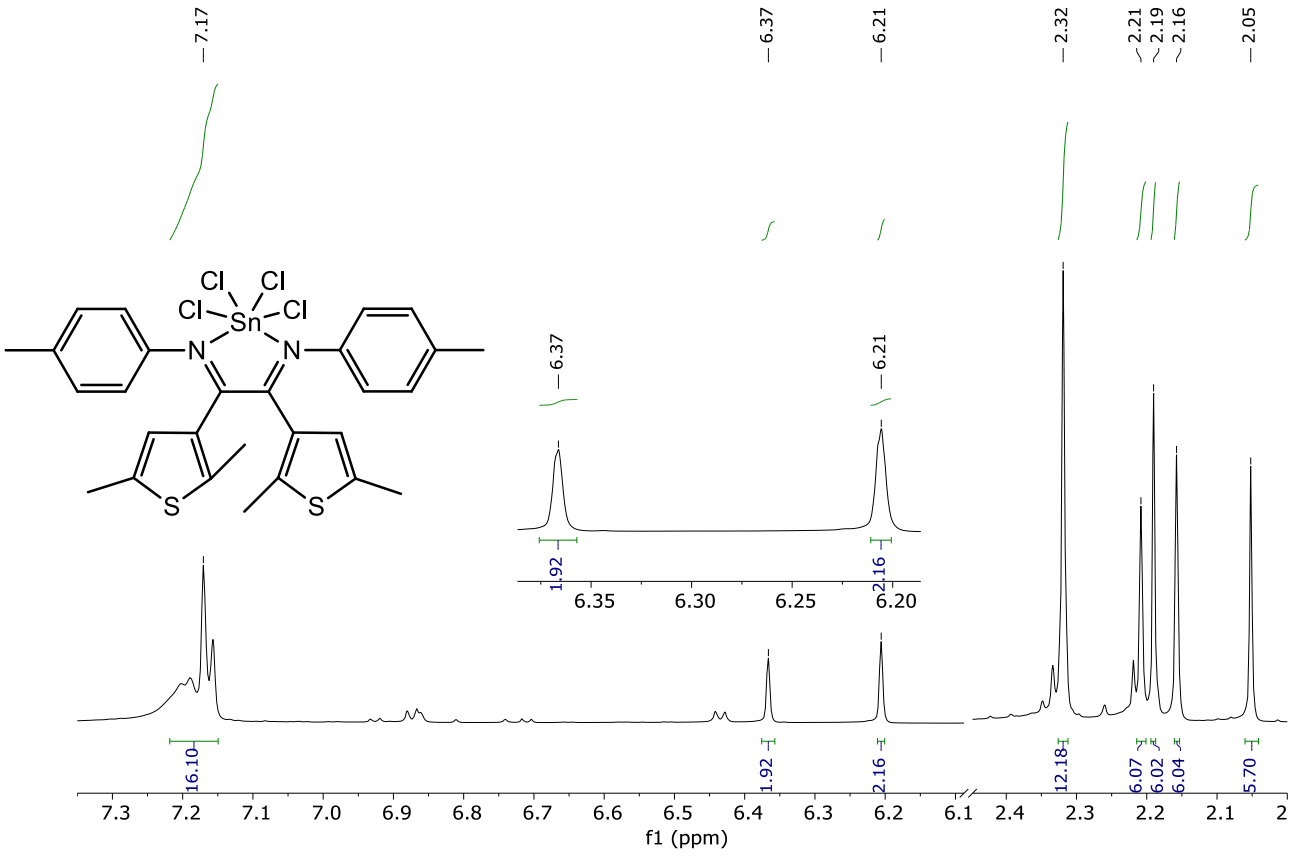

Figure S66: *^{1}H NMR spectrum (600 MHz, THF-d_8) of* ***101****.*

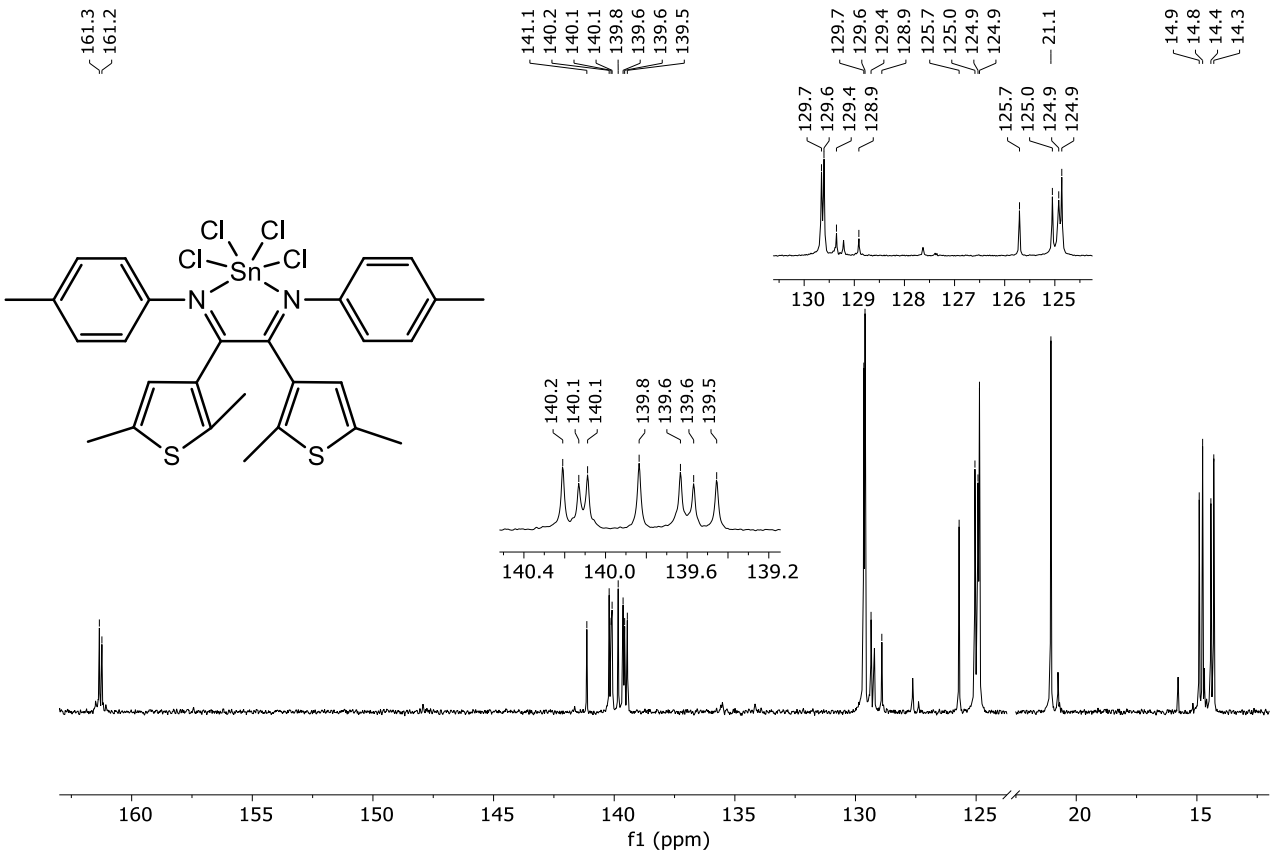

Figure S67: *$^{13}C\{^{1}H\}$ NMR spectrum (150 MHz, THF-d_8) of* ***101****.*

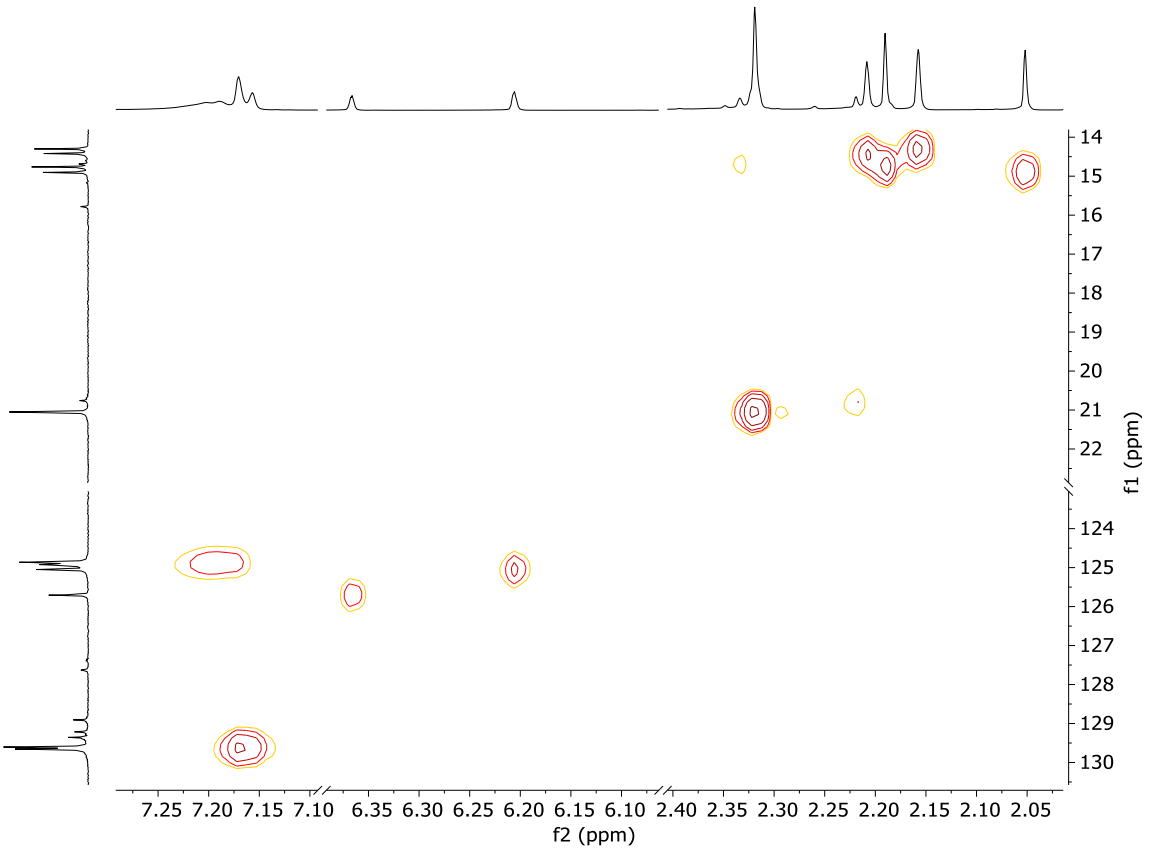

Figure S68: *HSQC spectrum (600/150 MHz, THF-$_8$) of* ***101****.*

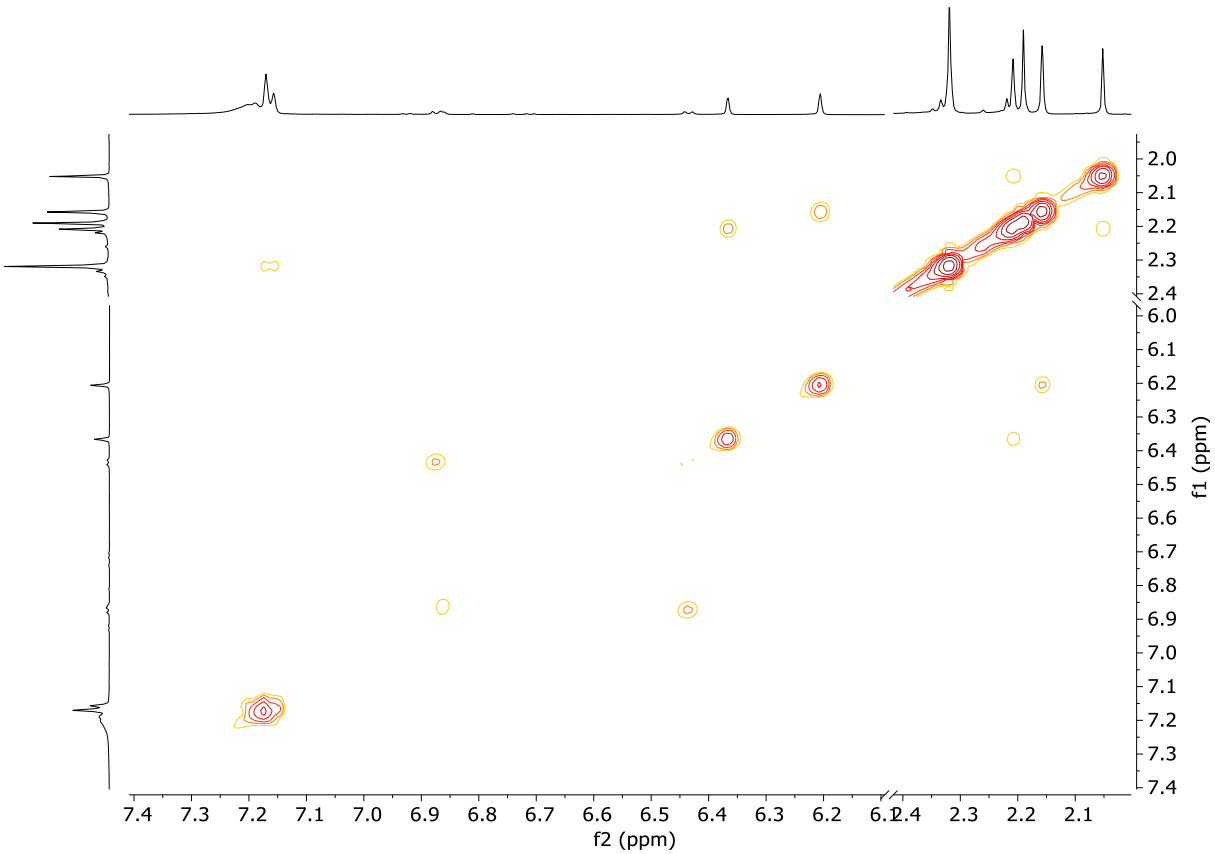

Figure S69: *H,H-COSY spectrum (600 MHz, THF-d_8) of* ***101****.*

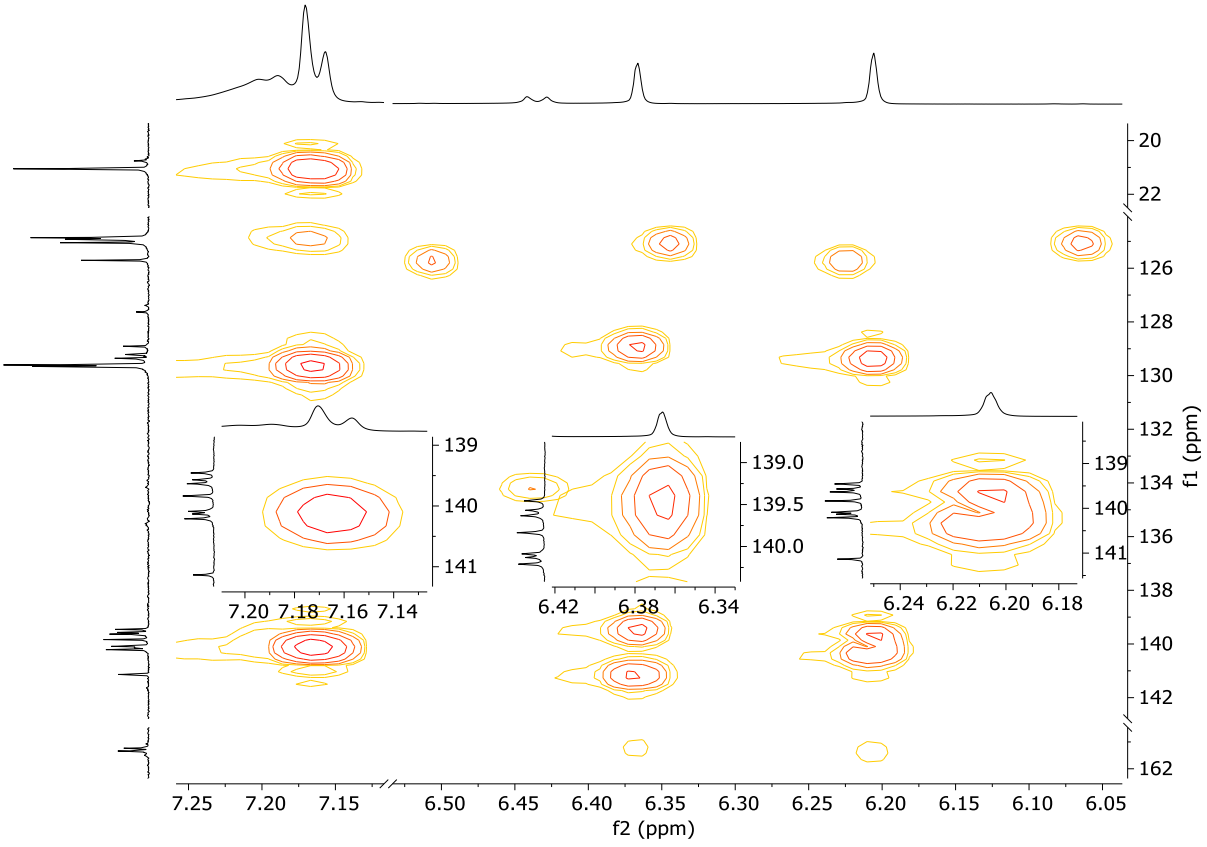

Figure S70: *HMBC aromatic area spectrum (600/150 MHz, THF-d_8) of* ***101****.*

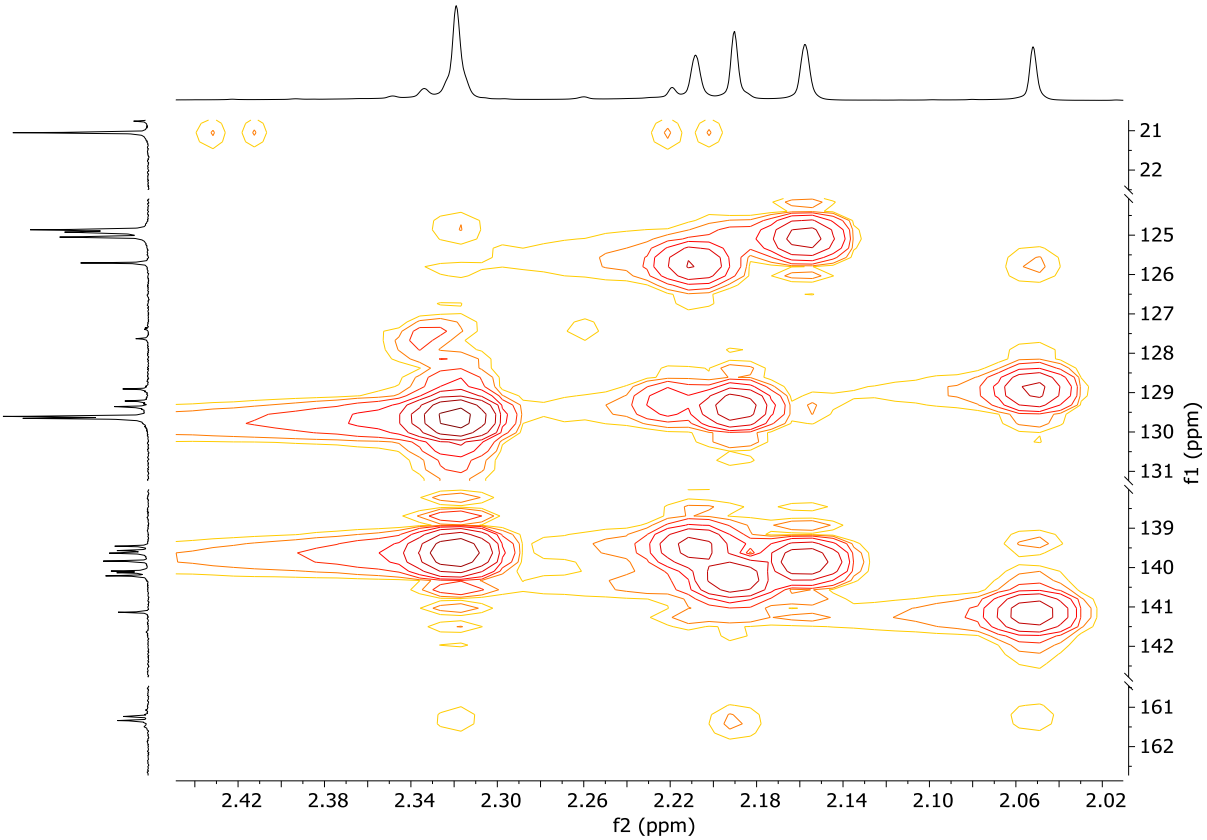

Figure S71: *HMBC aliphatic area spectrum (600/150 MHz, THF-d_8) of* ***101****.*

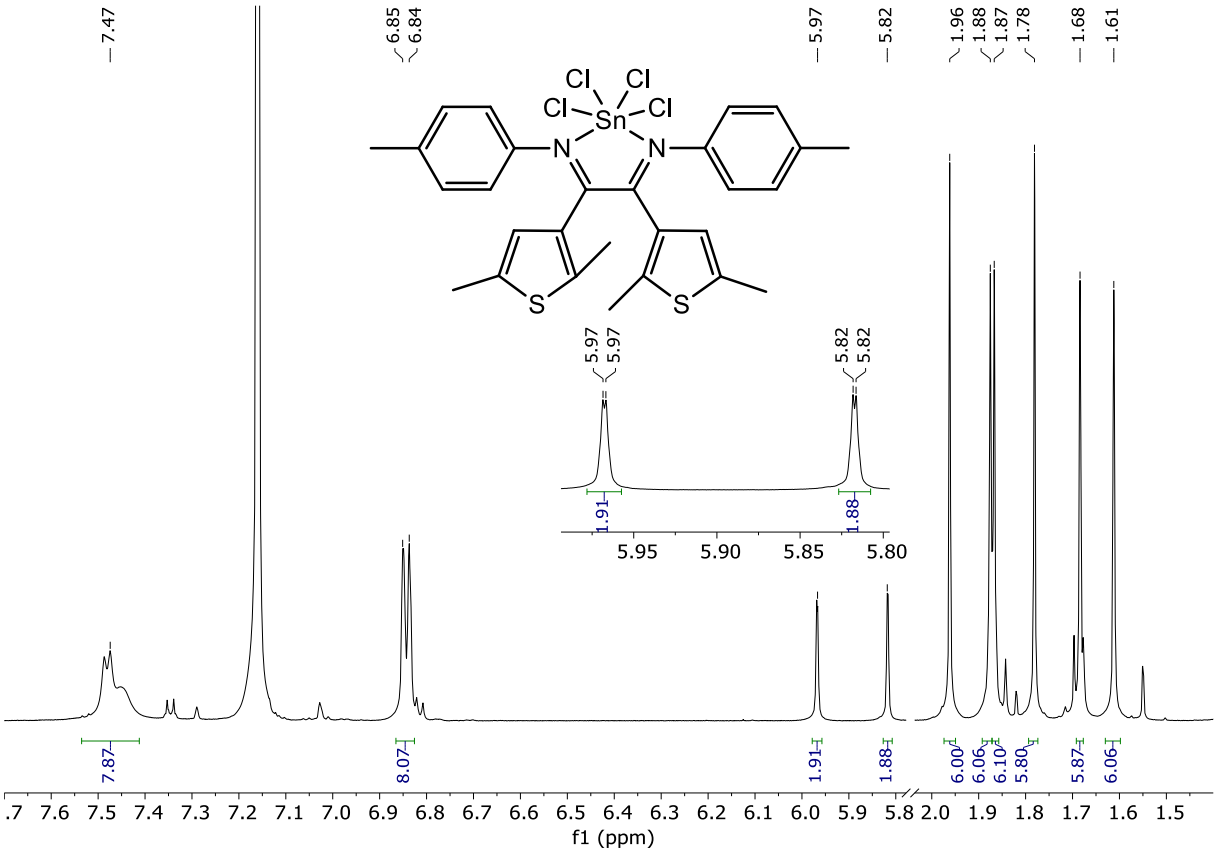

Figure S72: *^{1}H NMR spectrum (600 MHz, C_6D_6) of* ***101****.*

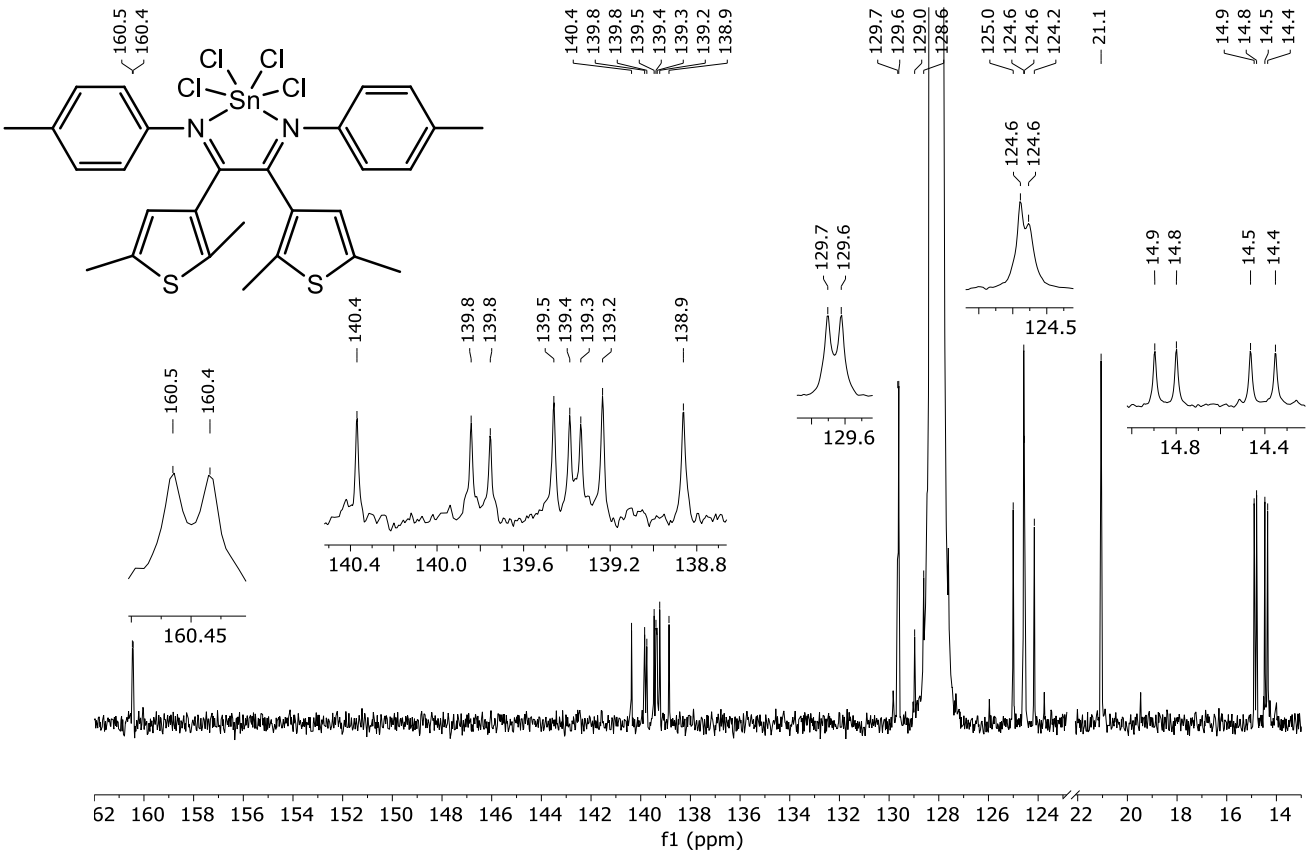

Figure S73: *$^{13}C\{^{1}H\}$ NMR spectrum (150 MHz, C_6D_6) of* ***101****.*

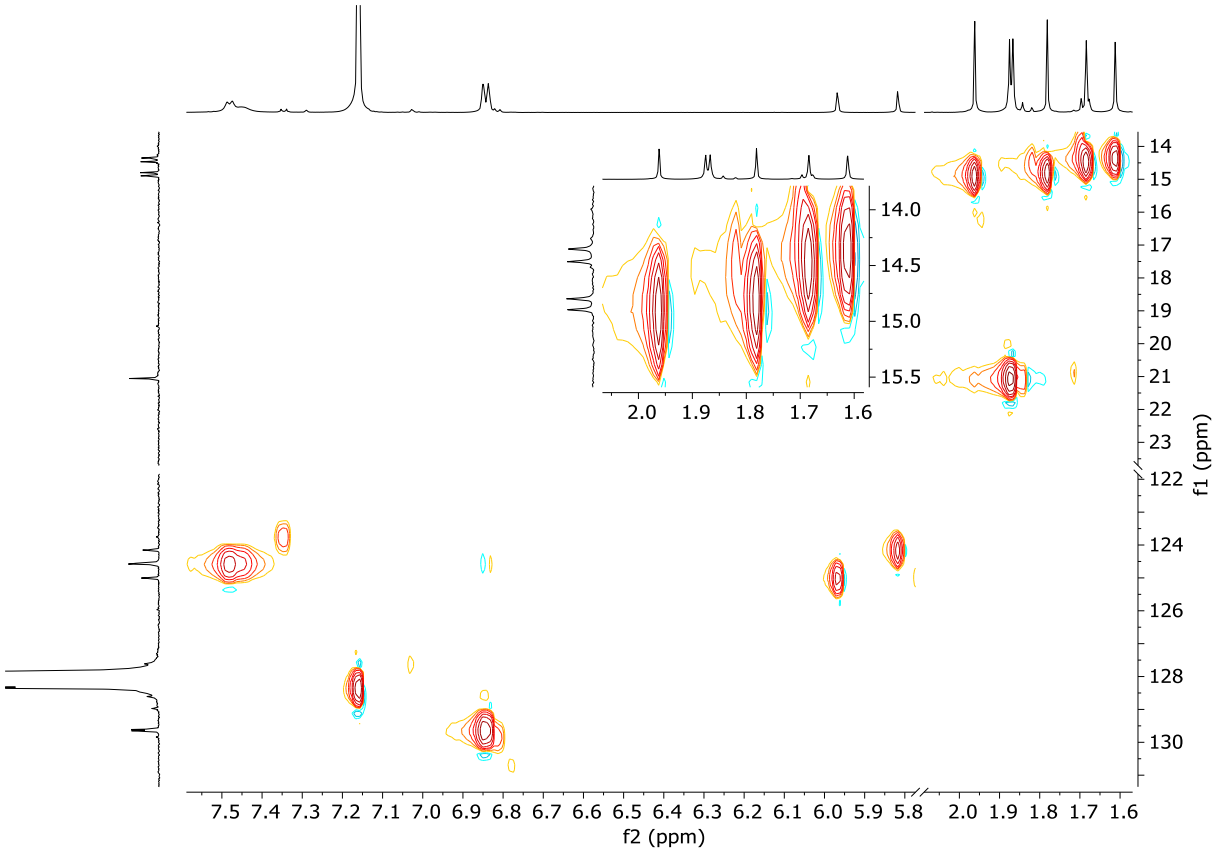

Figure S74: *HSQC spectrum (600/150 MHz, C_6D_6) of* ***101****.*

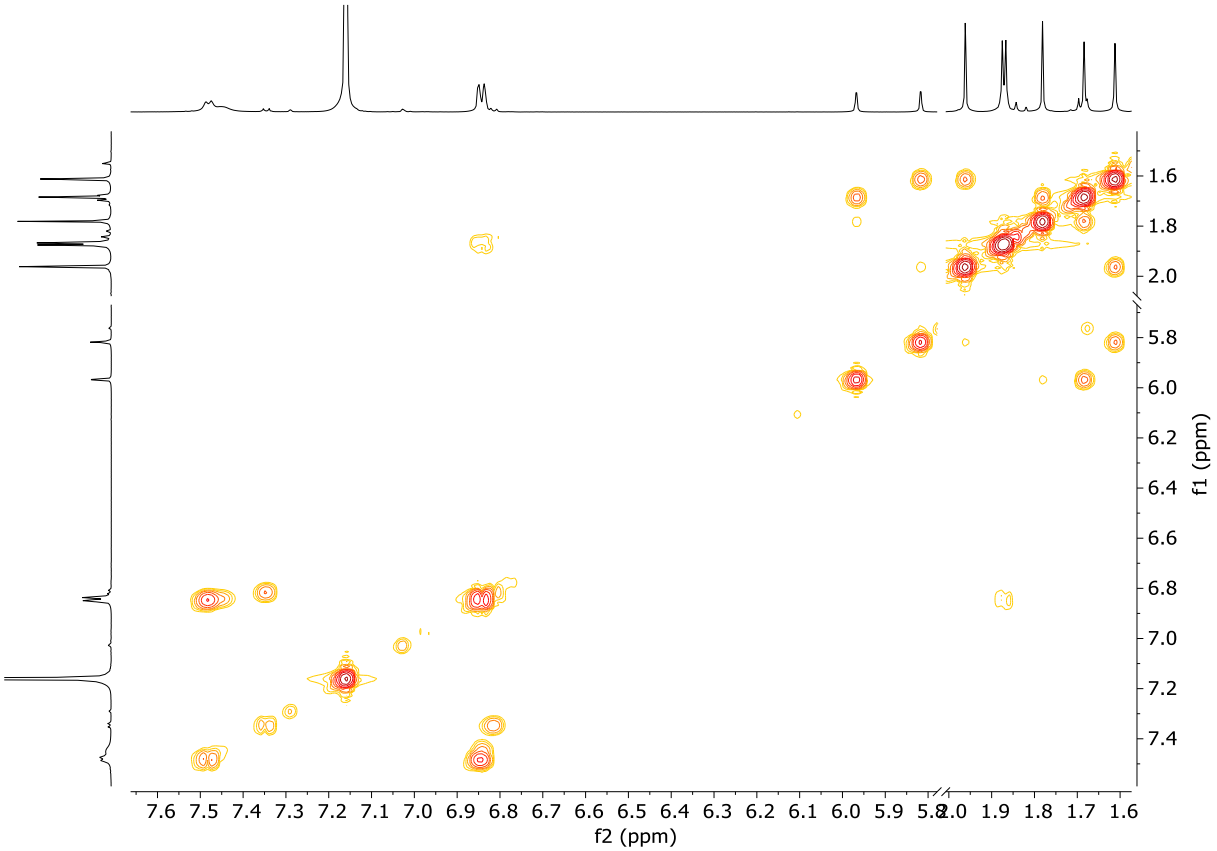

Figure S75: *H,H-COSY spectrum (600 MHz, C_6D_6) of* ***101****.*

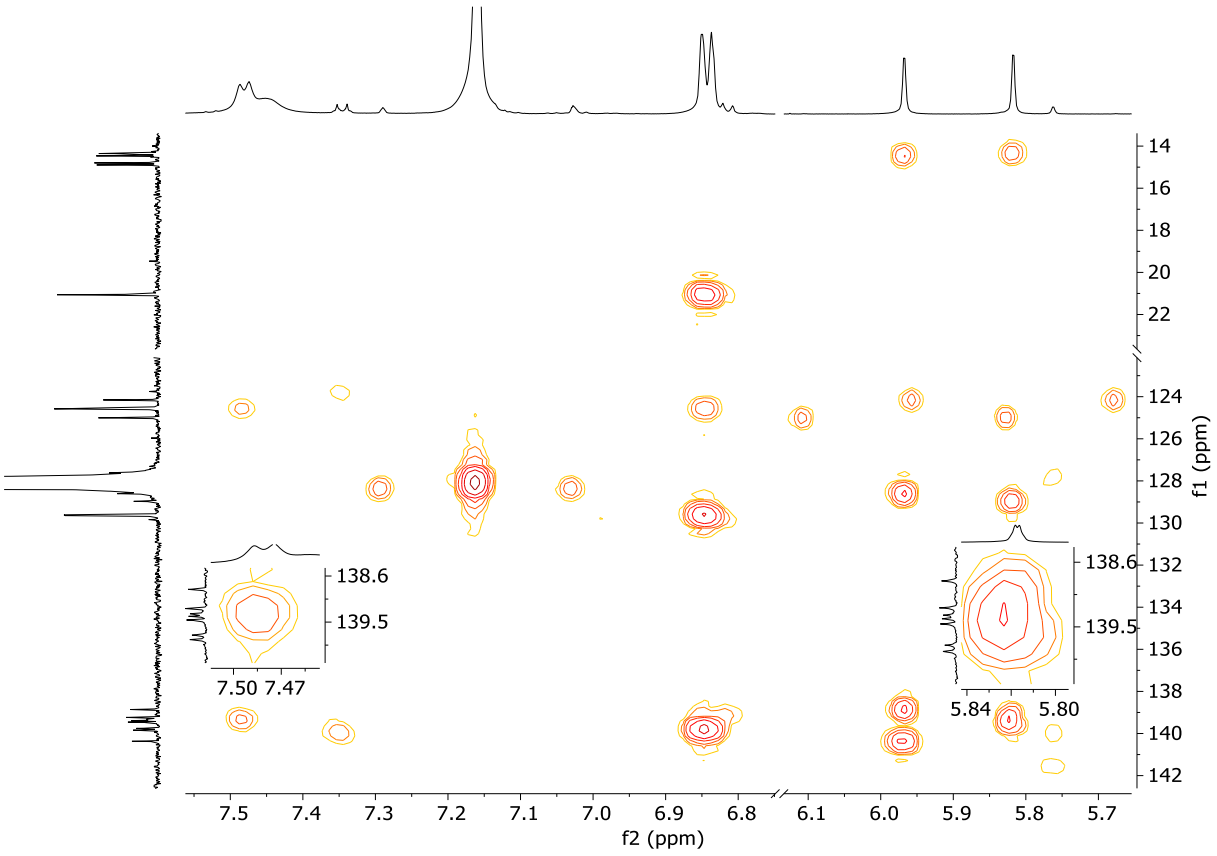

Figure S76: *HMBC aromatic area spectrum (600/150 MHz, C_6D_6) of* ***101****.*

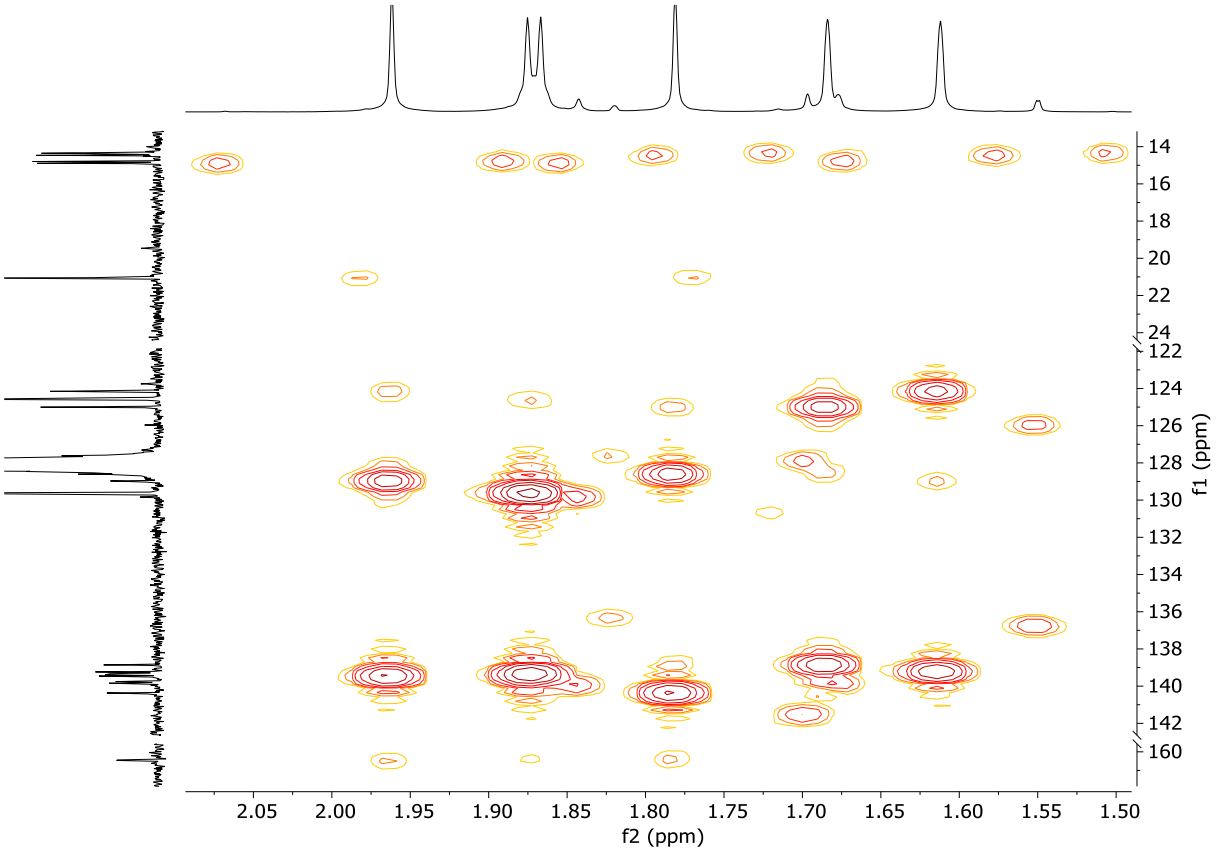

Figure S77: *HMBC aliphatic area 1 spectrum (600/150 MHz, C_6D_6) of* ***101****.*

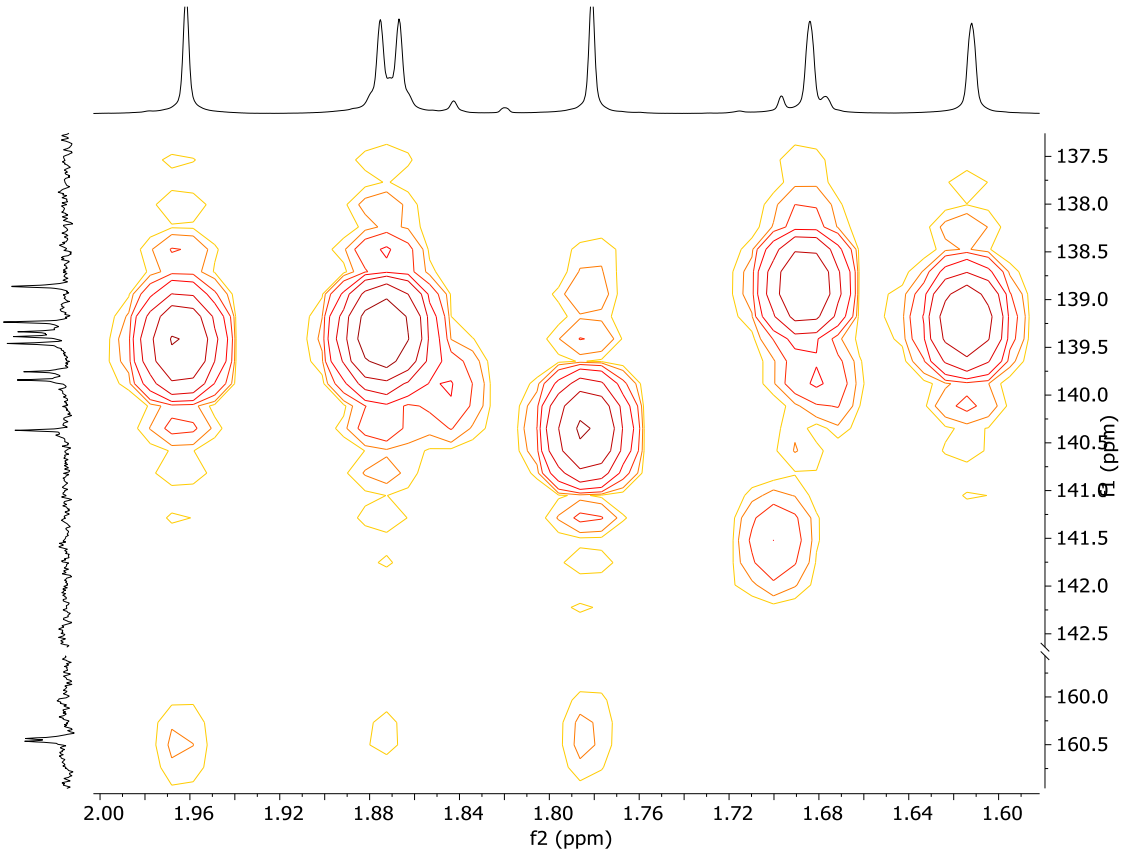

Figure S78: *HMBC aliphatic area 2 spectrum (600/150 MHz, C_6D_6) of* ***101****.*

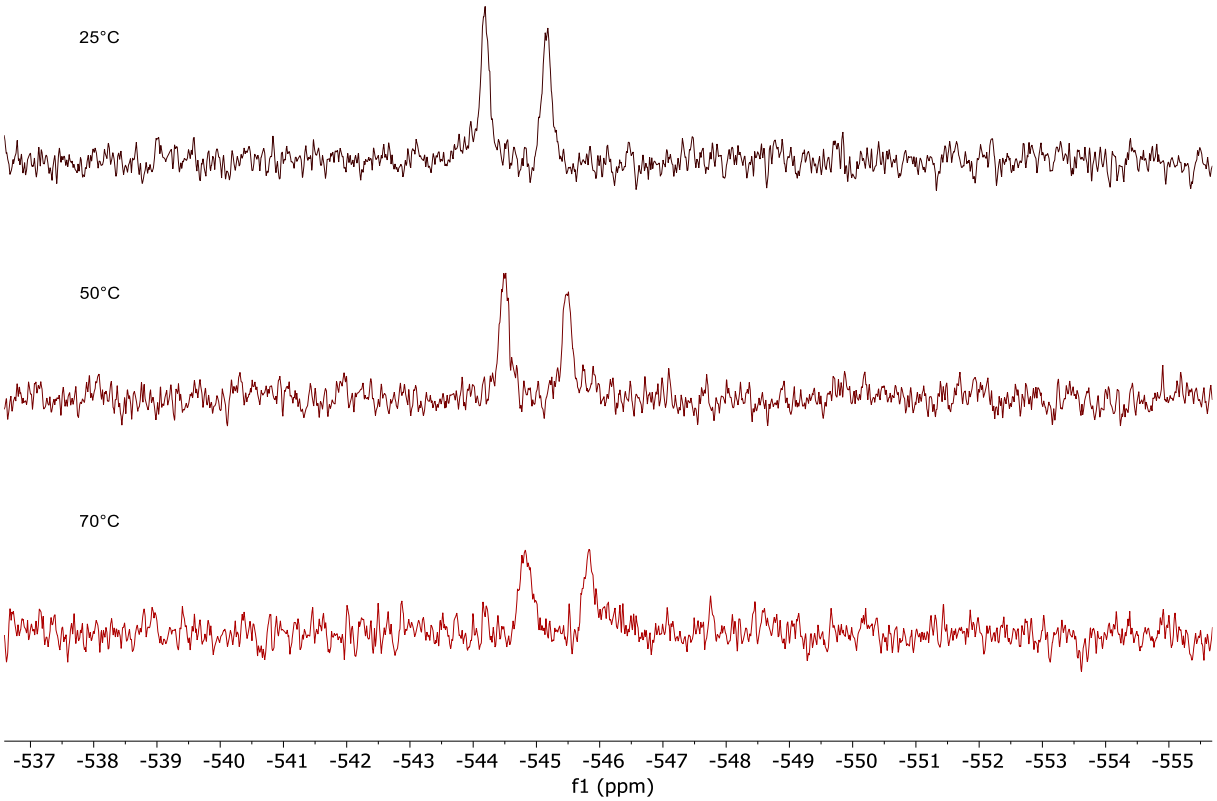

Figure S79: *^{119}Sn NMR spectrum of temperature measurement (150 MHz, C_6D_6) of* ***101****.*

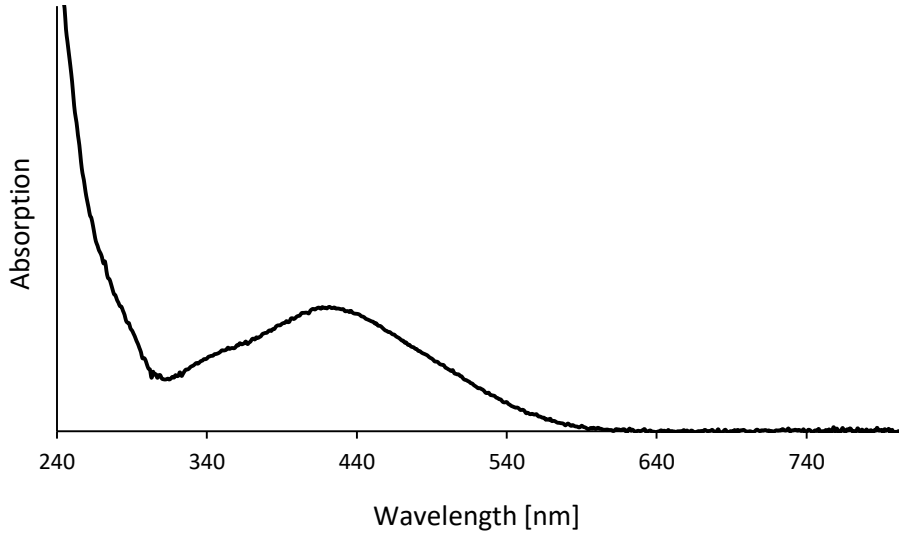

Figure S80: *UV/Vis spectrum of* ***101*** *in DCM.*

Synthesis and Characterization of (α-Diketone)$SnCl_4$ (102)

α-Diketone (0.08 g, 0.29 mmol, 1.1 eq.) was dissolved in 5 mL toluene and treated with $SnCl_4$ (30 µL, ρ = 2.23 g/cm^3, 0.26 mmol, 1.0 eq.). Instantly a dark red to black precipitate occurred. The suspension was stirred at rt for 2 h before removal of the solvent under reduced pressure and washing the crude product with small portions of *n*-hexane led to **102** as deep red to brown solid. Crystals suitable for X-ray crystallography were obtained *via* slow diffusion of *n*-hexane into a saturated solution of **102** in DCM. **Yield:** 0.13 g (0.25 mmol, 94%); **Mp:** 135-138 °C; **^{1}H NMR:** (360 MHz, CD_2Cl_2): δ 6.89-6.86 (m, 2H, c), 2.96 (s, 6H, a), 2.42-2.40 (m, 6H, b) ppm; **^{13}C{1H} NMR:** (90 MHz, CD_2Cl_2): δ 182.3 (g), 167.9 (b), 138.5 (c), 131.1 (a), 128.0 (d), 18.7 (e), 15.1 (f) ppm; **^{119}Sn NMR:** (90 MHz, CD_2Cl_2): δ -491.4 ppm; **UV/Vis** (CH_2Cl_2): λ_{max} = 271, 530 nm; $\lambda_{shoulder}$ = 314 nm.-

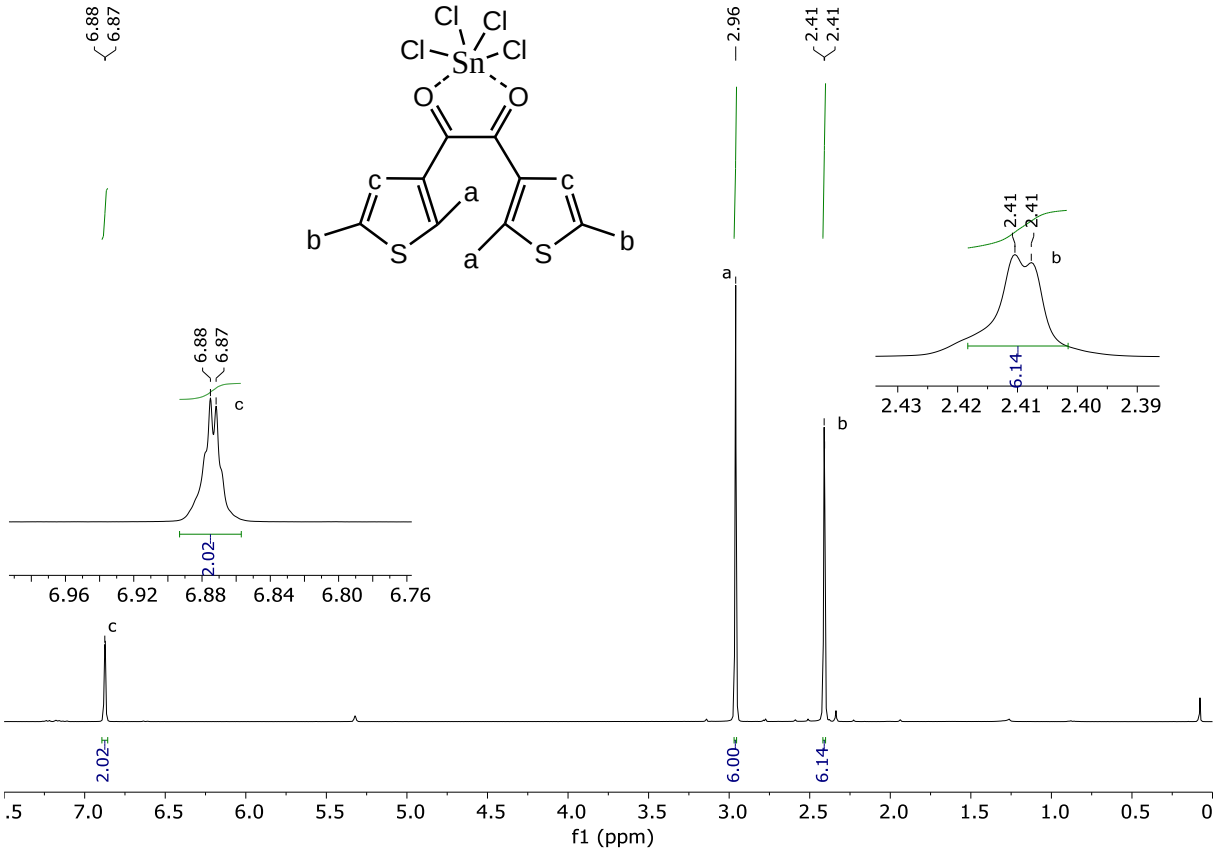

Figure S81: *^{1}H NMR spectrum (360 MHz, CD_2Cl_2) of* ***102****.*

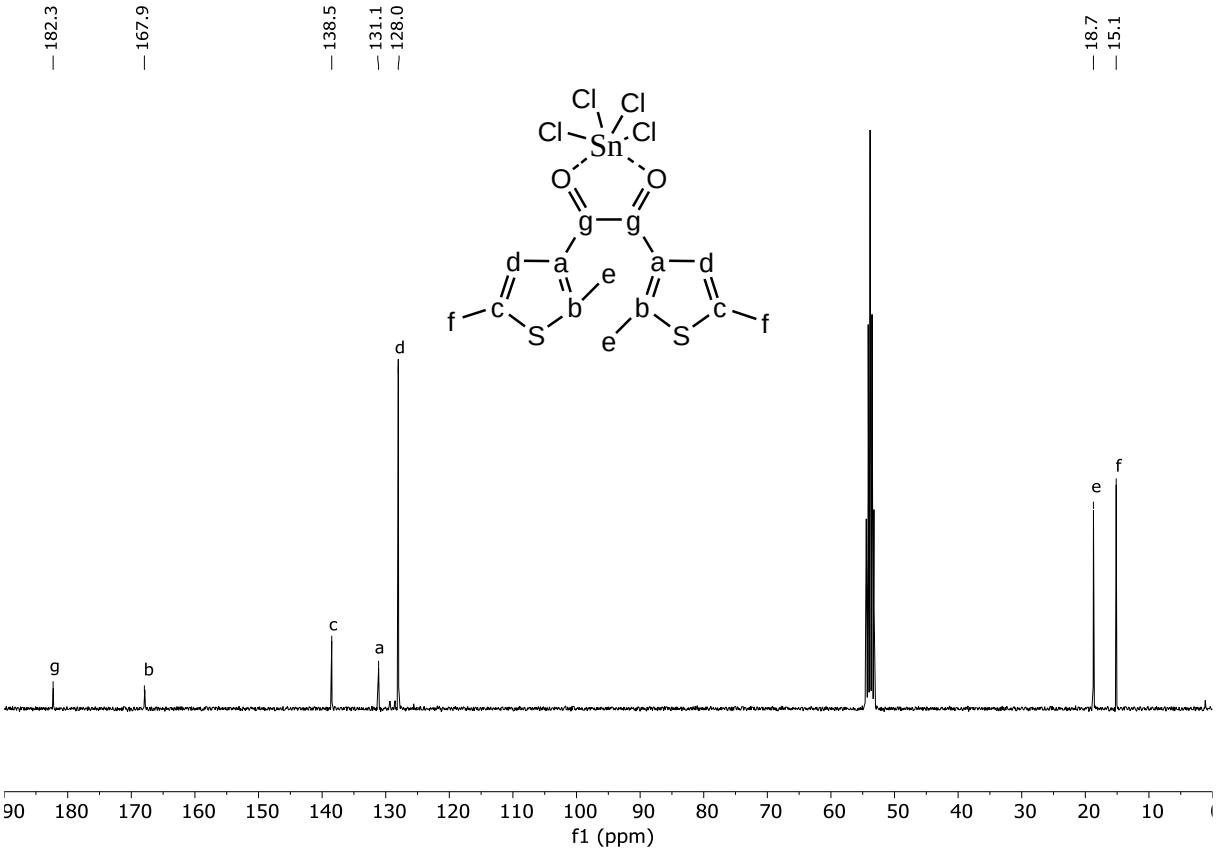

Figure S82: *$^{13}C\{^{1}H\}$ NMR spectrum (90 MHz, CD_2Cl_2) of* ***102****.*

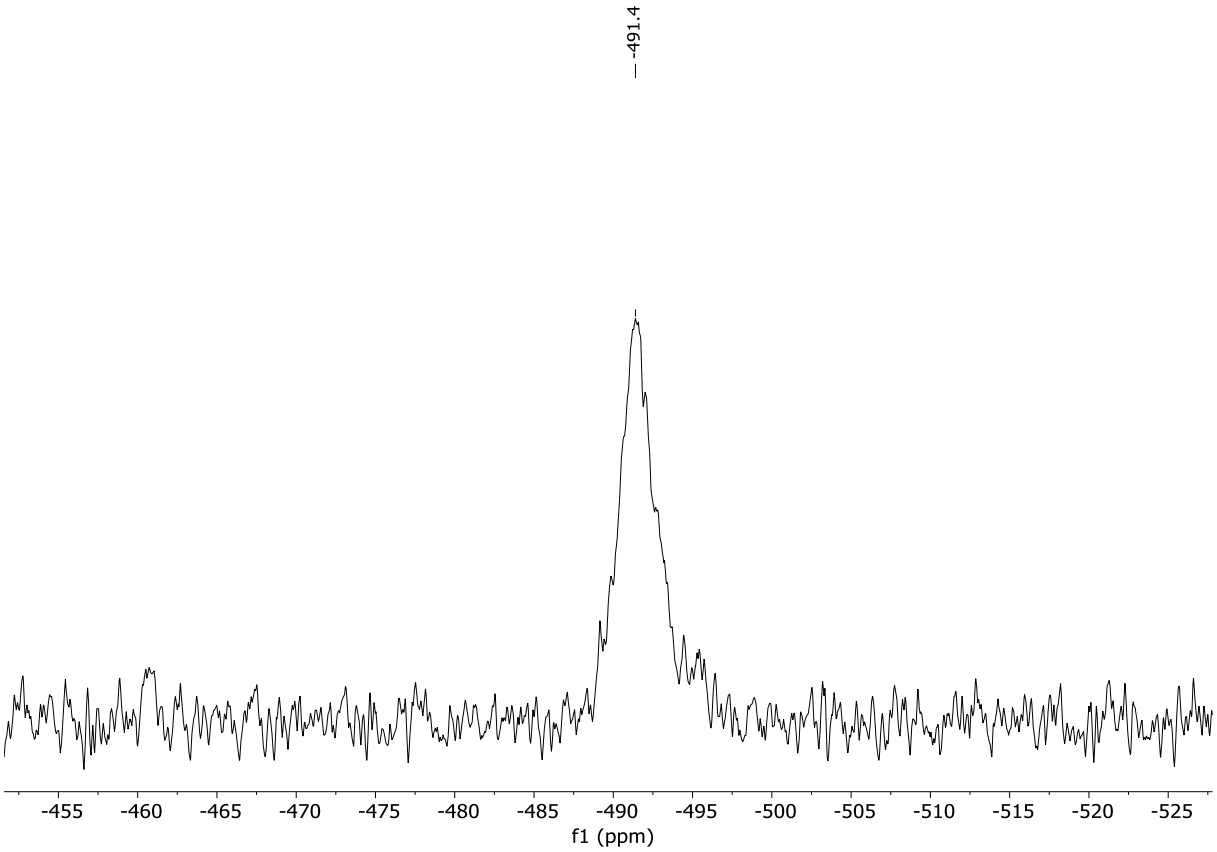

Figure S83: *^{119}Sn NMR spectrum (90 MHz, CD_2Cl_2) of* ***102****.*

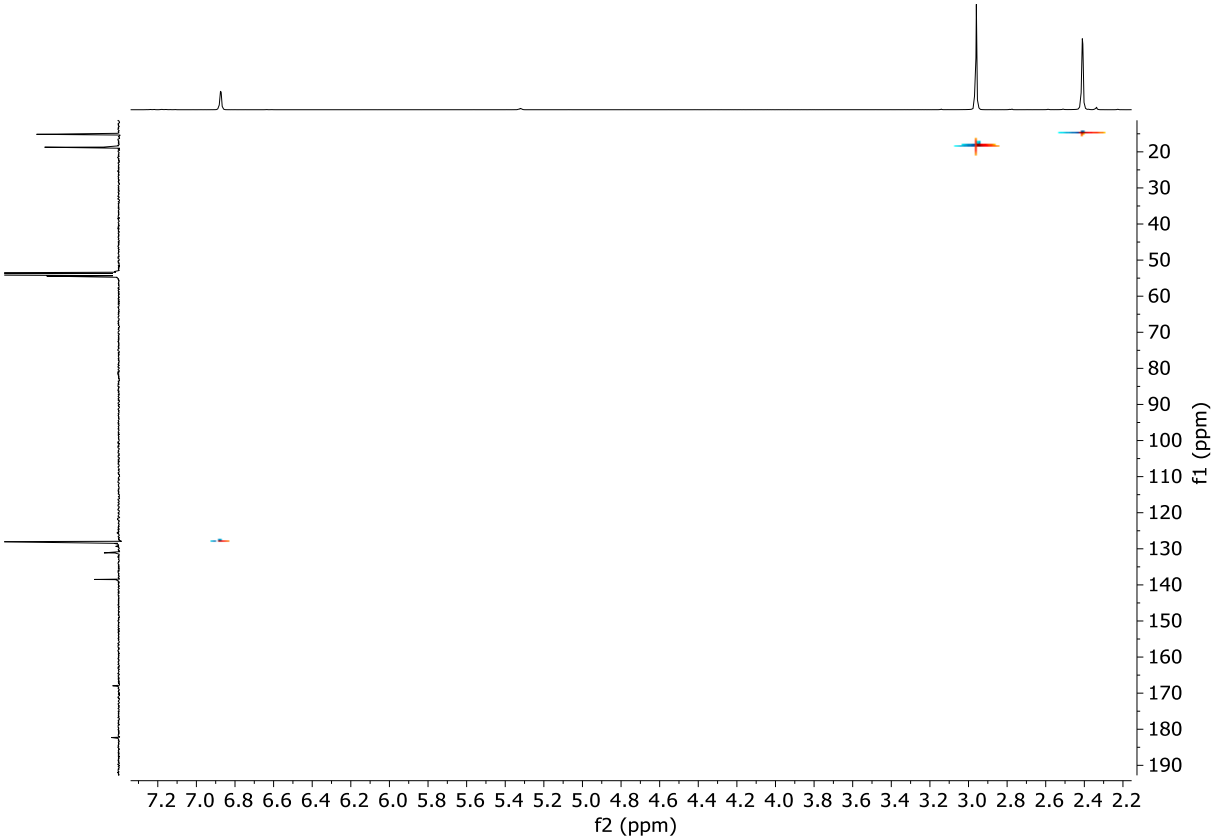

Figure S84: *HSQC spectrum (360/90 MHz, CD_2Cl_2) of* ***102****.*

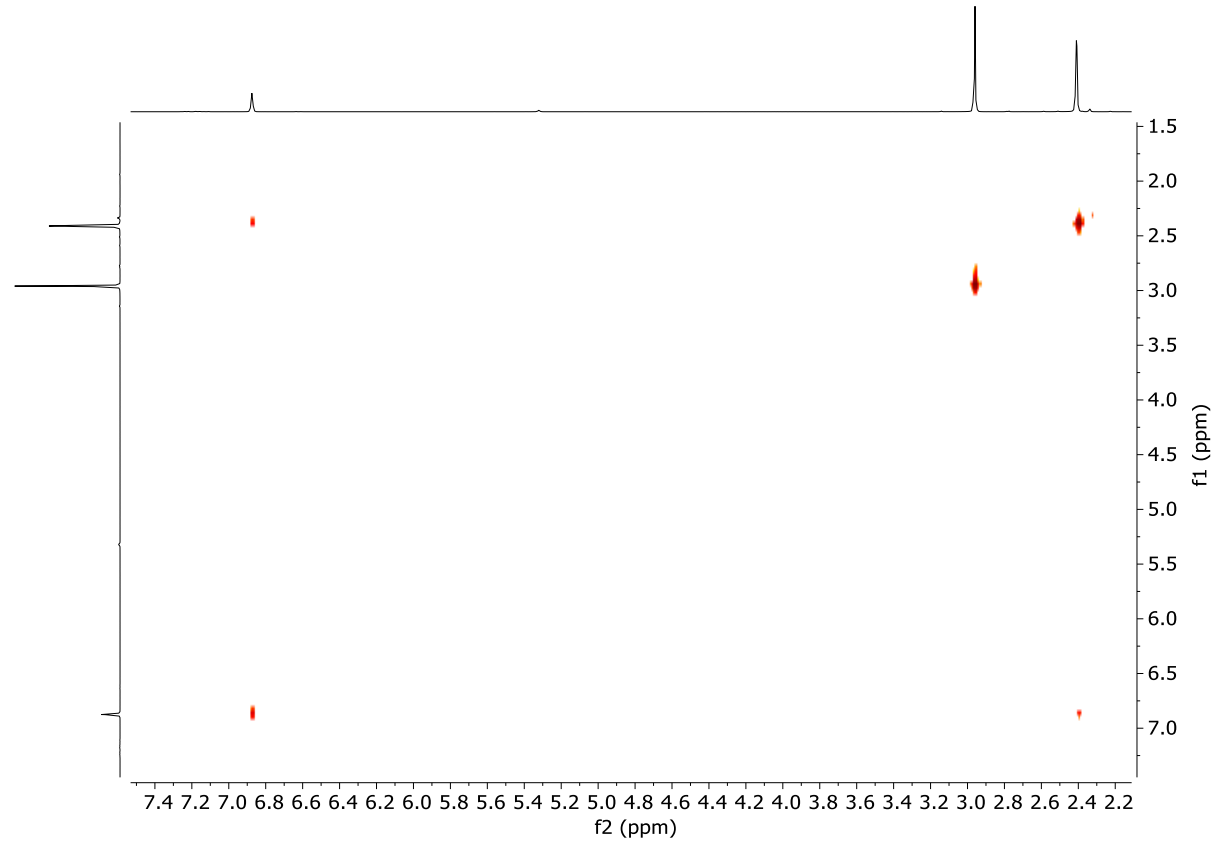

Figure S85: *H,H-COSY spectrum (360 MHz, CD_2Cl_2) of* ***102****.*

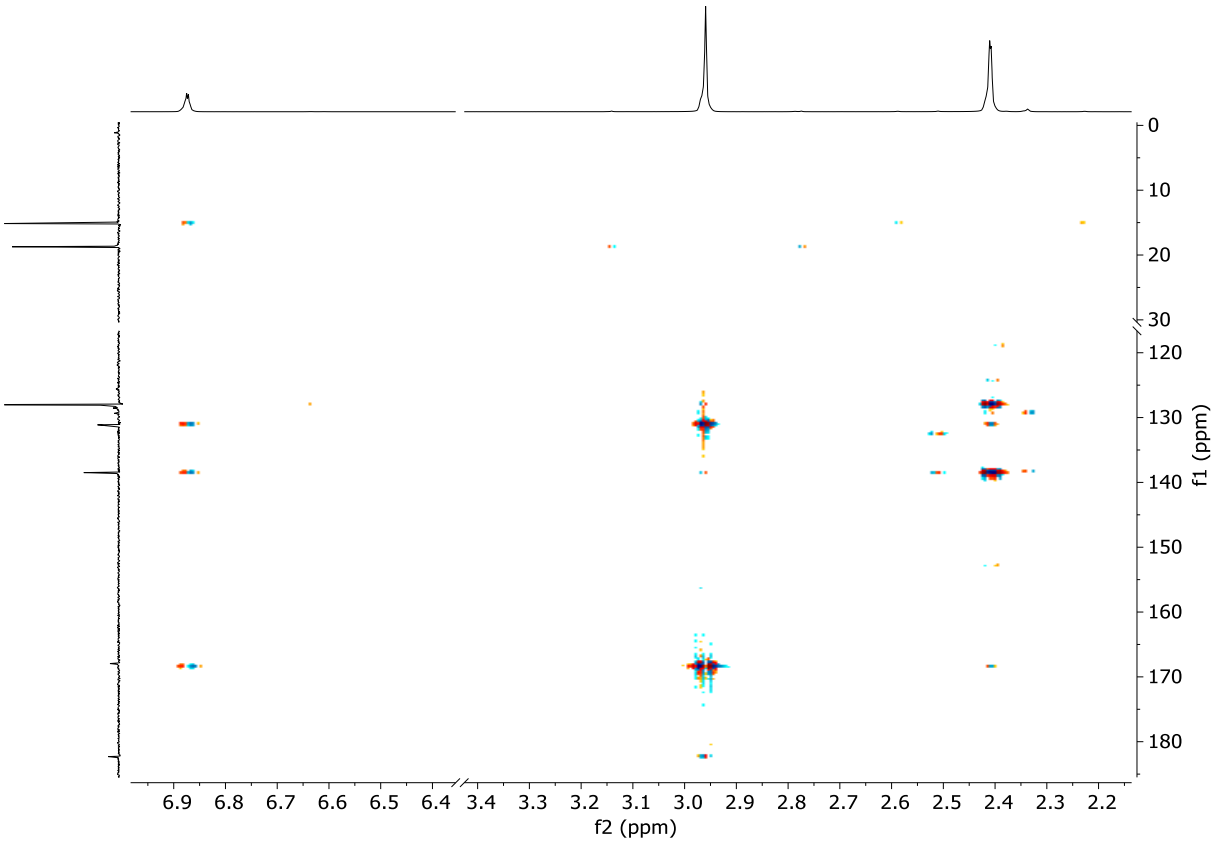

Figure S86: *HMBC spectrum (360/90 MHz, CD_2Cl_2) of* ***102****.*

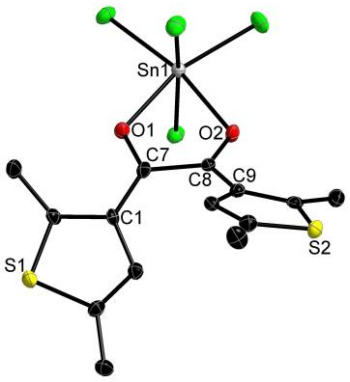

Figure S87: *X-ray crystal structure of* ***102*** *at 50% ellipsoid probability. Hydrogen atoms are omitted for clarity. Selected bond lengths [Å]: C1-C7 = 1.413(5), C7-C8 = 1.551(5), C7-O1: 1.256(4), C8-O2: 1.253(4), C8-C9 = 1.420(3), O1-Sn: 2.196(2), O2-Sn: 2.220(2).*

Table S5: *Crystal data for (α-diketone)$SnCl_4$ (**102**).*

	(α-diketone)$SnCl_4$ (**102**)
Formula	$C_{14}H_{14}Cl_4O_2S_2Sn$
Formula weight, g mol^{-1}	538.86
Crystal system	Monoclinic
Space group	$P2_1/n$
a, Å	9.5988 (4)
b, Å	11.4729 (5)
c, Å	18.0339 (8)
α, º	90
β, º	97.095 (2)
γ, º	90
V, Å^3	1970.80 (15)
Z	4
ρ_{calcd}, Mg m^{-3}	1.816
μ (Mo *Kα*), mm^{-1}	2.054
F(000)	1056
θ range, deg	2.9 – 28.3
Index ranges	$-11 \le h \le 11$
	$-14 \le k \le 14$
	$-22 \le l \le 22$
No. of reflns collected	44496
Completeness to θ_{max}	99.9%
No. indep. Reflns	4019
No. obsd reflns with($I>2\sigma(I)$)	3135
No. refined params	212
GooF (F^2)	1.022
R_1 (F) ($I > 2\sigma(I)$)	0.0300
wR_2 (F^2) (all data)	0.0688
Largest diff peak/hole, e Å^{-3}	0.666 / -0.874

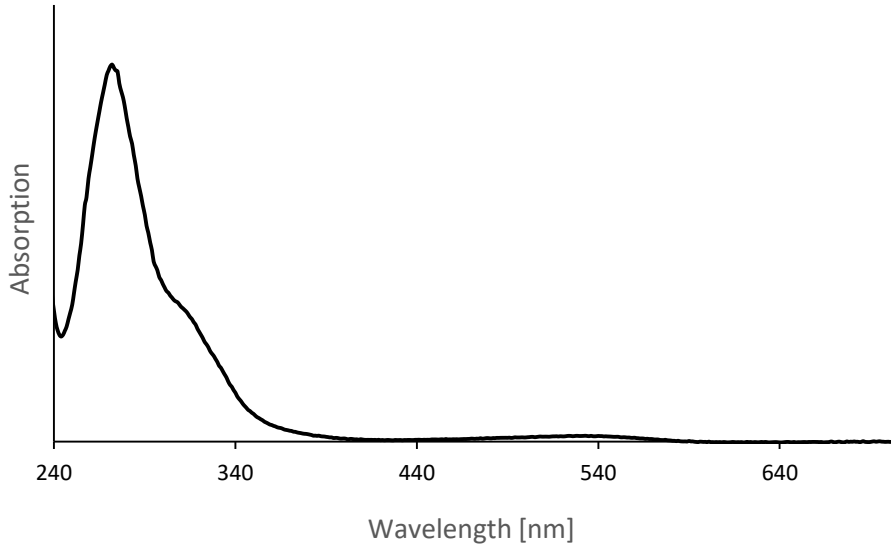

Figure S88: *UV/Vis spectrum of* ***102*** *in DCM.*

Synthesis and Characterization of (α-Diimine)Re(CO)$_3$Br (106)

α-Diimine **91** (120 mg, 0.27 mmol, 1.1 eq.) and Re(CO)$_5$Br (100 mg, 0.25 mmol, 1.0 eq.) were dissolved in 15 mL dry toluene and the resulting mixture was heated up to 100 °C for 2 h upon which a drastic color change from pale yellow to deep red occurred. Thereafter the solution was ventilated under inert conditions to remove liberated CO and stirred again for 2 h at 100 °C, then 4 h at rt. Removal of the solvent under reduced pressure and washing with small portions of *n*-hexane led to pure product **106** as deep red solid. Crystals suitable for X-ray crystallography were obtained *via* slow evaporation of the solvents of **106** dissolved in DCM/MeCN (1:2) at rt.

Yield: 190 mg (0.23 mmol; 95 %); **^{1}H NMR** (360 MHz, THF-d_8): δ 7.21 – 7.05 (m, 16H), 6.31 (s, 2H), 6.20 (s, 1H), 6.11 (s, 1H), 2.30 (s, 12H), 2.19 (s, 6H), 2.16 (s, 3H), 2.15 (s, 6H), 2.07 (s, 6H) 2.04 (s, 3H) ppm; **^{13}C{1H} NMR** (90 MHz, THF-d_8): δ 197.1, 196.7, 185.4, 185.3, 174.0, 173.9, 149.6, 149.2, 140.2, 139.5, 138.3, 138.3, 138.1, 137.9, 137.7, 132.2, 131.5, 131.2, 129.9, 129.8, 129.7, 126.6, 126.4, 126.1, 126.0, 123.0, 122.9, 122.7, 122.7, 20.9, 14.6, 14.6, 14.5, 14.4, 14.4 ppm; **UV/Vis** (THF): λ_{max} = 340 nm, 509 nm; **CV** (referenced to Fc/Fc$^+$, THF): $E_{1/2}^{red}$ = -1.29 V, E^c_p = -2.15 V, E^a_p = -1.99 V.-

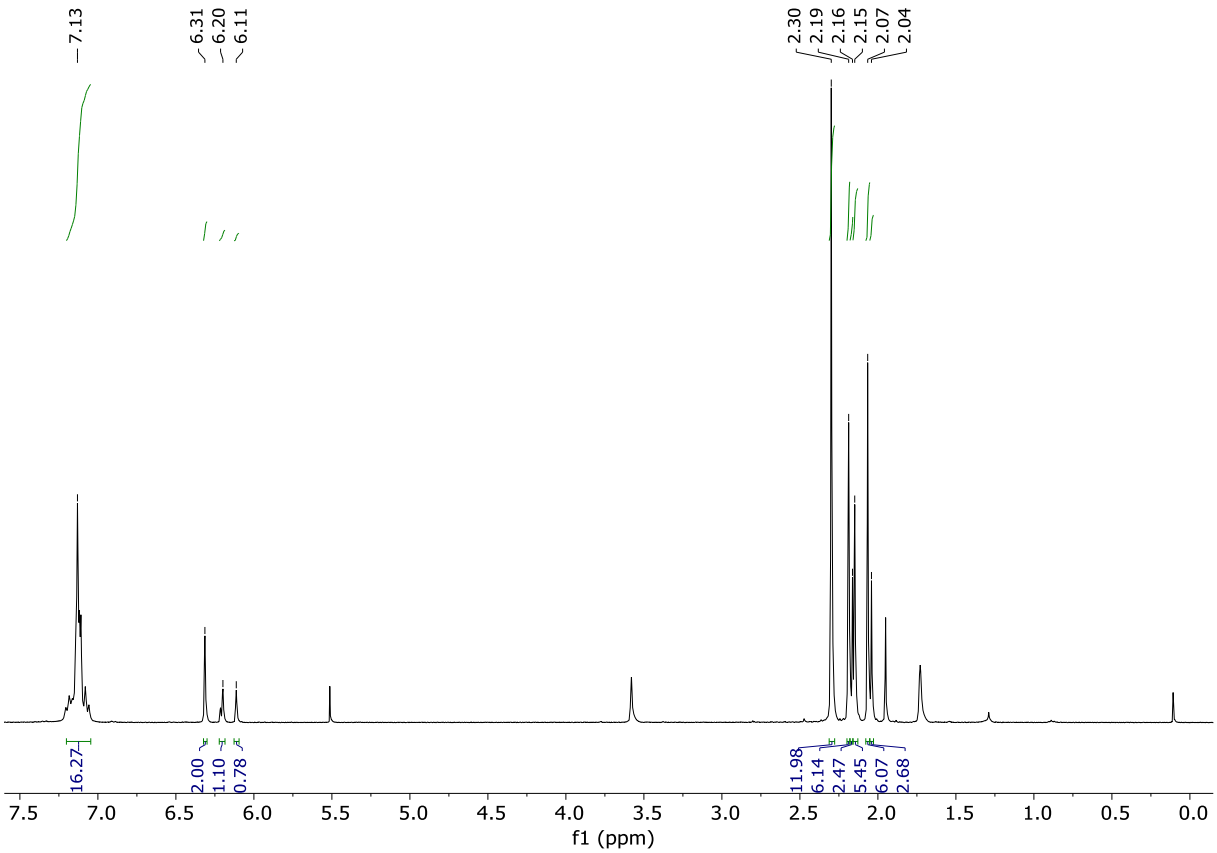

Figure S89: *^{1}H NMR spectrum (360 MHz, THF-d_8) of* ***106****.*

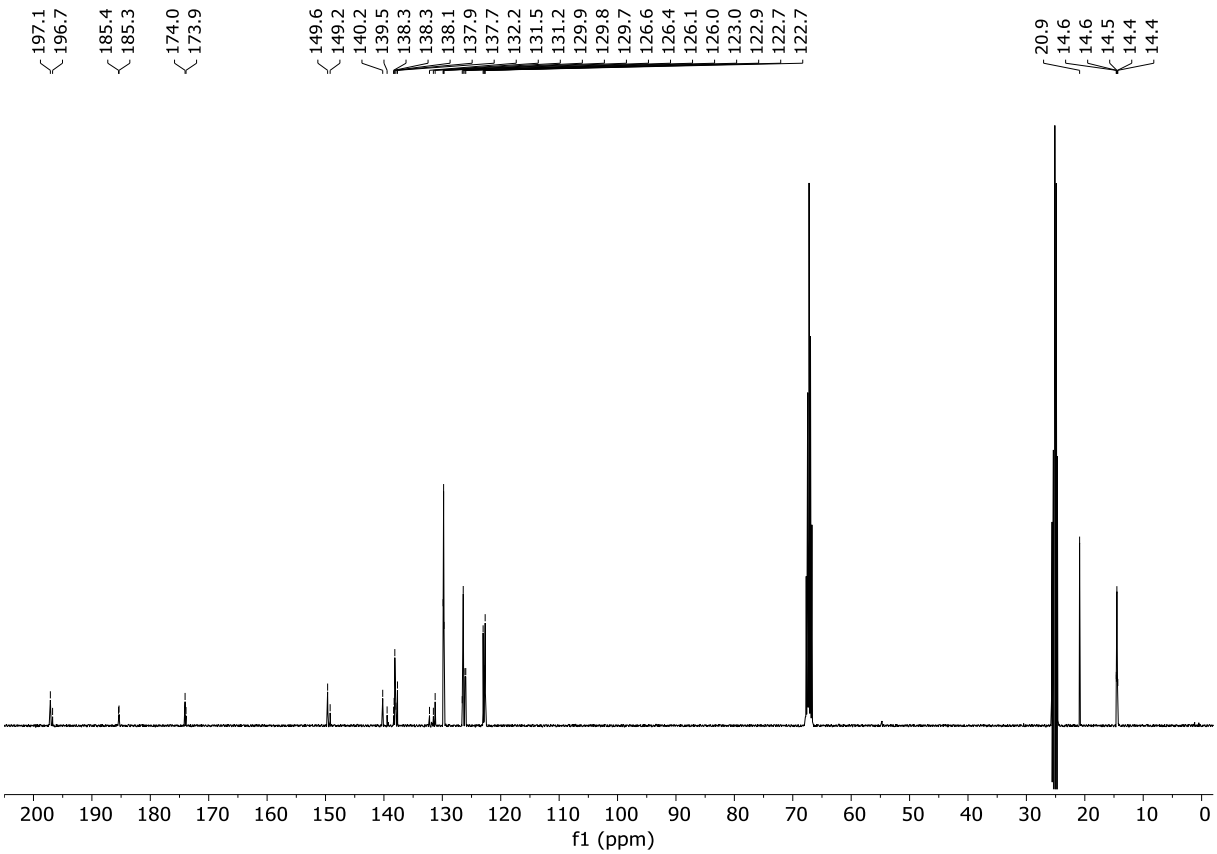

Figure S90: *$^{13}C\{^{1}H\}$ NMR spectrum (90 MHz, THF-d_8) of* ***106****.*

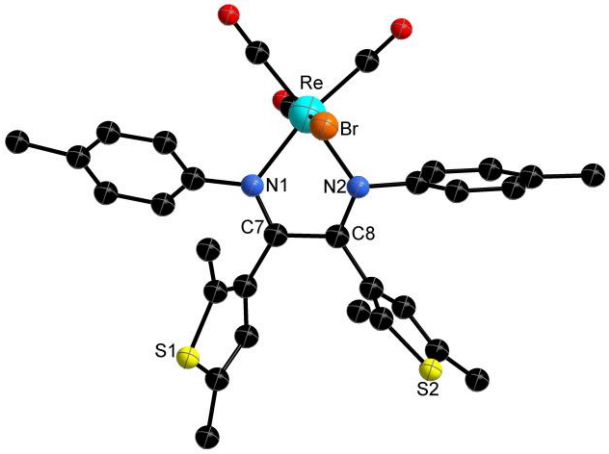

Figure S91: *X-ray crystal structure of* ***106*** *at 50% ellipsoid probability. Hydrogen atoms are omitted for clarity. Selected bond lengths [Å]: C7-C8 = 1.492(1), C7-N1: 1.314(1), N1-Re: 2.166(8), C8-N2: 1.314(1), N2-Re: 2.122(9).*

Table S6: *Crystal data for (α-diimine)Re(CO)$_3$Br (**106**).*

	(α-diimine)Re(CO)$_3$Br (**106**)
Formula	$C_{31}H_{28}BrN_2O_3ReS_2$
Formula weight, g mol^{-1}	806.78
Crystal system	Monoclinic
Space group	$P2_1/n$
a, Å	11.9162 (8)
b, Å	13.0322 (9)
c, Å	20.1562 (14)
α, °	90
β, °	96.547 (2)
γ, °	90
V, Å^3	3109.7 (4)
Z	4
ρ_{calcd}, Mg m^{-3}	1.723
μ (Mo *K*α), mm^{-1}	5.361
F(000)	1576
θ range, deg	2.33–28.28
Index ranges	$-14 \leq h \leq 14$
	$-16 \leq k \leq 15$
	$-24 \leq l \leq 24$
No. of reflns collected	78317
Completeness to θ_{max}	99.9%
No. indep. Reflns	6113
No. obsd reflns with($I>2\sigma(I)$)	5343
No. refined params	367
GooF (F^2)	1.109
R_1 (F) ($I > 2\sigma(I)$)	0.0263
wR_2 (F^2) (all data)	0.0504
Largest diff peak/hole, e Å^{-3}	1.173 / -1.570

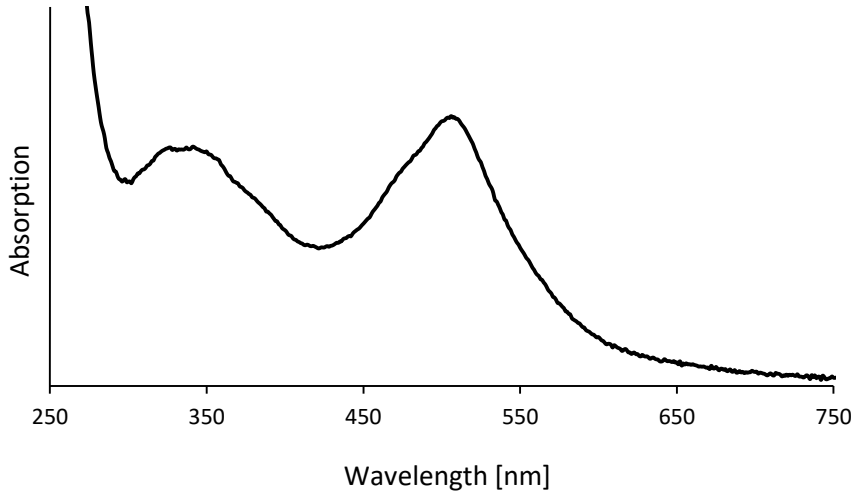

Figure S92: *UV/Vis spectrum of* ***106*** *in THF.*

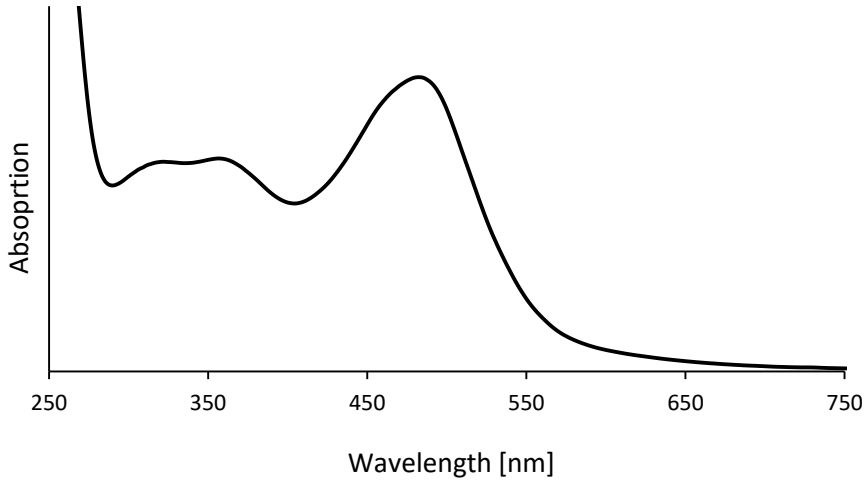

Figure S93: *UV/Vis spectrum of* ***106*** *in MeCN.*

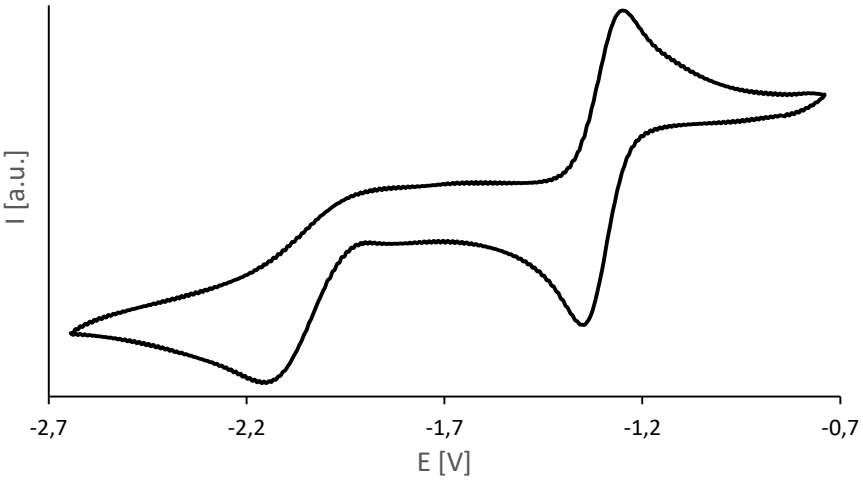

Figure S94: *CV of* ***106*** *(THF, [TBA]PF_6/0.1 M), scan rate 200 mV/s, potentials plotted vs Fc/Fc^+.*

Synthesis and Characterization of (α-Diimine)$_2$MnBr$_2$ (112)

α-Diimine ligand **91** (75 mg, 0.16 mmol, 1.1 eq.) and $Mn(CO)_5Br$ (41 mg, 0.15 mmol, 1.0 eq.) were dissolved in 5 mL dry toluene and the resulting mixture was heated up to 60 °C for 3 h. The solution changed color from yellow to green and then purple. After ventilation under inert conditions to remove liberated CO, the solution was stirred again overnight at rt, becoming brown-red in color. Removal of the solvent under reduced pressure and washing with small portions of cold *n*-hexane led to an amorphous brown crude product, which was redissolved in a small amount of dry THF. Slow diffusion of pentane into this solution led to crystallization of **112**. Crystals suitable for X-ray crystallography were received using the same method.

Yield: 57 mg (0.05 mmol, 34 % total, 68 % adjusted); **HRMS** (ESI) *m/z*: $[M\text{-}Br]^+$ calculated for $C_{56}H_{56}BrMnN_4S_4^+$, 1046.19462, found 1046.19385.

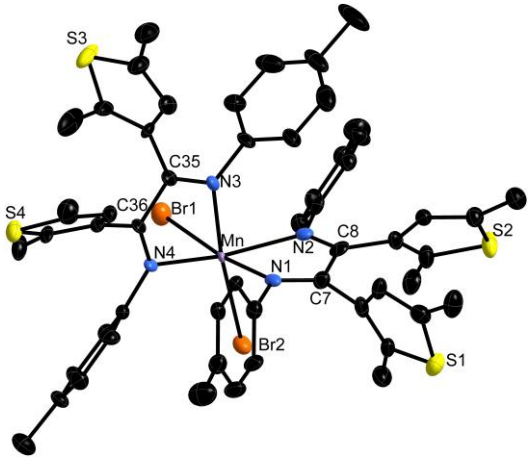

Figure S95: *X-ray crystal structure of **112**; 50% ellipsoid probability, hydrogen atoms are omitted for clarity. Selected bond lengths [Å]: C7-C8 = 1.513(1), C7-N1: 1.290(9), N1-Mn: 2.320(6), C8-N2: 1.280(9), N2-Mn: 2.290(6), C35-C36 = 1.502(10), C35-N3: 1.282(9), N3-Mn: 2.316(7), C36-N4: 1.285(9), N4-Mn: 2.293(6), Mn-Br1: 2.582(2), Mn-Br2: 2.592(1).*

Table S7: *Crystal data for (α-diimine)$_2$MnBr$_2$ (**112**).*

	(α-diimine)$_2$MnBr$_2$ (**112**)
Formula	$C_{56}H_{56}Br_2MnN_4S_4$
Formula weight, g mol^{-1}	1128.08
Crystal system	Triclinic
Space group	$P\bar{1}$
a, Å	14.9331 (10)
b, Å	23.7142 (17)
c, Å	24.6143 (17)
α, °	102.669 (2)
β, °	92.551 (2)
γ, °	103.648 (2)
V, Å^3	8221.5 (10)
Z	16
ρ_{calcd}, Mg m^{-3}	1.511
μ (Mo *Kα*), mm^{-1}	1.018
F(000)	3811
θ range, deg	2.52–20.59
Index ranges	$-20 \le h \le 20$
	$-31 \le k \le 31$
	$-33 \le l \le 33$
No. of reflns collected	431587
Completeness to θ_{max}	98.5%
No. indep. Reflns	42070
No. obsd reflns with($I>2\sigma(I)$)	14016
No. refined params	1846
GooF (F^2)	0.996
R_1 (F) ($I > 2\sigma(I)$)	0.1052
wR_2 (F^2) (all data)	0.2101
Largest diff peak/hole, e Å^{-3}	1.193 / -1.013

Synthesis and Characterization of [(α-Diimine)$_2$CuCl]$^+$·[CuCl$_2$]$^-$ (113)

α-Diimine ligand **91** (100 mg, 0.22 mmol, 1.1 eq.) was dissolved in 10 mL dry toluene and treated with CuCl (20 mg, 0.20 mmol, 1.0 eq.). The resulting mixture was heated up to 60 °C for 5 h, upon which a dark green solution formed. Removal of the solvent under reduced pressure and washing of the crude product with small portions of cold *n*-hexane led to pure product **113** as dark green powder. Crystals suitable for X-ray crystallography were received *via* slow diffusion of pentane into a saturated solution of **113** in THF.

Yield: 107 mg (0.19 mmol, 95 %); **UV/Vis** (toluene): λ_{max} = 369 nm, 616 nm, 762 nm; **HRMS** (ESI) *m/z*: $[M]^+$ calculated for $C_{56}H_{56}CuN_4S_4^+$, 975.26783, found 975.26645.

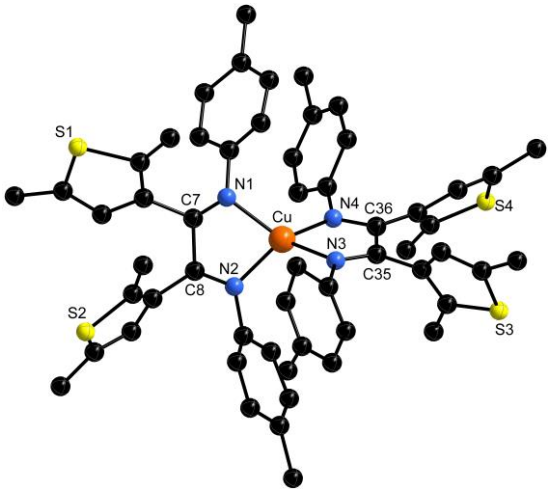

Figure S96: *X-ray crystal structure of **113** shown without $CuCl_2^-$. Due to insufficient data collection in search for crystal structures of other compositions only an image is given here.*

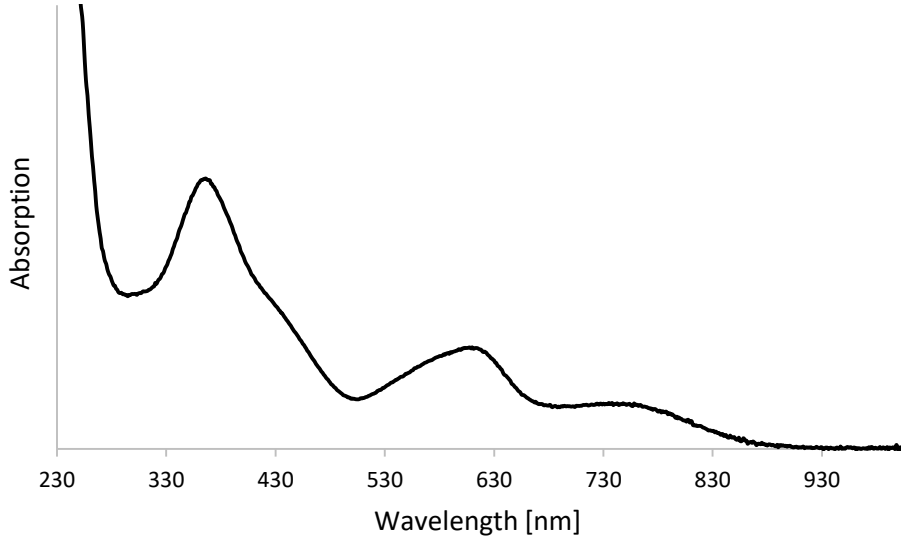

Figure S97: *UV/Vis spectrum of **113** in THF.*

Synthesis and Characterization of (Endiolato)Ga-FLP Adduct (114)

Over the course of the synthesis procedure exposure to light was reduced to a minimum by wrapping aluminium foil around the reaction vessel.

α-Diketone ligand **90** (105 mg, 0.38 mmol, 1.05 eq.) was dissolved in 15 mL dry pentane and treated with Ga-FLP (200 mg, 0.36 mmol, 1.0 eq.). The solution instantly turned red and an ocher precipitate formed. After stirring overnight the precipitate was filtered off and washed with small portions of cold pentane to afford **114** as ocher powder. Crystals suitable for X-ray crystallography were received *via* slow diffusion of *n*-hexane into a saturated solution of **114** in DCM. Compound **114** should be stored in darkness due to occurring photoreaction.

Yield: 273 mg (0.33 mmol, 91 %); **^{1}H NMR** (600 MHz, C_6D_6): δ 7.78 (d, $^{3}J_{HP}$ = 47.3 Hz, 1H, PC=CH), 7.54 (d, $^{3}J_{HH}$ = 7.4 Hz, 2H, *o*-HPh), 7.12 (t, $^{3}J_{HH}$ = 7.7 Hz, 2H, *m*-HPh), 7.06 (s, 1H, thienyl-H), 7.01 (t, $^{3}J_{HH}$ = 7.4 Hz, 1H, *p*-HPh), 6.50 (br. s, 4H, *m*-HMes), 6.36 (br. s, 1H, thienyl-H), 2.84 (br. s, 12H, *o*-CH_3), 2.20 (br. s, 3H, thienyl-CH_3), 2.16 (s, 3H, thienyl-CH_3), 1.95 (s, 3H, thienyl-CH_3), 1.91 (s, 6H, *p*-CH_3), 1.61 (br. s, 18H, Ga^{t}Bu$_2$), 1.33 (s, 3H, thienyl-CH_3) ppm; **^{13}C{1H} NMR** (150 MHz, C_6D_6): δ 158.7 (d, $^{2}J_{CP}$ = 8.5 Hz, PC=*C*H), 155.4 (d, $^{1}J_{CP}$ = 11.5 Hz, P*C*=CH), 149.4 (d, $^{3}J_{CP}$ = 3.1 Hz, =C-O), 142.1 /142.0 (br s., *o*-CMes) / (br. s, *p*-CMes), 139.9 (d, $^{3}J_{CP}$ = 40.4 Hz, ipso-CPh), 137.1 (s, ipso-thienyl), 135.6 (s, thienyl-*C*-Me), 135.2 (br s., ipso-thienyl), 133.6 (br. s, thienyl-*C*-Me), 133.0 (d, $^{2}J_{CP}$ = 4.6 Hz, =C-O), 130.9 (br. s, *m*-CMes), 129.9 (s, *p*-CPh), 128.9 (s, *m*-CPh), 128.9 (s, *o*-CPh), 127.7 (s, thienyl-C-H), 127.6 (s, thienyl-*C*-Me), 126.5 (s, thienyl-C-H), 33.7 (Ga(C*Me*$_3$)$_2$), 25.5 (br. s, *o*-CH_3), 22.7 (s, Ga(*C*Me$_3$)$_2$) 20.8 (*p*-CH_3), 15.4 (s, thienyl-Me), 14.9, (s, thienyl-Me), 14.3 (s, thienyl-Me), 13.9 (s, thienyl-Me) ppm. Second thienyl-*C*-Me and ipso-CMes was not observed; **^{31}P{1H} NMR** (240 MHz, C_6D_6): δ = 84.5 (s); **HRMS** (ESI) *m/z*: $[M+H]^+$ calculated for $C_{48}H_{61}GaO_2PS_2^+$, 833.31008, found 833.30963; $[M+Na]^+$ calculated for $C_{48}H_{60}GaNaO_2PS_2^+$, 855.29203, found 855.29150.-

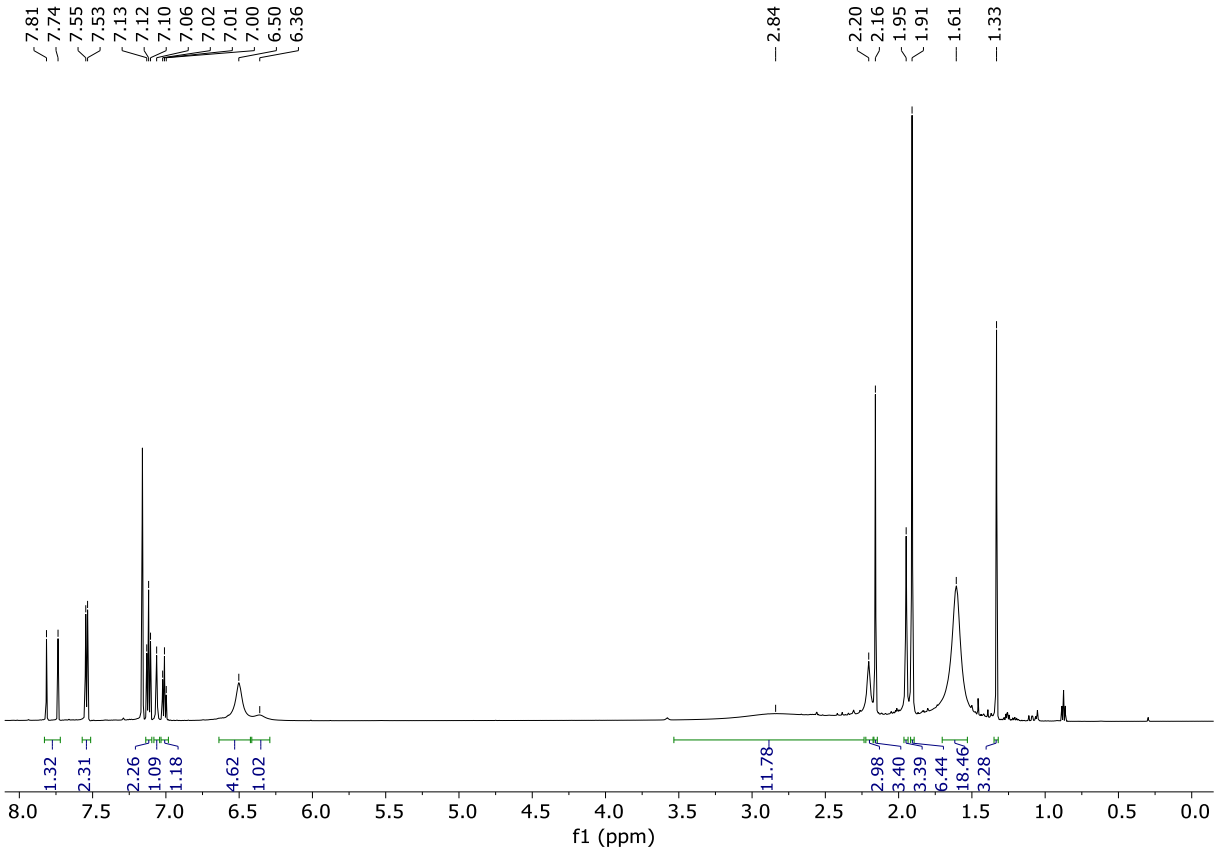

Figure S98: *^{1}H NMR spectrum (600 MHz, C_6D_6) of* ***114****.*

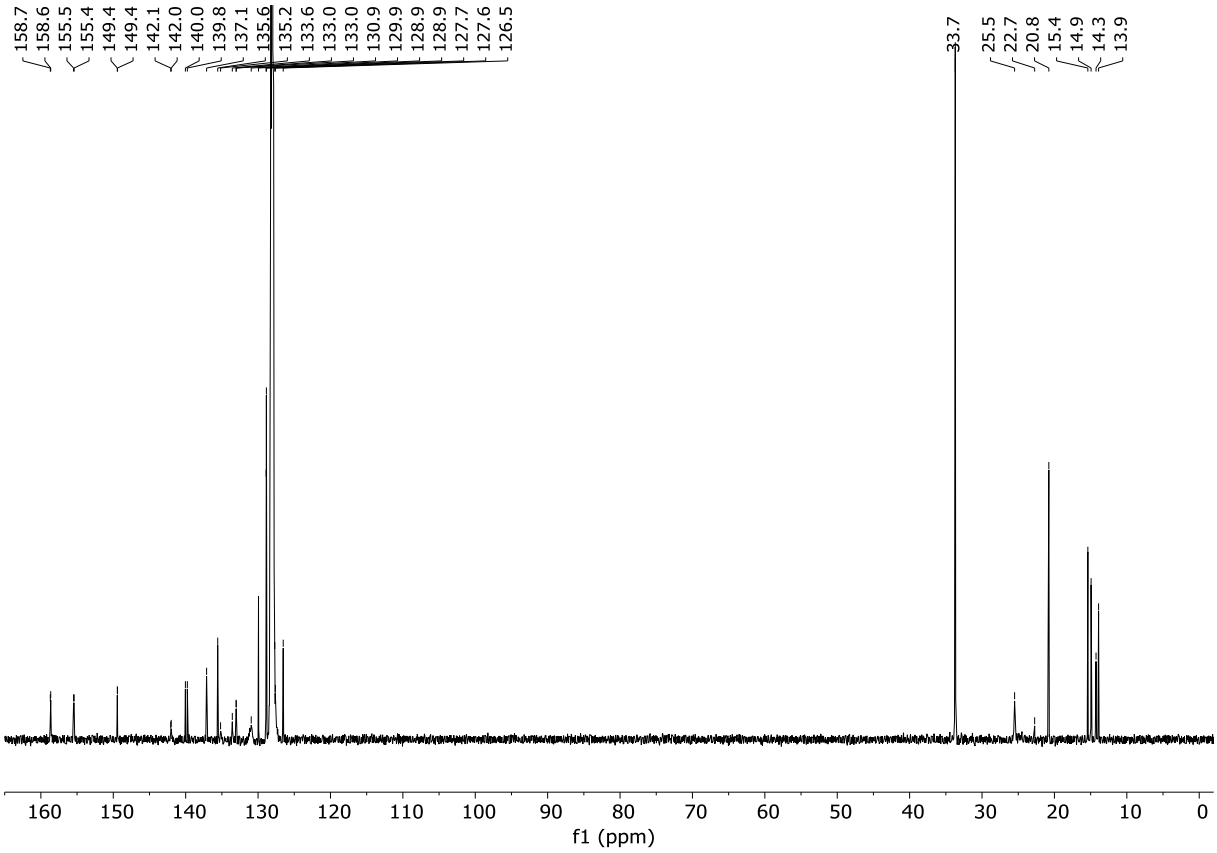

Figure S99: *$^{13}C\{^{1}H\}$ NMR spectrum (150 MHz, C_6D_6) of* ***114****.*

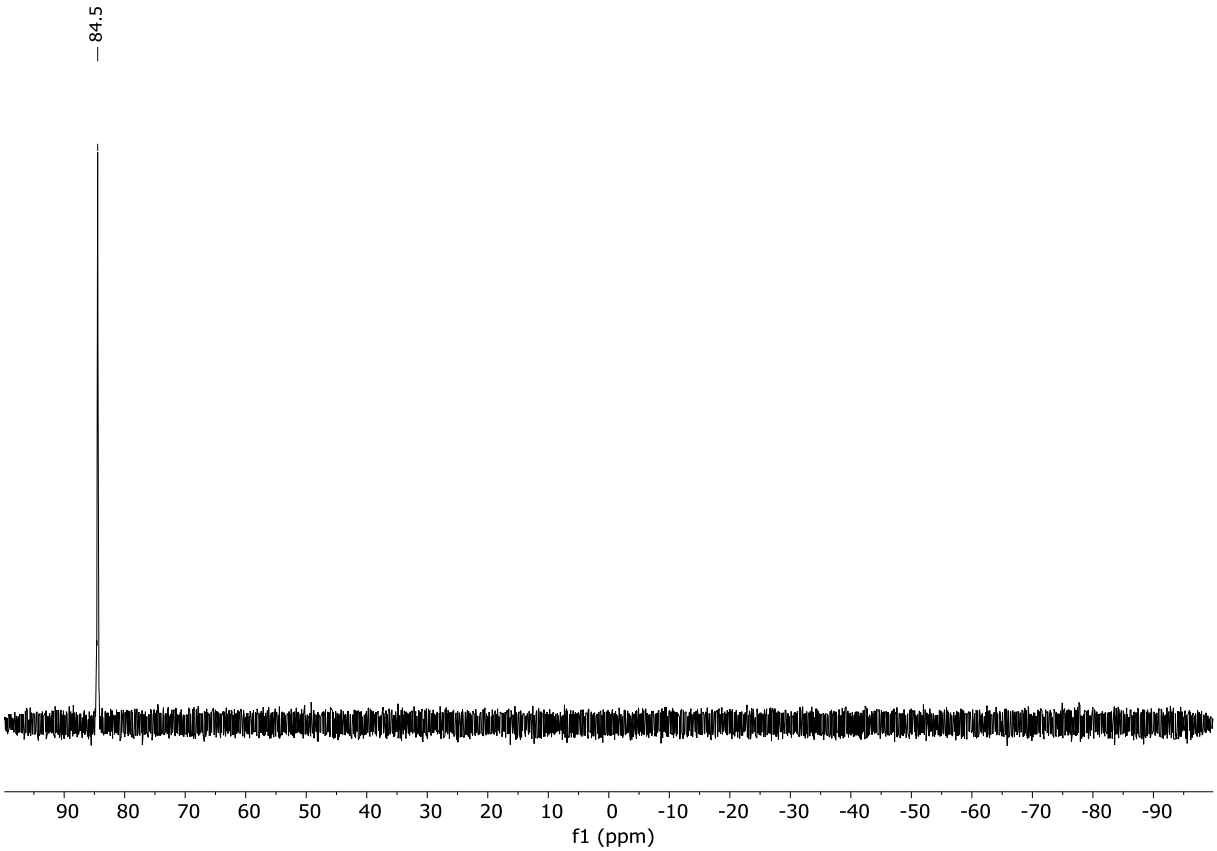

Figure S100: *$^{31}P\{^{1}H\}$ NMR spectrum (240 MHz, C_6D_6) of* ***114****.*

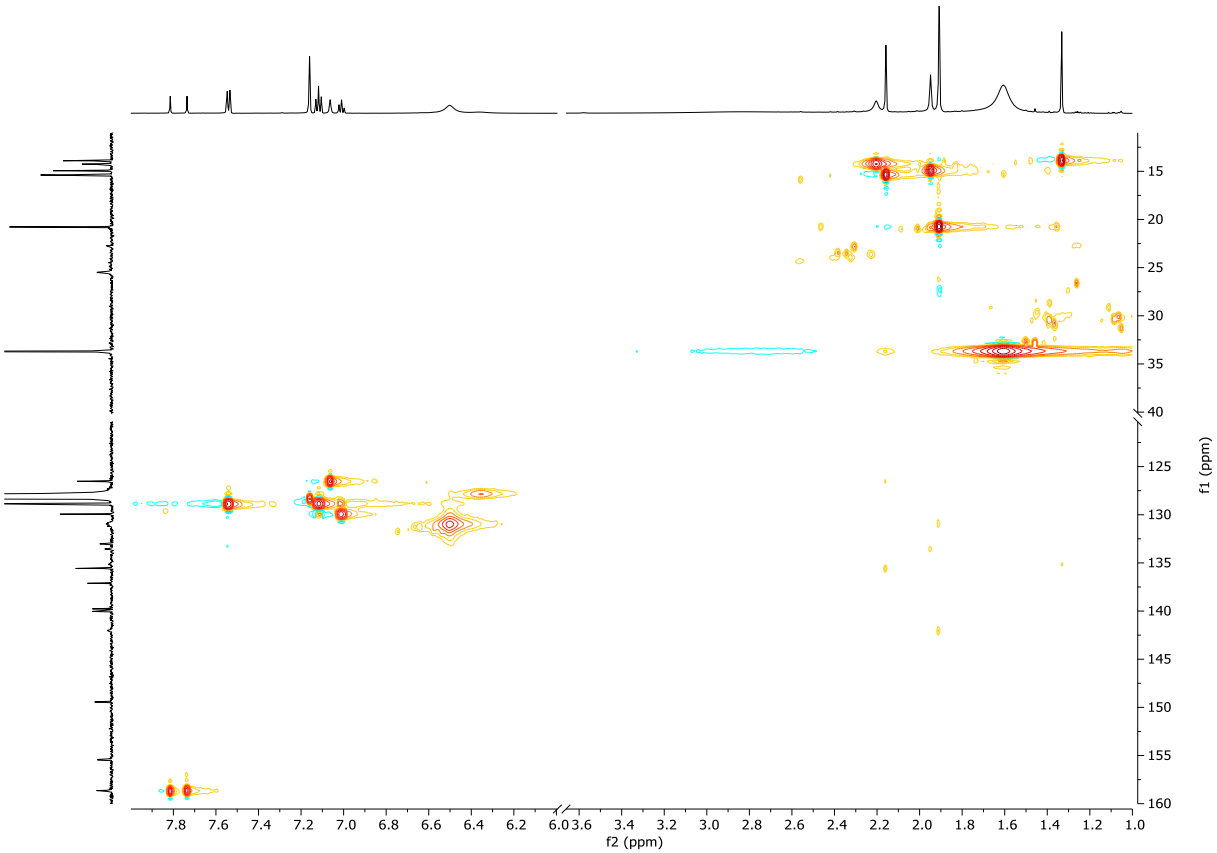

Figure S101: *HSQC spectrum (600/150 MHz, C_6D_6) of* ***114****.*

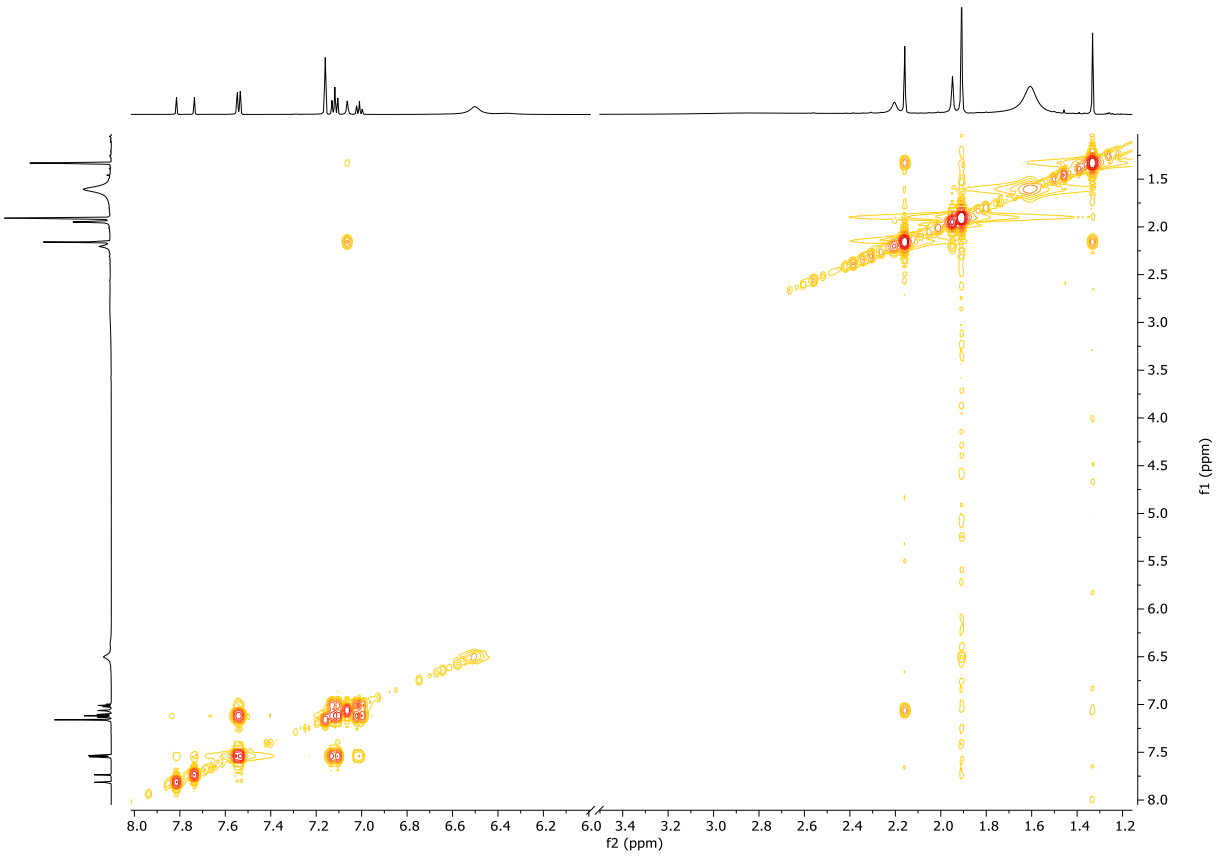

Figure S102: *H,H-COSY spectrum (600 MHz, C_6D_6) of* ***114****.*

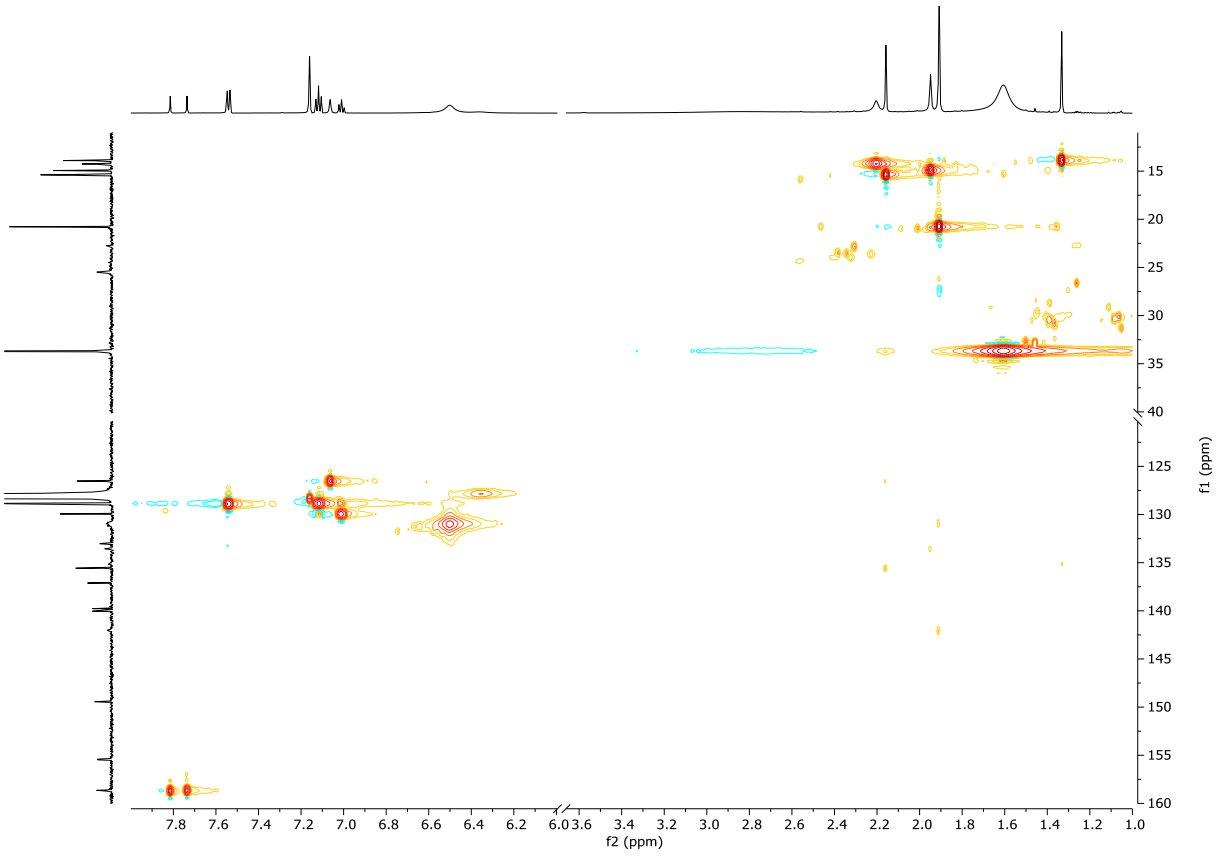

Figure S103: *HMBC spectrum (600/150 MHz, C_6D_6) of* ***114****.*

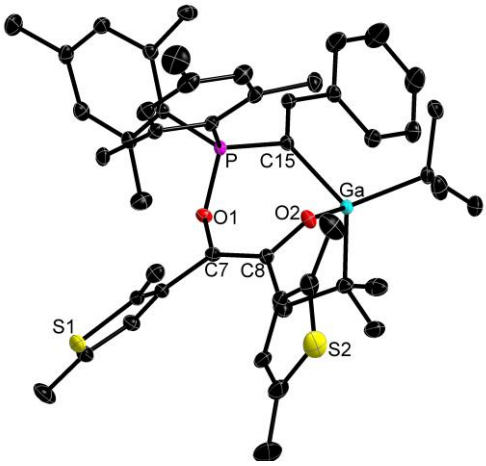

Figure S104: *X-ray crystal structure of* ***114*** *at 50% ellipsoid probability. Hydrogen atoms are omitted for clarity. Selected bond lengths [Å]: C7-C8 = 1.3535(1), C7-O1: 1.4340(1), O1-P: 1.5944(1), C8-O2: 1.3314(1), O2-Ga: 1.9414(1).*

Table S8: *Crystal data for (endiolato)Ga-FLP adduct (**114**).*

	(endiolato)Ga-FLP adduct (**114**)
Formula	$C_{48}H_{60}GaO_2PS_2$
Formula weight, g mol^{-1}	833.77
Crystal system	Triclinic
Space group	$P\bar{1}$
a, Å	11.6485 (5)
b, Å	11.9783 (5)
c, Å	18.2123 (8)
α, °	93.4620 (10)
β, °	98.2760 (10)
γ, °	108.4870 (10)
V, Å^3	2369.65 (18)
Z	2
ρ_{calcd}, Mg m^{-3}	1.169
μ (Mo *Kα*), mm^{-1}	0.71073
F(000)	884
θ range, deg	2.352–33.126
Index ranges	$-17 \leq h \leq 17$
	$-18 \leq k \leq 18$
	$-28 \leq l \leq 28$
No. of reflns collected	167592
Completeness to θ_{max}	99.4%
No. indep. Reflns	18137
No. obsd reflns with($I>2\sigma(I)$)	15943
No. refined params	503
GooF (F^2)	1.036
R_1 (F) ($I > 2\sigma(I)$)	0.0326
wR_2 (F^2) (all data)	0.0890
Largest diff peak/hole, e Å^{-3}	0.599 / -0.453

Synthesis and Characterization of (Endiolato)Al-FLP Adduct (115)

Over the course of the synthesis procedure exposure to light was reduced to a minimum by wrapping aluminium foil around the reaction vessel.

α-Diketone ligand **90** (114 mg, 0.41 mmol, 1.05 eq.) was dissolved in 15 mL dry pentane and treated with Al-FLP (200 mg, 0.39 mmol, 1.0 eq.). The solution instantly turned purple and an ocher precipitate formed. After stirring overnight the precipitate was filtered off and washed with small portions of cold pentane to afford **115** as ocher powder. Crystals suitable for X-ray crystallography were received *via* slow diffusion of *n*-hexane into a saturated solution of **115** in DCM. Compound **115** should be stored in darkness due to occurring photoreaction.

Yield: 262 mg (0.33 mmol, 85 %); **^{1}H NMR** (600 MHz, C_6D_6): δ 7.74 (d, $^3J_{HP}$ = 51.5 Hz, 1H, PC=CH), 7.66 (d, $^3J_{HH}$ = 7.4 Hz, 2H, *o*-HPh), 7.16 (overlapping with d_6-benzene t, $^3J_{HH}$ = 7.4 Hz, 2H, *m*-HPh), 7.03 (t, $^3J_{HH}$ = 7.4 Hz, 1H, *p*-HPh), 7.00 (s, 1H, thienyl-H), 6.48 (br. s, 4H, *m*-HMes), 6.34 (br. s, 1H, thienyl-H), 2.71 (br. s, 12H, *o*-CH_3), 2.17 (br. s, 3H, thienyl-CH_3), 2.12 (s, 3H, thienyl-CH_3), 1.95 (s, 3H, thienyl-CH_3), 1.89 (s, 6H, *p*-CH_3), 1.57 (br. s, 18H, Ga^{t}Bu$_2$), 1.25 (s, 3H, thienyl-CH_3) ppm; **^{13}C{1H} NMR** (150 MHz, C_6D_6): δ 160.4 (d, $^2J_{CP}$ = 5,3 Hz, PC=*C*H), 151.1 (br. s, P*C*=CH), 145.8 (d, $^3J_{CP}$ = 3.9 Hz, =C-O), 142.0 /142.0 (br s., *o*-CMes) / (br. s, *p*-CMes), 139.3 (d, $^3J_{CP}$ = 41.9 Hz, ipso-CPh), 135.7, 135.5, 133.8, 132.3 (d, $^2J_{CP}$ = 2.9 Hz, =C-O), 130.9 (br. s), 129.9, 129.1, 129.0, 128.5, 127.2, 126.2, 33.6 (s, Al(C*Me*$_3$)$_2$), 22.4 (s, *o*-CH_3), 20.4 (s, *p*-CH_3), 17.9 (br. s, Al(*C*Me$_3$)$_2$, 14.9 (s, thienyl-Me), 14.5, (s, thienyl-Me), 13.9 (s, thienyl-Me), 13.5 (s, thienyl-Me) ppm. Several aromatic signals are not observed due to overlapping with the signal of d_6-benzene; **^{31}P{1H} NMR** (240 MHz, C_6D_6): δ = 86.6 (s); **HRMS** (ESI) *m/z*: $[M+Na]^+$ calculated for $C_{48}H_{60}AlNaO_2PS_2^+$, 813.34799, found 813.34732.-

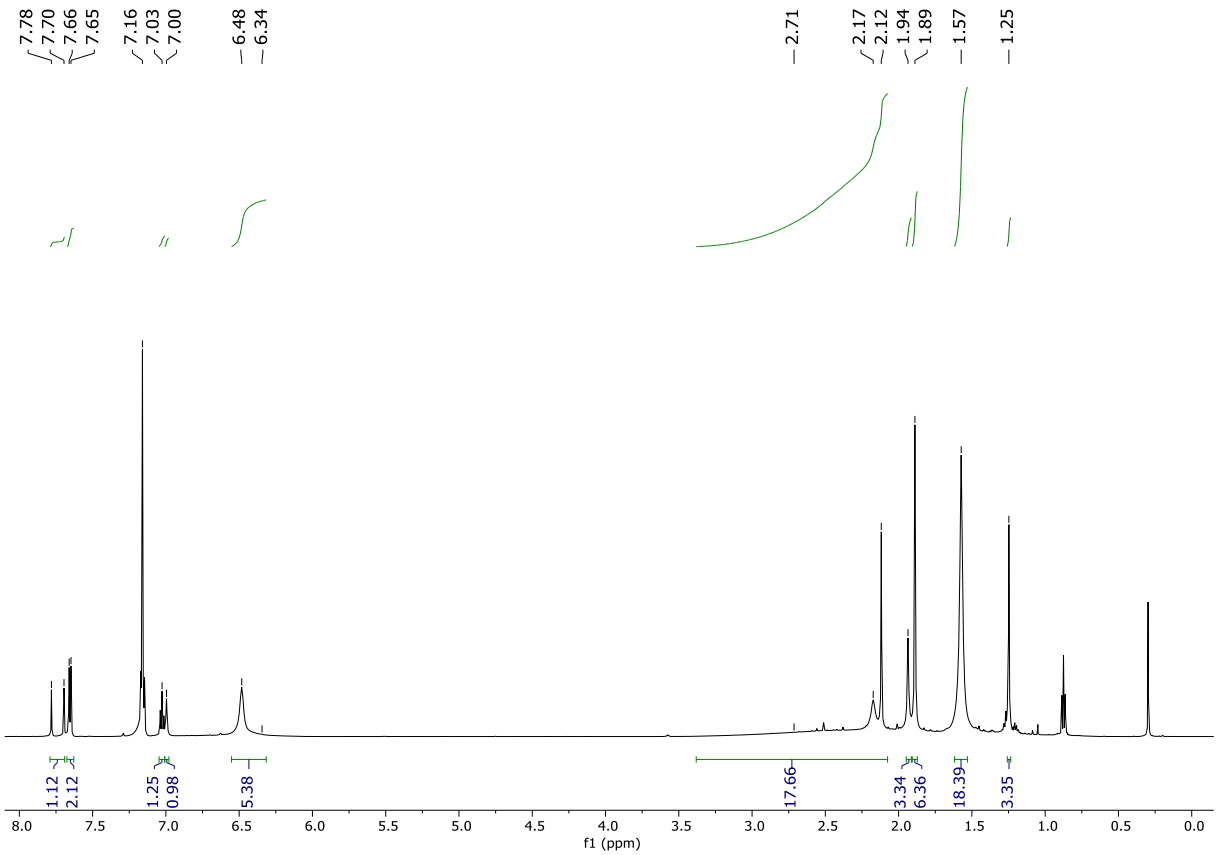

Figure S105: *^{1}H NMR spectrum (600 MHz, C_6D_6) of* ***115****.*

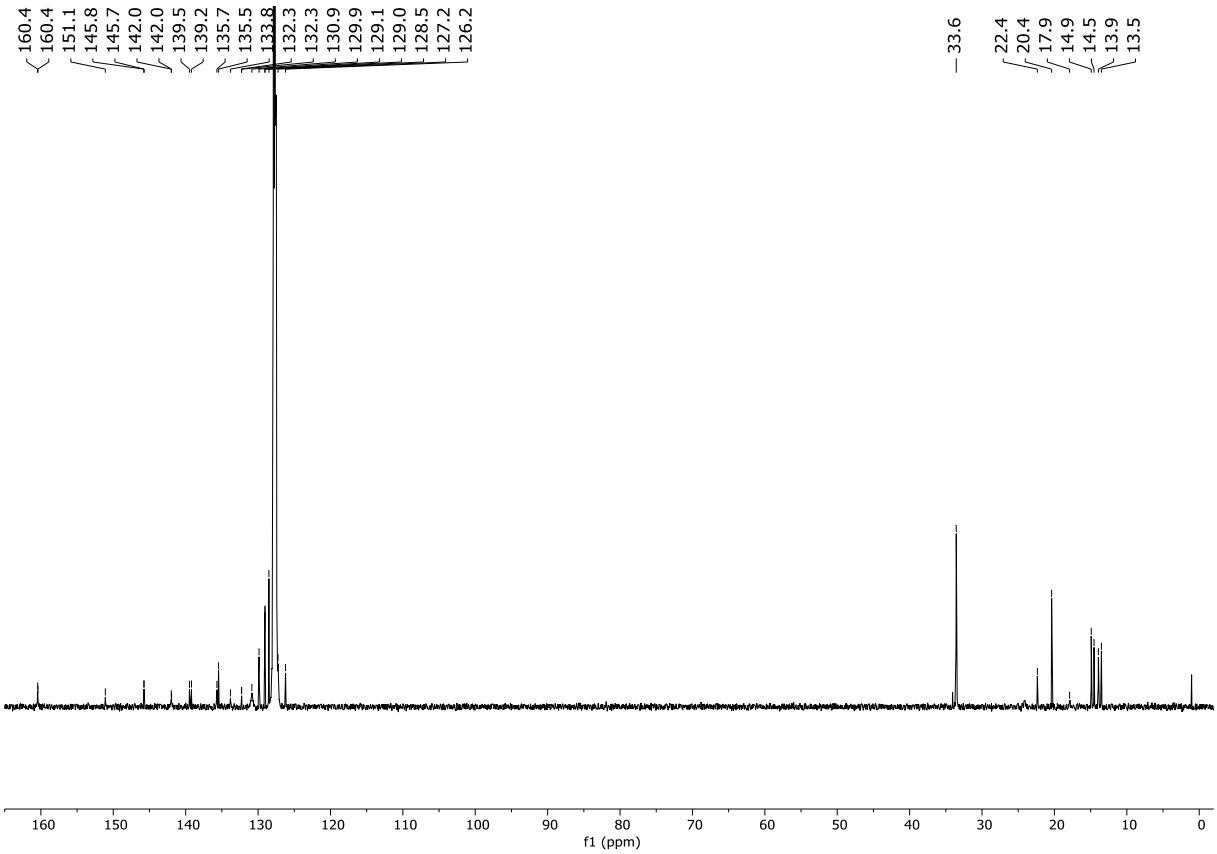

Figure S106: *$^{13}C\{^{1}H\}$ NMR spectrum (150 MHz, C_6D_6) of* ***115****.*

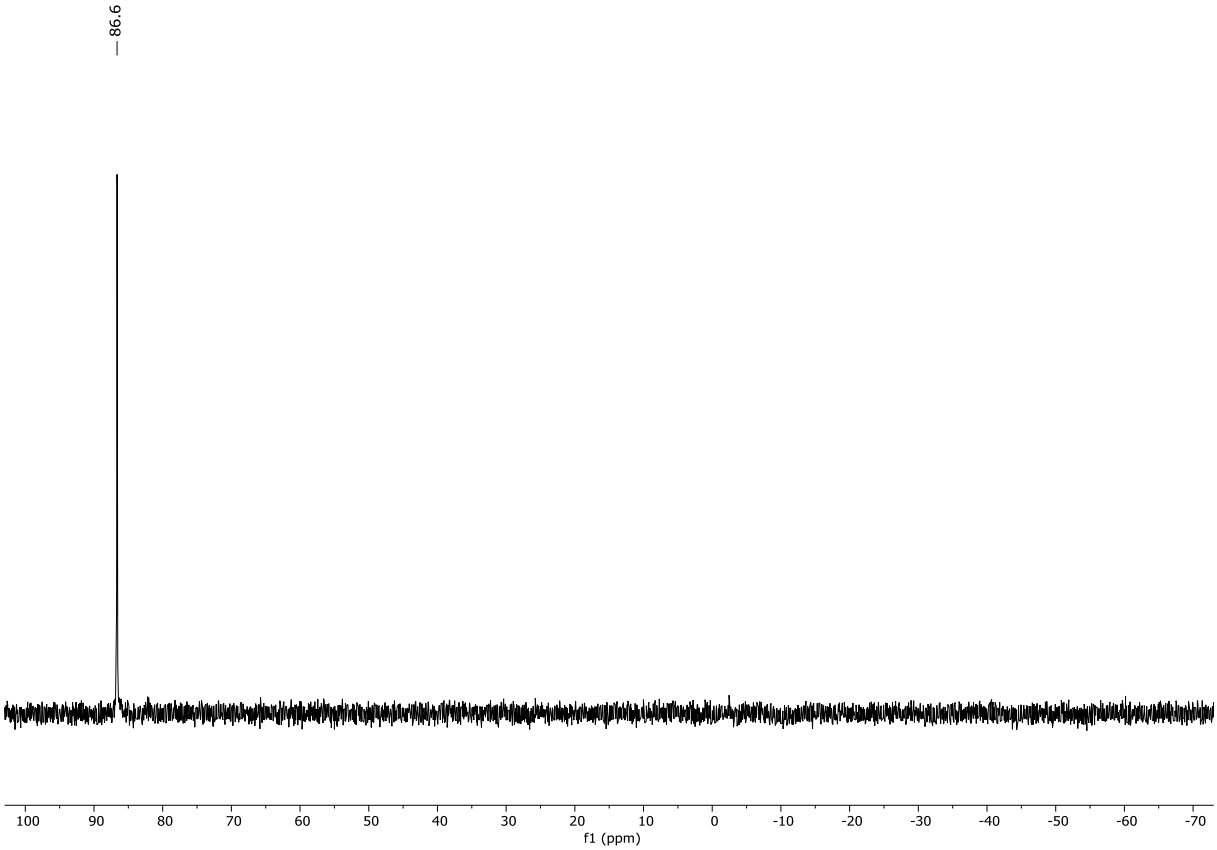

Figure S107: *$^{31}P\{^{1}H\}$ NMR spectrum (240 MHz, C_6D_6) of* ***115****.*

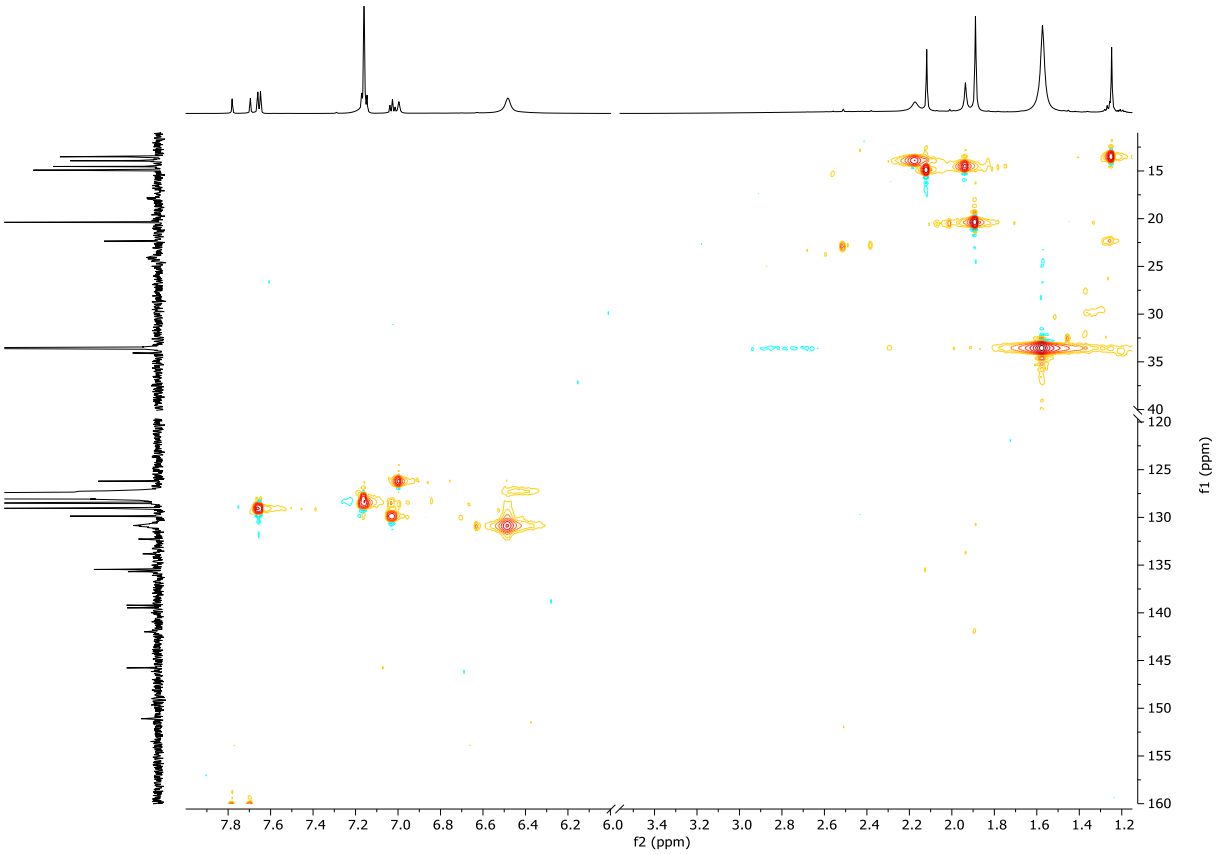

Figure S108: *HSQC spectrum (600/150 MHz, C_6D_6) of* ***115****.*

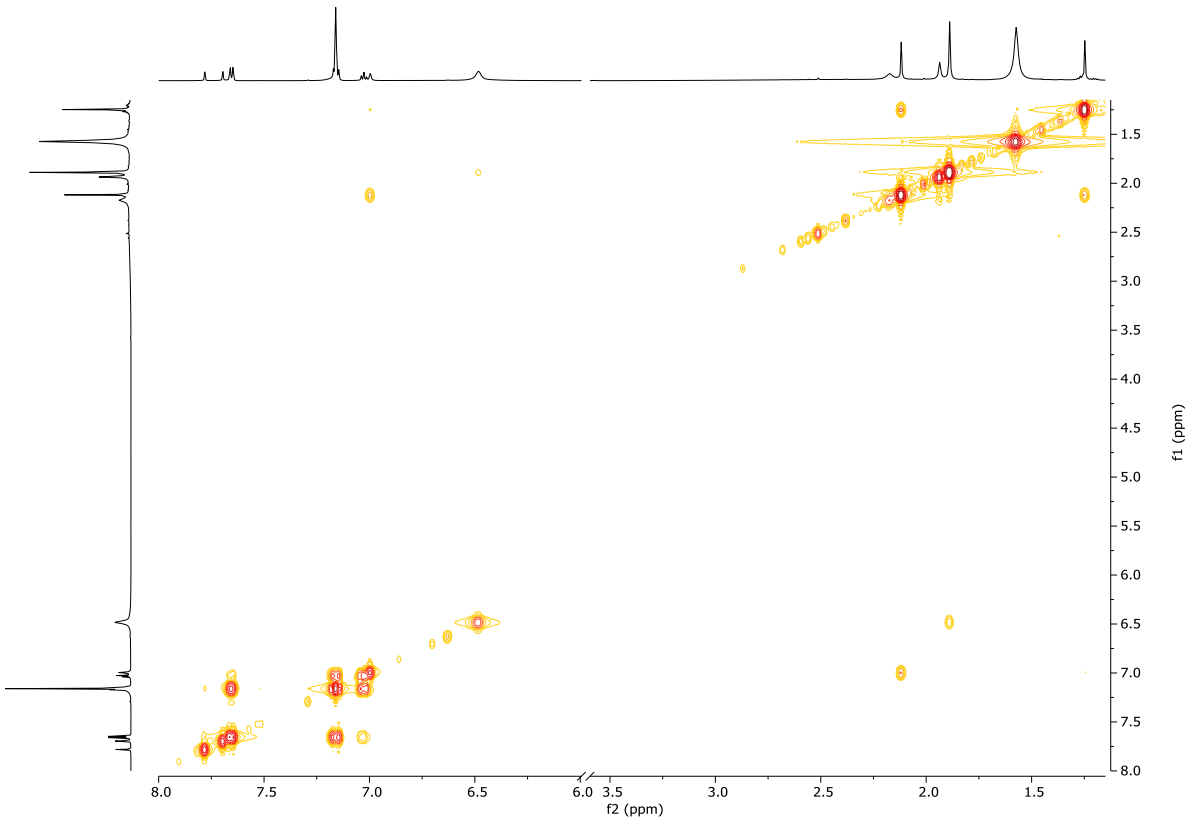

Figure S109: *H,H-COSY spectrum (600 MHz, C_6D_6) of* ***115****.*

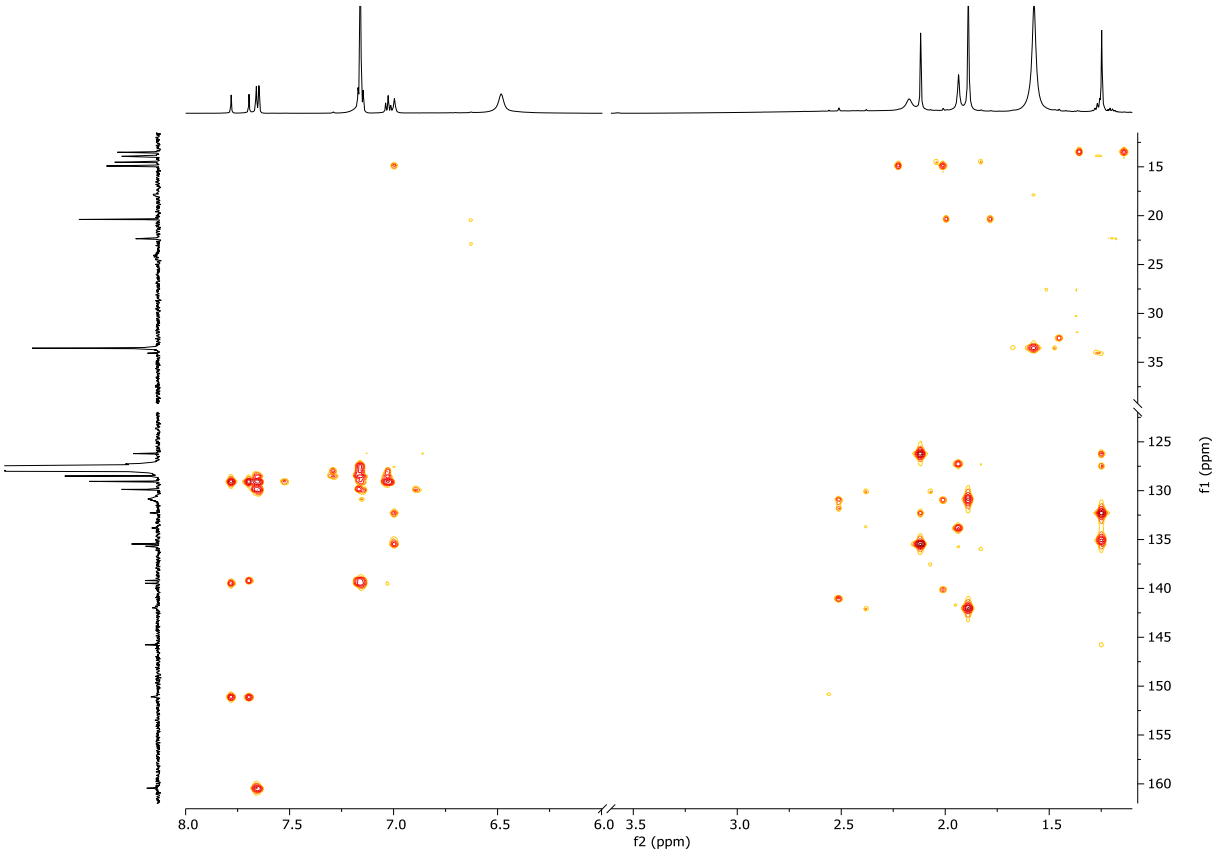

Figure S110: *HMBC spectrum (600/150 MHz, C_6D_6) of* ***115****.*

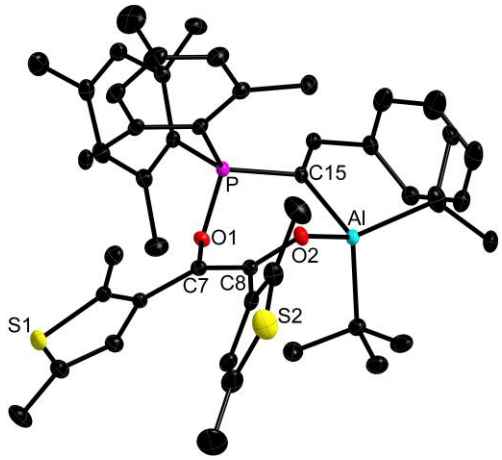

Figure S111: *X-ray crystal structure of* ***115*** *at 50% ellipsoid probability. Hydrogen atoms are omitted for clarity. Selected bond lengths [Å]: C7-C8 = 1.3461(2), C7-O1: 1.4334(1), O1-P: 1.5963(1), C8-O2: 1.383(1), O2-Al: 1.7994(1).*

Table S9: *Crystal data for (endiolato)Al-FLP adduct (**115**).*

	(endiolato)Al-FLP adduct (**115**)
Formula	$C_{48}H_{60}AlO_2PS_2$
Formula weight, g mol^{-1}	791.03
Crystal system	Triclinic
Space group	$P\bar{1}$
a, Å	11.6039 (9)
b, Å	11.9817 (7)
c, Å	18.1882 (12)
α, °	93.620 (2)
β, °	98.224 (3)
γ, °	108.565 (2)
V, Å^3	2356.6 (3)
Z	2
ρ_{calcd}, Mg m^{-3}	1.115
μ (Mo *Kα*), mm^{-1}	0.71073
F(000)	848
θ range, deg	2.243–28.323
Index ranges	$-15 \leq h \leq 15$
	$-15 \leq k \leq 14$
	$-24 \leq l \leq 24$
No. of reflns collected	60379
Completeness to θ_{max}	99.4%
No. indep. Reflns	11742
No. obsd reflns with($I>2\sigma(I)$)	10192
No. refined params	668
GooF (F^2)	1.028
R_1 (F) ($I > 2\sigma(I)$)	0.0352
wR_2 (F^2) (all data)	0.0948
Largest diff peak/hole, e Å^{-3}	0.453 / -0.304

Synthesis and Characterization of (Endiolato)$ReCl_2(PPh_3)_2$ (118)

α-Diketone ligand **90** (39 mg, 0.14 mmol, 1.0 eq.) was dissolved in 10 mL dry toluene and treated with $ReCl_3(CH_3CN)(PPh_3)_2$ (120 mg, 0.14 mmol, 1.0 eq.). (Note: although a reaction occurs suggesting a ratio of $ReCl_3(CH_3CN)(PPh_3)_2$ / *α*-diketone **90** of 2:1, a ratio of 1:1 was preferred to keep presence of $ReCl_3(CH_3CN)(PPh_3)_2$ after the reaction as low as possible. Abundant *α*-diketone ligand **90** can easily be removed *via* extraction with *n*-hexane.) The suspension was then heated to reflux, upon which a fast conversion to a dark purple solution could be observed. Stirring for another 48 h under reflux led to a solution blue-green in color. After removal of the solvent, the crude residue was dissolved in a small amount of DCM and overlayered with *n*-hexane. Over the course of several days, mainly dark red crystals formed. The supernatant was decanted, freed from solvent and the crude residue prepared for a second crystallization cycle as described before. This time mainly brown crystals in form of a rod formed, altogether with the prior described dark red crystals. The supernatant was decanted, and a small portion of *n*-hexane was added to the crystal mixture, followed by gentle shaking, which led to rod crystals break loose from the wall of the vessel. Decanting of the crystal suspension and washing with small portions of cold *n*-hexane led to pure product **118**. The obtained crystals were readily suitable for X-ray crystallography. For an increased yield the described procedure of the crystallization / decanting process was repeated one more time.

Yield: 24 mg (0.02 mmol, 16 %); **UV/Vis** (CH_2Cl_2): λ_{max} = 613 nm; **HRMS** (ESI) *m/z*: $[M]^+$ calculated for $C_{50}H_{44}Cl_2O_2P_2ReS_2^+$, 1059.11725, found 1059.11680.-

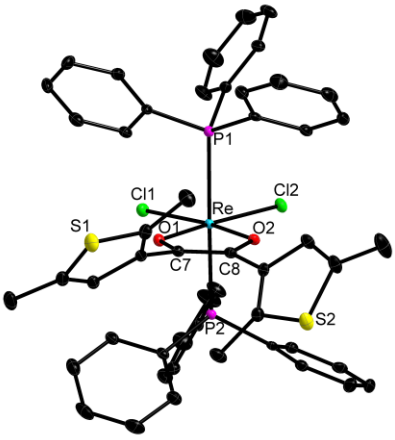

Figure S112: *X-ray crystal structure of* ***118*** *at 50% ellipsoid probability. Hydrogen atoms are omitted for clarity. Selected bond lengths [Å]: C7-C8 = 1.369(3), C7-O1: 1.345(3), O1-Re: 1.995(1), C8-O2: 1.342(3), O2-Re: 1.990(1), P1-Re: 2.488(1), P2-Re: 2.491(1).*

Table S10: *Crystal data for (endiolato)$ReCl_2(PPh_3)_2$ (**118**).*

	(endiolato)$ReCl_2(PPh_3)_2$ (**118**)
Formula	$C_{50}H_{44}Cl_2O_2P_2ReS_2 \cdot CH_2Cl_2$
Formula weight, g mol^{-1}	1144.76
Crystal system	Triclinic
Space group	$P\bar{1}$
a, Å	9.8895 (5)
b, Å	13.3448 (6)
c, Å	20.4711 (8)
α, °	72.947 (2)
β, °	88.468 (2)
γ, °	85.980 (2)
V, Å^3	2576.5 (2)
Z	2
ρ_{calcd}, Mg m^{-3}	1.476
μ (Mo *Kα*), mm^{-1}	2.746
F(000)	1146
θ range, deg	2.53–30.53
Index ranges	$-11 \leq h \leq 12$
	$-16 \leq k \leq 16$
	$-25 \leq l \leq 25$
No. of reflns collected	59486
Completeness to θ_{max}	100%
No. indep. Reflns	10691
No. obsd reflns with($I>2\sigma(I)$)	9981
No. refined params	565
GooF (F^2)	1.03
R_1 (F) ($I > 2\sigma(I)$)	0.0240
wR_2 (F^2) (all data)	0.0564
Largest diff peak/hole, e Å^{-3}	1.176 / -1.291

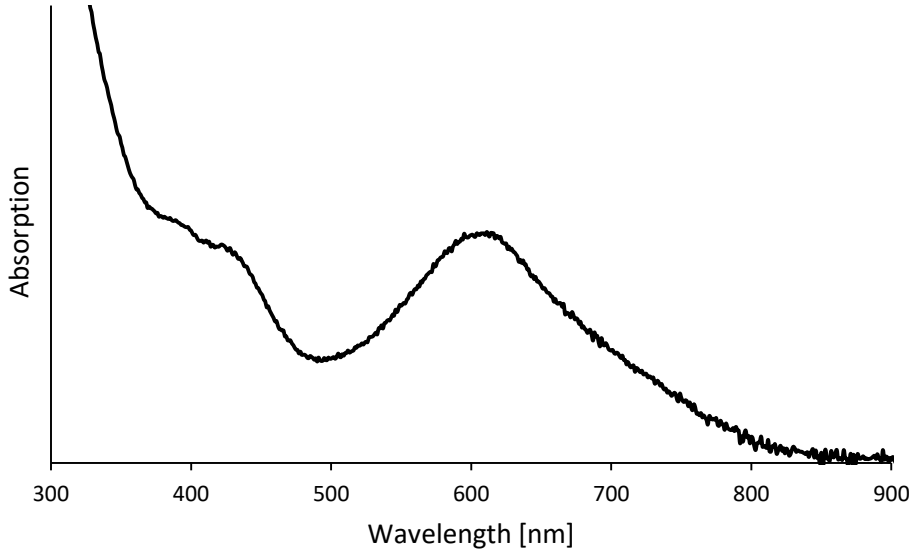

Figure S113: *UV/Vis spectrum of* ***118*** *in DCM.*

Erklärungen zur elektronischen Version und zur Überprüfung einer Dissertation

Hiermit bestätige ich gemäß §7, Abs. 7, Punkt 4, dass die zu Prüfungszwecken beigelegte elektronische Version meiner Dissertation identisch ist mit der abgegebenen gedruckten Version.

Ich bin mit der Überprüfung meiner Dissertation gemäß §6, Abs. 2, Punkt 5 mit qualifizierter Software im Rahmen der Untersuchung von Plagiatsvorwürfen einverstanden.

_____ _____

Ort, Datum Dirk Schlüter